Synthesis and Characterization of Zwitterion-Containing Acrylic (Block) Copolymers for Emerging Electroactive and Biomedical Applications

Tianyu Wu

Dissertation submitted to the faculty of the Virginia Polytechnic Institute and State University in partial fulfillment of the requirements for the degree of

Doctor of Philosophy
In
Macromolecular Science and Engineering

Timothy E. Long, Chair
S. Richard Turner
James R. Heflin
Richey M. Davis

August 31, 2012
Blacksburg, VA

Keywords: functional acrylate, block copolymer, controlled radical polymerization, zwitterion, ionic liquid, electromechanical transducer, nucleic acid delivery, and morphology

Copyright © 2012, Tianyu Wu

Synthesis and Characterization of Zwitterion-Containing Acrylic (Block) Copolymers for Emerging Electroactive and Biomedical Applications

Tianyu Wu

ABSTRACT

Conventional free radical polymerization of *n*-butyl acrylate with 3-[[2-(methacryloyloxy)ethyl](dimethyl)-ammonio]-1-propanesulfonate (SBMA) and 2-[butyl(dimethyl)amino]ethyl methacrylate methanesulfonate (BDMAEMA MS), respectively, yielded zwitterionomers and cationomers of comparable chemical structures. Differential scanning calorimetry (DSC), small-angle X-ray scattering (SAXS), and atomic force microscopy (AFM) revealed that zwitterionomers promoted more well-defined microphase-separation than cationic analogs. Dynamic mechanical analyses (DMA) of the copolymers showed a rubbery plateau region due to physical crosslinks between charges for zwitterionomers only. We attributed improved microphase-separation and superior elastomeric performance of the zwitterionomers to stronger association between covalently tethered charged pairs.

Zwitterionomer / ionic liquid binary compositions of poly(*n*BA-*co*-SBMA) and 1-ethyl-3-methylimidazolium ethylsulfate (EMIm ES) were prepared using both the "swelling' and the "cast with" methods. Dynamic mechanical analysis revealed that the "swollen" membranes maintained their thermomechanical performance with up to 18 wt% EMIm ES incorporation, while that of the "cast with" membranes decreased

gradually as the ionic liquid concentration in the composite membranes increased. Small-angle X-ray scattering results indicated that the “swollen” and the “cast with” membranes have different morphologies, with the ionic liquid distributed more evenly inside the “cast with” membranes. Impedance spectroscopy results showed that the “cast with” membranes had better ionic conductivity than the “swollen” membrane at high ionic liquid concentration, in agreement with our proposed model. The results indicated that the different processing methods had a significant impact on thermomechanical properties, ionic conductivities, as well as morphologies of the zwitterionomer / ionic liquid binary compositions.

Reversible addition-fragmentation chain transfer polymerization (RAFT) strategy afforded the synthesis of well-defined poly(sty-*b*-*n*BA-*b*-sty). 2-(Dimethylamino)ethyl acrylate (DMAEA), a tertiary amine-containing acrylic monomer, exhibited radical chain transfer tendency toward itself, which is undesirable in controlled radical polymerization processes. We employed a higher [RAFT] : [Initiator] ratio of 20 : 1 to minimize the impact of the chain transfer reactions and yielded high molecular weight poly[sty-*b*-(*n*BA-*co*-DMAEA)-*b*-sty] with relatively narrow PDIs. The presence of the tertiary amine functionality, as well as their quaternized derivatives, in the central blocks of the triblock copolymers afforded them tunable polarity toward polar guest molecules, such as ionic liquids. Gravimetric measurements determined the swelling capacity of the triblock copolymers for EMIm TfO, an ionic liquid. DSC and DMA results revealed the impact of the ionic liquid on the thermal and thermomechanical properties of the triblock copolymers, respectively. Composite membranes of DMAEA-derived triblock

copolymers and EMIm TfO exhibited desirable plateau moduli of ~ 100 MPa, and were hence fabricated into electromechanical transducers.

RAFT synthesized poly(sty-*b*-*n*BA-*b*-sty) triblock copolymer phase separates into long-range ordered morphologies in the solid state due to the incompatibility between the poly(*n*BA) phases and the poly(sty) phases. The incorporation of DMAEA into the central acrylic blocks enabled subsequent quaternization of the tertiary amines into sulfobetaine functionalities. Both DSC and DMA results suggested that the electrostatic interactions in the low T_g central blocks of poly(sty-*b*-*n*BA-*b*-sty) enhanced block copolymer phase separation. SAXS results indicated that the presence of the sulfobetaine functionalities in acrylate phases increased electron density differences between the phases, and led to better defined scattering profiles. TEM results confirmed that the block copolymers of designed molecular weights exhibited lamellar morphologies, and the lamellar spacing increased with the amount of electrostatic interactions for the zwitterionic triblock copolymers.

Acrylic radicals are more susceptible to radical chain transfer than their styrenic and methacrylic counterparts. Controlled radical polymerization processes (e.g. RAFT, ATRP and NMP) mediate the reactivity of the acrylic radical and enable the synthesis of well-defined linear poly(alkyl acrylate)s. However, functional groups such as tertiary amine and imidazole on acrylic monomers interfere with the controlled radical polymerization of functional acrylates. Model CFR and RAFT polymerization of *n*BA in the presence of triethylamine and *N*-methyl imidazole revealed the interference of the functional group on the polymerization of acrylate. Various RAFT agents, RAFT agent to initiator ratios, degree of polymerization and monomer feed concentrations were screened

with an imidazole-containing acrylate for optimized RAFT polymerization conditions. The results suggest that the controlled radical polymerization of functional acrylates, such as 2-(dimethylamino)ethyl acrylate and 4-((3-(1H-imidazole-1-yl)propanoyl)oxy)-butyl acrylate (ImPBA), remained challenging.

ACKNOWLEDGEMENTS

I would first like to thank my advisor, Dr. Timothy E. Long for allowing me the opportunity to conduct graduate research in his group. I truly appreciate the lessons that he taught me as a person and a scientist, the many opportunities that he brought upon me, and the freedom that he allowed me to pursue my scientific endeavors. I would also like to thank Dr. Robert B. Moore, Dr. S. Richard Turner, Dr. Richey M. Davis, and Dr. J. Randy Heflin for serving on my committee throughout my graduate career. Their suggestions and comments had enlightened me and resulted in publications at times. I'm also grateful to Dr. Frederick L. Beyer for allowing me the opportunity to spend a week at the U.S Army Research Laboratory working on small angle X-ray scattering (SAXS).

I would like to thank Dean Dr. Karen P. DePauw of the Graduate School at Virginia Tech for her support over the years. I first met Dean DePauw in her "Preparing the Future Professoriate" class and at monthly Graduate Student Assembly meeting. The PFP class gave me new perspectives toward graduate education and allowed me the opportunity to reflect on the possibility of pursuing a career in the academia. I also enjoyed my conversations with her on interdisciplinary education and research. As a student in the interdisciplinary Macromolecular Science and Engineering Program, I'm grateful to Dean DePauw for her sincere support.

I would like to thank Dr. Long, the Graduate School at Virginia Tech, the U.S. Army Research Office, the U.S. Army Research Laboratory, the Macromolecular and Interfaces Institute and the Chemistry Department at Virginia Tech for the funding that supported me through the past five years. I would also like to thank the "Chevron-Phillips

Chemical Professional Excellence Travel Award" for enabling me to attend the Gordon Research Conference in 2011.

I am grateful for all the assistance that I have received from various staff members over the years. Our administrative assistants Laurie Good, Tammy Jo Hiner, Valerie Owens, Naya Sou, and Teresa Dickerson all deserve a big "Thank You". I would also like to thank Steve McCartney, Dr. Niven Monsegue and Kathy Lowe for their knowledge of microscopy; Dr. Hugo Azurmendi and Geno Iannaccone for maintaining a functional NMR facility; Bill Bebout for mass spectrometry services; Tom Wertalik for his skilled glassblowing craftsmanship; Larry Jackson and Jim Hall for their assistance with various IT issues; John Burleson for his expertise with electronics and machinery.

Thanks to past and current members of the Long Research Group who I had the honor to work with, especially those who shared valuable time with me in the old Davidson Hall, which is now demolished for renovation. I would like to thank Dr. Rebecca Brown and Dr. Matthew Cashion for showing me the ropes of the Long Group and teaching me about the American culture. I would like to thank Dr. Takeo Suga for sharing with me his thoughts on pursuing an academic career and his demonstration of excellence. I would like to thank Dr. Eugene Joseph, a seasoned chemical engineer with extensive industrial experience, for sharing with me his experience and providing me with valuable suggestions from time to time. I would like to thank Dr. Christian Schreiner and Dr. Kevin Miller, my postdoc lab-mates, for their great company on many hiking excursions and their demonstration of good laboratory practices. In fact, Dr. Miller's lab notebook was the most well-organized that I've ever seen to-date. I will remember Dr. John Layman for his friendship and his acceptance to international cultures. I will also

remember Dr. Matthew Hunley for his extraordinary hospitality at tailgate parties and enthusiasm for Hokies. I would like to thank Dr. Shijing Cheng and Dr. Renlong Gao for reminding me of our Chinese culture half a world away.

This list of past and current group members should also include Dr. Taigyoo Park, Dr. Sean Ramirez, Dr. Erin Murphy, Dr. Adam Smith, Mr. Daisuke Yamamoto, Dr. Sharlene Williams, Dr. Andy Duncan, Dr. Gozde Ozturk, Dr. Emily Anderson, Dr. Matthew Green, Dr. Steve June, Mana Tamami, Mike Allen, Nancy Zhang, Ali Nebipasagil, Sean Hemp, David Inglefield, Chainika Jangu, Ashley Nelson, Alex Fersner, Alie Shultz, Keren Zhang and Evan Margaretta. I would like to thank each one of them for bringing their unique personality into this dynamic group, and the past five years have been quite a learning experience for me personally.

Few of the chapters in this dissertation were accomplished without valuable inputs from our collaborators. I would like to thank Dr. Gilles Divoux for his expertise on electrochemistry and sharing of his experience and value; Mingqiang Zhang for his expertise on SAXS measurement; Dong Wang for his knowledge and skills on electro-mechanical actuator fabrication; Jianbo Hou for his insightful discussions on ion transport in membranes.

I would like to thank my family for their love and unconditional support every step of my way throughout the years. I owe a huge debt of gratitude to my Mom, Yili He for her guidance and unwavering support throughout my life. I would like to thank my grandpa Baoqi He, a visiting chemist in the US in 1940s, and grandma Mojie Zhu for their nurturing of me as I grew up. I'm also grateful to the families of my aunts Yiping He and Yiling He for providing me with shelters in North America.

Finally, as I wrote this acknowledgement in preparation of my PhD defense, I became increasingly aware that many individuals and organizations had helped me with setting this stage. I would like to thank all those that go unnamed for making my past five years colorful.

Attribution

Dr. Frederick L. Beyer, Dr. Rebecca H. Brown, Professor Robert B. Moore and Professor Timothy E. Long co-authored **Chapter 3**. Dr. Beyer of Army Research Laboratory (ARL) provided access to the small angle X-ray scattering (SAXS) instrument at ARL and shared valuable experience concerning data processing and interpretation. Professor Moore and Professor Long are both faculty members of the Department of Chemistry at Virginia Tech, while Dr. Brown was a graduate student in the Long Research Lab. Dr. Brown suggested the topic of comparing sulfobetaine methacrylate (SBMA) with its cationic analog bearing a bromide anion, and Professor Moore suggested the modification of the cationic analog through ion exchange for methanesulfonate anions. Professor Long provided the financial support and the oversight for this project.

Dr. Gilles M. Divoux, Mr. Mingqiang Zhang, Professor Robert B. Moore, and Professor Timothy E. Long co-authored **Chapter 4**. Both Dr. Divoux and Mr. Zhang were members of the Moore Research Group. Professor Moore granted access to the SAXS instrument in his group for this collaboration; Mr. Zhang performed the SAXS analysis on all samples, while Dr. Divoux conducted the impedance analysis on these samples. Professor Long provided the financial resources for the other aspects of this project.

Mr. Dong Wang, Mr. Mingqiang Zhang, Professor James R. Heflin, Professor Robert B. Moore and Professor Timothy E. Long co-authored **Chapter 5**. Mr. Wang is a graduate student in Professor Heflin's group in Department of Physics at Virginia Tech. They fabricated the actuators and evaluated their electro-responsiveness. Mr. Zhang and

Professor Moore enabled morphological characterization of the block copolymers using the small angle X-ray scattering instrument in their group.

Mr. Mingqiang Zhang, Professor Robert B. Moore, and Professor Timothy E. Long co-authored **Chapter 6** on "Impact of Electrostatic Interactions in the Low Tg Center Blocks on the Thermomechanical Properties and the Morphological Development of ABA Triblock Copolymers". Mr. Zhang and Professor Moore enabled the SAXS characterization of the acrylic triblock copolymers.

Dr. Shijing Cheng, Mr. Sean T. Hemp, and Professor Timothy E. Long co-authored **Chapter 7**. Dr. Cheng and Mr. Hemp were both graduate students in the Long Research Group. Dr. Cheng provided suggestions regarding the synthesis of the novel imidazole-containing acrylates, while Mr. Hemp performed the size exclusion chromatography analysis of the hompolymers. Professor Long provided the financial support and the oversight for this project.

Table of Contents

List of Figures

List of Schemes

List of Tables

Chapter 1 Introduction

1.1 Scientific Rationale and Perspective

This dissertation explores the potential of zwitterions in acrylic copolymer for emerging applications. Chapter 2 reviews the general synthetic strategies toward polyzwitterions, and focuses on recent advances in the synthesis of betaine-containing block copolymers. They exhibit unique antifouling performance and affinity toward polar guest molecules due to the placement of opposite charges in zwitterion-containing polymers.

Meanwhile, poly(acrylate)s are an important class of macromolecules that exhibit much lower glass transition temperatures than their methacrylic analogs. The T_gs for poly(acrylic acid), poly(ethyl acrylate), poly(*n*-butyl acrylate), poly(2-ethylhexyl acrylate) and poly(lauryl acrylate) are 130 °C, -8 °C, -43 °C, -58 °C and -17 °C, respectively.[1] The sub-ambient T_gs for most poly(acrylate)s permit segmental motions at ambient and higher temperatures, which enables the dissipation of mechanical energy in adhesive applications.[2] Bauer first reported the application of acrylic polymers in adhesive compositions in 1933.[3] 3M popularized the use of acrylic polymers in pressure sensitive adhesives in the 1950s. By late 1990s, poly(acrylate)-based products had 33% of the market share in the pressure sensitive adhesive business, and the growth rate had exceeded that of the GNP and remained steady.[4] Nielson and coworkers explored zwitterionic compounds as tackifiers or plasticizers in adhesive formulations and provided adhesive compositions comprising zwitterionic copolymers.[5, 6] Chapter 3 of this dissertation elucidated the impact of zwitterionic interactions on the thermomechanical

properties and the morphologies of acrylic copolymers, and 2-[butyl(dimethyl)amino]ethyl methacrylate methanesulfonate (BDMAEMA MS) was chosen as the cationic analog to 3-[[2-(methacryloyloxy)ethyl](dimethyl)ammonio]-1-propanesulfonate (SBMA), the zwitterionic monomer. Chapter 4 explored the potential of the zwitterionomer as the host matrices for polar guest molecules such as ionic liquids and revealed the impact of processing methods (e.g. "swelling" *vs.* "cast with") on the morphology and the property of the binary compositions.

Thermoplastic elastomers (TPEs) are polymers that exhibit both elastomeric behaviors and thermoplastic properties.[7, 8] Typical TPEs include styrenic block copolymers (e.g. SBS), multiblock copolymers (e.g. polyurethane elastomers) and hard polymer-elastomer combinations, where thermally reversible physical crosslinks such as glassy blocks, small crystallites and ionic aggregates lock flexible polymer chains into rubber-like networks.[9] In 2009, the styrenic block copolymers had 45% of the global TPE share by mass.[9] However, the polydiene-based central blocks of the styrenic block copolymers render them susceptible to oxidation and lack chemical tunability. Therefore, it is desirable to explore the potential of TPEs that contain more versatile poly(acrylate) central blocks. Matyjaszewski and coworkers investigated poly(*n*-butyl acrylate) (block) copolymers with advanced architectures for elastomeric performances.[10-14] Jerome and coworkers studied the mechanical properties and the morphologies of a series of ABA triblock copolymers that contained methyl methacrylate outer blocks and alkyl acrylate central blocks.[15-18] The authors correlated the elastomeric performance of the triblock copolymers with the molecular weights between entanglements (M_e) for the central blocks. Chapter 5 reported the synthesis of poly(sty-*b*-acrylate-*b*-sty) triblock copolymers

using RAFT polymerization strategy. The central acrylate block contained 2-(dimethylamino)ethyl acrylate, which drastically improved the affinity of the triblock copolymers toward ionic liquids for electro-active membrane applications. The presence of the tertiary amine functionalities in the triblock copolymers enabled facile quaternization with 1,3-propanesultone to derive zwitterion-containing triblock copolymers. Chapter 6 discussed the impact of electrostatic interactions in the low T_g central blocks on the morphological development, as well as the thermomechanical performance, of weakly segregated ABA triblock copolymers.

Finally, Chapter 7 reported the synthesis of novel imidazole-containing acrylates using Michael-addition reactions and their potential in electro-active applications and as nucleic acid delivery agents. Despite recent developments in controlled radical polymerization (CRP) techniques, the CRP of functional acrylates remained challenging due to the radical stability of acrylic radicals.[19] This chapter also summarized our efforts in controlling the radical polymerization of the novel imidazole-containing acrylates.

1.2 References

1. Auchter, G.; Aydin, O.; Zettl, A.; Satas, D., Acrylic Adhesives. In *Handbook of Pressure Sensitive Adhesive Technology*, Third Edition ed.; Satas, D., Ed. Satas & Associates: Warwick, Rhode Island, 1999.
2. Pocius, A. V., Adhesives. In *Physical Properties of Polymers Handbook*, Mark, J. E., Ed. Springer: New York, 2007.
3. Bauer, W. Adhesives. 1928-R74611, 575327, 19280510., 1933.
4. Satas, D., Pressure Sensitive Adhesives and Adhesive Products in the United States. In *Handbook of Pressure Sensitive Adhesive Technology*, Third Edition ed.; Satas, D., Ed. Satas & Associates: Warwick, Rhode Island, 1999.
5. Nielson, K. E.; Li, K.; Rayner, T. J. Adhesive compositions and adhesive tapes comprising novel zwitterionic copolymers. 1998-42980, 6133391, 19980317., 2000.
6. Nielson, K. E.; Li, K.; Rayner, T. J. Adhesive compositions with zwitterionic tackifiers and plasticizers for adhesive tape. 1998-40024, 6106940, 19980317., 2000.

7. Holden, G.; Bishop, E. T.; Legge, N. R. *Journal of Polymer Science Part C: Polymer Symposia* **1969,** 26, (1), 37-57.
8. Fetters, L. J.; Morton, M. *Macromolecules* **1969,** 2, (5), 453-458.
9. Drobny, J. G., In *Handbook of Thermoplastic Elastomers*, William Andrew Publishing: Norwich, New York, 2007; p 3.
10. Dufour, B.; Tang, C.; Koynov, K.; Zhang, Y.; Pakula, T.; Matyjaszewski, K. *Macromolecules (Washington, DC, U. S.)* **2008,** 41, (7), 2451-2458.
11. Pakula, T.; Zhang, Y.; Matyjaszewski, K.; Lee, H.-i.; Boerner, H.; Qin, S.; Berry, G. C. *Polymer* **2006,** 47, (20), 7198-7206.
12. Pakula, T.; Koynov, K.; Boerner, H.; Huang, J.; Lee, H.-i.; Pietrasik, J.; Sumerlin, B.; Matyjaszewski, K. *Polymer* **2011,** 52, (12), 2576-2583.
13. Juhari, A.; Mosnacek, J.; Yoon, J. A.; Nese, A.; Koynov, K.; Kowalewski, T.; Matyjaszewski, K. *Polymer* **2010,** 51, (21), 4806-4813.
14. Nese, A.; Mosnacek, J.; Juhari, A.; Yoon, J. A.; Koynov, K.; Kowalewski, T.; Matyjaszewski, K. *Macromolecules (Washington, DC, U. S.)* **2010,** 43, (3), 1227-1235.
15. Tong, J. D.; Jerome, R. *Macromolecules* **2000,** 33, (5), 1479-1481.
16. Tong, J. D.; Jerome, R. *Polymer* **2000,** 41, (7), 2499-2510.
17. Tong, J. D.; Leclere, P.; Doneux, C.; Bredas, J. L.; Lazzaroni, R.; Jerome, R. *Polymer* **2000,** 41, (12), 4617-4624.
18. Tong, J. D.; Leclere, P.; Rasmont, A.; Bredas, J. L.; Lazzaroni, R.; Jerome, R. *Macromol. Chem. Phys.* **2000,** 201, (12), 1250-1258.
19. Ahmad, N. M.; Charleux, B.; Farcet, C.; Ferguson, C. J.; Gaynor, S. G.; Hawkett, B. S.; Heatley, F.; Klumperman, B.; Konkolewicz, D.; Lovell, P. A.; Matyjaszewski, K.; Venkatesh, R. *Macromol. Rapid Commun.* **2009,** 30, (23), 2002-2021.

Chapter 2 Exploring the Potential of Zwitterion-Containing Block Copolymers for Emerging Applications

(*Tianyu Wu*, and *Timothy E. Long*)

2.1 Abstract

This review summarizes the general synthetic strategies toward polyzwitterions and focuses on recent advances in the synthesis of betaine-containing block copolymers. Polyzwitterions shared some characteristic that derived from their ionic nature with conventional polyelectrolytes and ionomers. However, due to the placement of opposite charges, they also exhibited unique antifouling performance and affinity toward polar guest molecules. Here, we attempted to correlate the physical properties of polyzwitterions with their molecular structures and shed light on their potential in emerging applications.

2.2 Introduction

Zwitterions are compounds that contain both cations and anions. In the case of polyzwitterions, the ionic functionalities of opposite charges may reside either on the same repeating unit or on different repeating units. The former are referred to as polybetaines, while the latter are referred to as polyampholytes. Zwitterionic polymers are an important subclass of charge-containing polymers, which have received considerable amount of interest over the past 50 years for their unique properties and commercial applications.

DuPont™ first commercialized Surlyn® A ionomer resins, which consisted of copolymers of ethylene and neutralized methacrylic acid, in March 1965. The term

ionomer refers to copolymers containing less than 10 mol% charged functionalities. Thanks to the temperature-dependent electrostatic interactions between the ionic functionalities, this new class of materials exhibited both the solid-state properties of crosslinked hydrocarbon polymers and the melt-flow properties of uncrosslinked hydrocarbon polymers.[1, 2] In addition, the presence of electrostatic interactions in Surlyn® A resins prevented lamellar crystals of the polyethylene components from forming larger spherulites. As a result, the ionomers appeared transparent.[3] Kinsey noted that the types and the amounts of the carboxylic acid comonomer, the types of the metal counter-cations and the molecular weights of the copolymers determined their suitability for applications in skin packaging, paper and coil coating and bonding wood to metal.

In late 1960s, DuPont™ developed another series of ionomers, Nafion®, for improving the membrane chlor-alkali cell technology. Nafion® is a perfluorosulfonated ionomer, which has sparked great interest over the past 20 years for its potential applications in proton exchange membrane fuel cells (PEMFC)[4] and electromechanical transducers.[5] All such applications involved the transport of ionic species across the polymeric membranes. Mauritz and coworkers long noted that the realization of such ionomers' potential in separation processes rests with the understanding, and optimizing, the structure-property relationships in these materials.[4, 6] More recently, Schmid-rohr et al. quantitatively simulated previously published small-angle scattering data of hydrated Nafion®, and suggested that the characteristic "ionomer peak" arose from long parallel but otherwise randomly packed water channels.[7] They reported that the water channels had average diameters of 2.4 nm, and concluded that the new model agreed well with Nafion®'s fast water and proton diffusion, as well as its persistence at low temperatures.

Another key characteristic of ionic polymers also involves the intrinsic interactions between positive and negative charges. Otocka reviewed early works on the formation of polyelectrolyte complexes in 1971.[8] The author termed such complexes polysalts, and noted that they were very compatible with mammalian tissue and exhibited good ionic permeability and swellability for potential application in medicine. Rembaum reported that mixing the aqueous solutions of a cationic ionene and an anionic calf thymus DNA resulted in a solid fibrous precipitate.[9] Polarizing microscopy results suggested that the helical configuration of DNA persisted in the complex. In recent years, especially since the presentation of the Nobel Prize in Physiology or Medicine in 2006 to Fire and Mello for their discovery of RNA interference-gene silencing by double-stranded RNA, the potential application of cationic polymers in nucleic acid therapeutics has sparked great interest.[10-13]

For zwitterionic polymers, the electrostatic interactions between the opposite charges are identical in nature compared with those in ionomers and polyelectrolytes. However, due to significant differences in the positioning of those charges, zwitterionic polymers exhibited unique physical properties. Over the past decade, Lowe and McCormick reviewed solution properties of polyzwitterions, and briefly summarized the synthesis of both polyampholytes and polybetaines;[14] Kudaibergenov et al. reviewed synthesis of polybetaines in detail, discussed their condensed state, as well as solution state, properties, and highlighted their applications in oil recovery, hydrometallurgy processes and a number of biomedical applications.[15]

A number of recent publications explored potential applications of betaine-containing block copolymers as antifouling, stimuli-responsive and bio-conjugate

forming materials in the solution and gel states, while a parallel effort focused on utilizing the high dipole moments of betaine functionalities as the hosting sites for polar guest molecules. In this review, we will briefly overview the synthesis of polyampholytes and their responses to salt addition and pH changes in solutions, and focus on the various synthetic strategies toward polybetaines and betaine-containing block copolymers for emerging applications.

2.3 Synthesis of Polyampholytes

Peiffer and Lundberg synthesized low charge density acrylamide-based polyampholytes and studied their solution properties in fresh and high ionic strength solutions.[16] The polyampholytes consisted of cationic methacrylamidopropyltrimethylammonium chloride (MAPTAC) and anionic sodium styrene sulfonate (SSS), or sodium vinyl sulfonate (SVS). The chemical structures of the comonomers are shown in **Figure 2.1**. They found that, at low charge densities, intermolecular interactions determined solution properties of the polyampholytes in fresh water, and salt addition led to the lowering of the solution viscosities. In comparison, at moderate charge densities, intra-molecular interactions dominated their behaviors, and, as the ionic strength of the solutions increased, intermolecular interactions became more dominant.

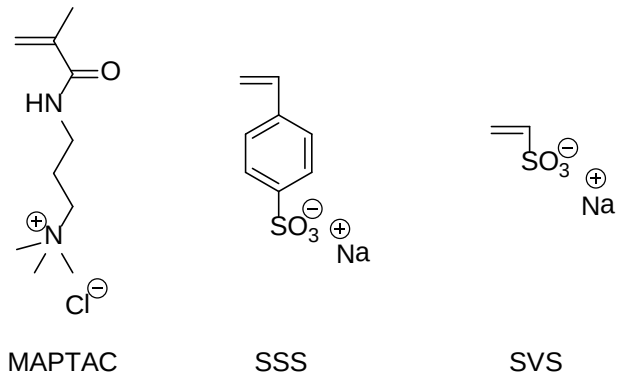

Figure 2.1 Chemical structures of MAPTAC, SSS and SVS

Baker and Prausnitz et al. copolymerized acrylamide with cationic MAPTAC and anionic SSS.[17] The authors maintained overall charge density in the copolymers at 4.7 mol%, but varied the molar ratio of the cations to the anions. They measured swelling equilibria of the copolymers in both water and NaCl solutions, and found that the hydrogels showed increasing insensitivity to solution ionic strength as their molar ratio of the cations to the anions approached unity.

English and coworkers studied ampholytic hydrogels consisted of 2-acryl-amido-2-methylpropane sulfonic acid (AMPS-H), acrylic acid, MAPTAC and *N*,*N*'-methylene-bis-acrylamide (BIS), the crosslinker.[18-21] The structures of the monomers, as well as the crosslinker, are shown in **Figure 2.2**. They studied the swelling behaviors of the hydrogels in aqueous solutions, and reported their normalized diameters (D/D_0) at equilibriums as a function of their charge imbalances and solution ionic strengths. Experimental results revealed that balanced polyampholytes collapsed at low salt concentrations and swelled at high salt concentrations; as the charge offset increased, the polyampholytes exhibited polyelectrolyte behaviors and decreased swelling with increasing salt concentrations. The authors demonstrated that an extension of the Flory-

Huggins theory incorporating a quasi-lattice screened Coulombic term for the hydrogel fixed charge groups agreed well with the observed results.

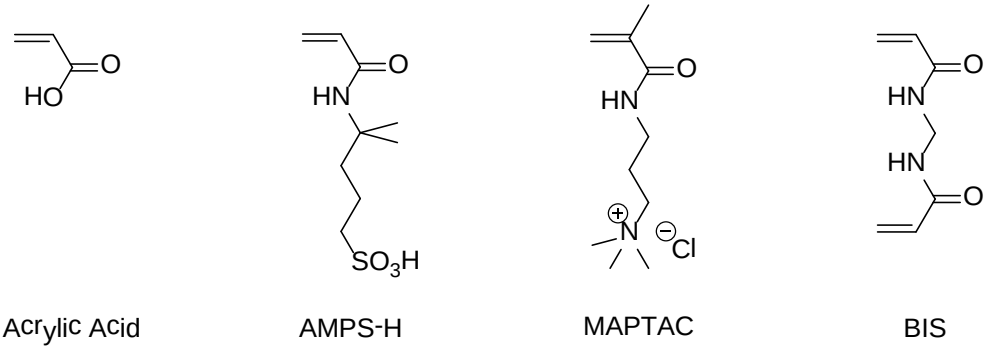

Figure 2.2. Chemical structures of acrylic acid, AMPS-H, MAPTAC and BIS

Gabaston and Armes et al. explored the chain extension of TEMPO-capped poly(SSS) with 2-vinylpyridine (2VP), 4-vinylbenzyltrimethyl ammonium chloride (VBTMACl), 4-(dimethylamino)methylstyrene (DMAMS), 4-vinylbenzyl alcohol and sodium 4-styrenecarboxylate, respectively.[22] Three of the five targeted diblock copolymers constituted polyampholytes under appropriate pHs. However, they found that the block addition of 2VP was inefficient, while VBTMACl addition resulted in insoluble products in a variety of aqueous and organic solvents. In comparison, poly(SSNa-*b*-DMAMS) was water soluble, and showed pH-responsive solubility in aqueous media.

2.4 Synthesis of Polybetaines

2.4.1 Synthesis of Polycarboxybetaines

Ladenheim and Morawetz first reported the synthesis of polycarboxybetaines in 1957.[23] They alkylated a poly(4-vinyl pyridine) precursor with an excess of ethyl bromoacetate in nitromethane, and obtained a poly(carboxybetaine) upon subsequent hydrolysis of the ester linkage. Other common synthetic strategies toward carboxybetaine

functionalities included alkylating tertiary amines with strained lactones, α,β-unsaturated acids,[24, 25] or haloalkylcarboxylates.[26, 27] Favresse and Laschewsky reported the synthesis of poly(carboxybetaine)s from diallyl-ammonium monomers.[26, 27] Representative structures of those polymers are shown in **Figure 2.3**. They varied the distance between the charges, and introduced hydrophobic fragments onto the monomers. They reported that monomers with four bulky substituents had limited polymerizability, and confirmed that the nucleophilicity of the anions, as well as their accessibility to the α-position of the cations, determined the thermal stability of the polymers.

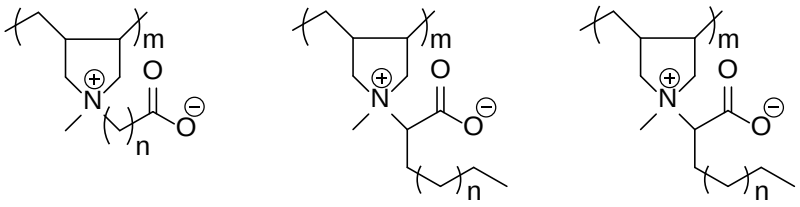

Figure 2.3 Representative chemical structures of polycarboxybetaines derived from diallylammonium monomers.[26]

Barboiu and coworkers demonstrated the reactions between pyridine and *N*-substituted imidazole compounds with α,β-unsaturated carboxylic acids, which yielded carboxybetaines.[24, 25] The authors reported that acrylic acid had significantly higher reactivity than other acids investigated, and ranked the reactivity of the four amines studied as follows: poly(*N*-vinylimidazole) ≈ 4-methyl pyridine > poly(4-vinylpyridine) > *N*-methylimidazole. **Figure 2.4** showed representative poly(carboxybetaine)s synthesized using this route.

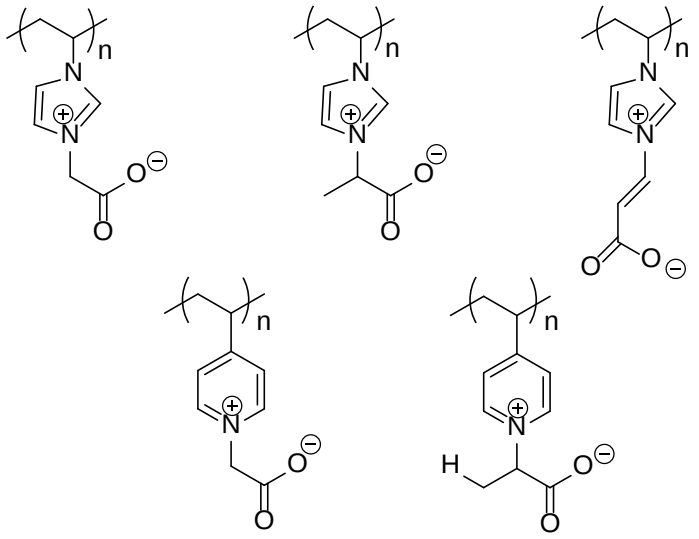

Figure 2.4 Representative structures of poly(carboxybetaines) synthesized using α,β-unsaturated carboxylic acids

In recent years, Jiang and coworkers probed the biocompatibility and antifouling characteristics of ATRP synthesized poly(carboxybetaine) homopolymers. They demonstrated for the first time that a glycine-based poly(carboxybetaine) maintained the stability of α-chmotrypsin, an enzyme, without sacrificing its bioactivity.[28] They also reported a "camptothecin"-mimic poly(carboxybetaine), which showed an acid/base-driven equilibrium (as shown in **Figure 2.5**) between an open carboxylate form (CB-OH) and a six membered lactone ring (CB-Ring).[29] The surface initiated "CB-OH" brushes exhibited ultralow fouling characteristics due to the presence of the carboxybetaine functionalities, while the "CB-Ring" showed reactivity toward nucleophiles. The authors provided experimental evidence that demonstrated the coexistence of an ultralow fouling background and its suitability for ligand immobilization for the first time.

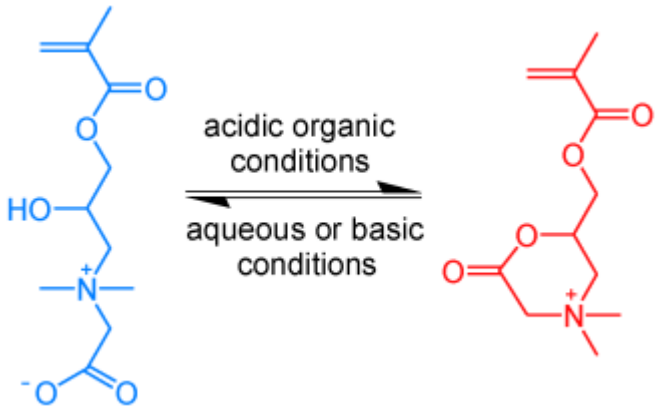

Figure 2.5 Acid/base-driven equilibrium of a "camptothecin"-mimic carboxybetaine.[30] Reprinted with permission from (*Angew. Chem. Int. Ed.* **2011**, 6102). Copyright (2011) John Wiley and Sons.

2.4.2 Synthesis of Polysulfobetaines

Roberts and Williams first demonstrated the synthesis of sulfobetaines from tertiary amines using strained sultones, such as 1,3-propanesultone and 1,4-butanesultone.[31] The process yielded salt-free monomers, or polymers, which are beneficial for the characterization of the material. Alternatively, Gauthier et al. reacted ethylenesulfonyl chloride with 2-(dimethylamino)ethyl methacrylate to obtain *N*,*N*-dimethyl-*N*-methacryloyloxyethyl-*N*-(2-sulfoethyl)ammonium betaine.[32] However, residue salts remained problematic. **Figure 2.6** listed representative sulfobetaine structures reported in the literature.

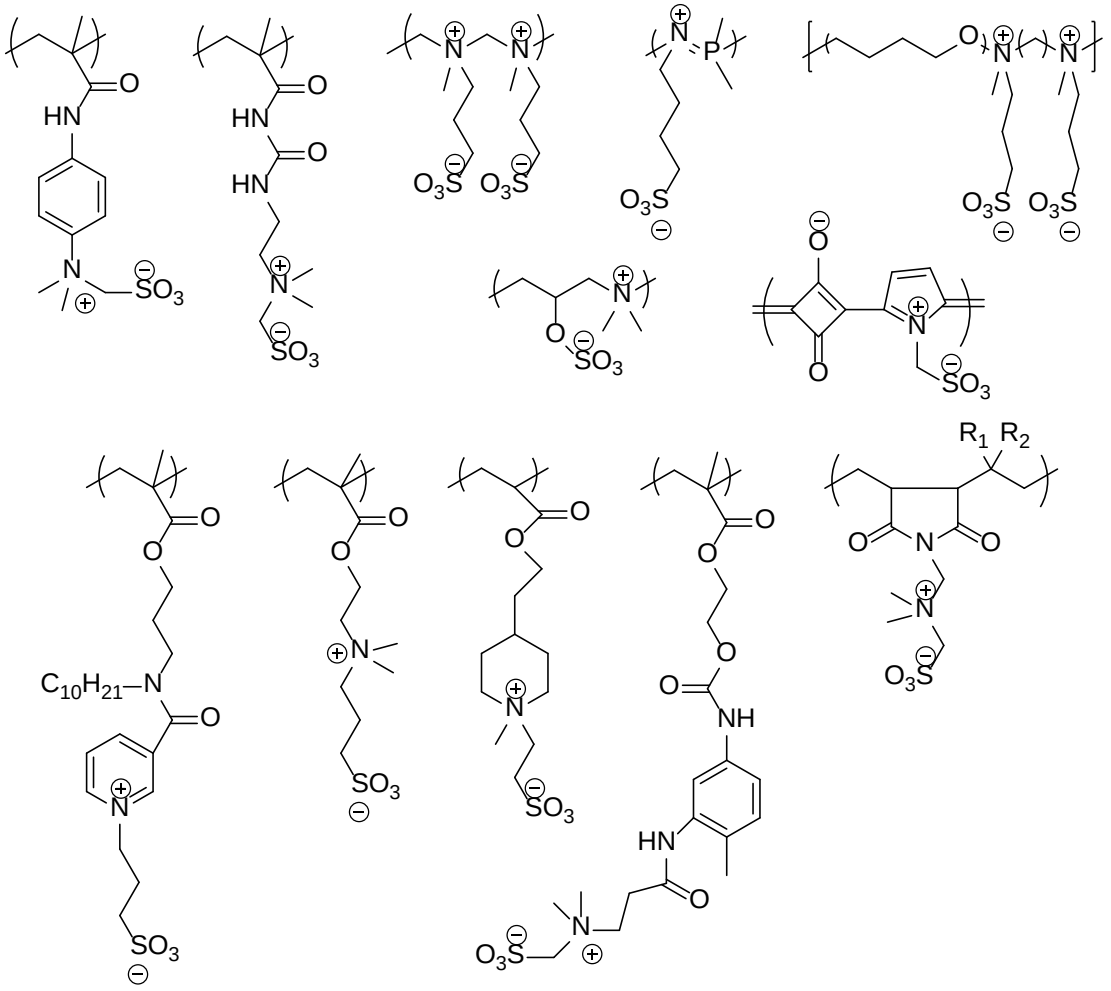

Figure 2.6 Representative polysulfobetaines reported in the literature

Lowe and Armes et al. demonstrated the functionalization of poly(2-(dimethylamino)ethyl methacrylate)s with 1,3-propanesultone to produce sulfopropylbetaine-containing homopolymers and copolymers.[33] They reported that the sulfobetaine-containing polymers formed polydisperse micelles in water, and exhibited anti-polyelectrolyte effect in aqueous NaCl solutions up to 0.1 M. Preliminary dissolution of the zwitterionic polymers in 2,2,2-trifluoroethanol resulted in near-monodisperse micelles.

Carr and Jiang demonstrated the impact of polymer backbone on the mechanical strength of zwitterionic hydrogels.[34] They compared hydrogels bearing sulfobetaine methacrylate and sulfobetaine vinylimidazole (SBVI) functionalities, and reported that the introduction of the vinylimidazole backbone improved tensile and compressive mechanical properties of the hydrogel by an order of magnitude. They also showed that surfaces coated with pSBVI exhibited exceptionally low nonspecific protein adsorption.

2.4.3 Synthesis of Polyphosphobetaines

Many phosphobetaines contain phosphorylcholine structures, which consist of quaternary ammonium cations and phosphate anions. They are synthetic analogs to phospholipids, such as the phosphatidylcholine (shown in **Figure 2.7**), in biological membranes.[35, 36] Nakaya and coworkers first reported the synthesis and polymerization of 2-bromoethoxyphenoxyphosphoryl methacrylate as a polymeric phospholipid analog in 1974.[37] They also demonstrated the synthesis and polymerization of 2-(methacryloyloxy)ethyl 2-aminoethyl hydrogen phosphate, a polymerizable phosphobetaine, in 1977.[38] Both of these works were a part of an effort to incorporate lipid structures into polymer matrixes for biomimetic membranes.[37-42] McKee et al. reported that lecithin self-assembled into worm-like micelles in aqueous solutions at high concentrations, and demonstrated the electro-spinning of such solutions into biologically based fibers and high-surface-area membranes.[43]

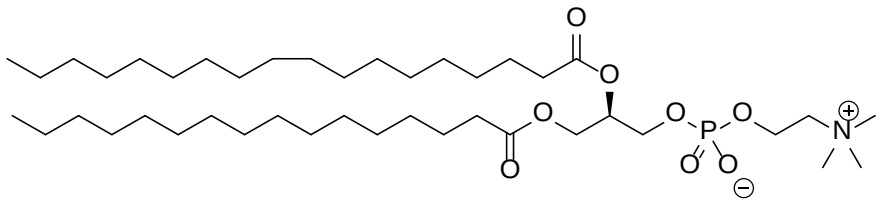

Figure 2.7. Chemical structure of phosphatidylcholine

Figure 2.8 illustrates a common synthetic approach toward polymerizable phosphobetaines.[41] The hydroxyl-terminated polymerizable motifs, such as (meth)acrylates, (meth)acrylamides and styrenes, were first reacted with 2-chloro-2-oxo-1,3,2-dioxaphospholane, and subsequently ring opened with trimethyl amine.

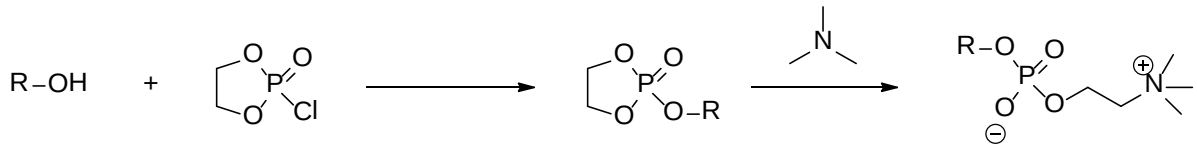

Figure 2.8 Synthesis of polymerizable phosphobetaines

2-Methacryloyloxyethyl phosphorylcholine (MPC) is a commercially available polymerizable phosphobetaine, which has been the subject of many recent publications. Chen and Jiang et al. evaluated anti-fouling characteristics of phosphorylcholine-terminated self-assembled monolayers (PC SAM).[44] They found that the PC SAMs formed from a basic assembly solution had N/P ratios closer to 1:1 than those formed from an acidic assembly solution. They attributed the better antifouling performance of the former PC SAMs to their balanced charge and minimized dipoles. **Figure 2.9** shows representative structures of polyphosphobetaines that contain the zwitterionic functionality in either the main-chain or side-chain.

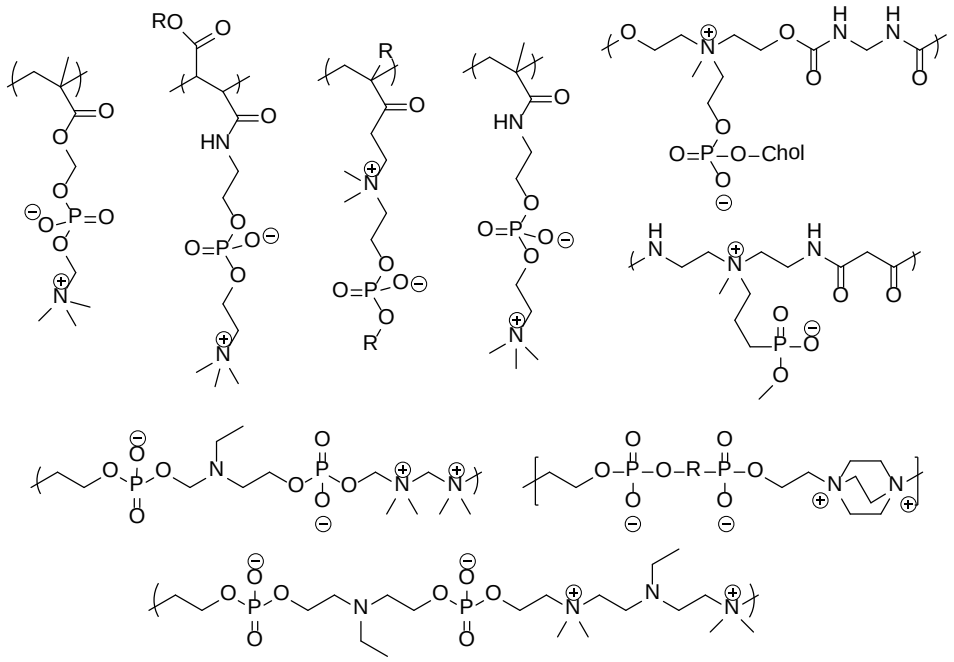

Figure 2.9 Representative polyphosphobetaines that have been published in the literature

2.5 Anti-fouling and Biomimetic Characteristics of Zwitterionic Polymers

Bio-fouling refers to the undesirable accumulation of microorganisms, plants, algae, or animals on wetted structures. In biomedical applications, the formation of a blood clot inside a blood vessel is termed thrombosis, which obstructs the flow of blood through the circulatory system.[45] In marine environment, the accumulation of bioorganisms on ships' hull increases its drag, and reduces the overall hydrodynamic performance of the vessel. For ultrafiltration membranes, the adsorption and deposition of biomacromolecules on the membrane surfaces and/or pore walls reduce permeate flux with operation time.[46] A well-known strategy for rendering surfaces anti-fouling characteristics involves the incorporation of poly(ethylene glycol) both into polymers and as surface-grafted chains.[47, 48] Grunze et al. correlated the molecular conformation of oligo(ethylene glycol) (OEG)-terminated self-assembled alkanethiolate monolayers (SAM) with the ability of these films to resist protein adsorption.[49] They found that the

predominantly crystalline helical and the amorphous forms of OEG on gold substrates are resistant to protein adsorption, while a densely packed "all trans" form of methoxy-terminated tri(ethylene glycol) present on silver surfaces adsorbed protein, in agreement with the hypothesis that the binding of interfacial water by the OEG moieties contributed significantly to their ability to resist protein adsorption. Whitesides et al. systematically screened a number of functional groups on SAMs, and reported that electrically neutral hydrophilic functionalities, such as oligo(sarcosine), *N*-acetylpiperazine and permethylated sorbitol, exhibited effective anti-fouling characteristics.[50] The authors also pointed out that all of these functionalities contained hydrogen-bond acceptors but not donors.

However, PEG autoxidizes relatively rapidly in the presence of oxygen or transition metal ions found in most biochemical environments.[51] As a result, there still is a great interest in the search for alternative nonfouling materials.[44, 45, 52] Hayward and Chapman noted that the extracellular surfaces and the cytoplasmic surfaces of plasma membranes of red blood cells exhibited drastically different protein adsorption characteristics.[53] The two surfaces differed mainly in the concentrations of the electrically neutral phospholipids. The authors attributed the thromboresistance of the extracellular membranes to its higher concentration of phosphorylcholine functionalities, and demonstrated that polymeric phospholipids had non-thrombogenic characteristics.

Lobb and Armes et al. first demonstrated controlled polymerization of poly(MPC-DEA) diblock copolymers using ATRP in methanol in 2001, but noted that MPC auto-polymerized in aqueous media within 5 min at 20 °C.[54] The chemical structure of the MPC-DEA diblock copolymer is shown in **Figure 2.10**. ^{1}H NMR results revealed that the

diblock copolymers existed as unimers in acidic aqueous solutions, but formed micelles under basic conditions. The authors reported that the diblock copolymers exhibited resistance to protein adsorption upon coating onto PET substrates as expected.

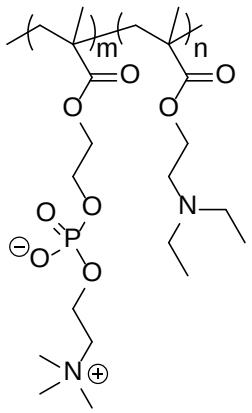

Figure 2.10 Chemical structure of the MPC-DEA diblock copolymer

Shao and Jiang et al. used molecular simulations to study the differential hydration of carboxybetaine and sulfobetaine.[52] They reported that the hydration of the cations in the two betaines was similar, and there were more coordinated water molecules around the cations than around the anions. The authors also noted that the water molecules around the anions had sharper spatial distributions, more preferential dipole orientation, and longer residence time. Chen and Jiang examined key factors that contributed to the nonfouling behaviors of zwitterionic phosphorylcholine SAMs using both experiments and simulations.[44] They concluded that zwitterions with a balanced charge and minimized dipole are excellent candidates as nonfouling materials due to their strong hydration capacity via electrostatic interactions.

Ladd and Jiang et al. probed the interaction between human serum, as well as plasma, and six different homopolymers and self-assembled monolayer surfaces [e.g. oligo(ethylene glycol) methacrylate, sulfobetaine methacrylate, carboxybetaine

methacrylate, tetra(ethylene glycol) SAM, TMA-SA and TMA-CA].[55] The repeat units of the three polymers are shown in **Figure 2.11**. They found that the pCBMA surfaces had an improved resistance to nonspecific protein adsorption over the pOEGMA and pSBMA surfaces. The authors speculated that the shorter distance between the charges on CBMA monomers resulted in a stronger hydration layer, which contributed to this improvement. They also noticed that the polymer surfaces had an increased resistance to nonspecific protein adsorption compared to SAMs, and attributed this improvement to an increase in the surface packing density of the zwitterionic functionalities, as well as a steric repulsion from the flexible polymer brushes, on the surfaces.

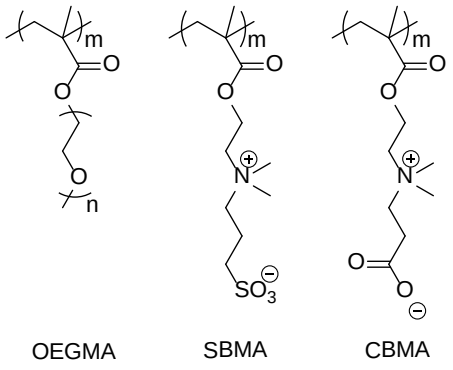

Figure 2.11 Chemical structures of the three polymers evaluated for resistance to nonspecific protein adsorption

In addition, Chen et al. further utilized the strong hydration of the phosphorylcholine-like functionalities, and demonstrated that a human-made poly(MPC) brush-coated surface had lower friction coefficients than those at natural synovial joints.[56] They reported that PMPC-brush coated surfaces had friction coefficient, μ, as low as 0.0004 at pressures as high as 7.5 MPa. While the mechanism of lubrication between articular cartilage surfaces is still not clear, the above observation should still have

relevance for boundary lubrication in human-made systems in devices, such as biomedical devices, where friction and wear are often an issue.

2.6 Solution Properties and Stimuli-Responsiveness of Zwitterionic Polymers

Lowe and McCormick recently reviewed aqueous solution properties of both polyampholytes and polybetaines.[14] They noted that the solution properties of zwitterionic polymers depended mainly on their Coulombic interactions between the cations and the anions. For polyampholytes, the solution viscosity and the coil size exhibited minima near their isoelectric points (IEP), the pH at which the polyampholytes were electrically neutral. Salt addition to polyampholyte solutions near their IEPs increased their solution viscosities and coil sizes. Such phenomena are referred to as the anti-polyelectrolyte effect. At pHs away from their IEPs, the polyampholytes showed solution properties similarly to those of polyelectrolytes.

Polybetaines also exhibited anti-polyelectrolyte effects, and lacked solubility in pure water in general. Lowe and McCormick attributed such insolubility of polybetaines to the ionic crosslinking associated with the formation of intra- and interchain ionic contacts.[14] Kathmann and McCormick et al. reported the syntheses of 2-(2-acrylamido-2-methyl-propyldimethylammonio) ethanoate (AMPDAE), 4-(2-acrylamido-2-methyl-propyldimethyl-ammonio) butanoate (AMPDAB) and 6-(2-acrylamido-2-methylpropyldimethylammonio) hexanoate (AMPDAH).[57-59] **Figure 2.12** showed the chemical structures of the carboxybetaine monomers, which had different spacer lengths between the opposite charges. The authors demonstrated the copolymerization of the carboxybetaine monomers with acrylamide in aqueous NaBr solutions, and probed the solution properties of the copolymers as a function of the pH and the ionic strength of the

solutions. They found that, as the spacer length between the opposite charges increased, the solubility of the copolymers containing higher zwitterion contents decreased. AMPDAE copolymers indeed exhibited both inter- and intra-molecular associations. Upon NaCl addition, the solutions viscosity increased due to the transition from intramolecular associations to intermolecular associations. At high pHs, salt addition dissociated intermolecular electrostatic associations and led to lower solution viscosities.

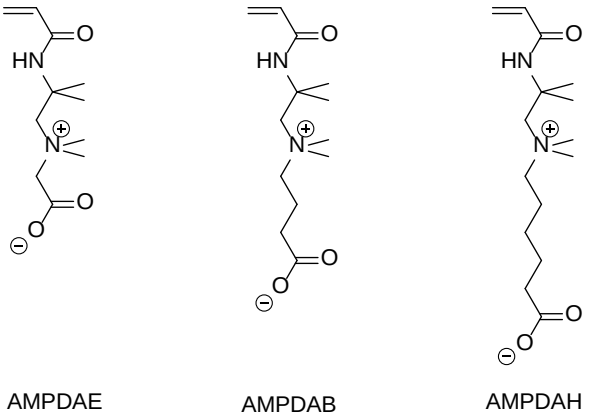

Figure 2.12. Chemical structures of AMPDAE, AMPDAB and AMPDAH

Johnson and McCormick et al. synthesized a series of terpolymers consisted of *N*-butylphenylacrylamide (BPAM), 3-(2-acrylamido-2-methylpropanedimethylammonio)-1-propanesulfonate (AMPDAPS), or 4-(2-acrylamido-2-methylpropyldimethylammonio)butanoate (AMPDAB), and acrylamide (AM) using micellar copolymerization.[60, 61] Low charge density copolymers contained 3.9-8.6 mol% betaine functionalities, while high charge density copolymers contained 17-25 mol% of the betaines. The hydrophobically modified terpolymers contained up to 1.0 mol% BPAM as the hydrophobe. **Figure 2.13** illustrates the general synthesis of the terpolymers. The authors reported that the hydrophobically modified polymers exhibited negative second virial coefficients, a common phenomenon observed for associative

polymers. Potentiomeric titration results confirmed that hydrophobic modification of carboxybetaine-containing terpolymers restricted polymer conformation in aqueous solutions and induced local dielectric effects, which led to higher pK_as for the terpolymers. Solution rheology results indicated that both pH and salt addition impacted the intra- and inter-molecular associations between the zwitterionic copolymers quite significantly.

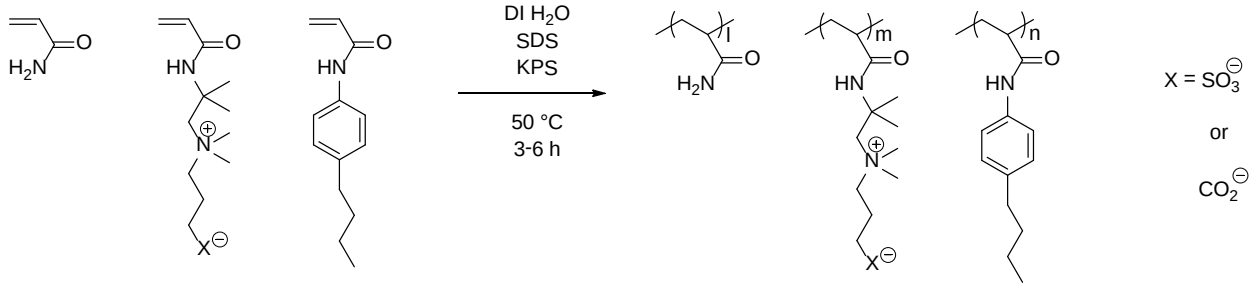

Figure 2.13 Synthesis of terpolymers containing AM, AMPDAPS (or AMPDAB) and BPAM

They also studied the interactions between low charge density hydrophobically modified polybetaines, as well as non-ionic HAM copolymer, and different types of surfactants. They found that, upon surfactant addition, changes in polymer solution viscosity were consistent with the Pathway 1 of the conceptual model shown in **Figure 2.14**.

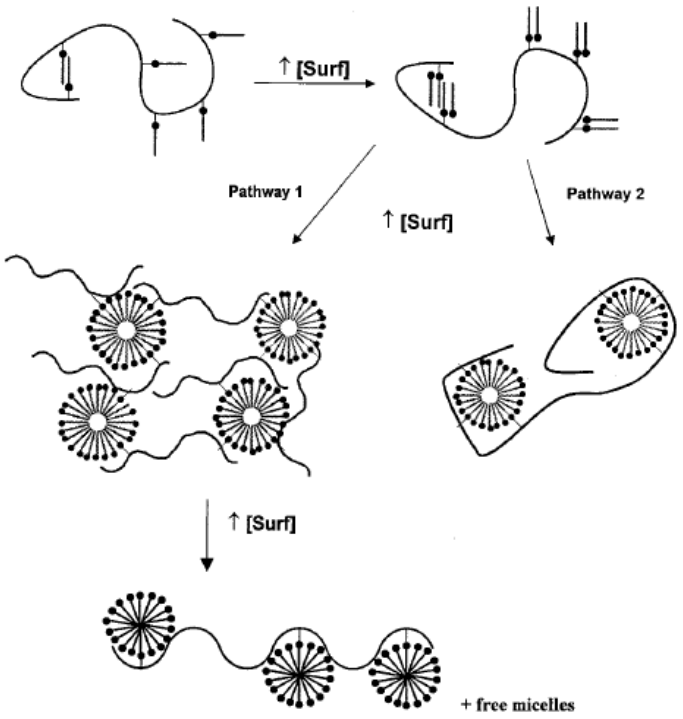

Figure 2.14. Proposed mechanism of surfactant-induced viscosity modification in hydrophobically-modified polymer solutions.[60] Reprinted with permission from (*J. Appl. Polym. Sci.* **2004**, 658). Copyright (2004) John Wiley and Sons.

Flores and McCormick et al. synthesized a triblock copolymer that consisted of a permanently hydrophilic poly(*N*,*N*-dimethylacrylamid) (PDMA) block, a salt-responsive poly(3-[2-(*N*-methyl acrylamido)ethyldimethylammonio]propanesulfate) (PMAEDAPS) center block and a pH-responsive poly(3-acrylamido-3-methyl butanoic acid) (PAMBA) block using RAFT polymerization.[62] The authors demonstrated that the well-defined ABC triblock copolymer underwent facile cross-linking and formed reversible polymeric micelles upon solution pH and ionic strength changes. **Figure 2.15** showed the chemical structure of $PDMA_{102}$-*b*-$PMAEDAPS_{64}$-*b*-$PAMBA_{69}$, and illustrated its reversible self-assembly.

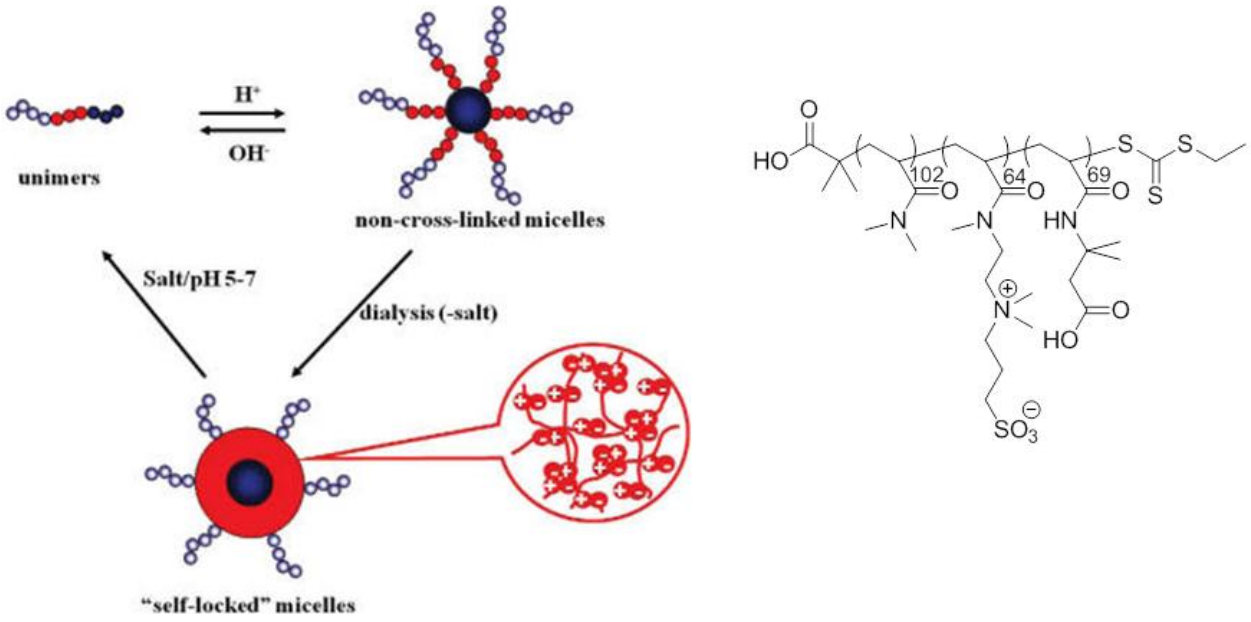

Figure 2.15 Reversible self-assembly of "self-locked" micelles of $PDMA_{102}$-*b*-$PMAEDAPS_{64}$-*b*-$PAMBA_{69}$ triblock copolymer.[62] Reprinted with permission from (*Macromolecules* **2009**, 4941). Copyright (2009) American Chemical Society.

Shen and Liu et al. studied the kinetics of vesicle formation and dissociation of $PDPA_{120}$-*b*-$PMPC_{25}$ upon pH changes using stopped-flow light scattering and laser light scattering.[63] They proposed that the formation of the polymeric vesicles followed a four-step process in ~ 400 s, during which 1) unimers first formed non-equilibrium aggregates, 2) the non-equilibrium aggregates, such as rodlike micelles, coalesced into lamellar nanostructures, which then curved into precursor vesicles, 3) the precursor vesicles rearranged to form quasi-equilibrium vesicles, 4) the quasi-equilibrium vesicles slowly coarsened toward the final stable vesicles. The authors also reported that the reversal of the polymeric vesicle formation process occurred much faster, and it was complete within ~ 5 ms.

Arotcarena and Laschewsky et al. focused their work on sulfobetaines, and demonstrated the RAFT synthesis of a diblock copolymer that consisted of a nonionic *N*-isopropylacrylamide (NIPA) block and a zwitterionic 3-[*N*-(3-methacrylamidopropyl)-*N*,*N*-dimethyl]ammonio-propane sulfonate (SPP) block in methanol.[64] The NIPA block had a lower critical solution temperature, whereas the SPP block exhibited an upper critical solution temperature. The authors reported that, through appropriate design of the block lengths, the diblock copolymers formed reversible micelles that stayed in the solution between 0 °C and 100 °C. Virtanen and Tenhu et al. studied the impact of NaCl on the solution properties of the above mentioned diblock copolymers.[65] They found that the addition of NaCl enhanced the solubility of the SPP block, but decreased the solubility of the NIPA block. The authors also noted that, at temperatures below the UCST or above the LCST, both polymer and salt concentrations impacted the formation of the aggregates and their sizes.

Thomas et al. compared aqueous solution properties of a sulfobetaine-containing copolymer and a carboxybetaine-containing copolymer of comparable structure and composition.[66] They observed macroscopic phase separation only for the sulfobetaine containing polymer, but detected the polyzwitterion to polycation transition for the carboxybetaine analog using potentiometric titration. The strong electrostatic interactions between the betaine functionalities might have contributed to their application in drag reduction and the formulation of pharmaceuticals, cosmetics and coatings as associating polymers.[67]

2.7 Self-Assembly of Zwitterionic Block Copolymers in Solutions

Block copolymers consist of two or more chemically different polymer segments, or blocks, connected by a covalent linkage.[68] Depending on the choice of the blocks, as well as the lengths of the blocks, they self-assemble into molecular-scale aggregates of nanometer sizes.[69-72] Discher and Eisenberg reviewed the self-assembly of polymer into vesicles,[73] and suggested that the amphiphilic lipids are the most useful concept to mimic and extend with block copolymers. In the case of zwitterion-containing polymers, the betaine monomers are synthetic analogs of the lipids, while diblock copolymers containing a polybetaine block and a hydrophobic block are amphiphilic polymers. Thus, it is interesting to explore the self-assembly of zwitterion-containing block for biological and microelectronic applications.

Chim and Roberts et al. evaluated poly(DMA-MPC) diblock copolymer as a potential new synthetic vector for gene delivery.[74] The MPC blocks contained 30 repeat units, and provided steric stabilization and colloidal stability to the polymer-DNA complexes, while the DMA blocks varied between 20 and 60 repeating units in lengths. Both transmission electron microscopy (TEM) and in situ atomic force microscopy (AFM) results suggested that the DNA complexes exhibited more condensed morphologies as the DMA blocks in the diblock copolymers became longer. However, the in situ AFM images indicated less condensed regions for the same highly condensed samples, which were in better agreement with DNase I degradation results. **Figure 2.16** plotted the percentage distribution of the different complex structures observed with different polymers at varying DNA concentrations using AFM. The authors concluded that copolymers with longer DMA blocks produced more condensed structures, whereas

systems with relatively longer MPC components appeared to hinder electrostatic complexation between the DNA and the copolymer.

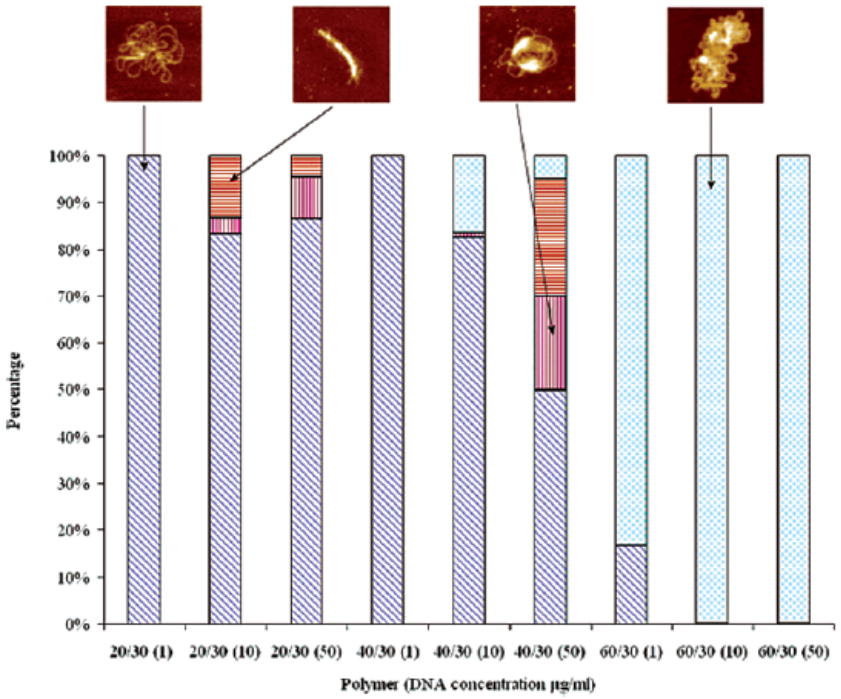

Figure 2.16 A percentage distribution chart of the different poly(DMA-MPC)/DNA complex structures observed at the same monomer in polymer to DNA ratio of 2:1, but different DNA concentrations using AFM.[74] Reprinted with permission from (*Langmuir* **2005**, 3591). Copyright (2005) American Chemical Society.

Sugihara and Armes et al. explored chain extension of a PMPC-based chain transfer agent with 2-hydroxypropyl methacrylate (HPMA), a water-soluble monomer, using RAFT.[75] Since PHPMA is a water-insoluble polymer, the authors demonstrated that the block copolymers underwent spontaneous self-assembly in water as the polymerization proceeded. They found that both PMPC/PHPMA block ratio and total solids concentration determined the final particle morphology (i.e. spheres, worm-like micelles, or vesicles) of the block copolymers in the aqueous media. **Figure 2.17** showed

a detailed phase diagram for $M_{25}H_x$-Y formulations, where 25 and x indicated MPC and HPMA block lengths, while Y indicated total solids concentration.

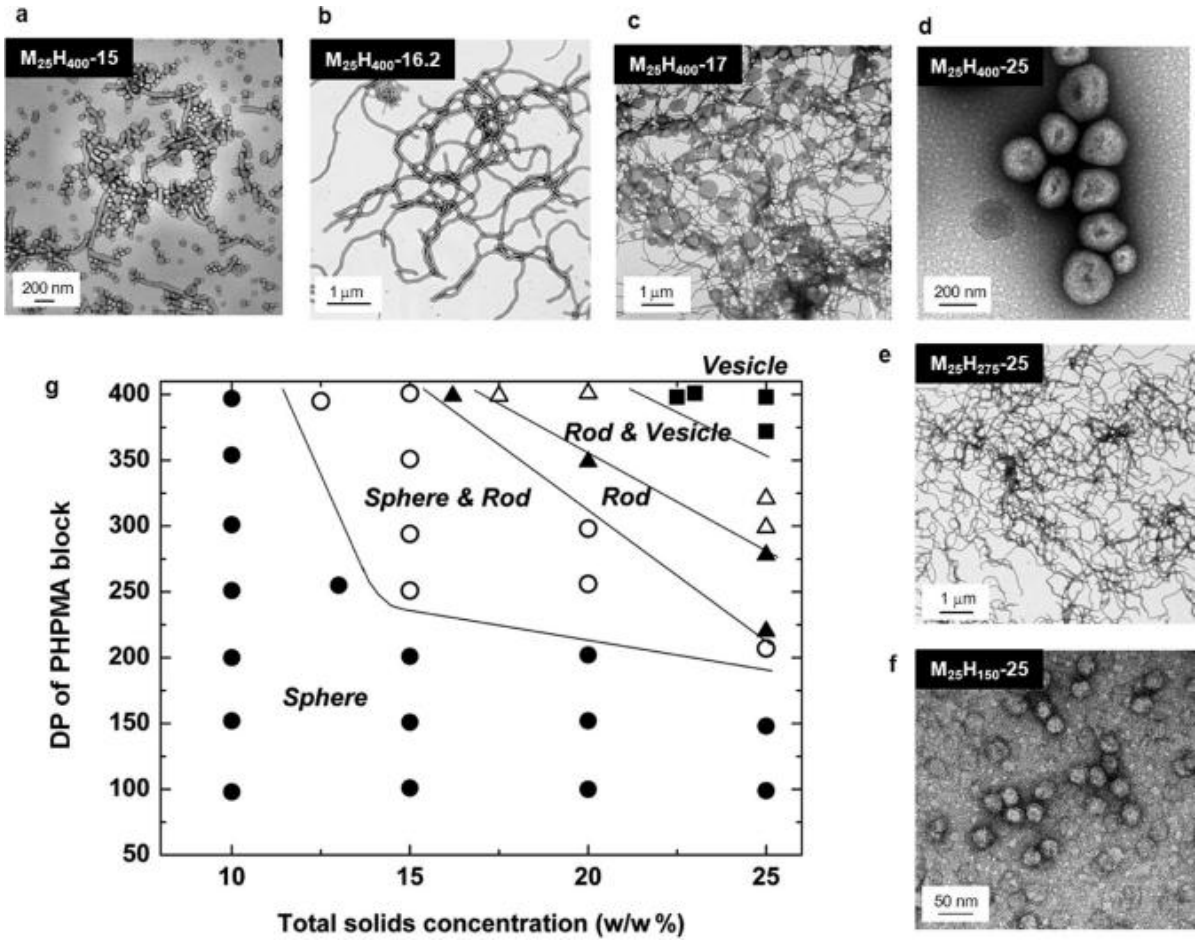

Figure 2.17 Detailed phase diagram constructed for the $M_{25}H_x$-Y formulation (where M denotes MPC and H denotes HPMA) by systematic variation of the mean target degree of polymerization of PHPMA (x) and the total solids concentration (Y) used for each synthesis.[75] Reprinted with permission from (*JACS*, **2011**, 15707). Copyright (2011) American Chemical Society.

Addison et al. reported the fabrication of hollow microcapsules from calcium carbonate cores and a cationic/zwitterionic pair of pH-responsive block copolymer micelles using the layer-by-layer technique for the first time.[76] The block copolymer

micelles consisted of cationic poly[2-(dimethylamino)-ethyl methacrylate-*b*-2-(diethylamino)ethyl methacrylate] and zwitterionic poly[2-(diethylamino)ethyl methacrylate-*b*-methacrylic acid]. The authors demonstrated the dissolution of the calcium carbonate cores with EDTA at a carefully selected pH. They confirmed using AFM, SEM and QCM that the micelle/micelle membranes maintained their structures during the process. The results suggested that such systems might have potential application in the encapsulation and triggered release of actives.

More recently, Cao and Jiang et al. reported the synthesis of a poly(lactic-*co*-glycolic acid)-poly(carboxybetaine) block copolymer through the use of a tert-butyl-protected carboxybetaine (CB-*t*Bu) monomer.[77] The chemical structures of the repeating units, as well as the reaction scheme, are shown in **Figure 2.18**. The cationic CB-*t*Bu exhibited good solubility in polar organic solvents, such as acetonitrile, which facilitated the addition of the hydrophobic PLGA block to the P(CB-*t*Bu) block. Subsequent hydrolysis of the *tert*-butyl group with TFA rendered the block copolymer amphiphilicity, which enabled the block copolymer to self-assemble into nanoparticles. The pairing between the carboxylate anions and the quaternary ammonium cations afforded the zwitterionic block copolymer resistance to non-specific protein adsorption. In addition, the carboxylate anions offered the polyzwitterions reactivity with amine-containing biomolecules. The authors evaluated the drug loading/releasing capability of the PLGA-PCB nanoparticles (NP) with docetaxel, studied their stability in biologically relevant media such as buffered saline solution of 10 wt% bovine serum albumin or 100% fetal bovine serum, and successfully demonstrated the functionalization of the NPs with amine-modified galactose ligands to target asialogly-coprotein receptors in

hepatoma cell lines in vitro. The authors concluded that the PCB-modified NPs were superior to PEGylated NPs because of their easy processing, extraordinary stability, and multifunctionality, which made them universal polymers for “theranostics”.

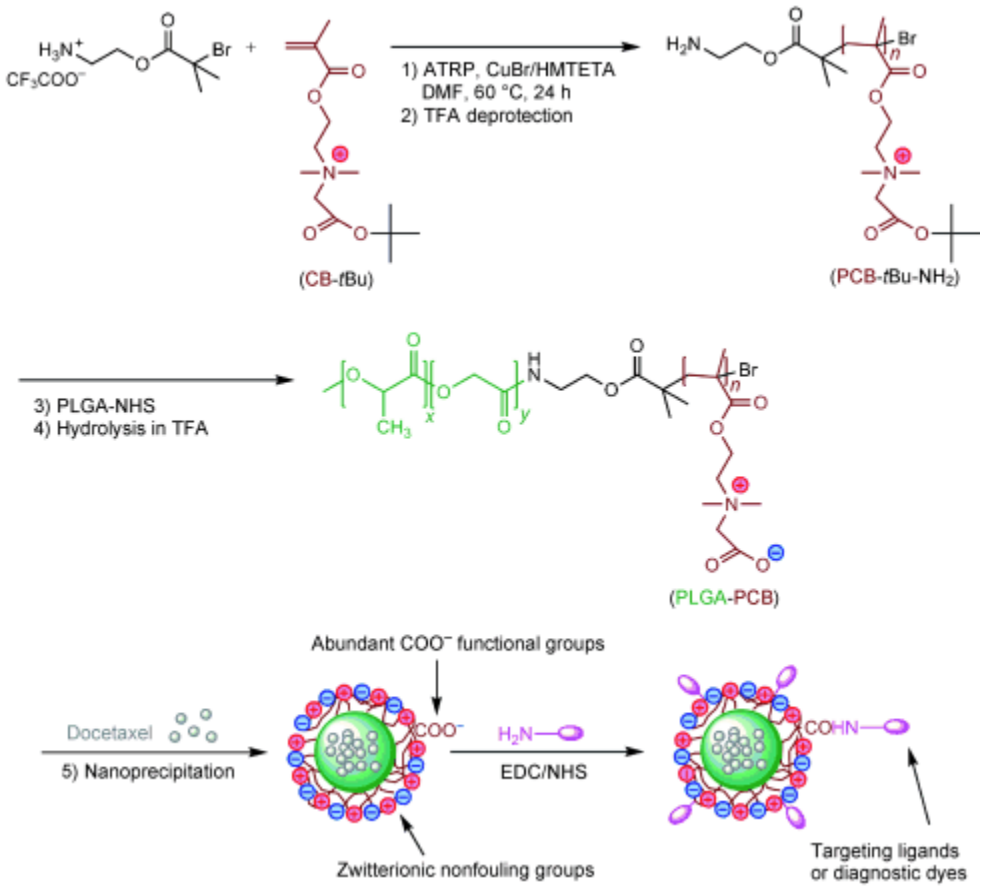

Figure 2.18 Synthesis of PLGA-PCB block copolymer, formation of PLGA-PCB/Docetaxel NPs, and functionalization of the NPs with targeting ligands or diagnostic dyes.[77] Reprinted with permission from (*Angew. Chem. Int. Ed.* **2010**, 3771). Copyright (2010) John Wiley and Sons

2.8 Solid State Properties of Zwitterionic Polymers

2.8.1 Thermomechanical Performance and Morphologies of Zwitterionononomers

The unique presence of opposite charges bridged through alkylene spacers offers betaine functionalities extremely high polarity. Typical electrical dipole moments of sulfobetaine-type zwitterions are reported as μ ~ 18.7-27.6 Debye (D) based on calculations,[78] whereas that of water is only 1.9 D. Therefore, strong electrostatic interactions are ubiquitous among zwitterions. Galin and coworkers studied extensively the solid state properties of ethyl acrylate and *n*-butyl acrylate (*n*BA) based sulfobetaine-containing copolymers.[79, 80] They found that the incorporation of zwitterionic functionalities afforded elastomeric properties, which were typical for ionomers with low T_g polymeric matrices.[79, 81-83] Detailed morphological studies revealed that zwitterionomers adopted morphologies that were in agreement with the Eisenberg-Hird-Moore multiplet-cluster model.[84]

Gauthier and coworkers synthesized a series of zwitterionomers based on *n*-butyl acrylate and 2-ethoxyethyl acrylate.[32, 85] They investigated the impact of spacer lengths between the opposite charges, as well as the bulkiness at the cationic sites, on the reactivity of the sulfobetaine methacrylates toward the acrylate monomers and the morphology, as well as the thermomechanical performances, of the resulting zwitterionic copolymers. The authors reported that the more hydrophobic sulfobetaine monomers had lower reactivity toward the acrylic monomers. They also noted that the intercharge spacing had little impact on the thermomechanical performance of the zwitterionomers, while the increase in the mechanical strengths of the zwitterionomers with increasing zwitterion contents was less pronounced for the bulky sulfobetaine methacrylates.

Porto and Borsali et al. investigated the morphologies of $PMPC_{30}$-*b*-$PDPA_{60}$ diblock copolymer films cast from various polar solvents using SAXS and (S)TEM.[86] They reported that films cast from ethanol at room temperature exhibited a thermodynamically quasi-stable cylindrical morphology, which underwent an order-order transition upon thermal annealing at 170 °C. **Figure 2.19** overlaid SAXS traces for the diblock copolymer cast from ethanol before and after thermal annealing. In comparison, films cast from methanol did not undergo similar transitions under the same experimental conditions. The authors also demonstrated that the diblock copolymer self-assembled into a lamellar morphology from aqueous solution at pH 4 at room temperature.

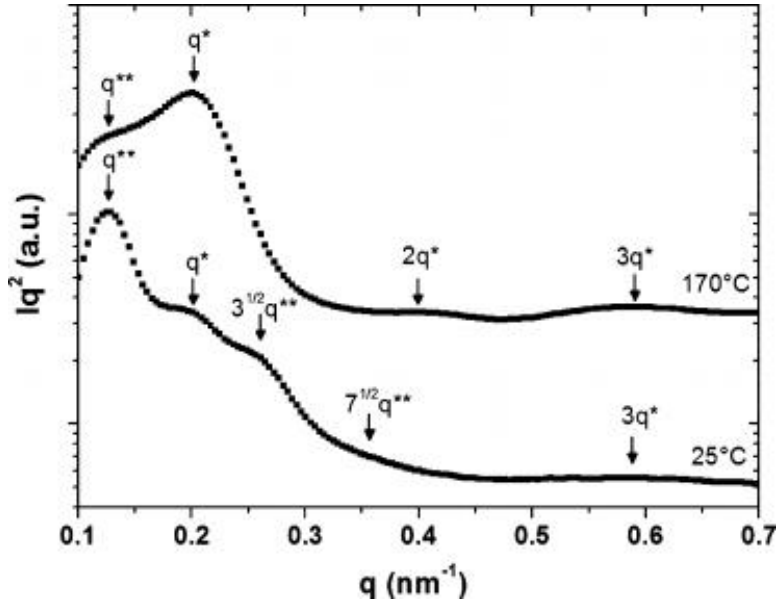

Figure 2.19 Variation of Iq^2 *vs.* q for $PMPC_{30}$-*b*-$PDPA_{60}$ films cast from 10% w/v ethanol both at room temperature and after annealing at 170 °C for 24 h, as indicated.[86] Reprinted with permission from (*Macromolecules* **2011**, 2240). Copyright (2011) American Chemical Society.

2.8.2 Zwitterion-Containing Polymers as Host Matrices for Polar Guest Molecules

The unique high dipole moments of polybetaines have afforded them potential as host matrices for polar guest molecules. Koberle and Laschewsky et al. synthesized a series of sulfobetaine-based homopolymers, and studied their compatibility with selected inorganic salts.[87, 88] They obtained homogeneous blends of the homopolymers and NaI up to stoichiometric amounts using a solution mixing method, but reported that NaCl addition led to phase-separated mixtures. NaCl addition resulted in T_g depression, while NaI addition increased the T_g of the homogeneous blends. X-ray scattering results revealed that characteristic scattering signals for the added salts were only observed for the phase-separated mixtures. The authors noted that the choices of both the anions and the cations impacted the miscibility of the salts with the zwitterionic polymers, while the selectivity of the anions agrees with the empirical "Hofmeister" lyotropic series, where homogeneous mixing is favored by "chaotropic" anions.[89] They concluded that the nature of the inorganic salts dominated miscibility, and tail-end type, ammoniopropnesulfonate-containing polyacrylamides were best suited for homogeneous blends.

They also introduced transition metal salts into a sulfobetaine copolymer, where one of the comomoner contained a zwitterionic chromophore. The chemical structure of the copolymer is shown in **Figure 2.20**. They reported halochromic effect for the polysulfobetaine upon salt incorporation, and conducted magnetic measurements on those blends. The results suggested that, depending on the choice the anion and the cation, homogeneous blends were obtained.[90]

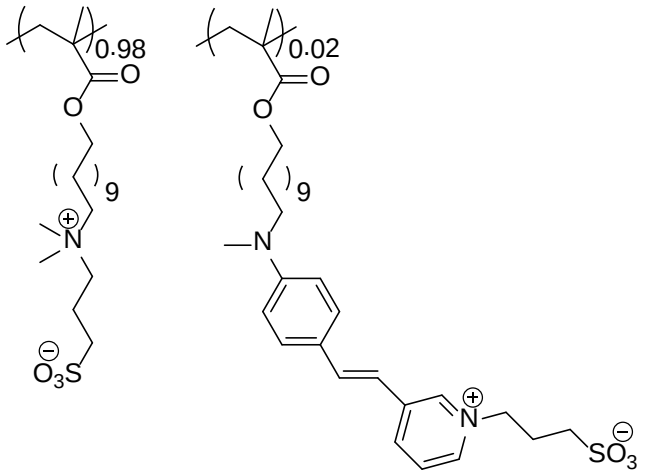

Figure 2.20 Chemical structure of a chromophore-containing polysulfobetaine[90]

Galin and coworkers have also demonstrated that these salt-polyzwitterion mixtures formed amorphous blends due to strong ion-dipole interactions that precluded salt segregation or crystallization within the zwitterionic matrix.[91, 92] This unique ability to dissolve large amounts of salts has sparked interest in polyzwitterions as polymeric host matrices for many polar guest molecules.

More recently, Strehmel and Laschewsky et al. conducted free radical polymerization of *n*-butyl methacrylate in a number of imidazolium, pyridinium and alkylammonium ionic liquids.[93] They found that the solvents had little influence on polymer tacticity, but impacted the degrees of polymerization quite significantly. More recently, they explored the copolymerization of *n*BMA and 3-[*N*-2-(methacryloyloxyethyl)-*N*,*N*-dimethyl-3-ammonio]propane sulfonate, a zwitterionic monomer.[94] They reported that the ionic liquids enabled copolymerization of monomers with highly different polarities, which were not accessible in common organic solvents. They also noted that the chemical compositions of the resulting copolymers depended on both the feed ratio of the monomers and the choice of the ionic liquid.

2.9 Conclusions

Polyzwitterions are unique charge-containing polymers that bear both covalently bound cations and anions. Earlier research efforts on polyzwitterions focused mainly on their responsiveness to salt addition and pH changes in aqueous solutions and on the thermoplastic performance of zwitterionomers. In this review, we identified structural characteristics of charge-containing polymers that contributed to their commercial applications as thermoplastic elastomers, proton-exchange membranes and nucleic acid delivering agents, and overviewed synthetic strategies toward polybetaines and betaine-containing block copolymers for similar emerging applications. Current literature results suggested that polybetaine and betaine-containing block copolymers had great potential as antifouling materials in biomedical applications. The strong association tendency of the betaine functionalities afforded polybetaines drag-reducing capabilities, and also encouraged their self-assembly in aqueous media. In addition, the high electrical dipole moments of the betaine functionalities afforded polybetaines high affinity toward polar guest molecules, such as ionic liquids, as the matrices for electromechanical transducers.

2.10 Reference

1. Broussard, J. P. *Mod. Packag.* **1967,** 40, (10), 173-5.
2. Broussard, J. P. *Mod. Packag.* **1967,** 40, (9), 157-61.
3. Kinsey, R. H. *Appl. Polym. Symp.* **1969,** 11, 77-94.
4. Mauritz, K. A.; Moore, R. B. *Chemical Reviews* **2004,** 104, (10), 4535-4586.
5. Shahinpoor, M. *Electrochimica Acta* **2003,** 48, (14–16), 2343-2353.
6. Mauritz, K. A.; Hopfinger, A. J. *Mod. Aspects Electrochem.* **1982,** 14, 425-508.
7. Schmidt-Rohr, K.; Chen, Q. *Nat Mater* **2008,** 7, (1), 75-83.
8. Otocka, E. P. *J. Macromol. Sci., Rev. Macromol. Chem.* **1971,** 5, (2), 275-94.
9. Rembaum, A. *Appl. Polym. Symp.* **1973,** No. 22, 299-317.
10. Davis, M. E. *Current Opinion in Biotechnology* **2002,** 13, (2), 128-131.
11. Merdan, T.; Kopecek, J.; Kissel, T. *Adv. Drug Delivery Rev.* **2002,** 54, (5), 715-758.
12. Neu, M.; Fischer, D.; Kissel, T. *J. Gene Med.* **2005,** 7, (8), 992-1009.

13. Gary, D. J.; Puri, N.; Won, Y.-Y. *Journal of Controlled Release* **2007,** 121, (1-2), 64-73.
14. Lowe, A. B.; McCormick, C. L. *Chem. Rev.* **2002,** 102, (11), 4177-4190.
15. Kudaibergenov, S.; Jaeger, W.; Laschewsky, A., Polymeric betaines: Synthesis, characterization, and application. In *Supramolecular Polymers Polymeric Betains Oligomers*, 2006; Vol. 201, pp 157-224.
16. Peiffer, D. G.; Lundberg, R. D. *Polymer* **1985,** 26, (7), 1058-1068.
17. Baker, J. P.; Stephens, D. R.; Blanch, H. W.; Prausnitz, J. M. *Macromolecules* **1992,** 25, (7), 1955-1958.
18. English, A. E.; Mafe, S.; Manzanares, J. A.; Yu, X. H.; Grosberg, A. Y.; Tanaka, T. *Journal of Chemical Physics* **1996,** 104, (21), 8713-8720.
19. English, A. E.; Tanaka, T.; Edelman, E. R. *Polymer* **1998,** 39, (24), 5893-5897.
20. English, A. E.; Tanaka, T.; Edelman, E. R. *Macromolecules* **1998,** 31, (6), 1989-1995.
21. Mafé, S.; Manzanares, J. A.; English, A. E.; Tanaka, T. *Physical Review Letters* **1997,** 79, (16), 3086-3089.
22. Gabaston, L. I.; Furlong, S. A.; Jackson, R. A.; Armes, S. P. *Polymer* **1999,** 40, (16), 4505-4514.
23. Harry Ladenheim, H. M. *Journal of Polymer Science* **1957,** 26, (113), 251-254.
24. Barboiu, V.; Streba, E.; Luca, C.; Radu, I.; Grigoriu, G. E. *Journal of Polymer Science Part A: Polymer Chemistry* **1998,** 36, (10), 1615-1623.
25. Barboiu, V.; Holerca, M. N.; Streba, E.; Luca, C. *Journal of Polymer Science Part A: Polymer Chemistry* **1996,** 34, (2), 261-270.
26. Favresse, P.; Laschewsky, A. *Polymer* **2001,** 42, (7), 2755-2766.
27. Philippe Favresse, A. L. *Macromolecular Chemistry and Physics* **1999,** 200, (4), 887-895.
28. Keefe, A. J.; Jiang, S. *Nat. Chem.* **2012,** 4, (1), 59-63.
29. Cao, Z.; Brault, N.; Xue, H.; Keefe, A.; Jiang, S. *Angew. Chem., Int. Ed.* **2011,** 50, (27), 6102-6104, S6102/1-S6102/9.
30. Cao, Z.; Brault, N.; Xue, H.; Keefe, A.; Jiang, S. *Angewandte Chemie International Edition* **2011,** 50, (27), 6102-6104.
31. Roberts, D. W.; Williams, D. L. *Tetrahedron* **1987,** 43, (6), 1027-1062.
32. Gauthier, M.; Carrozzella, T.; Penlidis, A. *Journal of Polymer Science Part a-Polymer Chemistry* **2002,** 40, (4), 511-523.
33. Lowe, A. B.; Billingham, N. C.; Armes, S. P. *Macromolecules* **1999,** 32, (7), 2141-2148.
34. Carr, L.; Cheng, G.; Xue, H.; Jiang, S. *Langmuir* **2010,** 26, (18), 14793-14798.
35. Keith, A. D.; Waggoner, A. S.; Griffith, O. H. *Proceedings of the National Academy of Sciences* **1968,** 61, (3), 819-826.
36. McConnell, H. M.; Hubbell, W. L. *Journal of the American Chemical Society* **1971,** 93, (2), 314-326.
37. Doiuchi, T.; Nakaya, T.; Imoto, M. *Makromolekulare Chemie* **1974,** 175, (1), 43-8.
38. Nakai, S.; Nakaya, T.; Imoto, M. *Makromolekulare Chemie* **1977,** 178, (10), 2963-7.
39. Nakaya, T.; Li, Y.-J. *Progress in Polymer Science* **1999,** 24, (1), 143-181.

40. Sugiyama, K.; Nakaya, T. *Makromolekulare Chemie, Rapid Communications* **1986,** 7, (10), 679-85.
41. Umeda, T.; Nakaya, T.; Imoto, M. *Makromolekulare Chemie, Rapid Communications* **1985,** 6, (4), 285-90.
42. Yamada, M.; Li, Y.; Nakaya, T. *Journal of Macromolecular Science, Pure and Applied Chemistry* **1995,** A32, (10), 1723-33.
43. McKee, M. G.; Layman, J. M.; Cashion, M. P.; Long, T. E. *Science* **2006,** 311, (5759), 353-355.
44. Chen, S.; Zheng, J.; Li, L.; Jiang, S. *Journal of the American Chemical Society* **2005,** 127, (41), 14473-14478.
45. Zhang, Z.; Chao, T.; Chen, S.; Jiang, S. *Langmuir* **2006,** 22, (24), 10072-10077.
46. Shi, Q.; Su, Y.; Zhao, W.; Li, C.; Hu, Y.; Jiang, Z.; Zhu, S. *Journal of Membrane Science* **2008,** 319, (1-2), 271-278.
47. Bailey, F. E., Jr.; Koleske, J. Y., *Poly(Ethylene Oxide)*. Academic Press: New York, 1976.
48. *Poly(ethyleneglycol) chemistry: biotechnical and biomedical applications*. Plenum Press: New York, 1992.
49. Harder, P.; Grunze, M.; Dahint, R.; Whitesides, G. M.; Laibinis, P. E. *The Journal of Physical Chemistry B* **1998,** 102, (2), 426-436.
50. Ostuni, E.; Chapman, R. G.; Holmlin, R. E.; Takayama, S.; Whitesides, G. M. *Langmuir* **2001,** 17, (18), 5605-5620.
51. Gaberc-Porekar, V.; Zore, I.; Podobnik, B.; Menart, V. *Current Opinion in Drug Discovery & Development* **2008,** 11, (2), 242-250.
52. Shao, Q.; He, Y.; White, A. D.; Jiang, S. *The Journal of Physical Chemistry B* **2010,** 114, (49), 16625-16631.
53. Hayward, J. A.; Chapman, D. *Biomaterials* **1984,** 5, (3), 135-142.
54. Lobb, E. J.; Ma, I.; Billingham, N. C.; Armes, S. P.; Lewis, A. L. *J. Am. Chem. Soc.* **2001,** 123, (32), 7913-7914.
55. Ladd, J.; Zhang, Z.; Chen, S.; Hower, J. C.; Jiang, S. *Biomacromolecules* **2008,** 9, (5), 1357-1361.
56. Chen, M.; Briscoe, W. H.; Armes, S. P.; Klein, J. *Science (Washington, DC, U. S.)* **2009,** 323, (5922), 1698-1701.
57. Kathmann, E. E.; McCormick, C. L. *Journal of Polymer Science Part A: Polymer Chemistry* **1997,** 35, (2), 243-253.
58. Kathmann, E. E.; White, L. A.; McCormick, C. L. *Polymer* **1997,** 38, (4), 871-878.
59. Kathmann, E. E.; White, L. A.; McCormick, C. L. *Polymer* **1997,** 38, (4), 879-886.
60. Johnson, K. M.; Fevola, M. J.; Lochhead, R. Y.; McCormick, C. L. *J. Appl. Polym. Sci.* **2004,** 92, (1), 658-671.
61. Johnson, K. M.; Fevola, M. J.; McCormick, C. L. *J. Appl. Polym. Sci.* **2004,** 92, (1), 647-657.
62. Flores, J. D.; Xu, X.; Treat, N. J.; McCormick, C. L. *Macromolecules (Washington, DC, U. S.)* **2009,** 42, (14), 4941-4945.
63. Shen, L.; Du, J.; Armes, S. P.; Liu, S. *Langmuir* **2008,** 24, (18), 10019-10025.

64. Arotcarena, M.; Heise, B.; Ishaya, S.; Laschewsky, A. *Journal of the American Chemical Society* **2002,** 124, (14), 3787-3793.
65. Virtanen, J.; Arotcarena, M.; Heise, B.; Ishaya, S.; Laschewsky, A.; Tenhu, H. *Langmuir* **2002,** 18, (14), 5360-5365.
66. Thomas David, B.; Armentrout, R. S.; McCormick Charles, L., Synthesis and Aqueous Solution Behavior of Novel pH Responsive, Zwitterionic Cyclocopolymers. In *Stimuli-Responsive Water Soluble and Amphiphilic Polymers*, American Chemical Society: 2000; Vol. 780, pp 101-114.
67. Schulz Donald, N.; Kitano, K.; Duvdevani, I.; Kowalik, R. M.; Eckert, J. A., Hydrocarbon-Soluble Associating Polymers as Antimisting and Drag-Reducing Agents. In *Polymers as Rheology Modifiers*, American Chemical Society: 1991; Vol. 462, pp 176-189.
68. Bates, F. S.; Fredrickson, G. H. *Annual Review of Physical Chemistry* **1990,** 41, (1), 525-557.
69. Cui, H.; Chen, Z.; Zhong, S.; Wooley, K. L.; Pochan, D. J. *Science (Washington, DC, U. S.)* **2007,** 317, (5838), 647-650.
70. Jain, S.; Bates, F. S. *Science (Washington, DC, U. S.)* **2003,** 300, (5618), 460-464.
71. Park, M.; Harrison, C.; Chaikin, P. M.; Register, R. A.; Adamson, D. H. *Science (Washington, D. C.)* **1997,** 276, (5317), 1401-1404.
72. Thurn-Albrecht, T.; Schotter, J.; Kastle, G. A.; Emley, N.; Shibauchi, T.; Krusin-Elbaum, L.; Guarini, K.; Black, C. T.; Tuominen, M. T.; Russell, T. P. *Science (Washington, D. C.)* **2000,** 290, (5499), 2126-2129.
73. Discher, D. E.; Eisenberg, A. *Science (Washington, DC, U. S.)* **2002,** 297, (5583), 967-973.
74. Chim, Y. T. A.; Lam, J. K. W.; Ma, Y.; Armes, S. P.; Lewis, A. L.; Roberts, C. J.; Stolnik, S.; Tendler, S. J. B.; Davies, M. C. *Langmuir* **2005,** 21, (8), 3591-3598.
75. Sugihara, S.; Blanazs, A.; Armes, S. P.; Ryan, A. J.; Lewis, A. L. *J. Am. Chem. Soc.* **2011,** 133, (39), 15707-15713.
76. Addison, T.; Cayre, O. J.; Biggs, S.; Armes, S. P.; York, D. *Langmuir* **2010,** 26, (9), 6281-6286.
77. Cao, Z.; Yu, Q.; Xue, H.; Cheng, G.; Jiang, S. *Angewandte Chemie International Edition* **2010,** 49, (22), 3771-3776.
78. Galin, M.; Chapoton, A.; Galin, J. C. *J. Chem. Soc. Perkin Trans.* **1993,** 2, 545.
79. Ehrmann, M.; Muller, R.; Galin, J. C.; Bazuin, C. G. *Macromolecules* **1993,** 26, (18), 4910-4918.
80. Mathis, A.; Zheng, Y. L.; Galin, J. C. *Polymer* **1991,** 32, (17), 3080-3085.
81. Ehrmann, M.; Galin, J. C. *Polymer* **1992,** 33, (4), 859-865.
82. Ehrmann, M.; Galin, J. C.; Meurer, B. *Macromolecules* **1993,** 26, (5), 988-993.
83. Ehrmann, M.; Mathis, A.; Meurer, B.; Scheer, M.; Galin, J. C. *Macromolecules* **1992,** 25, (8), 2253-2261.
84. Eisenberg, A.; Hird, B.; Moore, R. B. *Macromolecules* **1990,** 23, (18), 4098-4107.
85. Gauthier, M.; Carrozzella, T.; Snell, G. *Journal of Polymer Science Part B-Polymer Physics* **2002,** 40, (19), 2303-2312.
86. Porto, L. C.; Aissou, K.; Giacomelli, C.; Baron, T.; Rochas, C.; Pignot-Paintrand, I.; Armes, S. P.; Lewis, A. L.; Soldi, V.; Borsali, R. *Macromolecules* **2011,** 44, (7), 2240-2244.

87. Koberle, P.; Laschewsky, A. *Macromolecules* **1994,** 27, (8), 2165-2173.
88. Koeberle, P.; Laschewsky, A.; Lomax, T. D. *Makromol. Chem., Rapid Commun.* **1991,** 12, (7), 427-33.
89. CACACE, M. G.; LANDAU, E. M.; RAMSDEN, J. J. *Quarterly Reviews of Biophysics* **1997,** 30, (03), 241-277.
90. Koeberle, P.; Laschewsky, A. *Macromol. Symp.* **1994,** 88, (Frontiers in Polymerization), 165-75.
91. Galin, M.; Marchal, E.; Mathis, A.; Galin, J. C. *Polymers for Advanced Technologies* **1997,** 8, 75-86.
92. Galin, M.; Marchal, E.; Mathis, A.; Meurer, B.; Soto, Y. M. M.; Galin, J. C. *Polymer* **1987,** 28, (11), 1937-1944.
93. Strehmel, V.; Laschewsky, A.; Wetzel, H.; Görnitz, E. *Macromolecules* **2006,** 39, (3), 923-930.
94. Strehmel, V.; Wetzel, H.; Laschewsky, A.; Moldenhauer, E.; Klein, T. *Polymers for Advanced Technologies* **2008,** 19, (10), 1383-1390.

Chapter 3 Influence of Zwitterions on Thermomechanical Properties and Morphology of Acrylic Copolymers: Implications for Electro-Active Applications

(*Tianyu Wu,*[†] *Frederick L. Beyer,*[‡,*] *Rebecca H. Brown,*[†] *Robert B. Moore,*[†] *and Timothy E. Long*[†,*])

[†]*Department of Chemistry, Macromolecules and Interfaces Institute, Virginia Tech, Blacksburg, Virginia 24061-0212;* [‡]*Army Research Laboratory, Aberdeen Proving Ground, Maryland 21005-5069*

*Corresponding authors: rick.beyer@us.army.mil and telong@vt.edu

Reprinted with permission from (*Macromolecules* **2011**, 8056). Copyright (2011) American Chemical Society.

3.1 Abstract

n-Butyl acrylate based zwitterionomers and ionomers containing 3-[[2-(methacryloyl-oxy)ethyl](dimethyl)ammonio]-1-propanesulfonate (SBMA) and 2-[butyl(dimethyl)amino]ethyl methacrylate methanesulfonate (BDMAEMA MS), respectively, were synthesized using conventional free radical polymerization. Size-exclusion chromatography confirmed the molecular weights of the copolymers exceeded the critical molecular weight between entanglements (M_e) for poly(*n*-butyl acrylate). Differential scanning calorimetry (DSC), small-angle X-ray scattering (SAXS), and atomic force microscopy (AFM) revealed that zwitterionomers promoted more well-defined microphase-separation than cationic analogs. Dynamic mechanical analyses (DMA) of the copolymers showed a rubbery plateau region due to physical crosslinks

between charges for zwitterionomers only. Since SBMA and BDMAEMA MS have very similar chemical structures, we attributed improved microphase-separation and superior elastomeric performance of the zwitterionomers to stronger association between covalently tethered charged pairs.

Key Words: zwitterion, elastomer, morphology, ionic association, X-ray scattering

3.2 Introduction

Charge-containing polymers have attracted considerable scientific attention over the past 20 years.[1-3] They offer tremendous impact in emerging technologies ranging from energy[4] and water purification[5] to biotechnology.[6] A unique combination of physical properties of ionomeric membranes is the ionic conductivity of low molar mass electrolytes and viscoelastic response of polymers in the solid state. For example, our research group demonstrated the fabrication of ionic polymer transducers from branched sulfonated polysulfones.[7] The mechanical strength of the membranes drastically decreased upon introduction of ionic liquids to impart ionic conductivity. For electro-active applications, it is desirable for ionomeric membranes to maintain mechanical strength despite the presence of plasticizing conductive electrolytes. Recently, we investigated the versatility of zwitterion-containing acrylic copolymers to absorb ionic liquids,[8] and zwitterionomers maintained mechanical strengths upon swelling with 10 wt% ionic liquid.

Zwitterions are charged molecules that contain equal numbers of covalently bound cations and anions. The unique presence of opposite charges bridged through alkylene spacers offers zwitterions extremely high polarity. Typical dipole moments of sulfobetaine-type zwitterions are reported as $\mu \sim 18.7\text{-}27.6$ Debye (D) based on

calculations,[9] whereas water is only 1.9 D. Therefore, strong electrostatic interactions are ubiquitous among zwitterions. Galin and coworkers studied extensively the solid state properties of ethyl acrylate and *n*-butyl acrylate (*n*BA) based sulfobetaine-containing copolymers.[10, 11] They found that the incorporation of zwitterionic functionalities afforded elastomeric properties, which were typical for ionomers with low T_g polymeric matrices.[10, 12-14] Detailed morphological studies revealed that zwitterionomers adopted morphologies that were in agreement with the Eisenberg-Hird-Moore multiplet-cluster model.[15] In addition, Laschewsky et al. have shown that polymeric betaines have remarkable miscibility with various inorganic and metal salts approaching stoichiometric quantities.[16] Galin and coworkers have also demonstrated that these salt-polyzwitterion mixtures formed amorphous blends due to strong ion-dipole interactions that precluded salt segregation or crystallization within the zwitterionic matrix.[17, 18] This unique ability to dissolve large amounts of salts has sparked interest in polyzwitterions as polymeric host matrices for many polar guest molecules.

While zwitterionic polymers have exhibited many unique physical properties, their difference from cationic or anionic polymers is not well-established. Lee and coworkers investigated the difference in solution properties between poly(sulfobetaine)s homopolymers and their corresponding cationic polymers.[19-21] However, the cationic models contained iodide anions rather than monovalent sulfonate anions, which are present in sulfobetaines. Our work describes 2-(*n*-butyldimethylamino)ethyl 2-methacrylate methanesulfonate (BDMAEMA MS), as shown in **Figure 3.1**, along with 3-[[2-(methacryloyloxy)ethyl](dimethyl)ammonio]-1-propanesulfonate (SBMA), a zwitterionic monomer. Copolymerization of both charge-containing monomers with *n*BA

elucidates the influence of tethered counterions on the solid-state properties and morphology of zwitterionomers. Thermogravimetric analysis (TGA), differential scanning calorimetry (DSC) and dynamic mechanical analysis (DMA) probed thermal stability, glass transition temperatures, and thermomechanical behavior of the copolymers respectively. Small-angle X-ray scattering (SAXS) and atomic force microscopy (AFM) imaging results showed the morphological differences between the two copolymer series. A correlation between the elastomeric performance of the copolymers and their morphologies revealed the impact of zwitterionic interactions and ammonium ionic interactions with mobile counteranions. Fundamental understanding of structure-morphology relationships will guide the design of future charge-containing polymers for advanced transducer applications.

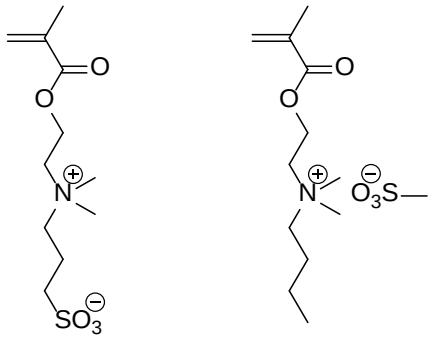

Figure 3.1 SBMA and BDMAEMA MS monomers

3.3 Experimental

Materials. Zwitterionic monomer, 3-[[2-(methacryloyloxy)ethyl](dimethyl)ammonio]-1-propanesulfonate (SBMA), was generously provided by Raschig GmbH. *n*-Butyl acrylate (*n*BA, Alfa Aesar, 98+%) and 2-(dimethylamino)ethyl methacrylate (DMAEMA, Aldrich, 98%) were deinhibited using neutral alumina columns. *n*BA was further distilled under reduced pressure from calcium hydride. Azobisisobutyronitrile (AIBN, Aldrich, 98%) was recrystallized from methanol. Dimethyl sulfoxide (DMSO, Alfa Aesar, 99.9+%), hydroquinone (Alfa Aesar, 99%), 1-bromobutane (Aldrich, 98%), silver methanesulfonate (AgMS, Aldrich), diethyl ether (Mallinckrodt, anhydrous) were used as received. Ultrapure water having a resistivity of 18.2MΩ·cm was obtained using a Millipore Direct-Q5 purification system.

Synthesis of 2-(*N*-butyl-*N*,*N*-dimethylamino)ethyl methacrylate methanesulfonate (BDMAEMA MS). DMAEMA (30.0 g, 0.191 mol), 1-bromobutane (52.3 g, 0.388 mol), methylene chloride (40 mL, 35 vol%) and hydroquinone (6.0 g) were added to a 250-mL, round-bottomed flask with a magnetic stir bar. The reaction mixture was sparged with N_2 for 15 min and placed into an oil bath at 50 °C for 72 h. The product, 2-(*N*-butyl-*N*,*N*-dimethylamino)ethyl methacrylate bromide (BDMAEMA Br), was precipitated into and washed with dry ether, recrystallized from acetone and dried under reduced pressure (0.5 mmHg) at room temperature. A yield of 70% was obtained. Anion exchange of BDMAEMA Br was then conducted at room temperature. AgMS (1.00 g, 4.92 mmol) and BDMAEMA Br (1.45 g, 4.93 mmol) were dissolved in 15 mL and 5 mL Milli-Q water respectively in 20-mL scintillation vials. After full dissolution, the AgMS solution was transferred to a 120-mL amber container and the BDMAEMA Br

solution was subsequently added in the absence of light. Both vials were thoroughly rinsed with Milli-Q water after solution transfer. The reaction was allowed to equilibrate in the dark overnight, although the precipitation of AgBr was instantaneous. The BDMAEMA MS solution was finally filtered through a fine fritted funnel and lyophilized dry. A yield of 97% was obtained. ^{1}H NMR (400 MHz, D_2O, δ): 0.95 (t, J = 8.0 Hz, 3H), 1.38 (m, 2H), 1.78 (m, 2H), 1.94 (s, 3H), 2.80 (s, 3H), 3.17 (s, 6H), 3.40 (m, 2H), 3.77 (m, 2H), 4.63 (m, 2H), 5.79 (s, 1H), 6.16 (s, 1H).

Synthesis of poly(*n*BA-*co*-SBMA) and poly(*n*BA-*co*-BDMAEMA MS). A typical copolymerization of poly(*n*BA-*co*-SBMA) containing 10 mol% SBMA is described as follows: *n*BA (5.00 g, 39.1 mmol), SBMA (1.21 g, 4.33 mmol) and AIBN (31.1 mg) were charged to a 150-mL round-bottomed flask with a magnetic stir bar. DMSO (51.1 mL, 90 wt%) was added to dissolve the monomers. The reaction mixture was sparged with N_2 for 15 min, and placed into an oil bath at 65 °C for 24 h. The polymer was precipitated into water and allowed to equilibrate in ultrapure water for a week. A yield of 90% was obtained. The final product was monomer-free, as confirmed using ^{1}H NMR spectroscopy, and any residual DMSO was removed with reduced pressure at 65 °C for 3 days.

The syntheses of poly(*n*BA-*co*-BDMAEMA MS) were conducted under similar conditions with 10 wt% monomer in the reaction mixture and 0.5 wt% AIBN based on total monomer. However, the cationic analogs were first isolated with vacuum stripping of DMSO due to very different solubility. The products were subsequently dissolved in methanol and diluted with ultrapure water. The product solutions remained homogeneous upon H_2O addition and upon removal of methanol. Purification of the copolymers was

performed using exhaustive dialysis, and ^{1}H NMR spectra also confirmed the absence of residue monomer. Typical yields of 85% were achieved.

Instrumentation. ^{1}H NMR spectra were obtained on a Varian Unity 400 MHz spectrometer in D_2O, $CDCl_3$, and CD_3OD. Size exclusion chromatography (SEC) determined the molecular weights of the copolymers at 50 °C in DMF with 0.01 M LiBr at 1 mL min^{-1} flow rate. The DMF SEC system was equipped with a Waters 717plus autosampler, a Waters 1525 HPLC pump, two Waters Styragel HR5E (DMF) columns, and a Wyatt miniDAWN multiangle laser light scattering (MALLS) detector. Absolute molecular weights, as well as the specific refractive index increments (*dn/dc*) for all the samples, were determined using the Wyatt Astra V software package.

Thermogravimetric analysis (TGA) of the samples employed a TA Q500 from 25 °C to 700 °C at a heating rate of 10 °C·min^{-1} under N_2 atmosphere. Differential scanning calorimetry (DSC) measurements were performed on a TA Q100 instrument at a heating and cooling rate of 10 °C/min from -90 °C. The first heat scans were concluded at 120 °C, and traces of the second heats are reported. Dynamic mechanical analysis (DMA) was performed on a TA Q800 analyzer in tension mode, at 1 Hz frequency, 15 μm amplitude, and 3 °C/min heating rate from -90 °C. The copolymer membranes were cast from 0.1 g·mL^{-1} chloroform solutions into Teflon® molds to achieve film thicknesses of approximately 0.30 mm. The films were dried at 25 °C overnight, and subsequently heated at 65 °C for 72 h under vacuum prior to physical characterizations.

A Veeco MultiMode scanning probe microscope was used with Veeco MPP-21100-10 tips with spring constants of 3 N/m, for tapping-mode AFM imaging. Samples

were imaged at a set-point to free-air amplitude ratio of 0.6 and at magnifications of 600 nm ×600 nm.

Small angle X-ray scattering data were collected with a customized, pinhole collimated 3 m camera. X-rays were generated with a Rigaku Ultrax18 rotating Cu anode generator operated at 45 kV and 100 mA and then filtered with Ni foil to select the Cu K_α doublet (λ = 1.542 Å). Two-dimensional data sets were collected using a Molecular Metrology multiwire area detector at both 50 cm and 150 cm from the detector. Raw data were corrected for absorption and background noise and subsequently azimuthally averaged. The corrected data were placed on an absolute scale using a secondary standard, type 2 glassy carbon, and the data at both camera lengths were subsequently merged into one continuous data set for each sample. All data reduction and analysis were performed using Igor Pro v6.12A from Wavemetrics, Inc, using a suite of procedures developed at the Argonne National Laboratory.[22]

3.4 Results and Discussions

3.4.1 Synthesis and Characterization of BDMAEMA MS

The synthesis of BDMAEMA MS is illustrated in **Figure 3.2**. The structure of this novel monomer was confirmed using ^{1}H NMR spectroscopy (**Figure S3.1**), ^{13}C NMR spectroscopy (**Figure S3.2**), and elemental analysis (**Table S3.1**). A melting point of 160 °C was observed in the first heat of the DSC. There are earlier reports of quaternized DMAEMAs bearing a butyl group and various halide anions, such as Cl, Br and I, or PF_6 anion.[23-26] In our study, we designed BDMAEMA MS to serve as the appropriate cationic analog to SBMA as shown in **Figure 3.1**. Both structures contain quaternary ammonium cations and monovalent sulfonate anions. The butyl group in BDMAEMA MS was chosen to match the spacer length between charges in SBMA.

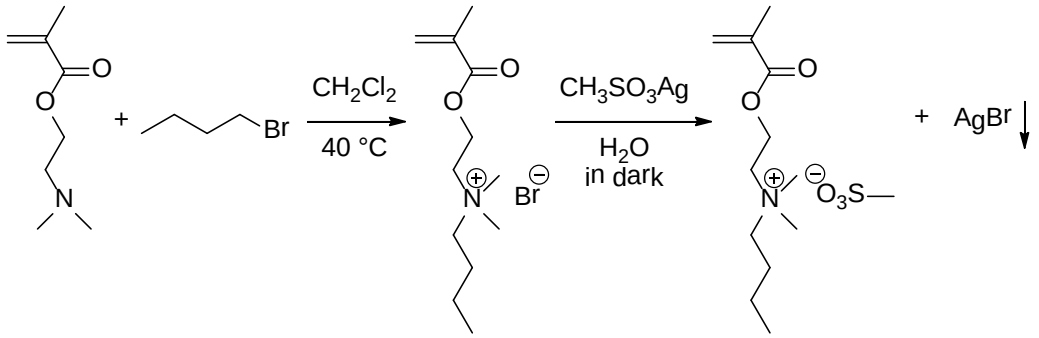

Figure 3.2. Synthesis of BDMAEMA Br in the presence of free radical inhibitor (hydroquinone) and subsequent anion exchange to BDMAEMA MS

3.4.2 Synthesis and Structural Characterization of Poly(*n*BA-*co*-SBMA) and Poly(*n*BA-*co*-BDMAEMA MS)

Zwitterionic copolymers containing 3, 6, and 9 mol% SBMA were synthesized using conventional free radical copolymerization in DMSO. A typical synthesis of poly(*n*BA-*co*-SBMA) is depicted in **Figure 3.3**.The reactions reached high conversions

in 24 h. ^{1}H NMR spectra confirmed that the products were monomer-free. The amount of SBMA in the copolymer was determined using ^{1}H NMR spectroscopy. However, any compositional drift due to high conversion was not determined.

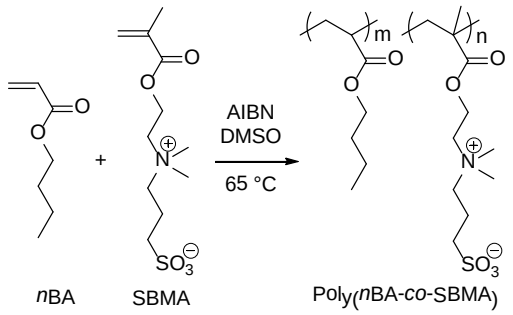

Figure 3.3. Synthesis of Poly(*n*BA-*co*-SBMA) using conventional free radical polymerization

The cationic analogs containing 7, 10, 15 and 22 mol% BDMAEMA MS were synthesized under similar conditions to those for zwitterionomers. However, the product isolation step was quite different due to very different solubility between the zwitterionomers and their cationic analogs. Nevertheless, the absence of the monomers in the final products was also confirmed using ^{1}H NMR spectra. The copolymer compositions were confirmed using ^{1}H NMR spectroscopy.

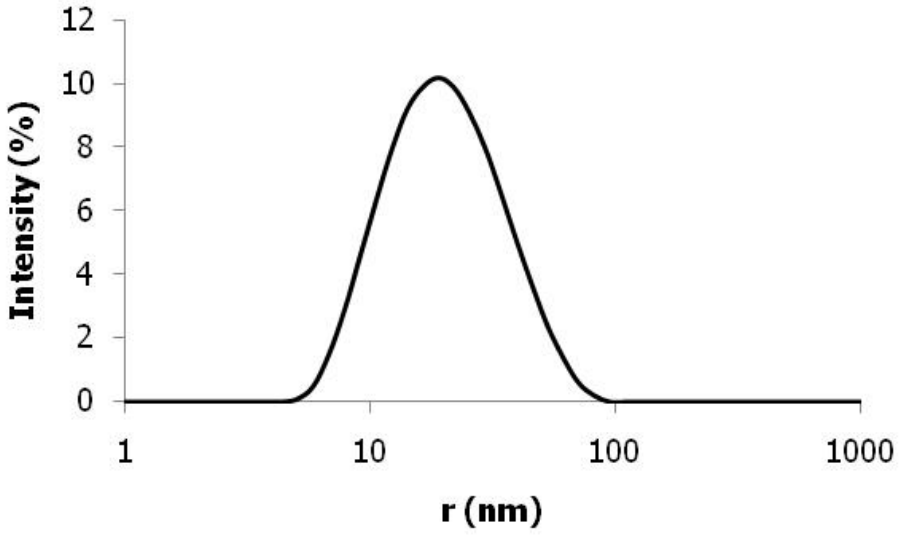

Figure 3.4. DLS intensity *vs* radius plot of poly(*n*BA_{91}-*co*-$SBMA_9$) in DMF with 0.01 M LiBr

The molecular weight determination of charge-containing polymers using size exclusion chromatography often presents a challenge due to ionic association of the polymers in solution. We demonstrated the use of dynamic light scattering in the screening of suitable SEC solvents for water-soluble ionenes.[27] In this current study, we adopted the same methodology and determined that DMF with 0.01 M LiBr was a suitable SEC eluent for both poly(*n*BA-*co*-SBMA) and poly(*n*BA-*co*-BDMAEMA MS). **Figure 3.4** is a representative DLS trace of poly(*n*BA_{91}-*co*-$SBMA_9$) in DMF with 0.01 M LiBr. The single peak with an average diameter of 23 nm suggested the absence of aggregation in the SEC solvent system.

SEC reproducibility tests confirmed that the SEC condition was suitable for both copolymer systems, except for the cationic analog containing 22 mol% BDMAEMA MS. We attributed the irreproducibility of this sample to the interaction between the polymer and the column at high BDMAEMA MS compositions. **Table 3.1** lists the absolute

molecular weights of the copolymers, as well as their specific refractive index increments. Since the average molecular weight between chain entanglements (M_e) for poly(*n*BA) is 28k,[28] our samples were of sufficient molecular weight for reliable thermomechanical property characterization. Molecular weight distribution values above 2.0 were typical of *n*BA-containing polymers synthesized with free radical processes.[29, 30]

Table 3.1 Size exclusion chromatographic analysis

Copolymer Composition	*dn/dc* (mL/g)	M_n (kg/mol)	M_w (kg/mol)	M_w / M_n
poly(nBA$_{97}$-*co*-SBMA$_3$)	0.045	87.1	461	5.28
poly(nBA$_{94}$-*co*-SBMA$_6$)	0.049	183	472	2.57
poly(nBA$_{91}$-*co*-SBMA$_9$)	0.050	162	404	2.49
poly[nBA$_{93}$-co-BDMAEMA MS$_7$]	0.047	115	294	2.55
poly[nBA$_{90}$-co-BDMAEMA MS$_{10}$]	0.051	88.7	228	2.56
poly[nBA$_{87}$-co-BDMAEMA MS$_{15}$]	0.042	246	252	1.03

3.4.3 Thermal Characterization of Zwitterionomers and Cationic Analogs

The thermal stability of the copolymers was determined using thermogravimetric analysis. **Figure 3.5** shows representative TGA traces of copolymers containing 9 mol% SBMA and 10 mol% BDMAEMA MS. The 5% mass loss temperatures of poly(*n*BA-*co*-SBMA) were ~300 °C, while poly(*n*BA-*co*-BDMAEMA MS) was similar. Burch and Manring showed that the thermal degradation of quaternary ammonium-containing polymers follow the Hofmann elimination mechanism.[31] Since the MS anion in BDMAEMA MS has similar basicity to the sulfonate group in SBMA, it was expected that the copolymer containing 9 mol% SBMA would have similar 5% weight loss

temperature to its cationic analog. TGA results also suggested that enhanced mobility of MS anions in BDMAEMA MS did not facilitate abstraction of β-H of the quaternary ammonium to initiate the degradation process.

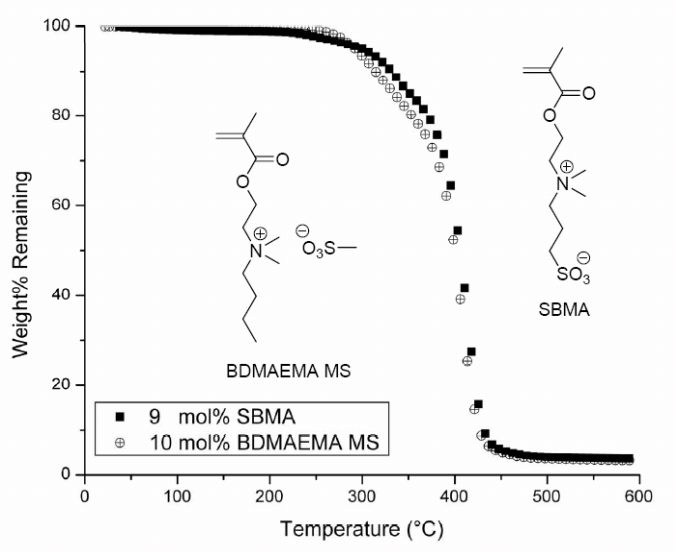

Figure 3.5. TGA of poly(*n*BA-*co*-SBMA) and poly(*n*BA-*co*-DBMAEMA MS) containing ~ 10 mol% of charged units

Table 3.2. Glass transition temperatures of zwitterionomers and their cationic analogs

Copolymer Composition	T_g (°C)
poly(nBA)	-47
poly(nBA_{97}-*co*-$SBMA_3$)	-44
poly(nBA_{94}-*co*-$SBMA_6$)	-42
poly(nBA_{91}-*co*-$SBMA_9$)	-40
poly(SBMA)	203
poly[nBA_{93}-co-(BDMAEMA MS)$_7$]	-35
poly[nBA_{90}-co-(BDMAEMA MS)$_{10}$]	-26
poly[nBA_{85}-co-(BDMAEMA MS)$_{15}$]	-5
poly[nBA_{78}-co-(BDMAEMA MS)$_{22}$]	19
poly(BDMAEMA MS)	83

Differential scanning calorimetry results exhibited one glass transition temperature for all copolymers, and T_g values are summarized in **Table 3.2**. For the zwitterionomers, the glass transition temperatures increased only slightly from -47 °C for poly(*n*BA) to -40 °C for copolymers containing 9 mol% SBMA. Considering that the glass transition temperature of poly(SBMA) was 203 °C, the observed T_g corresponded to the poly(*n*BA)-rich phase. This was an indication that the zwitterionomers presented biphasic morphologies, and the lack of a second T_g was likely due to low SBMA contents in the copolymers in agreement with a previous report on similar copolymers.[14] In comparison, the T_g of the cationic analog containing 7 mol% BDMAEMA MS was -35 °C, higher than the 9 mol% zwitterionomer. Further increasing the charged contents in the cationic

analog to 22 mol% resulted in a glass transition temperature of 19 °C for the copolymer. The different trends of T_g increase with increasing charge contents suggested that the zwitterionomers provided a more well-defined microphase-separated morphology than their cationic analogs.

3.4.4 Mechanical Characterization of Zwitterionomers and Their Cationic Analogs

Dynamic mechanical analysis provided the thermomechanical behavior of the copolymers. **Figure 3.6** shows the DMA traces of the zwitterionomers and their cationic analogs. In agreement with the DSC results, the glass transitions for both 6 and 9 mol% zwitterionomers appeared at approximately the same temperature, while the cationic analogs increased steadily with increasing charge contents in the copolymers. Due to the frequency dependence of polymer chain segmental motion, the glass transition temperatures of the samples measured using DMA were higher than values measured using DSC. More importantly, rubbery plateaus were observed only for zwitterionomers, in sharp contrast for cationic analogs. Gauthier and Eisenberg were among the first to systematically study similar rubbery plateaus observed in poly(sty) based ionomers.[32] They attributed the presence of rubbery plateaus to the physical cross-linking induced by ionic associations between metal cations and carboxylate anions. Here, we attributed rubbery plateaus for zwitterionomers to similar strong ionic interactions between the zwitterionic functionalities.

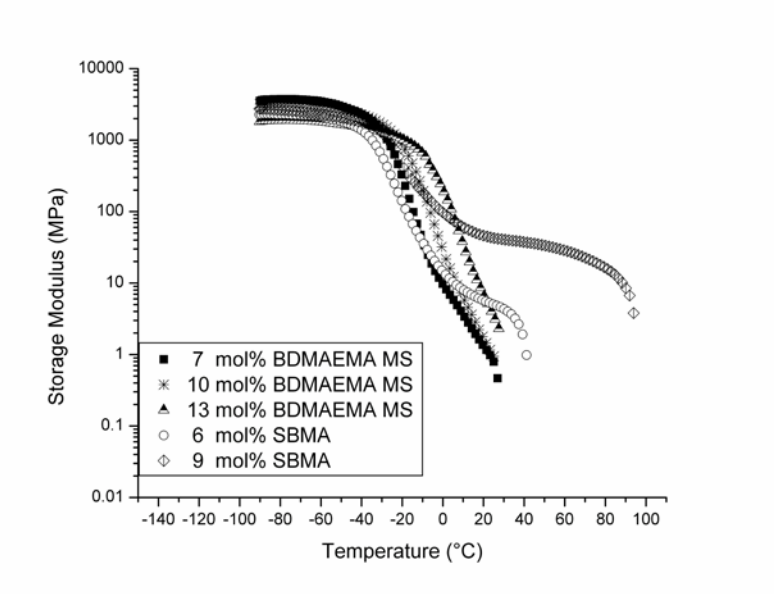

Figure 3.6. Storage modulus *vs* temperature profiles for poly(*n*BA-*co*-SBMA) and poly(*n*BA-*co*-BDMAEMA MS) containing varying amounts of charged units

Schmuck et al. demonstrated with a low molecular weight bis-zwitterion model that the zwitterionic species self-assembled in a head-to-tail fashion.[33] Bredas et al. predicted with theoretical calculations that the clustered zwitterions in polymers adopt an extended conformation with their dipoles aligning in an antiparallel fashion to favor interchain electrostatic interactions.[34] Based on these conclusions, we hypothesize that the charged zwitterions arrange in a head-to-tail fashion as illustrated in **Figure 3.7(a)**. Due to the covalent linkage between the cation and the anion on a zwitterion, the binding interactions between two zwitterionic functionalities represent ion-ion interactions (~250 kJ/mol).[35] In comparison, much weaker dipole-dipole interactions (~2 kJ/mol) between opposite charges are present in typical ionomers. The bulkiness of the quaternary ammonium cations in BDMAEMA MS, as well as their organic nature, should further contribute to the lack of rubbery plateau behavior for the cationic polymers. This is in agreement with what Page et al. reported for Nafion^{TM} neutralized with alkylammonium

cations,[36] however, experimental confirmation of such molecular level arrangements is lacking.

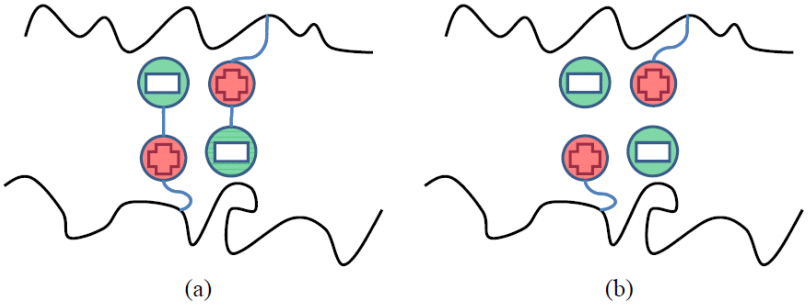

Figure 3.7. Simplified illustration of the possible charge interactions in (a) zwitterionomers and (b) cationic analogs

3.4.5 Morphologies of Zwitterionomers and Their Cationic Analogs

The morphologies of poly(*n*BA-*co*-SBMA) and poly(*n*BA-*co*-BDMAEMA MS) were probed using small-angle X-ray scattering (SAXS) and atomic force microscopy (AFM). Scattering profiles of the zwitterionomers and their cationic analogs, plotted as intensity *vs* the scattering vector magnitude, q, are shown in **Figure 3.8**. A scattering peak near $q \approx 0.15$ Å^{-1} was observed for each of the zwitterionomer samples, and the peak intensities decreased with decreasing sulfobetaine content in the copolymers. Scattering profiles containing such "ionomer peaks" are characteristic of charge-containing polymers.[15] The presence of the ionomer peaks was attributed to the different electron densities of the ionic aggregates and the surrounding matrix. These data indicated the presence of a microphase-separated morphology of zwitterion-rich domains in a matrix of *n*BA, consistent with the presence of physical crosslinks as indicated using DMA. In comparison, the scattering peaks of the cationic analogs were very broad and

weak with maxima around q ≈ 0.20 Å^{-1}. The weaker scattering intensities for the cationic analog samples suggested more phase mixing than the zwitterionomers in agreement with DSC findings.

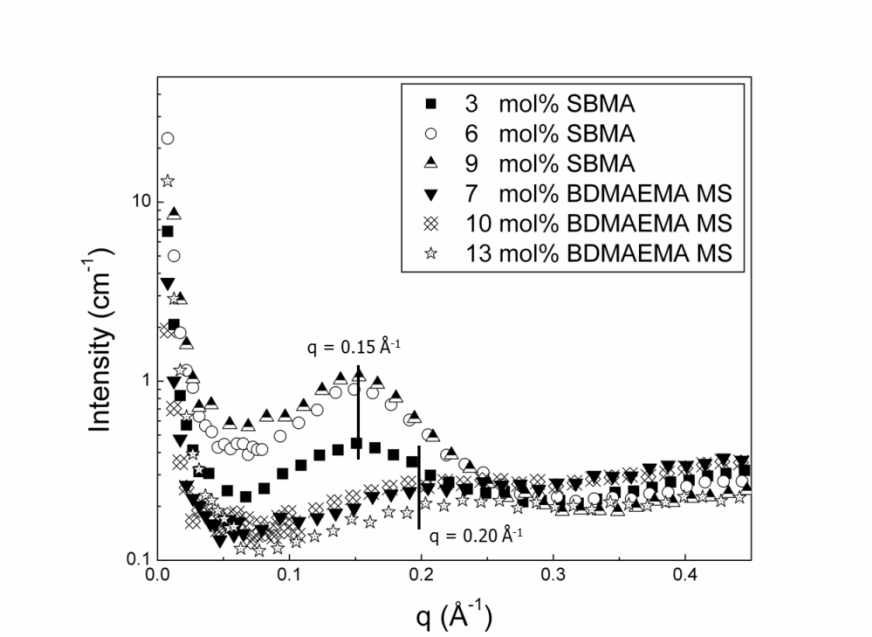

Figure 3.8. SAXS intensity *vs* scattering vector (q) traces for poly(*n*BA-*co*-SBMA) and poly(*n*BA-*co*-BDMAEMA MS) containing varying amounts of charged units

The SAXS profiles of both the zwitterionomers and the cationic analogs were fit using a liquid-like interparticle interference model as proposed by Yarusso and Cooper, and incorporating the Percus-Yevick structure factor, first used by Kinning and Thomas to model the scattering from spherical morphologies in block copolymers and later applied to ion-containing polymer by Ding et al.[37-40] The following general equation describes the scattered intensity of a sample from this model:

$$\frac{I}{I_e V} = \frac{1}{v_p}\left(\frac{4\pi R_1^3}{3}\right)^2 \Delta\rho^2 \emptyset^2 (qR_1) S(q, R_{cc}, R_1, v_p)$$

where I_e is the scattering from a single electron, V is the scattering volume, v_p is the volume of material per ionic aggregate, R_1 is the radius of the ionic aggregate, R_{ca} is the radius of closest approach, and Δρ is the difference in electron densities between the ionic aggregates and the matrix. $\Phi(qR_1)$ and $S(q, R_{ca}, R_1, v_p)$ are the form factor and the structure factor, respectively. The calculation of the Percus-Yevick structure factor followed the detailed expressions of Ding et al.[40] A Lorentzian peak, centered between 0.48 $Å^{-1}$ and 0.49 $Å^{-1}$, was added to the intensity function to represent poly(*n*-butyl acrylate) interchain scattering[41] and to improve the high-q fit. **Figure 3.9** shows that the model fits the SAXS data of the 9 mol% SBMA sample and the 15 mol% BDMAEMA MS sample very well over the q range between 0.07 $Å^{-1}$ and 0.41 $Å^{-1}$. Similarly good fits were also obtained for the other samples investigated in this study. The fitting parameters (Δρ, R_1, R_{ca} and v_p) as a function of copolymer contents are summarized in **Table 3.3**.

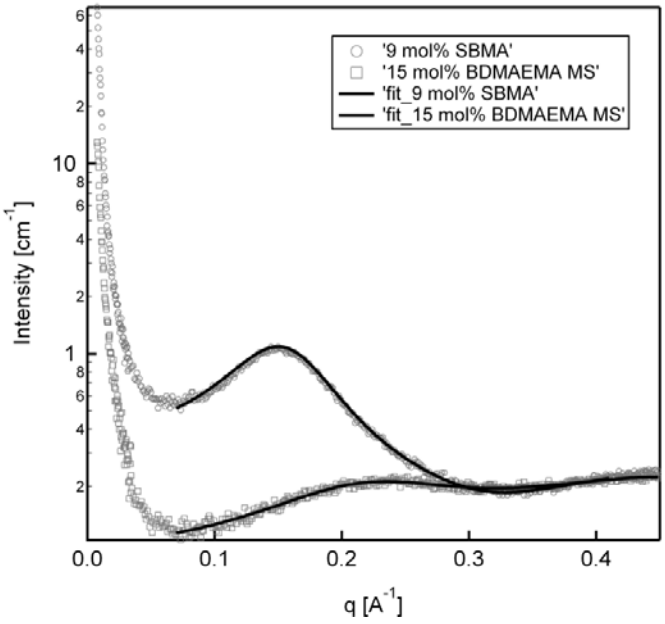

Figure 3.9. Fitting of representative SAXS traces of both the zwitterionomers and the cationic analogs to the Kinning-Thomas model.

The R_1 values for the zwitterionomers were close to what Ehrmann et al. reported for the R_g, which is a measure of the size of the scattering entities of similar zwitterionomers based on Guinier analysis.[14] The modeling of the SAXS data for quaternary ammonium-based cationomers is not well-documented in the literature. Hence, we compared our fits for the cationic analogs with those for common anionic ionomers, and found that our R_1 values matched what Kutsumizu et al. and Tsujita et al. reported for partially neutralized poly(ethylene-*co*-methacrylic acid) ionomers.[42, 43]

Table 3.3. Summary of the fitting parameters for zwitterionomers and their cationic analogs

Copolymer Composition	$\Delta\rho$ (10^{21} cm^{-3})	R_1 (nm)	R_{ca} (nm)	v_p (nm^3)
poly(nBA$_{91}$-*co*-SBMA$_9$)	46.5	1.33	1.96	115
poly(nBA$_{94}$-*co*-SBMA$_6$)	46.6	1.27	1.96	112
poly(nBA$_{97}$-*co*-SBMA$_3$)	46.5	1.10	1.86	127
poly[nBA$_{87}$-co-(BDMAEMA MS)$_{15}$]	100	0.585	1.27	48.8
poly[nBA$_{90}$-co-(BDMAEMA MS)$_{10}$]	111	0.633	1.23	62.0
poly[nBA$_{93}$-co-(BDMAEMA MS)$_7$]	97.7	0.647	1.25	98.7

Increasing charge content appeared to lead to substantially different morphological changes between the zwitterionomers and their cationic analogs, although the weak scattering of the cationic analogs prevented drawing firm conclusions from the resulting fit parameters. Hence, the main focus of our data interpretation was on the trends in zwitterionomers. Specifically, an increase in charge content for the zwitterionomers resulted in an increase in R_1, the radius of the ionic aggregate, but very

little change in v_p. Since the density of ionic aggregates is proportional to $1/v_p$, these results suggested that the number of ionic aggregates per unit volume remained relatively constant with increasing charge content in the zwitterionomer series. Conversely, increasing charge content in the cationic analogs resulted in an increased number of smaller aggregates (decreasing R_1 and decreasing v_p), as one can reliably conclude based on the weakly microphase-separated morphologies indicated by the scattering from the cationic analogs. However, this analysis of the SAXS data was in agreement with the DMA results for the zwitterionomers, as higher ion dissociation temperatures in DMA were observed for samples with higher charge contents, which also possessed larger ionic aggregates. Similar conclusions were not made for the cationic analogs as a rubbery plateau was not observed for any of the cationic analogs.

Furthermore, the comparison between the zwitterionomers and the cationic analogs revealed that the zwitterionomers contained fewer, but larger, ionic aggregates than the cationic analogs in a given sample volume. Considering that the rubbery plateaus in DMA were only observed for the zwitterionomers, the SAXS results supported our hypothesis that the binding interactions between the charges in the zwitterionomers were stronger than those in the cationic analogs.

AFM results are shown in **Figure 3.10**. For the zwitterionomers, clear evidence of surface microphase separation was observed at very low zwitterion incorporation of 3 mol%. In comparison, the surface of the cationic analog that contained 10 mol% BDMAEMA MS appeared very smooth; even at 22 mol% of charge composition, the cationic analog still appeared less phase-separated than the 3 mol% zwitterionomer. This trend agreed with the SAXS findings. Due to different resolution limits of the two

characterization techniques, the dimensions of the features observed using AFM are not comparable with those determined with SAXS. Nevertheless, the AFM results confirmed that the cationic analogs were more phase mixed than the zwitterionomers, consistent with the SAXS and DSC findings.

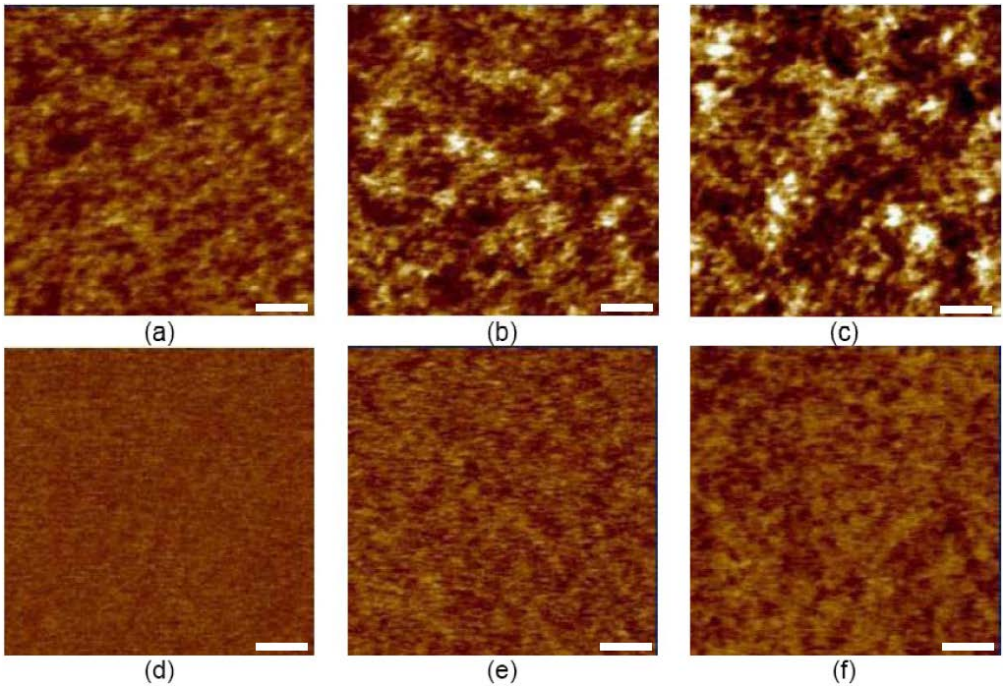

Figure 3.10. AFM phase images of zwitterionomers and their cationic analogs: samples (a~c) contains 3, 6 and 9 mol% SBMA respectively; samples (d~f) contains 10, 15 and 22 mol% BDMAEMA MS respectively. The scale bars are 100 nm; light phases represent higher modulus ionic aggregates.

3.5 Conclusions

We successfully designed and synthesized BDMAEMA MS as the cationic analog to SBMA. *n*BA based acrylic copolymers containing SBMA and BDMAEMA MS of varying charge compositions were polymerized. ^{1}H NMR results showed good agreement

between the monomer feed and copolymer compositions. The molecular weights of the copolymers were characterized using SEC in DMF with 0.01 M LiBr relative to polystyrene standards. Small- angle X-ray scattering traces from both zwitterionomers and cationic analogs were fit very well, using a hard sphere model combined with a structure factor incorporating liquid-like interparticle interference.[37-40] The modeling results revealed that the zwitterionomers contained fewer, but larger, ionic aggregates than the cationic analogs in a given sample volume. The superior elastomeric performances observed for the zwitterionomers compared to their cationic analogs coincided with their more well-defined microphase-separated morphologies. The stronger ion-ion interactions in the zwitterionomers were thus postulated to produce rubbery plateaus in DMA and better mechanical performance. The stronger zwitterionic interaction offers the potential to uptake conductive diluents, such as ionic liquids, while maintaining their mechanical strength for advanced electro-mechanical applications. Future efforts may involve comparing the zwitterionomers with polymer blends and other more polar ionomers to further elucidate the impact of zwitterionic interactions.

3.6 Acknowledgements

This material is based upon work supported by the U.S. Army Research Laboratory and the U.S. Army Research Office under grant number W911NF-07-1-0339. Parts of this work were carried out using instruments in the Nanoscale Characterization and Fabrication Laboratory, a Virginia Tech facility operated by the Institute for Critical Technology and Applied Science. The authors also acknowledge Dr. Andrew Duncan at the U.S. Army Research Laboratory for his assistance with the collection of small-angle X-ray scattering data.

Supporting Information Available. Detailed NMR and elemental analysis of BDMAEMA MS. Composition analysis of poly(*n*BA-*co*-SBMA) and poly(*n*BA-*co*-BDMAEMA MS) using ^{1}H NMR spectroscopy. This information is available free of charge via the Internet at http://pubs.acs.org/.

3.7 References

1. Mauritz, K. A.; Moore, R. B. *Chemical Reviews* **2004,** 104, (10), 4535-4586.
2. Duncan, A. J.; Leo, D. J.; Long, T. E. *Macromolecules* **2008,** 41, (21), 7765-7775.
3. Williams, S. R.; Long, T. E. *Progress in Polymer Science* **2009,** 34, (8), 762-782.
4. Hickner, M. A.; Ghassemi, H.; Kim, Y. S.; Einsla, B. R.; McGrath, J. E. *Chemical Reviews* **2004,** 104, (10), 4587-4611.
5. Ho Bum Park, Benny D. F., Zhong-Bio Zhang, Mehmet Sankir, James E. McGrath,. *Angewandte Chemie International Edition* **2008,** 47, (32), 6019-6024.
6. De Smedt, S. C.; Demeester, J.; Hennink, W. E. *Pharmaceutical Research* **2000,** 17, (2), 113-126.
7. Duncan, A. J.; Leo, D. J.; Long, T. E.; Akle, B. J.; Park, J. K.; Moore, R. B. In *Electromechanical performance and membrane stability of novel ionic polymer transducers constructed in the presence of ionic liquids*, Proc. SPIE, 2009; 2009; pp 728711/1-728711/11.
8. Brown, R. H.; Duncan, A. J.; Choi, J. H.; Park, J. K.; Wu, T. Y.; Leo, D. J.; Winey, K. I.; Moore, R. B.; Long, T. E. *Macromolecules* **2010,** 43, (2), 790-796.
9. Galin, M.; Chapoton, A.; Galin, J. C. *J. Chem. Soc. Perkin Trans.* **1993,** 2, 545.
10. Ehrmann, M.; Muller, R.; Galin, J. C.; Bazuin, C. G. *Macromolecules* **1993,** 26, (18), 4910-4918.
11. Mathis, A.; Zheng, Y. L.; Galin, J. C. *Polymer* **1991,** 32, (17), 3080-3085.
12. Ehrmann, M.; Galin, J. C. *Polymer* **1992,** 33, (4), 859-865.
13. Ehrmann, M.; Galin, J. C.; Meurer, B. *Macromolecules* **1993,** 26, (5), 988-993.
14. Ehrmann, M.; Mathis, A.; Meurer, B.; Scheer, M.; Galin, J. C. *Macromolecules* **1992,** 25, (8), 2253-2261.
15. Eisenberg, A.; Hird, B.; Moore, R. B. *Macromolecules* **1990,** 23, (18), 4098-4107.
16. Koberle, P.; Laschewsky, A. *Macromolecules* **1994,** 27, (8), 2165-2173.
17. Galin, M.; Marchal, E.; Mathis, A.; Galin, J. C. *Polymers for Advanced Technologies* **1997,** 8, 75-86.
18. Galin, M.; Marchal, E.; Mathis, A.; Meurer, B.; Soto, Y. M. M.; Galin, J. C. *Polymer* **1987,** 28, (11), 1937-1944.
19. Lee, W.-F.; Lee, C.-H. *Polymer* **1997,** 38, (4), 971-979.
20. Lee, W.-F.; Tsai, C.-C. *Polymer* **1994,** 35, (10), 2210-2217.
21. Lee, W.-F.; Tsai, C.-C. *Polymer* **1995,** 36, (2), 357-64.
22. Ilavsky, J.; Jemian, P. R. *Journal of Applied Crystallography* **2009,** 42, (2), 347-353.

23. Hamid, S. M.; Sherrington, D. C. *Polymer* **1987,** 28, (2), 325-331.
24. Oya, T.; Kunita, K.; Araki, K.; Iwai, Y.; Sonokawa, K.; Sasaki, T. Lithographic printing plate precursor and lithographic printing method. EP 2006738 A2 2008-11283, 2008.
25. Ushakova, V. N.; Kipper, A. I.; Afanakina, N. A.; Samarova, O. E.; Klenin, S. I.; Panarin, E. F. *Vysokomol. Soedin., Ser. A Ser. B* **1995,** 37, (6), 933-8.
26. Yuan, H.; Li, C.; Zhu, Y.; Huang, B. Manufacture of amphiphilic cation flocculant with high molecular weight for wastewater treatment. CN 1721339 A 20060118, 2006.
27. Layman, J. M.; Borgerding, E. M.; Williams, S. R.; Heath, W. H.; Long, T. E. *Macromolecules* **2008,** 41, (13), 4635-4641.
28. Tong, J. D.; Jerome, R. *Polymer* **2000,** 41, (7), 2499-2510.
29. Ahmad, N. M.; Charleux, B.; Farcet, C.; Ferguson, C. J.; Gaynor, S. G.; Hawkett, B. S.; Heatley, F.; Klumperman, B.; Konkolewicz, D.; Lovell, P. A.; Matyjaszewski, K.; Venkatesh, R. *Macromolecular Rapid Communications* **2009,** 30, (23), 2002-2021.
30. Barner-Kowollik, C. *Macromolecular Rapid Communications* **2009,** 30, (23), 1961-1963.
31. Burch, R. R.; Manring, L. E. *Macromolecules* **1991,** 24, (8), 1731-5.
32. Gauthier, M.; Eisenberg, A. *Macromolecules* **1990,** 23, (7), 2066-74.
33. Schmuck, C.; Rehm, T.; Klein, K.; Gröhn, F. *Angewandte Chemie International Edition* **2007,** 46, (10), 1693-1697.
34. Bredas, J. L.; Chance, R. R.; Silbey, R. *Macromolecules* **1988,** 21, (6), 1633-1639.
35. Atkins, P.; de Paula, J., In *Atkins' Physical Chemistry*, 7th ed.; 2002; p 700.
36. Page, K. A.; Cable, K. M.; Moore, R. B. *Macromolecules* **2005,** 38, (15), 6472-6484.
37. Yarusso, D. J.; Cooper, S. L. *Macromolecules* **1983,** 16, (12), 1871-80.
38. Percus, J. K.; Yevick, G. J. *Phys. Rev.* **1958,** 110, 1-13.
39. Kinning, D. J.; Thomas, E. L. *Macromolecules* **1984,** 17, (9), 1712-18.
40. Ding, Y. S.; Register, R. A.; Yang, C.; Cooper, S. L. *Polymer* **1989,** 30, (7), 1213-20.
41. Miller, R. L.; Boyer, R. F.; Heijboer, J. *J. Polym. Sci., Polym. Phys. Ed.* **1984,** 22, (12), 2021-41.
42. Kutsumizu, S.; Tagawa, H.; Muroga, Y.; Yano, S. *Macromolecules* **2000,** 33, (10), 3818-3827.
43. Tsujita, Y.; Hayashi, N.; Yamamoto, Y.; Yoshimizu, H.; Kinoshita, T.; Matsumoto, S. *Journal of Polymer Science Part B: Polymer Physics* **2000,** 38, (10), 1307-1311.

3.8 Supplemental Information

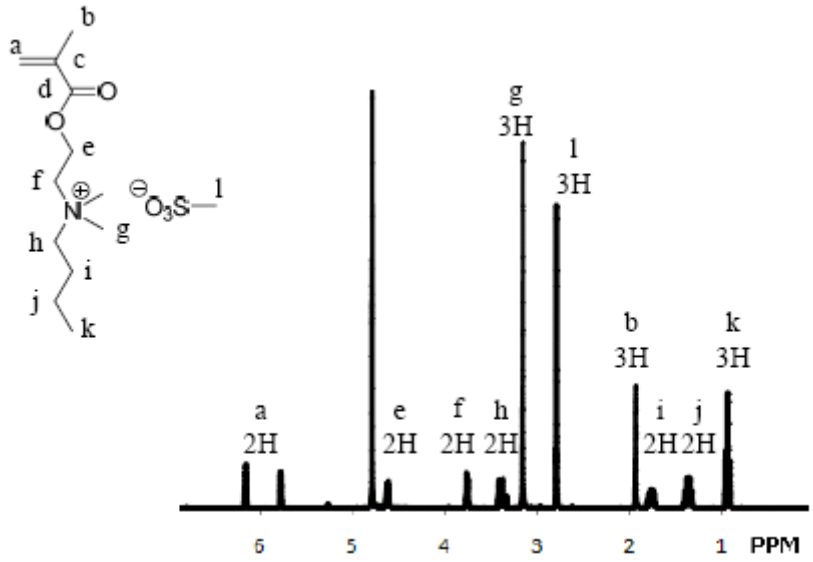

Figure 3.11 ^{1}H NMR of BDMAEMA MS in D_2O

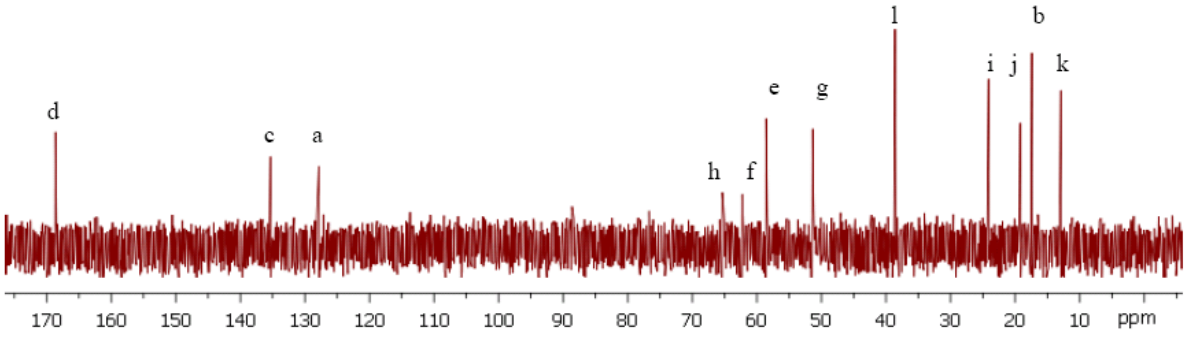

Figure 3.12 ^{13}C NMR of BDMAEMA MS in D_2O

Table 3.4 Elemental analysis results of BDMAEMA MS

Element	Theory (wt%)	Found (wt%)
C	50.46	50.49
H	8.80	8.79
O	25.85	26.03
N	4.53	4.49
S	10.36	10.33

Figure 3.13 is the ^{1}H NMR of poly(*n*BA-*co*-SBMA) in $CDCl_3$. Peak 'a' at 0.95 ppm was assigned to the methyl group on *n*BA, and peak 'b' at 3.36 ppm was assigned to the two methyl groups on the quaternized "*N*" of SBMA. The amount of SBMA in the copolymer was determined using the following equation:

$$SBMA\ mol\% = \frac{b}{b + 2a} \cdot 100\%$$

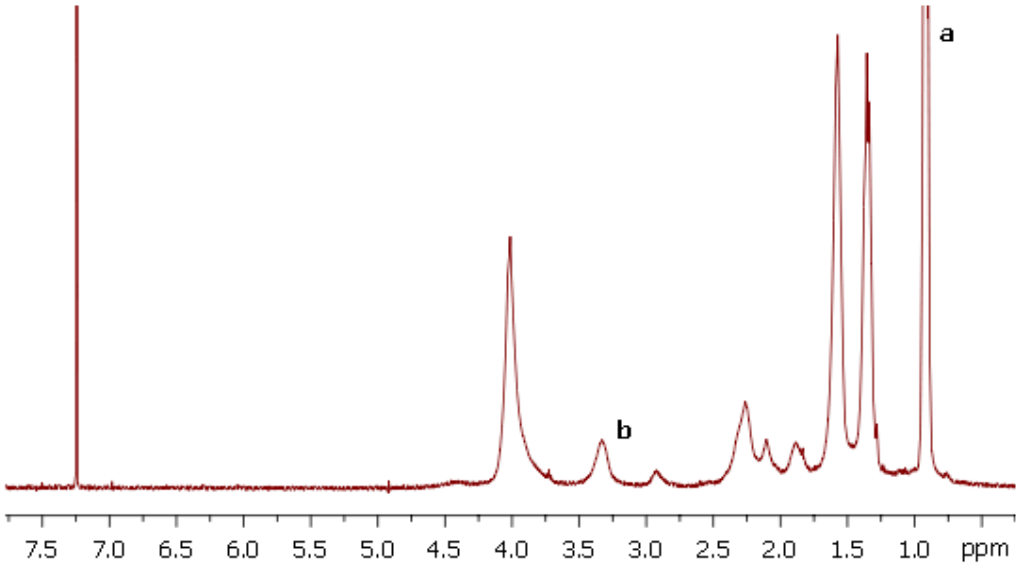

Figure 3.13 ^{1}H NMR of poly(*n*BA-*co*-SBMA) in $CDCl_3$

Figure 3.14 is the ^{1}H NMR of poly(*n*BA-*co*-BDMAEMA MS) in CD_3OD. Peak 'c' at 0.97 ppm was assigned to the methyl group on *n*BA, and peak 'd' at 1.05 ppm and the shoulder "e' on its left were assigned to the two methyl groups on BDMAEMA MS. The copolymer compositions were determined using the following equation:

$$BDMAEMA\ MS\ mol\% = \frac{(d+e)}{2c+d+e} \cdot 100\%$$

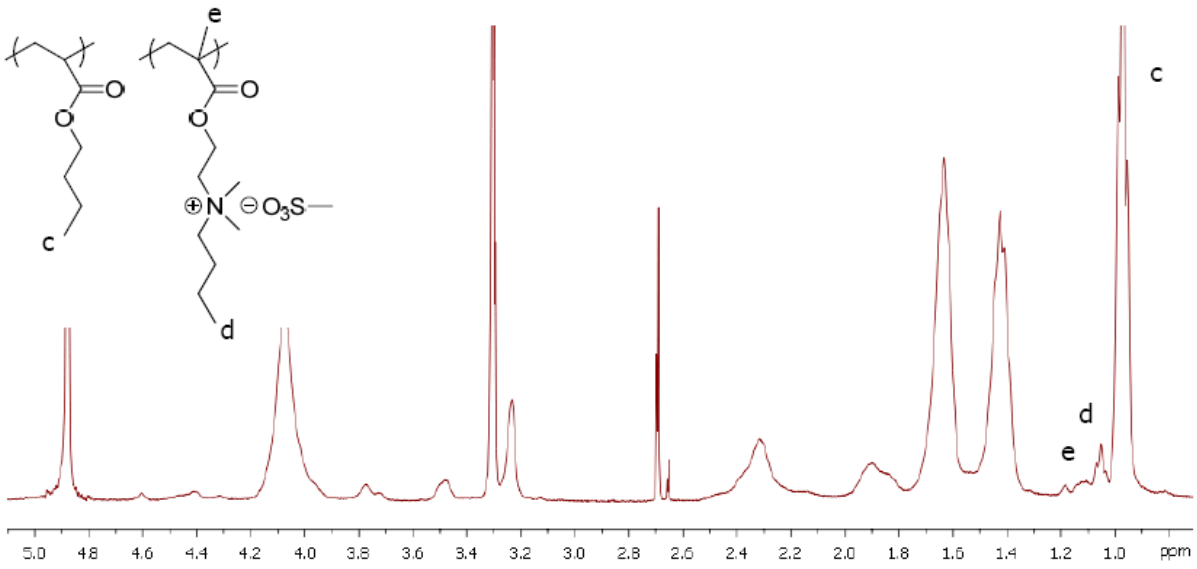

Figure 3.14 ^{1}H NMR of poly(*n*BA-*co*-BDMAEMA MS) in CD_3OD

Chapter 4 Impact of Compositing Strategies on the Thermomechanical Performance, Ionic Conductivities and Morphologies of Zwitterionomer / Ionic Liquid Composite Membranes

(*Tianyu Wu, Gilles M. Divoux, Mingqiang Zhang, Robert B. Moore, and Timothy E. Long**)

Department of Chemistry, Macromolecules and Interfaces Institute, Virginia Tech, Blacksburg, Virginia 24061-0212

4.1 Abstract

Zwitterionomer / ionic liquid composite membranes of poly(*n*BA-*co*-SBMA) and 1-ethyl-3-methylimidazolium ethylsulfate (EMIm ES), the ionic liquid, were prepared using both the "swelling' and the "cast with" methods. Dynamic mechanical analysis revealed that the "swollen" membranes maintained their thermomechanical performance with up to 18 wt% EMIm ES incorporation, while that of the "cast with" membranes decreased gradually as the ionic liquid concentration in the composite membranes increased. Small-angle X-ray scattering results indicated that the "swollen" and the "cast with" membranes have different morphologies, with the ionic liquid distributed more evenly inside the "cast with" membranes. Impedance spectroscopy results showed that the "cast with" membranes had better ionic conductivity than the "swollen" membrane at high ionic liquid concentration, in agreement with our proposed model. We attributed the differences in thermomechanical properties, ionic conductivities, as well as morphologies of the between the "swollen" and the "cast with" zwitterionomer / ionic liquid composite membranes to the impact of different membrane fabrication process.

Key Words: zwitterion, ionic liquid, composite, morphology, ionic conductivity

4.2 Introduction

Ionic liquids are salts that exhibit low melting points typically below 100 °C.[1] Walden reported the first room temperature ionic liquid, ethylammonium nitrate (EAN), in 1914.[2] However, it was the discovery of imidazolium-based ionic liquids, which exhibited lower melting points and wider electrochemical windows, in 1982 that provided impetus for recent dramatic increase in activity in the area.[3] Over the past decade, imidazolium-based ionic liquids have received considerable interest for their structural tenability, chemical and thermal stabilities, low vapor pressure and high ionic conductivity.[4] They have found applications not only as solvents in chemical synthesis and extraction,[5-10] but also as electrolytes and doping agents in lithium batteries,[11] solar cells,[12] catalytic membranes[13] and electromechanical transducers.[14-16] For example, Fukushima et al. fabricated a bucky gel actuator with an ionic liquid doped poly(vinylidene fluoride-*co*-hexafluoropropylene) internal electrolyte layer that operated quickly in air and for a long time.[17] Leo and coworkers demonstrated that ionic liquid-swollen Nafion™ membranes afforded actuators better stability than those solvated with water when operated in air.[14, 18]

Meanwhile, polybetaines are unique zwitterionic polymers that contain covalently bound cations and anions on each repeat unit. Typical betaine functionalities, such as ammonioalkanesulfonate, have very high electric dipole moments ($\mu \sim 18.7$-27.6 D as derived from dielectric measurements in solutions).[19] The higher polarities of betaine functionalities allow them to form strong ion-dipole interactions with polar guest

molecules, which preclude salt segregation or crystallization within the matrices. Koberle et al. studied miscibility of sulfobetaine-type poly(zwitterion)s with various types of inorganic salts.[20] They found that, different from typical polycations and polyanions, the highly dipolar sulfobetaine functionalities afforded the polyzwitterions miscibility with selected inorganic salts, such as NaI, up to stoichiometric amounts and beyond. Galin et al. reported that, upon salt incorporation, the glass transition temperatures of the polysulfobetaine matrices responded similarly regardless of the salt type, with the exception of a zwitterionic salt.[21] The compatibility of polyzwitterions with polar guest molecules afforded them potential as the host matrix in composite membranes for electro-active applications. Cardoso et al. investigated the impact of different salts on the ionic conductivities of polysulfobetaines up to stoichiometric amount of salt incorporation.[22] They found that the zwitterionomers exhibited higher ionic conductivities either in their pure states or at high salt concentrations. More recently, Brown et al. introduced 1-ethyl-3-methylimidazolium ethylsulfate (EMIm ES), a room temperature ionic liquid, into two series of zwitterionomer membranes.[23] They found that the rate of EMIm ES uptake at room temperature into the zwitterionomer membranes depended on the pairing of the IL and the zwitterionomer. They also reported that the incorporation of ionic liquid into the zwitterionomer membranes impacted their morphologies and improved their ionic conductivities.

While the influence of polar guest molecules on the performance and bulk properties of charge-containing polymer matrices are well documented,[17, 18, 23-25] the impact of the processes through which those polar molecules are introduced into the polymer membranes is not well understood. In this study, we incorporated EMIm ES into

zwitterionomer membranes both during and post membrane formation. The former process is referred to as the "cast with" method, while the latter process is referred to as the "swelling" method. Through employing dynamic mechanical analysis (DMA), small-angle X-ray scattering (SAXS), and impedance spectroscopy, we aim to elucidate the impact of the two fabrication processes on the thermomechanical properties, morphologies, as well as the ionic conductivities, of these composite membranes. Such understanding may provide guidance toward the fabrication of polymer / ionic liquid composite membranes for electro-active applications.

4.3 Experimental

Materials. Zwitterionic monomer, [2-(methacryloyloxy)ethyl]-dimethyl-(3-sulfopropyl)-ammonium hydroxide (SBMA, Aldrich, 97%), 1-ethyl-3-methylimidazolium ethylsulfate (EMIm ES, Fluka, BASF quality ≥ 95%), dimethyl sulfoxide (DMSO, Alfa Aesar, 99.9+%) and chloroform (Optima®, Fischer Scientific) were used as received. *n*-Butyl acrylate (*n*BA, Alfa Aesar, 98+%) was deinhibited via passing through neutral alumina column and further distilled under reduced pressure from calcium hydride. Azobisisobutyronitrile (AIBN, Aldrich, 98%) was recrystallized from methanol.

Synthesis of poly(*n*BA-*co*-SBMA). The synthesis of poly(*n*BA-*co*-SBMA) was previously described in detail in the literature.[26] Here, *n*BA (10.0 g, 78.1 mmol), SBMA (2.43 g, 8.71 mmol) and AIBN (62.9 mg, 0.383 mmol) were charged to a 250-mL round-bottomed flask with a magnetic stir bar. DMSO (102 mL, 90.0 wt%) was added to dissolve the monomers. The reaction mixture was sparged with N_2 for 15 min, and placed into an oil bath at 65 °C for 24 h. The polymer was precipitated into water, and

equilibrated in deionized water for a week. A yield of 90% was obtained. The final product was monomer free, as confirmed via ^{1}H NMR, and any residual DMSO was removed under vacuum at 65 °C for 3 days.

Preparing poly(*n*BA-*co*-SBMA) / EMIm ES composite membranes. Poly(*n*BA-*co*-SBMA) / EMIm ES composite membranes were prepared using both the "swelling" and the "cast with" methods. In the "swelling" approach, a zwitterionomer master membrane was first cast from 0.1 g·mL^{-1} chloroform solutions into a PTFE mold to achieve film thickness of approximately 0.30 mm. The master film was dried at room temperature overnight, and annealed at 65 °C for 72 h under vacuum. The master membrane was then cut into 30 mm × 20 mm rectangular pieces, and immersed into EMIm ES. The swelling of the zwitterionomer membranes was carried out at 65 °C under vacuum to minimize the impact of moisture uptake. The swollen membranes were periodically taken out, blotted with Kimwipe to remove excess of ionic liquid at the surfaces, and weighed to determine the amount of ionic liquid uptake in the membranes using the following equation:

$$wt\%\ uptake = \frac{m - m_0}{m_0} \times 100\%$$

where m_0 is the initial dry mass of the film and m is the mass of the swollen film at a given time. Once the desired ionic liquid uptake levels were reached, the swollen membranes were transferred to PTFE sheet covered petri dishes, and stored at 25 °C under vacuum for further characterizations.

In the "cast with" approach, predetermined amounts of poly(*n*BA-*co*-SBMA) and EMIm ES were first dissolved in chloroform at a concentration of 0.1 g polymer per mL

chloroform, and then cast into PTFE molds to achieve film thicknesses of approximately 0.30 mm. The composite membranes were dried at room temperature overnight prior to annealing at 65 °C under vacuum for 72 h. The "cast with" membranes were also stored at 25 °C under vacuum prior to characterizations. For both the "swollen" and the "cast with" membranes, the targeted amount of EMIm ES in the composite membranes were 3, 6, 9, 12, 15 and 18 wt% based on the dry mass of the zwitterionomer.

Instrumentation. ^{1}H NMR spectra were obtained on a Varian Unity 400 MHz spectrometer in $CDCl_3$. Size exclusion chromatography (SEC) was used, as previously described,[27] to determine the relative molecular weight of the copolymer to polystyrene standards in DMF with 0.01 M LiBr. Dynamic mechanical analysis (DMA) was performed on a TA Q800 analyzer in tension mode, at 1 Hz frequency, 15 μm amplitude, and 3 °C/min heating rate from -90 °C.

Small angle X-ray scattering (SAXS) data were collected using a Rigaku S-Max 3000 SAXS system, equipped with 3 pinholes and a copper rotating anode emitting X-ray with a wavelength of 0.154 nm (Cu Kα). Two-dimensional SAXS patterns were obtained using a fully integrated 2D multiwire, proportional counting, gas-filled detector, with an exposure time of 1 hour. Raw data were corrected for absorption and background noise, and then azimuthally averaged. The corrected data were calibrated against Type 2 glassy carbon, a secondary standard, and placed onto an absolute scale. The data collected at two sample-to-camera distances, 1603 mm and 939 mm respectively, were merged into one continuous data set for each sample. All data reduction and analysis were performed using Igor Pro v6.12A from Wavemetrics, Inc, using a suite of procedures developed at the Argonne National Laboratory.[28]

All conductivity measurements were performed at room temperature using a Solatron 1260 frequency response analyzer coupled with a Solatron 1287 electrochemical interface. The through-plane conductivity measurement cell was custom-made with circular copper electrodes. The applied pressure was calibrated using a Fuji Prescale® Tactile Surface Pressure Indicating film. Circular samples were cut with a 10 mm-diameter hollow punch and placed between the two electrodes. A frequency sweep between 10 MHz and 1 Hz was performed with an AC signal of 100 mV amplitude. The resistivity of a sample was determined from the complex impedance spectrum, and the conductivity was subsequently derived. Averages of at least three separate measurements were reported. ZPlot and ZView software packages were used to acquire and analyze the data, respectively.

4.4 Results and Discussions

4.4.1 Synthesis of poly(*n*BA-*co*-SBMA)

The synthesis of the zwitterionomer was described in detail in our previous publication.[23] **Figure 4.1** depicts the conventional free radical polymerization of poly(*n*BA-*co*-SBMA). The reaction reached high conversion in 24 h. The ^{1}H NMR spectrum of the product (shown in supplemental information, **Figure S4.1**) confirmed that the product was monomer-free and contained 8 mol% SBMA. SEC in DMF with 0.01 M LiBr determined that the copolymer had M_n of 66 kg/mol, exceeding the molecular weight between entanglements (M_e, 28 kg/mol) for poly(*n*BA),[29] and PDI of 2.5. The same batch of zwitterionomer was used for this entire study, and is referred to as poly(nBA$_{92}$-*co*-SBMA$_8$) in later text to indicate its molar composition.

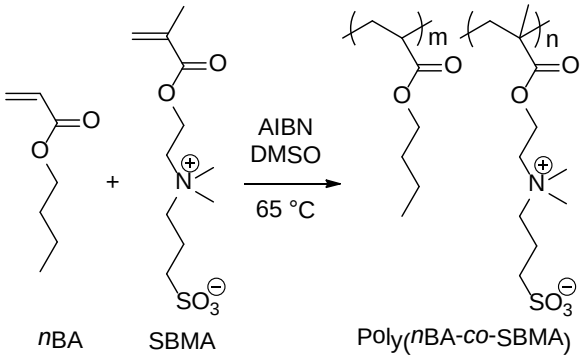

Figure 4.1 Synthesis of Poly(*n*BA-*co*-SBMA) using conventional free radical polymerization

4.4.2 Preparation poly(nBA$_{92}$-*co*-SBMA$_8$) / EMIm ES composite membranes.

Figure 4.2 shows the chemical structure of 1-ethyl-3-methylimidazolium ethylsulfate (EMIm ES). It is a water-miscible IL with a melting point of -65 °C and bulk conductivity of 3.82 mS·cm^{-1} at 298K. Brown et al. investigated the swelling behavior of poly(*n*BA-*co*-SBMA) with varying SBMA compositions at room temperature.[23] They reported the EMIm ES swelling profile for poly(nBA$_{91}$-*co*-SBMA$_9$), and noted that zwitterionomers containing less than 6 mol% SBMA functionalities were unable to take up measurable amounts of EMIm ES at room temperature after 1200 h. Here, we maintained the dry thicknesses of all swollen membranes through the use of a master membrane, and subjected them to a higher swelling temperature ,at 65 °C, to accelerate the swelling process.

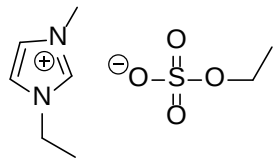

Figure 4.2 Chemical structure of 1-ethyl-3-methylimidazolium ethylsulfate (EMIm ES).

Figure 4.3 shows the swelling profiles for poly(*n*BA_{92}-*co*-$SBMA_8$) samples with different targeted swelling levels (hollowed data points). The legend indicated the actual EMIm ES concentrations in the swollen membranes at the end of the swelling processes. The filled data points are room temperature swelling profile adopted from the previous study for a similar sample containing 9 mol% SBMA.[23] Since all dry films used for the swelling study were cut from the same master film, the thicknesses of the dry membranes were maintained. The overlapping of hollowed data points indicated good reproducibility of the swelling studies and minimal variation in swelling kinetics for samples targeted at different swelling levels. The steeper slope observed for samples swollen at 65 °C suggested higher rates of ionic liquid uptake at higher temperatures. As a result, we were able to achieve ~18 wt% IL uptake in 40 h. In comparison, Brown et al. reported a 20 wt% EMIm ES uptake in 250 h for a similar sample at room temperature.[23] For the "cast with" samples, the amount of polymer and ionic liquid in the cast solutions determined the weight percent of ionic liquid in the composite membranes. Since the zwitterionomer used in this study contained 8 mol% SBMA, a composite membrane containing 13.5 wt% EMIm ES would bear equimolar of zwitterionic functionalities and ionic liquid.

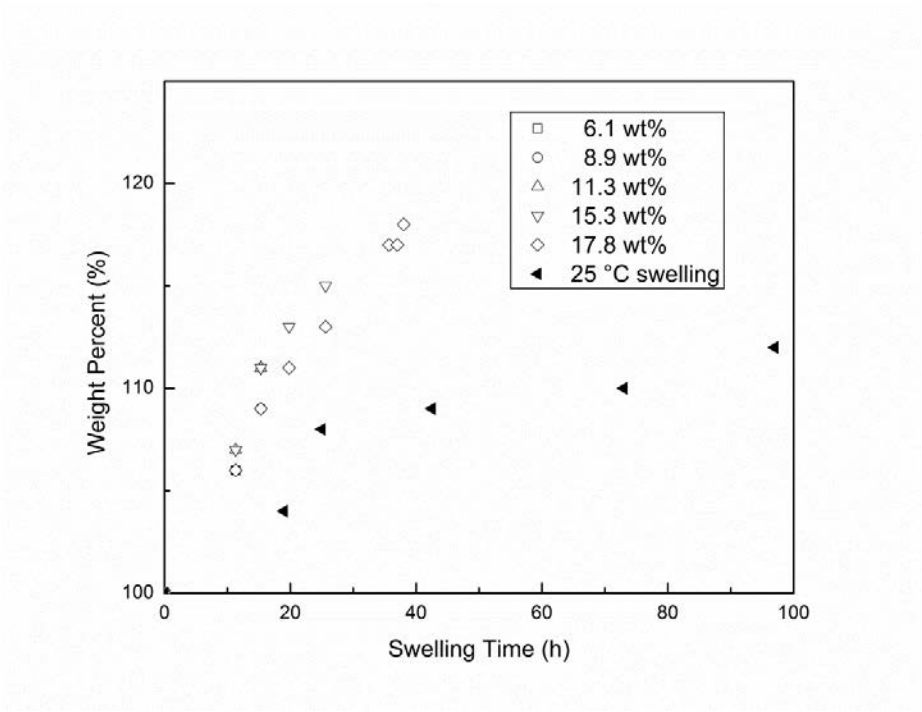

Figure 4.3. Swelling behavior of poly(nBA$_{92}$-*co*-SBMA$_8$) at 65 °C as a function of time. Filled data points illustrate the swelling profile for a similar sample at 25 °C.[23]

4.4.3 Dynamic mechanical analysis of poly(nBA$_{92}$-*co*-SBMA$_8$) / EMIm ES composite membranes.

Figure 4.4 and **Figure 4.5** show the DMA traces for the "swollen" and the "cast with" membranes with different amount of IL incorporation, respectively. The DMA traces for the "dry" samples in both figures are the same, and it is a typical storage modulus *vs.* temperature trace for poly(*n*BA-*co*-SBMA). The first transition at ~ -33 °C corresponds to the glass transition of the *n*BA-rich phase. The transition temperature is slightly higher than the $T_{g,\ DSC}$ (-46 °C) for poly(*n*BA) due to the mechanistic difference between the two characterization techniques. The second transition at ~ 110 °C is referred to as the flow temperature. It corresponds to the dissociation of the clustered phase, where chain mobility is reduced due to strong electrostatic interactions between the

zwitterionic functionalities.[30, 31] In between the two transition temperatures, the storage moduli of the dry zwitterionomer exhibited a plateau at ~ 10 MPa. The presence of this rubbery plateau is indicative of a zwitterionomer's biphasic morphology, in agreement with what Ehrmann et al. and Gauthier et al. had reported.[30, 32] In an earlier study, we compared thermomechanical property of zwitterionomers with that of structurally similar cationomers, and attributed the superior elastomeric performance, specifically broader rubbery plateaus, of the zwitterionomers to the stronger electrostatic interactions between the sulfobetaine functionalities, which served as the physical crosslinks in the membranes. [33]

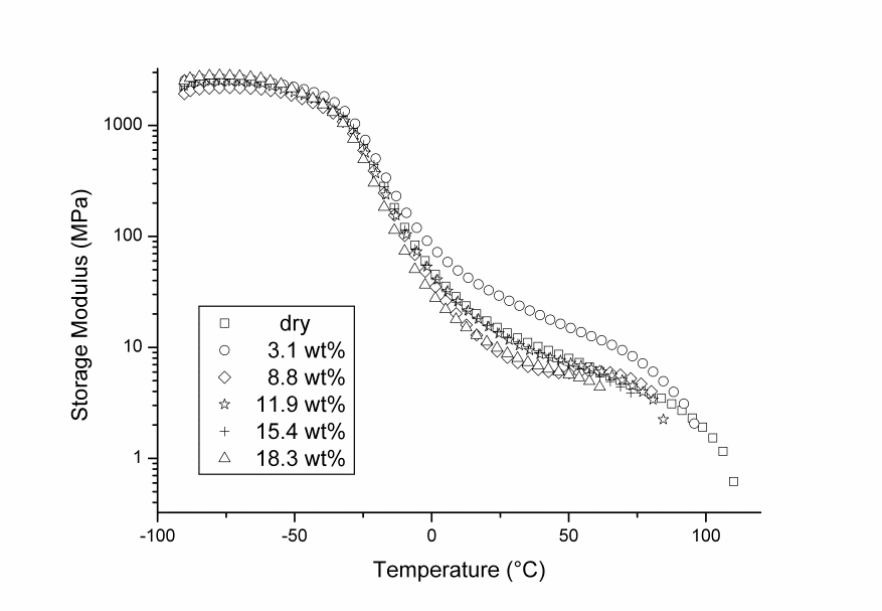

Figure 4.4. DMA traces for the "swollen" zwitterionomer / EMIm ES composite membranes.

For the "swollen" membranes, the DMA storage modulus *vs* temperature traces were almost identical with respect to their EMIm ES contents. Specifically, despite the flow occurred at lower temperatures for "swollen" samples with higher ionic liquid

contents, the glass transition temperatures of the *n*BA-rich phases, as well as the plateau moduli, of the "swollen" membranes were unaffected upon ionic liquid incorporation. In comparison, the "cast with" membranes showed that both transition temperatures decreased with increasing ionic liquid contents in the membranes. However, the flow temperatures decreased more rapidly than the glass transition temperatures. As a result, the breadth of the rubbery plateaus for the "cast with" membranes shortened gradually upon ionic liquid incorporation. At ionic liquid concentrations of 6 wt% and higher, the two thermomechanical transitions became so close that the rubbery plateaus became slopes instead. Since we attributed the second thermomechanical transition to the dissociation of the zwitterion-rich clustered phase, the DMA results suggested that the incorporation of ionic liquid into the zwitterionomer membranes weakened the electrostatic interactions between the sulfobetaine functionalities much more significantly through the "cast with" process than through the "swelling" process. Furthermore, the lowering of the glass transition temperatures with increasing IL concentrations in the "cast with" membranes indicated that more ionic liquid resided in the *n*BA-rich phase in "cast with" membranes with higher IL contents.

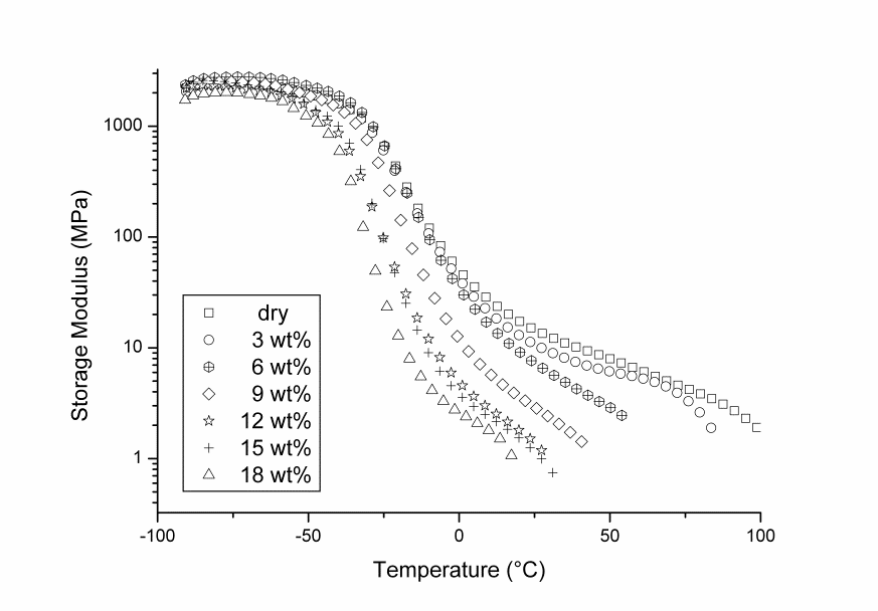

Figure 4.5 DMA traces for the "cast with" zwitterionomer / EMIm ES composite membranes.

4.4.4 Morphologies of poly(*n*BA_{92}-*co*-$SBMA_8$) / EMIm ES composite membranes

The morphologies of the zwitterionomer / ionic liquid composite membranes were probed using small-angle X-ray scattering (SAXS). Scattering profiles of the “swollen” and the “cast with” membranes, plotted as intensity *vs.* the scattering vector magnitude, q, are shown in **Figure 4.6** and **Figure 4.7**, respectively. A scattering peak near $q \approx 0.15$ $Å^{-1}$ was observed for the dry zwitterionomer membrane, in agreement with our previous report.[33] Such scattering profile is typical of charge-containing polymers,[31] and the scattering peak is referred to as the “ionomer peak”. It reflects the periodic arrangement of and the different electron densities between the zwitterionic aggregates and their surrounding matrix.

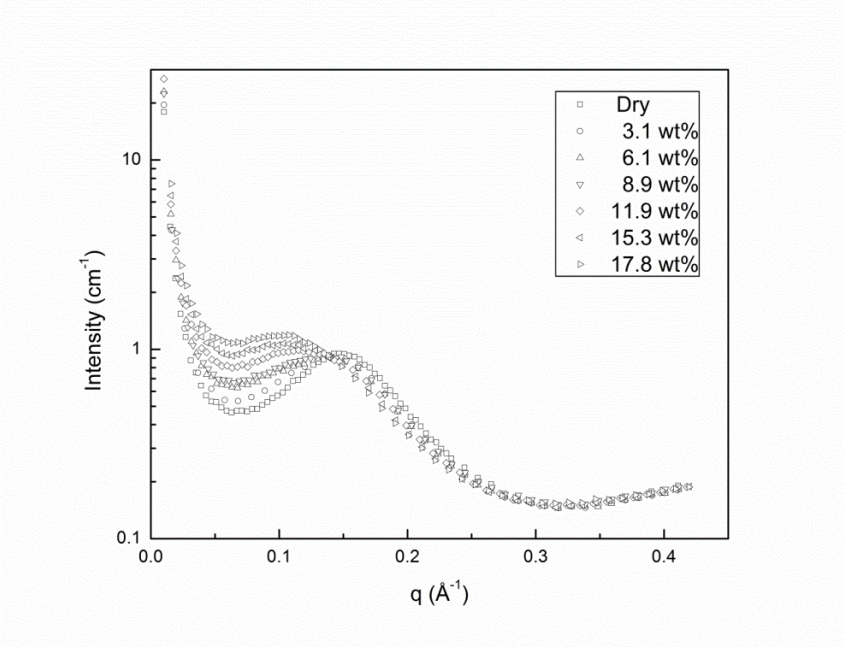

Figure 4.6. SAXS intensity *vs.* scattering vector (q) traces for the "swollen" zwitterionomer / ionic liquid composite membranes containing varying amounts of ionic liquid

Upon ionic liquid incorporation, the scattering profiles for the "swollen" membranes broadened gradually with increasing ionic liquid contents in the membranes. Specifically, all scattering traces overlapped very nicely at q higher than 0.3 $Å^{-1}$. However, as the peak positions of the scattering profiles shifted slowly toward lower q with increasing IL concentrations, the slope on the high q side of the scattering peak decreased gradually, while the low q side of the scattering peak shouldered. Slight increases in the scattering intensities were also observed for "swollen" membranes with higher IL contents. In comparison, the shape of the scattering profiles for the "cast with" membranes seemed unaffected with up to 18 wt% ionic liquid incorporation. All scattering traces for the "cast with" samples also overlapped very nicely at q higher than 0.3 $Å^{-1}$. However, the slopes on the high q side of the scattering peaks were maintained as

the scattering peaks shifted toward lower q. No shouldering on the low q side of the scattering peaks was observed as the scattering intensities increased slightly upon incorporation of ionic liquid into the “cast with” membranes.

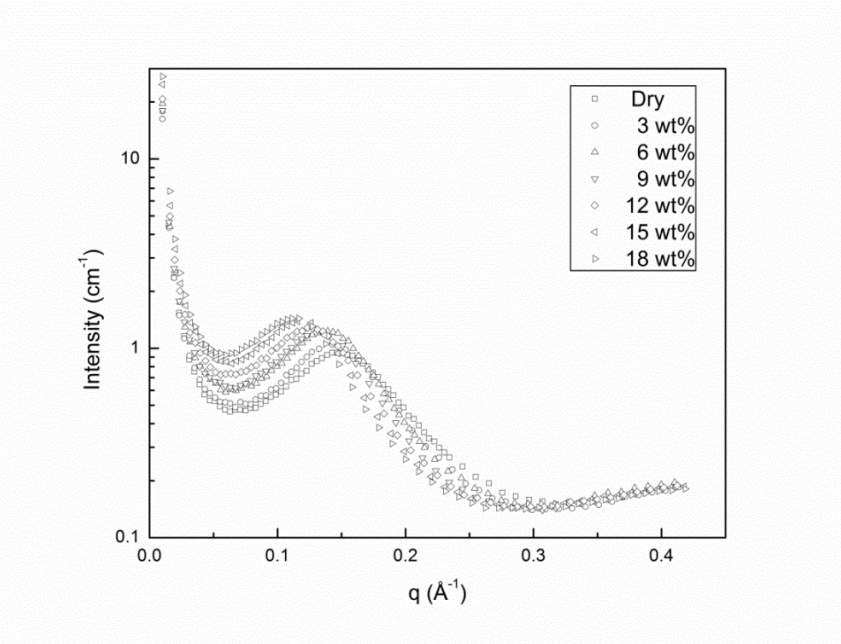

Figure 4.7. SAXS intensity *vs.* scattering vector (q) traces for the “cast with” zwitterionomer / ionic liquid composite membranes containing varying amounts of ionic liquid

All scattering traces for the composite membranes suggested micro-phase separated morphologies with zwitterionic aggregates dispersed in a matrix of *n*BA. The broadening of the scattering profiles for the “swollen” samples indicated that a portion of the morphological features that existed in the dry zwitterionomer membrane were not affected by the incorporation the ionic liquid. We speculate that it is these unaffected morphological features that helped to maintain the thermomechanical performance of the “swollen” membranes.

Quantitative analyses of the SAXS data were performed for both the "swollen" and the "cast with" samples, as we have previously described,[27] using a liquid-like interparticle interference model as proposed by Yarusso and Cooper, and incorporating the Percus-Yevick structure factor, first used by Kinning and Thomas to model the scattering from spherical morphologies in block copolymers and later applied to ion-containing polymer by Ding et al.[34-37] The following general equation describes the scattered intensity of a sample from this model:

$$\frac{I}{I_e V} = \frac{1}{v_p}\left(\frac{4\pi R_1^3}{3}\right)^2 \Delta\rho^2 \emptyset^2(qR_1) S(q, R_{ca}, R_1, v_p)$$

where I_e is the scattering from a single electron, V is the scattering volume, v_p is the volume of material per ionic aggregate, R_1 is the radius of the ionic aggregate, R_{ca} is the radius of closest approach, and $\Delta\rho$ is the difference in electron densities between the ionic aggregates and the matrix. $\Phi(qR_1)$ and $S(q, R_{ca}, R_1, v_p)$ are the form factor and the structure factor, respectively. The calculation of the Percus-Yevick structure factor followed the detailed expressions of Ding et al.[37] A Lorentzian peak, centered at 0.41 $Å^{-1}$ was added to the intensity function to represent poly(*n*-butyl acrylate) interchain scattering[38] and to improve the high-q fit.

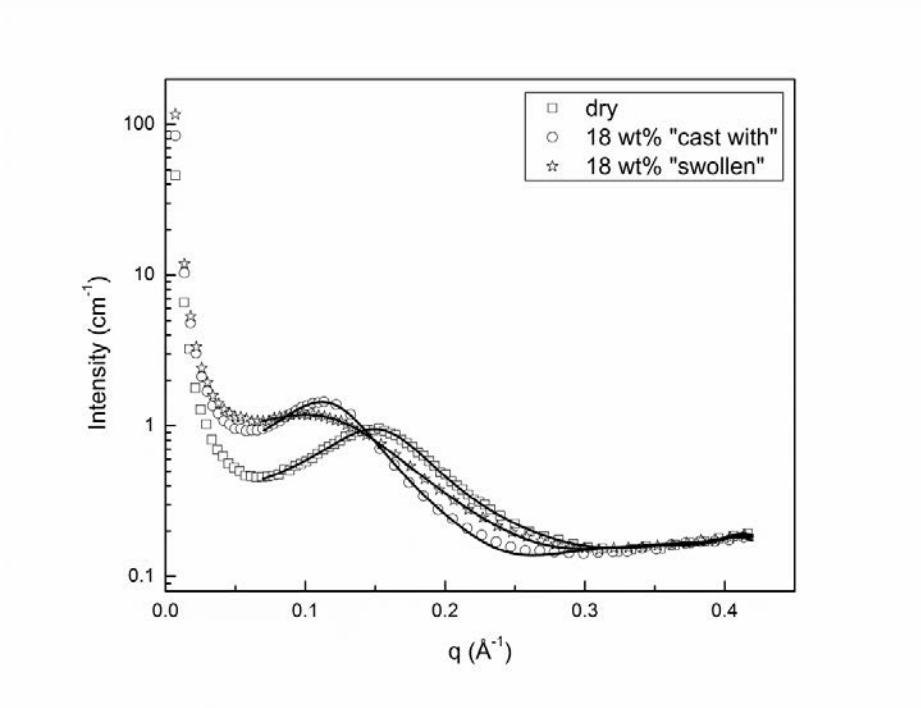

Figure 4.8. Fitting of the SAXS traces for the dry zwitterionomer membrane and composite membranes with the highest IL contents to the Kinning-Thomas model.

Good fits were obtained for all samples investigated in this study over the q range between 0.07 $Å^{-1}$ and 0.41 $Å^{-1}$. **Figure 4.8** shows representative modeling results for the dry zwitterionomer, as well as the "swollen" and the "cast with" samples containing the highest ionic liquid contents. The fitting parameters ($\Delta\rho$, R_1, R_{ca} and v_p) as a function of ionic liquid contents in the membranes are summarized in **Table 4.1**.

For the "cast with" samples, $\Delta\rho$, the difference in electron density between the zwitterionic aggregates and the matrix, were maintained at all ionic liquid concentrations investigated. Considering that the ionic liquid should have different bulk electron density from either the *n*BA-rich phase or the zwitterion-rich phase, the modeling results suggested that the ionic liquid was distributed rather evenly across the membrane during a "cast with" process. Therefore, a portion of the incorporated IL should reside inside the

zwitterionic aggregates in a “cast with” membrane. Consequently, the size of the zwitterionic aggregates, R_1, should increase, also in agreement with the modeling results. The presence of the polar guest molecules inside the zwitterionic aggregates would weaken the electrostatic interactions between sulfobetaine functionalities, and, hence, contribute to the loss of mechanical performance for the “cast with” membranes.

Table 4.1 Summary of the fitting parameters for “dry”, “swollen” and “cast with” zwitterionomer membranes

	IL Contents (wt%)	$\Delta\rho$ (10^{21} cm^{-3})	R_1 (nm)	R_{ca} (nm)	v_p (nm^3)
Swollen	3.1	42	1.38	2.00	138
	6.1	45	1.38	2.00	168
	8.9	46	1.38	2.00	172
	11.9	52	1.40	2.00	230
	15.3	52	1.47	2.03	286
	17.8	58	1.50	2.19	381
Dry	0.0	40	1.38	2.00	116
Cast with	3.0	40	1.45	2.10	131
	6.0	40	1.53	2.17	144
	9.0	40	1.54	2.21	165
	12.0	40	1.59	2.27	192
	15.0	40	1.66	2.37	232
	18.0	40	1.71	2.46	272

In comparison, for the “swollen” samples containing less than 12 wt% ionic liquid, significant increases in Δρ with increasing IL contents in the membranes were observed. Such changes in Δρ, coupled with little change in R_1, indicated that the incorporated ionic liquid resided mainly outside the zwitterionic aggregates. As a result, the strong electrostatic interactions between the sulfobetaine functionalities persisted in the “swollen” membranes.

Figure 4.9 is a simplified illustration of the possible local arrangement of ionic liquid with respect to the zwitterionic aggregates for both “swollen” and “cast with” membranes. Based on the DMA and the SAXS results, we hypothesize that, during the IL swelling process, the ionic liquid was attracted to the polar zwitterionic phase, but resided outside the zwitterionic aggregates. As a result, the physical crosslinks that resulted from the zwitterionic interactions persisted, and the mechanical performance of the “swollen” membranes was maintained at 18 wt% IL incorporation. In comparison, during the “cast with” process, the ionic liquid likely intercalated into the zwitterionic aggregates, hence weakened the electrostatic interactions that provided the physical crosslinks and shortened the rubbery plateaus of the composite membranes with gradual increase of ionic liquid contents.

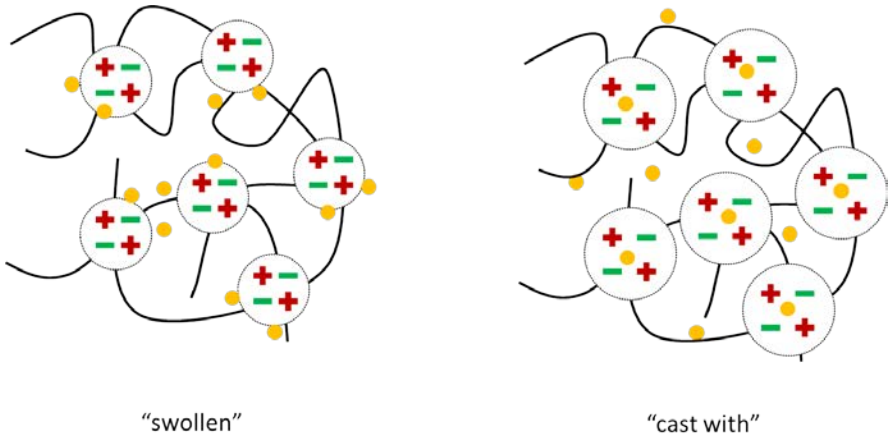

Figure 4.9. Possible arrangement of ionic liquid in 'swollen" and "cast with" zwitterionomer membranes

4.4.5 Ionic conductivities of poly(*n*BA$_{92}$-*co*-SBMA$_8$) / EMIm ES composite membranes

The thru-plane ionic conductivity of the composite membranes was measured using alternative current impedance spectroscopy under ambient conditions. **Figure 4.10** shows the ionic conductivity of the composite membranes as a function of their ionic liquid contents. The neat zwitterionomer exhibited characteristics of a pure resistor in impedance spectroscopy, and is not ionic conductive. The "cast with" membranes showed a 5 orders of magnitude increase in ionic conductivity, as their ionic liquid contents increased from 3 wt% to 18 wt%. This increase agreed with our proposed morphological model that the ionic liquid distributed more evenly inside the "cast with" membranes. In comparison, at low to moderate ionic liquid concentrations (< 12 wt%), the "swollen" membranes had similar ionic conductivity values to those of the "cast with" membranes. However, for the "swollen" membranes, the exponential increase in ionic conductivity reached plateau after 12 wt% of ionic liquid incorporation. It is likely

that the persistence of the zwitterionic aggregates in the “swollen” membranes hindered formation of ion-conductive channels.

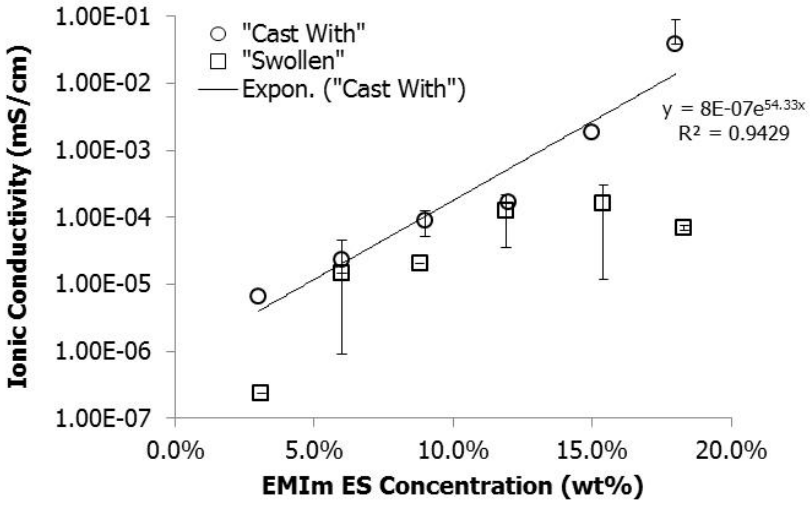

Figure 4.10. Ionic conductivity of both “swollen” and “cast with” zwitterionomer / ionic liquid composite membranes as a function of EMIm ES concentration

4.5 Conclusions

Zwitterionomer / ionic liquid composite membranes prepared using the “swelling” and the “cast with” methods exhibited very different thermomechanical performance, morphologies and ionic conductivity. Dynamic mechanical analysis showed that the “swollen” membranes maintained their thermomechanical performance with up to 18 wt% EMIm ES, while that of the “cast with” membranes decreased gradually as the ionic liquid contents in the composite membranes increased. Quantitative analysis of the SAXS data revealed that the sample preparation method impacted the distribution of ionic liquid inside the composite membranes. Specifically, for the “swollen” membranes, the zwitterionic aggregates existed prior to the introduction of ionic liquid into the membranes, and they resisted the intercalation of ionic liquid during the swelling process.

Conversely, for the "cast with" membranes, the presence of the polar guest molecules during the membrane casting process hindered the formation of the zwitterionic aggregates, which functioned as the physical crosslinks in the "swollen" membranes. Impedance spectroscopy results showed that the ionic conductivity for the "swollen" membranes plateaued at ionic liquid concentrations higher than 12 wt%. This deviation from the exponential increase in ionic conductivity was likely the result of the persistence of the zwitterionic aggregates in the "swollen" membranes as well.

In summary, the zwitterionic aggregates in poly(*n*BA-*co*-SBMA) served as both the physical crosslinks and the host sites for ionic conductive guest molecules. Upon ionic liquid incorporation, a trade-off between thermomechanical performance and ionic conductivity of the composite membranes was observed. In order for the matrix polymer to maintain its mechanical performance during the compositing process, it is necessary to have reinforcing mechanism, such as crystallinity or hydrophobic interactions, that won't be disrupted by the polar guest molecules.

4.6 Acknowledgements

This material is based upon work supported by the U.S. Army Research Laboratory and the U.S. Army Research Office under grant number W911NF-07-1-0339.

4.7 References

1. Visser, A. E.; Swatloski, R. P.; Reichert, W. M.; Mayton, R.; Sheff, S.; Wierzbicki, A.; Davis, J. H.; Rogers, R. D. *Environmental Science & Technology* **2002,** 36, (11), 2523-2529.
2. Walden, P. *Bull. Acad. Imp. Sci. St.-Petersbourg* **1914**, 405-22.
3. Wilkes, J. S.; Levisky, J. A.; Wilson, R. A.; Hussey, C. L. *Inorganic Chemistry* **1982,** 21, (3), 1263-1264.
4. Green, M. D.; Long, T. E. *Polymer Reviews* **2009,** 49, (4), 291-314.
5. Przemyslaw, K. *Progress in Polymer Science* **2004,** 29, (1), 3-12.

6. Zhu, S.; Wu, Y.; Chen, Q.; Yu, Z.; Wang, C.; Jin, S.; Ding, Y.; Wu, G. *Greem Chemistry* **2006,** 8, (4), 325-327.
7. El Seoud, O. A.; Koschella, A.; Fidale, L. C.; Dorn, S.; Heinze, T. *Biomacromolecules* **2007,** 8, (9), 2629-2647.
8. Pinkert, A.; Marsh, K. N.; Pang, S.; Staiger, M. P. *Chemical Reviews* **2009,** 109, (12), 6712-6728.
9. Huddleston, J. G.; Rogers, R. D. *Chem. Commun. (Cambridge)* **1998**, (16), 1765-1766.
10. Visser, A. E.; Swatloski, R. P.; Reichert, W. M.; Davis, J. H., Jr.; Rogers, R. D.; Mayton, R.; Sheff, S.; Wierzbicki, A. *Chem. Commun. (Cambridge)* **2001**, (1), 135-136.
11. Luo, S.; Zhang, Z.; Yang, L. *Chinese Science Bulletin* **2008,** 53, (9), 1337-1342.
12. Papageorgiou, N.; Athanassov, Y.; Armand, M.; Bonhote, P.; Pettersson, H.; Azam, A.; Gratzel, M. *Journal of the Electrochemical Society* **1996,** 143, (10), 3099-3108.
13. Carlin, R. T.; Fuller, J. *Chem. Commun. (Cambridge)* **1997**, (15), 1345-1346.
14. Bennett, M. D.; Leo, D. J.; Wilkes, G. L.; Beyer, F. L.; Pechar, T. W. *Polymer* **2006,** 47, (19), 6782-6796.
15. Ding, J.; Zhou, D.; Spinks, G.; Wallace, G.; Forsyth, S.; Forsyth, M.; MacFarlane, D. *Chemistry of Materials* **2003,** 15, (12), 2392-2398.
16. Lu, W.; Fadeev, A. G.; Qi, B.; Smela, E.; Mattes, B. R.; Ding, J.; Spinks, G. M.; Mazurkiewicz, J.; Zhou, D.; Wallace, G. G.; MacFarlane, D. R.; Forsyth, S. A.; Forsyth, M. *Science* **2002,** 297, (5583), 983-987.
17. Fukushima, T.; Asaka, K.; Kosaka, A.; Aida, T. *Angewandte Chemie International Edition* **2005,** 44, (16), 2410-2413.
18. Bennett, M. D.; Leo, D. J. *Sensors and Actuators A: Physical* **2004,** 115, (1), 79-90.
19. Galin, M.; Chapoton, A.; Galin, J. C. *Journal of the Chemical Society-Perkin Transactions 2* **1993**, (3), 545-553.
20. Koberle, P.; Laschewsky, A. *Macromolecules* **1994,** 27, (8), 2165-2173.
21. Galin, M.; Marchal, E.; Mathis, A.; Galin, J.-C. *Polymers for Advanced Technologies* **1997,** 8, (2), 75-86.
22. Cardoso, J.; Huanosta, A.; Manero, O. *Macromolecules* **1991,** 24, (10), 2890-2895.
23. Brown, R. H.; Duncan, A. J.; Choi, J. H.; Park, J. K.; Wu, T. Y.; Leo, D. J.; Winey, K. I.; Moore, R. B.; Long, T. E. *Macromolecules* **2010,** 43, (2), 790-796.
24. Ishioka, T.; Kobayashi, M. *Macromolecules* **1990,** 23, (12), 3183-6.
25. Gebel, G.; Lambard, J. *Macromolecules* **1997,** 30, (25), 7914-7920.
26. Wu, T.; Beyer, F. L.; Brown, R. H.; Moore, R. B.; Long, T. E. *Macromolecules* **2011**.
27. Wu, T.; Beyer, F. L.; Brown, R. H.; Moore, R. B.; Long, T. E. *Macromolecules* **2011,** 44, (20), 8056-8063.
28. Ilavsky, J.; Jemian, P. R. *Journal of Applied Crystallography* **2009,** 42, (2), 347-353.
29. Tong, J. D.; Jerome, R. *Polymer* **2000,** 41, (7), 2499-2510.

30. Ehrmann, M.; Muller, R.; Galin, J. C.; Bazuin, C. G. *Macromolecules* **1993,** 26, (18), 4910-4918.
31. Eisenberg, A.; Hird, B.; Moore, R. B. *Macromolecules* **1990,** 23, (18), 4098-4107.
32. Gauthier, M.; Carrozzella, T.; Snell, G. *Journal of Polymer Science Part B-Polymer Physics* **2002,** 40, (19), 2303-2312.
33. Wu, T. Y.; Beyer, F. L.; Brown, R. H.; Moore, R. B.; Long, T. E. *Macromolecules* **2011,** 44, (20), 8056-8063.
34. Yarusso, D. J.; Cooper, S. L. *Macromolecules* **1983,** 16, (12), 1871-80.
35. Percus, J. K.; Yevick, G. J. *Phys. Rev.* **1958,** 110, 1-13.
36. Kinning, D. J.; Thomas, E. L. *Macromolecules* **1984,** 17, (9), 1712-18.
37. Ding, Y. S.; Register, R. A.; Yang, C.; Cooper, S. L. *Polymer* **1989,** 30, (7), 1213-20.
38. Miller, R. L.; Boyer, R. F.; Heijboer, J. *J. Polym. Sci., Polym. Phys. Ed.* **1984,** 22, (12), 2021-41.

4.8 Supplemental Information

Figure 4.11 is the ^{1}H NMR of poly(*n*BA-*co*-SBMA) in $CDCl_3$. Peak 'a' at 0.95 ppm was assigned to the methyl group on *n*BA, and peak 'b' at 3.36 ppm was assigned to the two methyl groups on the quaternized "*N*" of SBMA. The amount of SBMA in the copolymer was determined using the following equation:

$$SBMA\,mol\% = \frac{b}{b+2a} \cdot 100\%$$

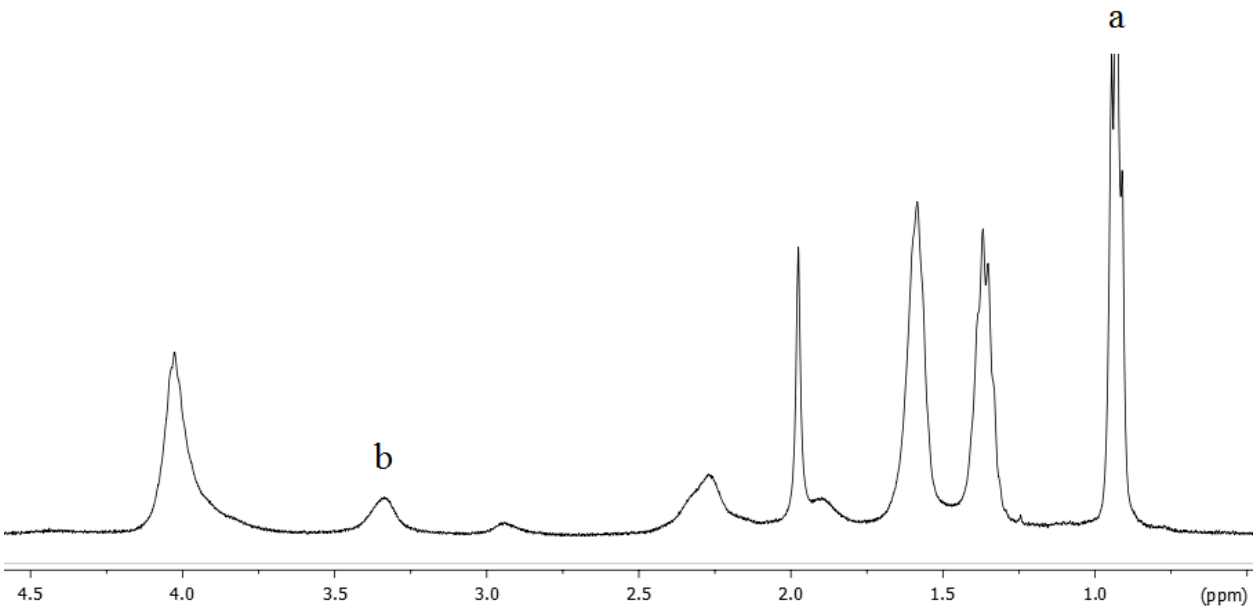

Figure 4.11 ^{1}H NMR of poly(*n*BA-*co*-SBMA) in $CDCl_3$

Chapter 5 RAFT Synthesis of Poly(sty-*b*-acrylate-*b*-sty) with Tunable Polarity as Host Matrices to Ionic Liquids for Electro-Active Applications

(Tianyu Wu,[†] Dong Wang,[‡] Mingqiang Zhang,[†] James R. Heflin,[‡] Robert B. Moore,[†] and Timothy E. Long[†,])*

[†]*Department of Chemistry, Macromolecules and Interfaces Institute;* [‡]*Department of Physics, Virginia Tech, Blacksburg, Virginia 24061*

*To whom correspondence should be addressed: Email telong@vt.edu

5.1 Abstract

2-(Dimethylamino)ethyl acrylate (DMAEA) imparts versatile functionality to poly[Sty-*b*-(*n*BA-*co*-DMAEA)-*b*-Sty] ABA triblock copolymers. A controlled synthetic strategy minimized chain transfer reactions and enabled the preparation of high molecular weight ABA triblock copolymers with relatively narrow PDIs using reversible addition-fragmentation chain transfer (RAFT) polymerization. The presence of tertiary amine functionality and their zwitterionic derivatives in the central blocks of the triblock copolymers afforded tunable polarity toward ionic liquids. Gravimetric measurements determined the swelling capacity of the triblock copolymers for EMIm TfO and EMIm ES ionic liquids (IL). A correlation of DSC, DMA and SAXS results revealed the impact of ionic liquid incorporation on the thermal transitions, thermomechanical properties, and morphologies of the triblock copolymers. IL-containing membranes of DMAEA-derived triblock copolymers and EMIm TfO exhibited desirable rubbery plateau moduli of ~ 100 MPa and electro-mechanical actuation to a 4 V electrical stimulus. Maintaining the mechanical ductility of polymer matrices, while increasing their ion-conductivity, is paramount for future electro-active devices.

Key Words: acrylate, block copolymer, membrane, ionic liquid, actuator, SAXS

5.2 Introduction

Electromechanical transducers are devices that exhibit coupling between electrical stimuli and mechanical response.[1] Over the past decade, electro-active polymers have attracted increasing interest due to their flexibility, light weight, facile processability, and low fabrication cost.[1-4] One emerging class of electro-active polymers for electromechanical transducers is ion-containing polymers such as Nafion®. A typical ionic polymer transducer (IPT) assembly consists of an ionic polymer membrane between two conductive electrodes. Akle and Leo proposed that mobile ions within the device accumulated at the electrodes upon charging the IPT, resulting in volume change and bending actuation.[5] However, typical Nafion®-based IPTs operate under hydrated conditions, where the hydrated protons serve as the mobile cations. As a result, their performance deteriorates as water evaporates and electrolysis occurs over time.[6]

Ionic liquids are organic salts that exhibit low melting points, typically below 100 °C.[7] Their structural tunability, chemical and thermal stabilities, low vapor pressure and high ionic conductivity render them promising substitutes for water in IPT applications.[8, 9] Watanabe and coworkers explored the compatibility of various ionic liquid / homopolymer pairs,[10] and they reported that polymerization of methacrylic monomers in the presence of various ionic liquids resulted in homogeneous ionic gels with desirable high ionic conductivity.[11, 12] Lodge and coworkers also proposed that incorporating ionic liquids into block copolymer matrices afforded mechanical integrity and persistent nanostructure to the ionic liquids.[13] They further demonstrated the impact of EMIm-TFSI, an ionic liquid, on the phase behavior and the ionic conductivity of poly(styrene-

ethylene oxide) diblock copolymers.[14, 15] Our research group has explored the use of polar sulfobetaine functionalities for desirable interactions with 1-ethyl-3-methylimidazolium ethyl sulfate, EMIm-ES.[16] We found that the ionic liquid preferentially swelled the zwitterionic domains and significantly impacted thermomechanical performance and ionic conductivity of the zwitterionomer membranes.

More recently, Choi and Colby et al. studied ionic conduction and dielectric response of poly(imidazolium acrylate) homopolymers with various counteranions and alkyl tail lengths on the pendant imidazolium structures.[17] They employed a physical model of electrode polarization to separate the ionic conductivity of the poly(imidazolium acrylate)s into number density of conducting ions and their mobility. Their analyses of the static dielectric constants revealed the presence of more ionic aggregates in poly(imidazolium acrylate)s with longer alkyl tails, in agreement with the X-ray scattering results. Gwee, Winey and Elabd et al. investigated the effect of morphology on the ion transport of this ionic liquid in poly(sty-*b*-MMA).[18] They observed higher through-plane conductivities in cylindrical morphologies with non-conducting polystyrene cylinders than in lamellar morphologies. They also reported that the ionic conductivity was direction-independent when the morphologies have a continuous conductive path. Imaizumi et al. also further studied the morphology and the viscoelastic properties of ion-gels that consisted of a well-defined poly(sty-*b*-MMA-*b*-sty) triblock copolymer and EMIm-TFSI using AFM and rheology, respectively.[19] They demonstrated that the ion-gel actuator bent softly toward the anode under less than 3.0 V of low applied voltage. However, due to the semi-crystalline behavior of poly(ethylene oxide) and the high glass transition temperatures of polystyrene and poly(methyl

methacrylate), earlier block copolymers were brittle in the absence of diluents, which complicated device fabrication.

In this study, we synthesized poly(sty-*b*-acrylate-*b*-sty) ABA triblock copolymers using the RAFT strategy. The central acrylic block contained quaternizable tertiary amine functionalities and exhibited low glass transition temperatures, which afforded flexible triblock copolymer membranes. The tertiary-amine containing acrylic phase and their zwitterionic derivatives exhibited tunable affinity for ionic liquids. Electro-mechanical transducers fabricated from these triblock copolymers showed electro-responsiveness. A correlation of differential scanning calorimetry (DSC), dynamic mechanical analysis (DMA), and small-angle X-ray scattering (SAXS) results elucidated the influence of ionic liquid incorporation on the thermal, thermomechanical, and morphological characteristics of the triblock copolymers and their IL-swollen membranes. To our knowledge, this is the first demonstration of non-PEG-based polymer that exhibited both a low glass transition temperature and compatibility with ionic liquids.

5.3 Experimental

Materials. Carbon disulfide (Aldrich, ≥99%), tetrabutylammonium hydrogen sulfate (Aldrich, ≥99%), 1,3-propanesultone (Aldrich, 99+%), Stoddard solvents (EMD), chloroform (Fischer Scientific, Optima®), acetone (Fischer Scientific, HPLC grade), methanol (Fischer Scientific, HPLC grade), hydrochloric acid (Fischer Scientific, certified ACS Plus), sodium hydroxide (Spectrum Chemical, ACS Reagent), 1-ethyl-3-methylimidazolium trifluoromethane-sulfonate (EMIm TfO, IoLiTec Inc., 99%), and 1-ethyl-3-methylimidazolium ethylsulfate (EMIm ES, Fluka, BASF quality ≥ 95%) were used as received. Styrene (Sty, Aldrich, ReagentPlus®, ≥99%), *n*-butyl acrylate (*n*BA,

Alfa Aesar, 98+%), and 2-(dimethylamino)ethyl acrylate (DMAEA, Aldrich, 98%) were deinhibited using neutral alumina columns and further distilled under reduced pressure from calcium hydride. Azobisisobutyronitrile (AIBN, Aldrich, 98%) was recrystallized from methanol.

RAFT synthesis of polystyrene precursor with S,S'-bis(α,α'-dimethyl-α"-acetic acid)-trithiocarbonate (TTC). The RAFT agent (TTC) was synthesized according to a literature procedure.[20] In a typical polymerization reaction, styrene (20 g, 0.19 mol), TTC (16.3 mg, 58 μmol), and AIBN (0.98 mg, 6.0 μmol) were charged to a 100-mL, round-bottomed flask equipped with a magnetic stir bar. The reaction mixture was subjected to three freeze-pump-thaw cycles to remove oxygen prior to polymerization and then placed into an oil bath at 65 °C. The reaction product had a targeted molecular weight of 345 kg/mol at full conversion. Aliquots were removed from the reaction flask under ultrahigh purity nitrogen atmosphere using a syringe at pre-determined time intervals throughout the polymerization. ^{1}H NMR spectroscopy and size exclusion chromatography (SEC) results determined the reaction kinetics and the product molecular weights, respectively. The reaction reached desired monomer conversion after 80 h. The reaction product was precipitated from THF into methanol and dried in a vacuum oven at 65 °C overnight.

Synthesis of poly[Sty-*b*-(*n*BA-*co*-DMAEA)-*b*-Sty]. In a typical central block insertion reaction, poly(Sty) precursor (1.0 g, 60 kg/mol, 17 μmol), *n*BA monomer (6.7 g, 52 mmol), and AIBN (0.3 mg, 1.8 μmol) were charged to a 50-mL, round-bottomed flask equipped with a magnetic stir bar. The molarity of AIBN was typically 1/10 of the poly(Sty) precursor, while the compositions of the acrylate monomers were either 100%

*n*BA or a 90/10 (molar ratio) *n*BA/DMAEA mixture. The reaction mixture was subjected to three freeze-pump-thaw cycles and then placed into an oil bath at 65 °C for 4 h. The reaction product was finally precipitated from THF into methanol and dried in a vacuum oven at 65 °C overnight. The triblock copolymer containing 10 mol% DMAEA in the central block is abbreviated as poly[Sty-*b*-(*n*BA-*co*-DMAEA)-*b*-Sty] or as DMAEA triblock copolymer.

Functionalization of poly[Sty-*b*-(*n*BA-*co*-DMAEA)-*b*-Sty] for sulfobetaine-containing derivatives. The molar concentration of DMAEA in poly[Sty-*b*-(*n*BA-*co*-DMAEA)-*b*-Sty] was calculated from the ^{1}H NMR spectra as obtained in $CDCl_3$ (see supporting information). In a typical functionalization reaction, poly[Sty-*b*-(*n*BA-*co*-DMAEA)-*b*-Sty] (1.0 g) and chloroform (6 mL) were charged to a 50-mL, round-bottomed flask equipped with a magnetic stir bar. Upon dissolution of the neutral triblock copolymer in chloroform, two equivalents of 1,3-propanesultone were charged to the reaction mixture. The reaction was refluxed for 20 h, and the final product was precipitated into methanol and vacuum dried. The sulfobetaine-containing triblock copolymer is abbreviated as poly[Sty-*b*-(*n*BA-*co*-SB-DMAEA)-*b*-Sty] or SB-DMAEA triblock copolymer.

Preparation of ionic liquid swollen poly(Sty-*b*-acrylate-*b*-Sty) membranes. The poly(Sty-*b*-acrylate-*b*-Sty) triblock copolymers had varying compositions in the central blocks, i.e. 100% *n*BA, 90/10 *n*BA/DMAEA, and 90/10 *n*BA/SB-DMAEA. The triblock copolymer membranes were first cast from 0.1 $g \cdot mL^{-1}$ chloroform solutions into PTFE molds to achieve film thicknesses of approximately 0.30 mm. The cast films were dried at room temperature overnight and annealed at 120 °C for 8 h under vacuum. The

dry membranes were immersed into either EMIm TfO or EMIm ES at 60 °C and stored under vacuum to minimize the impact of moisture uptake. The swollen membranes were periodically removed from the ionic liquid, blotted to remove excess of ionic liquid at the surfaces, and weighed to determine the amount of ionic liquid uptake in the membranes. The mass uptake of the ionic liquid was calculated using the following equation:

$$wt\%\ uptake = \frac{m - m_0}{m_0} \times 100\%$$

where m_0 is the initial dry mass of the film, and m is the mass of the swollen film at a given time. Once the amount of the ionic liquid uptake in the membranes plateaued, the swollen membranes were transferred to PTFE sheet covered petri dishes and stored at 25 °C under vacuum for further characterization.

Instrumentation. ^{1}H NMR spectra were obtained on a Varian Unity 400 MHz spectrometer in $CDCl_3$. Size exclusion chromatography (SEC) determined the molecular weights of the polymers at 35 °C in THF at 1 mL·min^{-1} flow rate. The THF SEC system was equipped with a Waters 717plus autosampler, a Waters 515 HPLC pump, three Polymer Laboratories PLGel 5µm Mixed-C columns, a Waters 2414 differential refractive index detector, and a Wyatt miniDAWN multiangle laser light scattering (MALLS) detector operating at a wavelength of 690 nm. Absolute molecular weights for poly(Sty) were calculated using the Wyatt ASTRA V software package with a specific refractive index increment value of 0.19.[21] Relative molecular weights to polystyrene standards for the triblock copolymer samples were reported using the Empower Pro software package.

Differential scanning calorimetry (DSC) measurements were performed on a TA Q100 instrument at a heating rate of 10 °C/min from -120 °C. The first heat scans were concluded at 150 °C, and traces of the second heats are reported. Dynamic mechanical analysis (DMA) was performed on a TA Q800 analyzer in tension mode at 1 Hz frequency, 15 μm amplitude, and 3 °C/min heating rate from -90 °C. Small angle X-ray scattering (SAXS) data were collected using a Rigaku S-Max 3000 SAXS system, equipped with 3 pinholes and a copper rotating anode emitting X-ray with a wavelength of 0.154 nm (Cu Kα). Two-dimensional SAXS patterns were obtained using a fully integrated 2D multiwire, proportional counting, gas-filled detector, with an exposure time of 1 hour. All SAXS data were analyzed using the SAXSGUI software package to obtain radially integrated SAXS intensity *vs.* scattering vector q plots. For all SAXS experiments, the sample-to-detector distance was 1603 mm, and the q range was calibrated using a silver behenate standard.

Fabrication and testing of poly(Sty-*b*-acrylate-*b*-Sty)-based electromechanical transducers. Electromechanical transducers were fabricated in a modified three-step process as previously reported.[22, 23] Specifically, the triblock copolymers were first cast from chloroform solutions at 0.1 $g \cdot mL^{-1}$ concentration onto silicone coated Mylar™ substrates with a drawdown blade set to 500 μm gap to achieve ~30 μm film thickness. Conductive network composite (CNC) coatings were then deposited onto the polymer membranes (~ 30 μm in thickness) using the layer-by-layer (LbL) technique[24] in order to provide a highly porous electronically and ionically conducting volume for storage of mobile ions. The 30-bilayer LbL CNCs were formed by alternately immersing the membrane in a cationic poly(allylamine hydrochloride) (PAH)

aqueous solution (10 mM, pH=4, Aldrich) and an anionic gold nanoparticle suspension (20 ppm, pH=9, diameter=3 nm, zeta potential=-40 mV, Purest Colloids Inc.) The alternate cationic and anionic layers were bound tightly through electrostatic self-assembly, generating uniform coatings with well-controlled thickness at the nanoscale through adjusting the number of layers. The membranes were subsequently immersed into EMIm TfO ionic liquid at 60 °C for 28 h. Gold foil (~ 50 nm in thickness) was finally hot pressed onto the outer surfaces of the devices at 60 °C and under 700 psi pressure for 20 s to serve as the electrodes. The actuator was then cut into 1 mm × 8 mm strips and subjected to a 4 V DC step voltage at 23 °C and 70% relative humidity. The bending response of the electromechanical transducer was recorded using a Sony HD Camcorder (Model HXR-MC1) with 30 fps.

5.4 Results and Discussions

5.4.1 RAFT synthesis of polystyrene and poly(Sty-*b*-acrylate-*b*-Sty) with S,S'-bis(α,α'-dimethyl-α"-acetic acid)-trithiocarbonate (TTC).

The past 15 years have witnessed rapid growth in the development and understanding of controlled radical polymerization (CRP) techniques, such as NMP,[25, 26] ATRP[27], and RAFT.[28] These strategies have enabled the incorporation of many functional monomers, which are typically incompatible with living ionic polymerization techniques, into polymers of advanced architectures and narrow polydispersity. Lai et al. first reported TTC-mediated RAFT polymerization of a variety of monomers and demonstrated the suitability of the short chain precursors for central block insertion reactions.[20] Ran et al. photo-initiated the synthesis of high molecular weight poly(Sty-*b*-*n*BA-*b*-Sty) triblock copolymers in the presence of TTC and demonstrated good

control.[29] However, to our knowledge, there is not a precedence of incorporating tertiary-amine containing acrylates into the central blocks of high molecular weight poly(Sty-*b*-acrylate-*b*-Sty)-type triblock copolymers for flexible membrane applications.

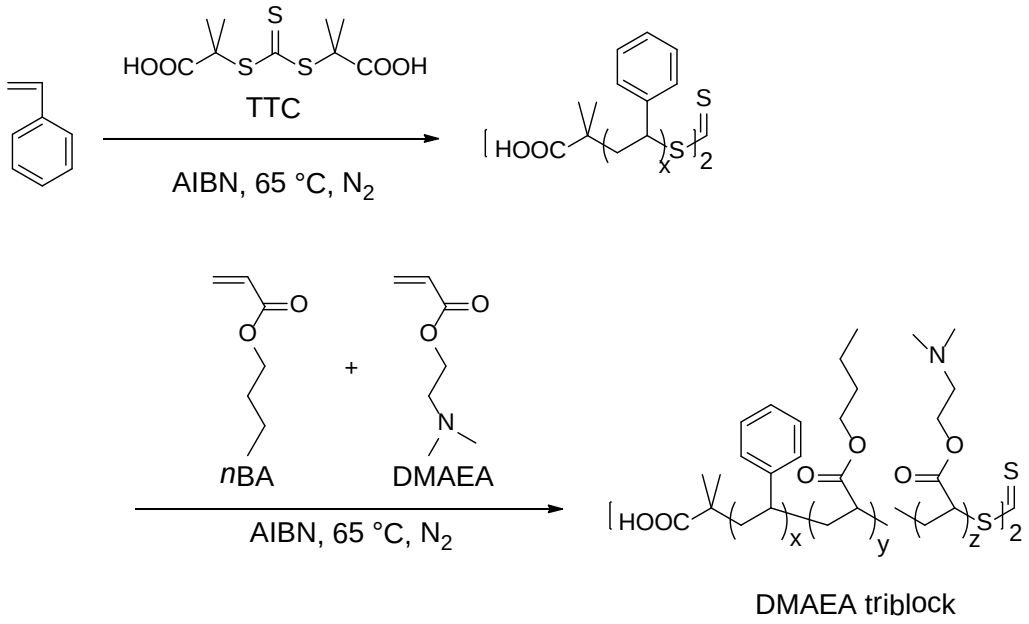

Scheme 5.1. Synthesis of poly[Sty-*b*-(*n*BA-*co*-DMAEA)-*b*-Sty] triblock copolymers, or DMAEA triblock

Scheme 5.1 illustrates the TTC-mediated RAFT polymerization of poly[Sty-*b*-(*n*BA-*co*-DMAEA)-*b*-Sty], where the central block contained a mixture of *n*BA and DMAEA units. Poly(Sty) precursor was first synthesized in bulk at a AIBN:TTC molar ratio of 1:10. The reaction exhibited pseudo-first order kinetics, and the molecular weights of the poly(Sty) products increased linearly as a function of the monomer conversion. Details of the reaction kinetics for TTC-mediated homopolymerization of styrene are provided in the supporting information.

The suitability of the poly(Sty) precursor for central block insertion depended on the choice of the acrylic monomers. Although the synthesis of poly(Sty-*b*-*n*BA-*b*-Sty)

was well controlled as indicated in **Table 5.4**, central block insertion reactions involving DMAEA presented challenges.[30] Conventional free radical polymerization of *n*BA in the presence of triethylamine (TEA) revealed that the propagating acrylic radicals chain transferred to TEA with a chain transfer constant (C_s) of 0.0240, which is on the same order of magnitude as chain transfer from poly(methyl acrylate) radicals to TEA (C_s ~ 0.0400).[21] Details of these calculations are also provided in the supporting information.

Since the success of controlled radical polymerization techniques rely on minimizing the propensity of propagating chain end to undergo undesirable chain transfer or termination, we targeted 10 mol% DMAEA in the acrylate monomer feed and reduced the molar AIBN:TTC ratio to 1:20 to improve the control over the central block insertion reaction. **Figure 5.1** shows the SEC chromatograms for the poly(Sty) precursor and poly[Sty-*b*-(*n*BA-*co*-DMAEA)-*b*-Sty] synthesized under these reaction conditions. The relative molecular weights of these polymers to poly(Sty) standards and their PDIs are summarized in **Table 5.3**. Three triblock copolymers were sampled from the same reaction at 4%, 6% and 12% monomer conversions. The shift of the SEC traces toward shorter elution time with increasing acrylate conversion indicated the growth of the central blocks for the triblock copolymers. Relatively narrow PDIs obtained for the triblock copolymers confirmed that the radical polymerization of the acrylates behaved in a controlled fashion. The tailing at the low molecular weight end of the distribution for the triblock copolymers suggested that chain transfer from the acrylic radicals to DMAEA was not completely eliminated during the polymerization process. Thus, the triblock copolymers presumably contained some poly[Sty-*b*-(*n*BA-*co*-DMAEA)] diblock contaminants. Nevertheless, a viable strategy for minimizing chain transfer to DMAEA

resulted in a library of poly[Sty-*b*-(*n*BA-*co*-DMAEA)-*b*-Sty] triblock copolymers for morphological studies and flexible host membranes for ionic liquids.

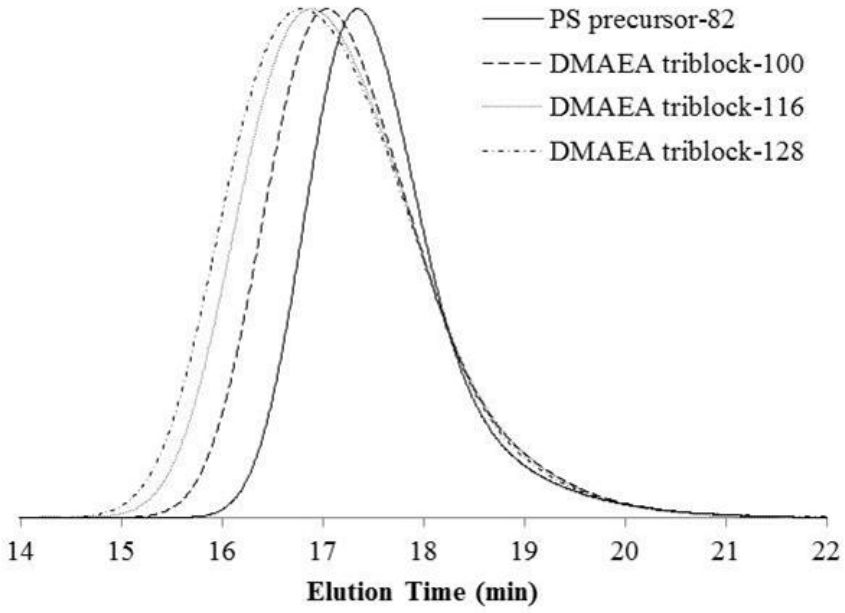

Figure 5.1 SEC traces for the PS precursor and DMAEA-containing triblock copolymers of varying central block lengths. All central blocks contained 10 mol% DMAEA. The abbreviations indicate the weight-average molecular weights of the final products (in $kg \cdot mol^{-1}$).

5.4.2 Functionalization of poly[Sty-*b*-(*n*BA-*co*-DMAEA)-*b*-Sty] for sulfobetaine-containing derivatives.

Scheme 5.2 illustrates the functionalization of poly[Sty-*b*-(*n*BA-*co*-DMAEA)-*b*-Sty] with 1,3-propanesultone. The characteristic ^{1}H NMR resonances for both neutral and sulfobetaine-containing triblock copolymers are shown in **Figure 5.14**. The ^{1}H NMR spectroscopic results confirmed complete conversion of DMAEA to its zwitterionic derivative in the triblock copolymer.

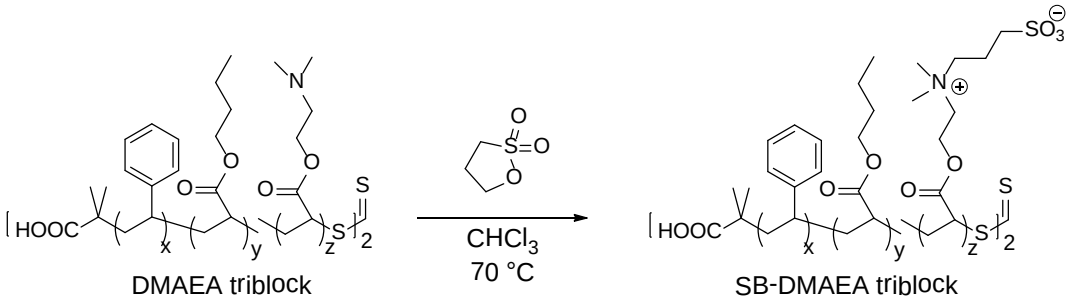

Scheme 5.2. Functionalization of DMAEA triblock copolymer with 1,3-propanesultone to form poly[Sty-*b*-(*n*BA-*co*-SBDMAEA)-*b*-Sty], or SB-DMAEA triblock

5.4.3 Swelling of poly(Sty-*b*-acrylate-*b*-Sty) triblock copolymers with ionic liquids.

The poly(Sty-*b*-acrylate-*b*-Sty) triblock copolymers varied in their central block compositions. Poly(Sty-*b*-*n*BA-*b*-Sty) contained a pure *n*BA central block, and both the DMAEA triblock and the SB-DMAEA triblock contained 90 mol% *n*BA in their central blocks. The SB-DMAEA triblock was directly derived from the DMAEA triblock. All three triblock copolymers had comparable relative molecular weights to polystyrene standards, and the values are listed in **Table 5.4**. **Figure 5.2** illustrates the chemical structures of the ionic liquids, and both EMIm TfO and EMIm ES contained 1-ethyl-3-methylimidazolium cations.

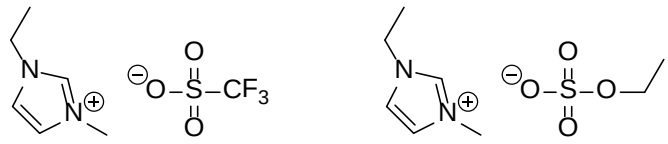

Figure 5.2. Chemical structures of the ionic liquids: (a) EMIm TfO and (b) EMIm ES

IL swelling studies were performed in a vacuum oven to reduce the impact of moisture uptake, and a 60 °C swelling temperature accelerated IL uptake. **Figure 5.3** and

Figure 5.4 show the swelling profiles for the triblock copolymers in EMIm TfO and EMIm ES, respectively. Poly(Sty-*b*-*n*BA-*b*-Sty) did not absorb appreciable ionic liquid (~ 0 wt%) in either EMIm TfO or EMIm ES over 100 h. Upon 10 mol% DMAEA incorporation into the central block, the tertiary amine-containing triblock copolymer exhibited significantly improved affinity toward EMIm TfO with a ~ 28 wt% uptake at equilibrium. However, it did not absorb EMIm ES; 0 wt% IL uptake was observed over 200 h.

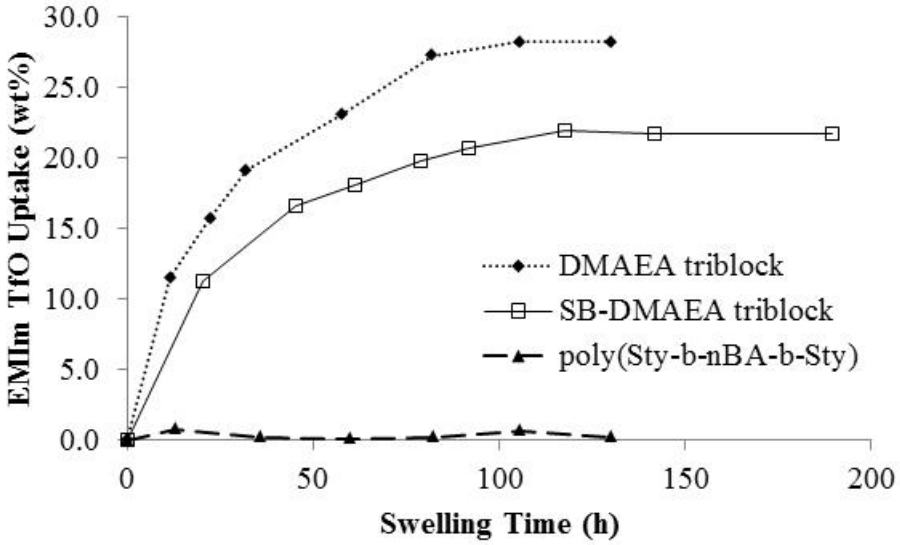

Figure 5.3. Swelling profiles for the triblock copolymers with EMIm TfO at 60 °C

In comparison, the SB-DMAEA triblock copolymer showed affinity toward both EMIm TfO and EMIm ES. While the zwitterionic triblock copolymer absorbed less EMIm TfO (~ 22 wt%) at a slower rate than the DMAEA triblock copolymer, swelling with EMIm ES achieved an equilibrium uptake of ~ 15 wt%. Tigelaar et al. studied water and ionic liquid uptake behavior of aromatic rigid-rod elastomeric polymers with imidazolium-trifluoromethanesulfonimide (imid-TFSI), imidazolium-trifluoromethanesulfonic acid (imid-CF_3SO_3H) and imidazolium-sulfuric acid (imid-

H_2SO_4). They reported similar dependence of equilibrium ionic liquid uptake on the pairing between the polymer matrix and the ionic liquid,[31] and they postulated that the observed difference was due to size differences between the ionic liquids and the free volume between the polymer chains. Nevertheless, our experimental results suggested that it is possible to adjust the affinity of the triblock copolymers toward polar guest molecules such as the ionic liquids.

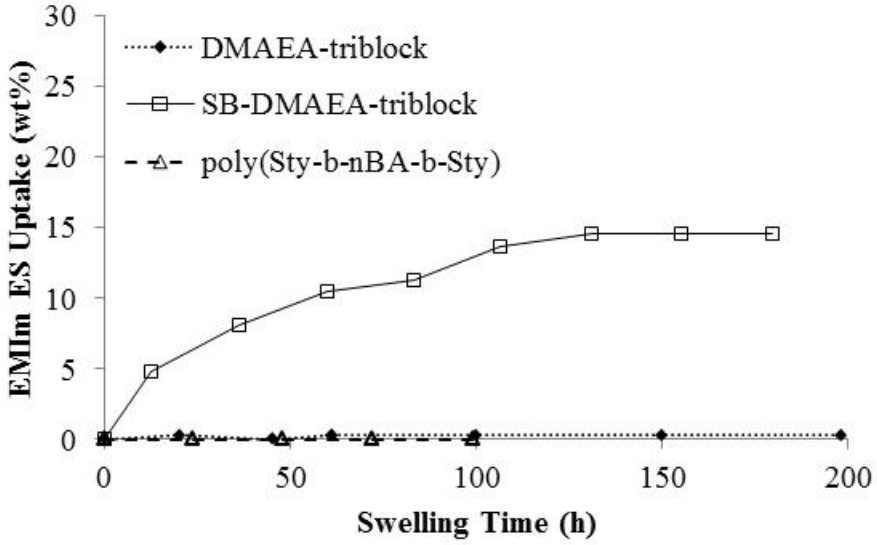

Figure 5.4. Swelling profiles for the triblock copolymers with EMIm ES at 60 °C

5.4.4 Thermal and thermomechanical properties of ionic liquid swollen poly(Sty-*b*-acrylate-*b*-Sty) membranes.

DSC results revealed the influence of the ionic liquids on the thermal transitions of the triblock copolymers. The glass transition temperatures of the triblock copolymers and their composites with ionic liquids, as well as the melting points of both EMIm TfO and EMIm ES, are summarized in **Table 5.1**. EMIm TfO exhibited a glass transition temperature of -95 °C and a melting temperature of -13 °C, while EMIm ES showed a glass transition temperature of -82 °C only, in agreement with earlier literature.[32, 33] The

presence of two T_gs for the triblock copolymers indicated microphase separation, which was independent of ionic liquid content. The higher T_g at ~ 100 °C corresponded to the poly(Sty) phase, and the lower T_g at ~ -40 °C corresponded to the acrylic phase.

The DSC results showed that the presence of either ionic liquid in the triblock copolymers had minimal impact on the glass transition temperatures of the poly(Sty) phase, suggesting that the ionic liquid resided mainly in the acrylic phase. The lower T_gs of the triblock copolymers increased noticeably upon EMIm TfO incorporation, while SB-DMAEA triblock copolymer showed minimal change with ~ 15 wt% EMIm ES incorporation. Koberle and Laschewsky studied the impact of stoichiometric amounts of NaI on the glass transition temperatures of sulfobetaine-containing homopolymers.[34] They observed increase in the glass transition temperatures of the homogeneous blends and attributed those increases to strong attractive interactions between the low molecular weight ions and the polymer-bound betaine functionalities. Similar molecular interactions presumably contribute to an increase in the T_g of SB-DMAEA triblock copolymer upon EMIm TfO incorporation. However, these interactions were not expected in neutral DMAEA triblock copolymers. Since EMIm TfO exhibited a melting point of -12 °C, higher than the T_g's of the acrylic phase, the addition of EMIm TfO may presumably reduce the amount of free volume in the triblock copolymers at temperatures below the melting point. As a result, the T_g's of the acrylic phase increased. Nevertheless, considering that poly(Sty-*b*-*n*BA-*b*-Sty) showed ~ 0 wt% uptake of either ionic liquid after 100 h of swelling, the impact of the chemical modifications in the central blocks of the triblock copolymers on their affinity toward polar guest molecules, such as the ionic liquids, was unexpected.

Table 5.1 Thermal transitions for the triblock copolymers with and without ionic liquids

Matrix	Ionic Liquid	$T_{g,1}$ (°C)	$T_{g,2}$ (°C)	T_m (°C)
DMAEA triblock copolymers	Without IL	-46	103	ND
	EMIm TfO (17-28 wt%)	-35 ± 1	106 ± 1	ND
SB-DMAEA triblock copolymers	Without IL	-36	105	ND
	EMIm TfO (22 wt%)	-30	106	ND
	EMIm ES (15 wt%)	-34	105	ND
/	EMIm TfO	-95	ND	-13
	EMIm ES	-83	ND	ND

ND = Not Detected

Figure 5.5 compares the DMA traces for the triblock copolymers with and without EMIm TfO. Rubbery plateaus spanning from -20 °C to 100 °C were observed for all samples. The presence of the ionic liquid only affected the glass transition temperatures of the acrylic phase, but the flow temperatures, which were associated with the T_g of the poly(Sty) phase, remained unchanged. This is in agreement with DSC data. The SB-DMAEA triblock copolymer in the neat state exhibited a plateau modulus about one order of magnitude higher than the neutral analog. However, upon ionic liquid incorporation, the plateau modulus for the sulfobetaine-containing triblock copolymer decreased significantly, while the DMAEA-containing triblock copolymer remained unchanged. We attributed this decrease in the storage modulus for the zwitterionic triblock copolymer to the dissociation of the strong electrostatic interactions between the sulfobetaine functionalities in the presence of ionic liquid. Since these electrostatic interactions are only present in the SB-DMAEA triblock copolymer, the observed different influences of EMIm TfO on the plateau moduli of the triblock copolymers was expected. Both IL composite membranes of DMAEA triblock and SB-DMAEA triblock

with EMIm TfO had plateau moduli of ~ 100 MPa, which was desirable for high moduli electro-active membranes.

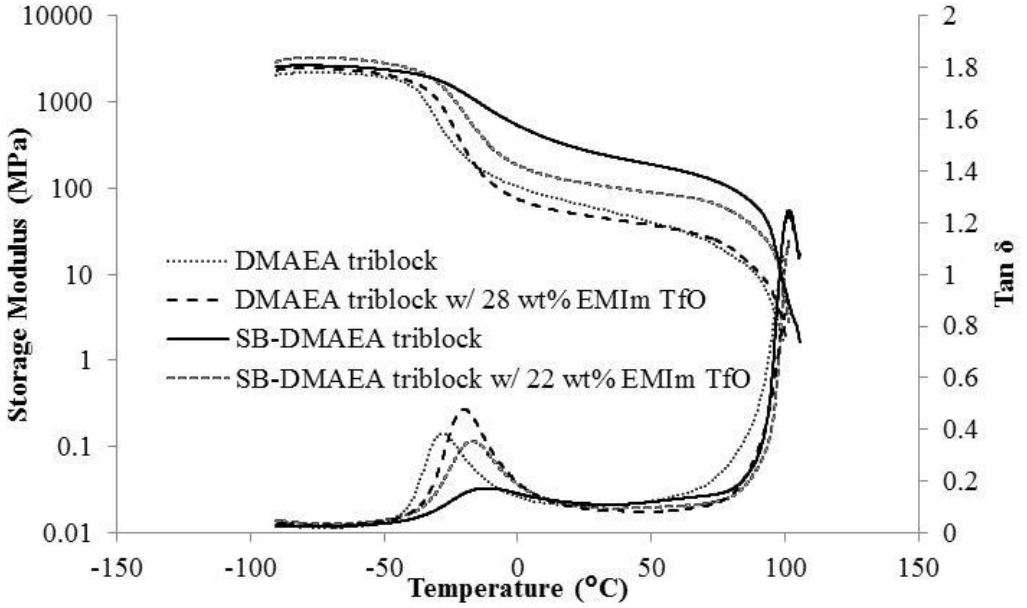

Figure 5.5. DMA traces for DMAEA triblock and SB-DMAEA triblock copolymers with and without EMIm TfO.

5.4.5 Morphologies of neat and ionic liquid swollen poly(Sty-*b*-acrylate-*b*-Sty) membranes.

Figure 5.6 compares SAXS traces for both DMAEA triblock and SB-DMAEA triblock copolymers without ionic liquid incorporation. The scattering trace for DMAEA triblock copolymer appeared featureless, while a distinctive scattering peak at ~1.5 nm^{-1} was observed for the SB-DMAEA triblock copolymer. We attributed a similar scattering peak earlier for a zwitterionic random copolymer to the difference in electron densities between the zwitterionic aggregates and their surrounding matrix.[35] In contrast, the presence of the sulfobetaine functionalities in the acrylic central blocks of the SB-DMAEA triblock copolymer likely resulted in ionic aggregation within the acrylic phase.

In addition, scattering signals at ~0.09 nm^{-1} and ~0.18 nm^{-1} for the SB-DMAEA triblock copolymer indicated that the strong electrostatic interactions between the sulfobetaine functionalities enhanced the long-range microphase separation of the triblock copolymer.

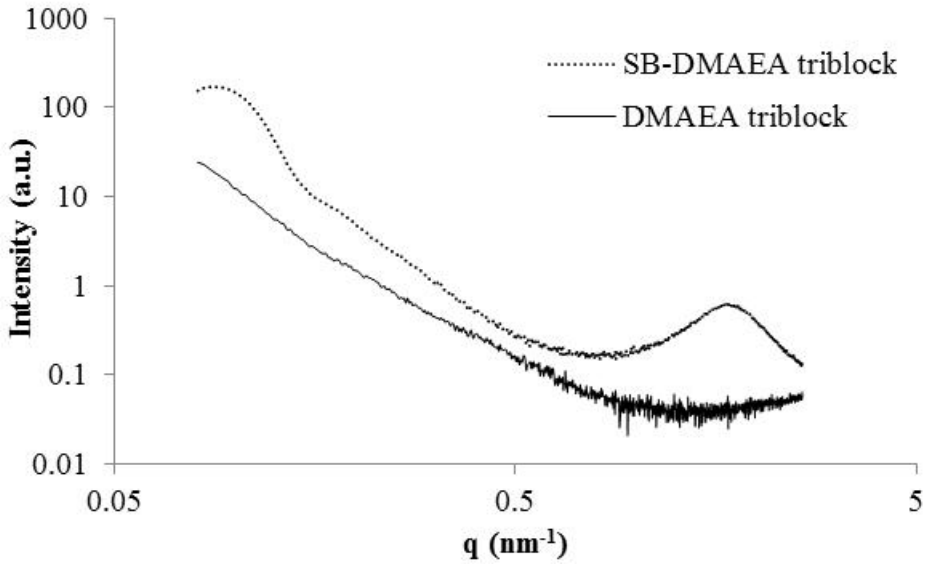

Figure 5.6. SAXS analysis of neat DMAEA- and SB-DMAEA-containing triblock copolymers in the absence of ionic liquids (ILs)

Figure 5.7 compares SAXS profiles for DMAEA triblock copolymer with and without EMIm TfO. The DMAEA triblock copolymer exhibited 0 wt% EMIm ES uptake over an extended period of time. Both DSC and DMA results suggested that EMIm TfO resided mainly in the acrylic phase of the composite membranes. SAXS analysis for the neat DMAEA triblock copolymer indicated the absence of a well-defined morphology. However, upon EMIm TfO incorporation into the acrylic phase, a scattering peak at ~0.09 nm^{-1} and a scattering shoulder at ~0.18 nm^{-1} appeared for the composite membrane. The scattering features were characteristic of a lamellar morphology with a lamellar spacing of ~70 nm. The SAXS results suggested that the presence of EMIm TfO

enhanced incompatibility between the polystyrene phase and the acrylic phase, which led to more well-defined morphology for the DMAEA triblock copolymer membrane.

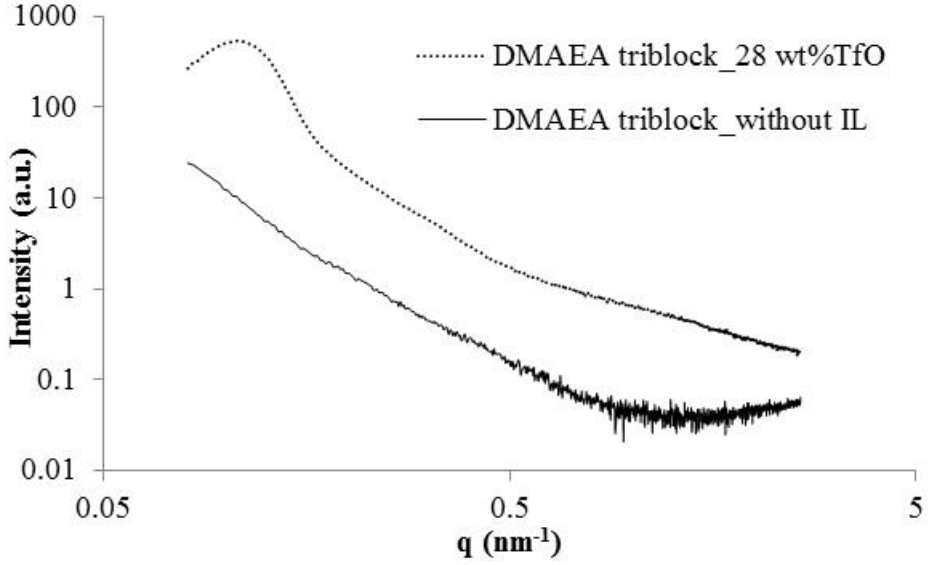

Figure 5.7. SAXS for DMAEA triblock copolymer without IL and with 28 wt% EMIm TfO

Figure 5.8 shows SAXS traces for SB-DMAEA triblock copolymer and composite membranes containing 22 wt% EMIm TfO and 15 wt% EMIm ES, respectively. The scattering features suggested that the long-range ordered morphologies of the neat SB-DMAEA triblock copolymer persisted upon ionic liquid incorporation. However, the ionomer peak shifted to lower q, which corresponded to an increase in the inter-cluster spacing with 15 wt% EMIm ES incorporation, and the peak broadened significantly with 22 wt% EMIm TfO. Gierke et al. attributed a similar increase in the mean inter-cluster spacing for water-swollen Nafion® membranes to the coalescence of adjacent ion clusters.[36] Bennett et al. studied the impact of EMIm TfO and EMIm TFSI on the morphology of Nafion® membranes.[37] They reported that the hydrophilic EMIm TfO was absorbed into the ionic clusters, while the hydrophobic EMIm TFSI resided at

least partially in the non-polar polymer matrix. Here, we attributed the difference in the SAXS traces for the EMIm TfO- and EMIm ES-swollen SB-DMAEA triblock copolymer membranes to the difference in polarity between the two ionic liquids. The tunability of the tertiary amine functionalities in the DMAEA triblock copolymer allowed us to adjust the polarity of the triblock copolymer and affinity toward polar guest molecules such as ionic liquids.

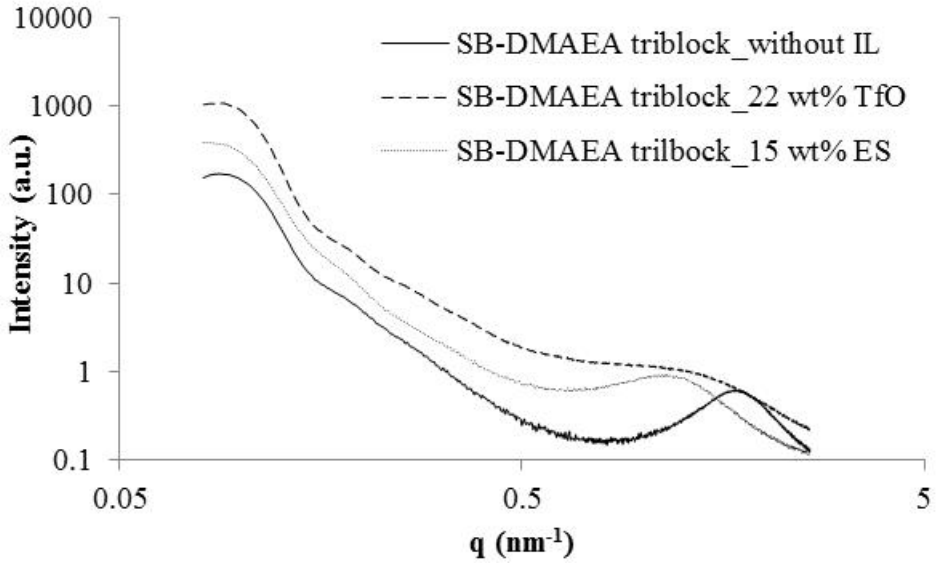

Figure 5.8. SAXS for SB-DMAEA triblock copolymer films without ionic IL, with 22 wt% EMIm TfO and with 15 wt% EMIm ES

5.4.6 Electro-responsiveness of poly(Sty-*b*-acrylate-*b*-Sty)-based actuators.

DMAEA triblock, SB-DMAEA triblock, and poly(Sty-*b*-*n*BA-*b*-Sty) were fabricated into electro-mechanical transducers according to a modified literature protocol.[23] **Figure 5.9** depicts the still images of the actuator fabricated from SB-DMAEA triblock copolymers under a 4 V step applied potential. Appreciable bending actuation was observed upon application of external electrical stimuli for both EMIm TfO-swollen DMAEA triblock and EMIm TfO-swollen SB-DMAEA triblock, but not for

poly(Sty-*b*-*n*BA-*b*-Sty), which did not show EMIm TfO uptake. Surprisingly, SB-DMAEA triblock copolymer swollen with EMIm ES also did not exhibit electro-responsiveness. As seen in **Figure 5.9**, the actuator initially bent toward the anode and later reversed the motion toward the cathode under the unipolar step potential. This bidirectional actuation behavior agreed with previous observation in ionic liquid-based actuation and was distinct from typical back-relaxation behavior.[38] It was ascribed to a faster motion of the smaller mobile cations followed by a slower motion of the larger mobile anions.

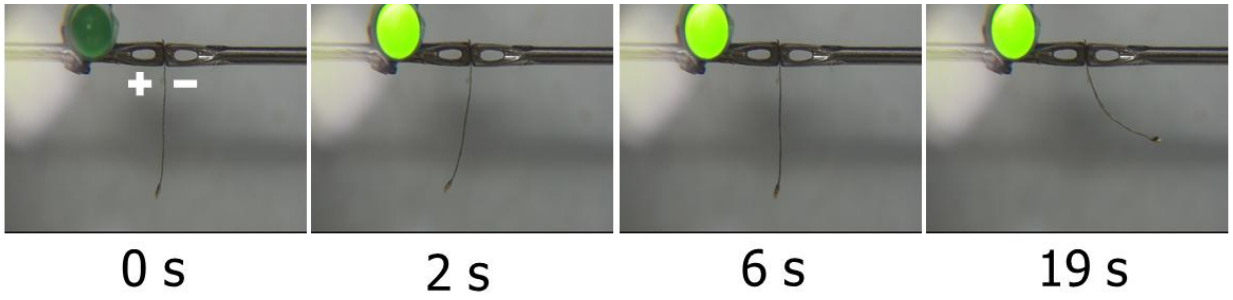

Figure 5.9. Images of electromechanical transducers fabricated from the SBDMAEA triblock copolymer with 58 wt% EMIm TfO

Since the bending actuation resulted from the accumulation of the mobile ions on both sides of the actuator, the bending curvature should be proportional to the charging of an equivalent resistor-capacitor (RC) circuit. Liu et al. simulated the ion motion in a similarly fabricated Nafion®-based IPT using a two-branch parallel RC circuit and obtained the characteristic time constants for both the cation motion and the anion motion.[38] They also successfully derived the maximum actuation curvature for their device. **Figure 5.10** shows that the equivalent RC circuit fits the actuation curvature for our SBDMAEA triblock copolymer-based actuator very well. Detailed fitting procedure and the fitting parameters are provided in the supporting information. While a more

comprehensive evaluation of the actuation curvature and the bending force is the subject of a future study, the current results indicated that the incorporation of DMAEA into the central blocks of poly(Sty-*b*-acrylate-*b*-Sty) enhanced affinity toward ionic liquids and enabled the electro-responsiveness of the triblock copolymer / EMIm TfO composite membranes.

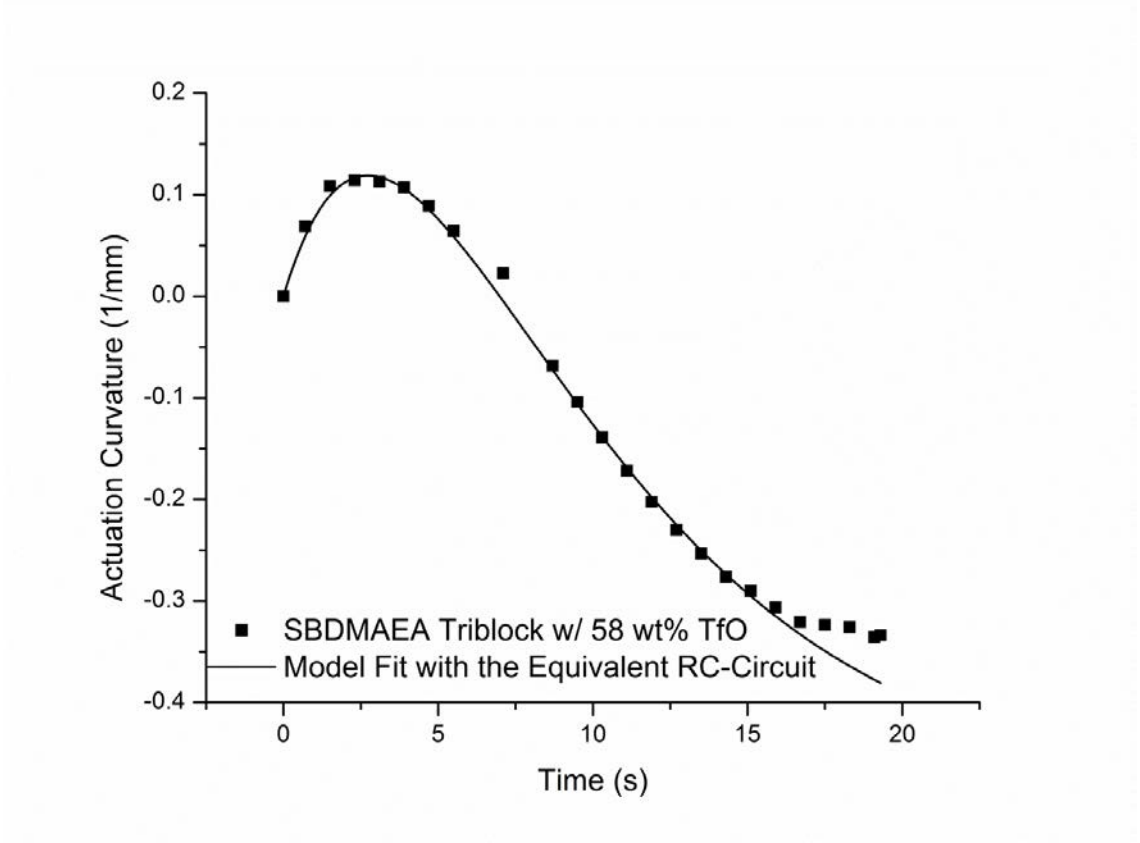

Figure 5.10. Actuation curvature for electromechanical transducer fabricated from the SBDMAEA triblock copolymer with 58 wt% EMIm TfO and the model fit with an equivalent RC-circuit[38]

5.5 Conclusions

We demonstrated the synthesis of high molecular weight poly[Sty-*b*-(*n*BA-*co*-DMAEA)-*b*-Sty] with relatively narrow PDIs employing the RAFT polymerization

strategy. The presence of the tertiary amine functionality in the central block of the triblock copolymers afforded tunable polarity toward polar guest molecules, such as ionic liquids. Both DMAEA triblock and SB-DMAEA triblock copolymers showed much improved affinity toward EMIm TfO, while their *n*BA counterpart did not absorb ionic liquid. Thermal and thermomechanical analyses of the block copolymer and their composite membranes revealed that they all had two distinctive glass transition temperatures at ~ -40 °C and ~ 100 °C. The lower T_g corresponded to the acrylate phase, where the ionic liquid resided, while the higher T_g corresponded to the IL-free poly(Sty) phase, which served as the physical crosslinks in the membranes. The triblock copolymer / EMIm TfO membranes exhibited rubbery plateaus between -20 °C and 100 °C and plateau moduli of ~ 100 MPa, both of which are desirable for applications in electromechanical transducers. SAXS results revealed that both quaternization of DMAEA to SB-DMAEA functionalities and the incorporation of ionic liquids into the acrylic phase facilitated the development of long-range ordered morphology in the triblock copolymers. Actuators fabricated from poly[Sty-*b*-(*n*BA-*co*-SBDMAEA)-*b*-Sty] indeed showed electro-responsiveness. Despite the high chain transfer constants for acrylic radicals to tertiary amines, the RAFT synthesis of poly[Sty-*b*-(*n*BA-*co*-DMAEA)-*b*-Sty] provided tunability for further understanding the structure-morphology-performance relationship of polymer-based electromechanical transducers.

5.6 Acknowledgements

This material is based upon work supported by the U.S. Army Research Office under grant number W911NF-07-1-0452 Ionic Liquids in Electro-Active Devices (ILEAD) MURI.

Supporting Information Available: reaction kinetics for the RAFT synthesis of polystyrene precursors; the structural confirmation of the triblock copolymers, and their molecular weight data; DSC traces for the triblock copolymer / ionic liquid binary compositions. This material is available free of charge via the Internet at http://pubs.acs.org.

5.7 References

1. Duncan, A. J.; Leo, D. J.; Long, T. E. *Macromolecules* **2008,** 41, (21), 7765-7775.
2. Pelrine, R.; Kornbluh, R.; Pei, Q. B.; Joseph, J. *Science* **2000,** 287, (5454), 836-839.
3. Shankar, R.; Krishnan, A. K.; Ghosh, T. K.; Spontak, R. J. *Macromolecules* **2008,** 41, (16), 6100-6109.
4. Gao, R.; Wang, D.; Heflin, J. R.; Long, T. E. *Journal of Materials Chemistry* **2012,** 22, (27), 13473-13476.
5. Akle, B. J.; Leo, D. J. *Smart Materials and Structures* **2007,** 16, (4), 1348.
6. Bennett, M. D.; Leo, D. J. *Sensors and Actuators A: Physical* **2004,** 115, (1), 79-90.
7. Visser, A. E.; Swatloski, R. P.; Reichert, W. M.; Mayton, R.; Sheff, S.; Wierzbicki, A.; Davis, J. H.; Rogers, R. D. *Environmental Science & Technology* **2002,** 36, (11), 2523-2529.
8. Green, M. D.; Long, T. E. *Polymer Reviews* **2009,** 49, (4), 291-314.
9. Armand, M.; Endres, F.; MacFarlane, D. R.; Ohno, H.; Scrosati, B. *Nature Materials* **2009,** 8, (8), 621-629.
10. Ueki, T.; Watanabe, M. *Macromolecules* **2008,** 41, (11), 3739-3749.
11. Noda, A.; Watanabe, M. *Electrochimica Acta* **2000,** 45, (8–9), 1265-1270.
12. Susan, M. A. B. H.; Kaneko, T.; Noda, A.; Watanabe, M. *Journal of the American Chemical Society* **2005,** 127, (13), 4976-4983.
13. Lodge, T. P. *Science* **2008,** 321, (5885), 50-51.
14. Meli, L.; Lodge, T. P. *Macromolecules* **2009,** 42, (3), 580-583.
15. Simone, P. M.; Lodge, T. P. *ACS Applied Materials & Interfaces* **2009,** 1, (12), 2812-2820.

16. Brown, R. H.; Duncan, A. J.; Choi, J. H.; Park, J. K.; Wu, T. Y.; Leo, D. J.; Winey, K. I.; Moore, R. B.; Long, T. E. *Macromolecules* **2010,** 43, (2), 790-796.
17. Choi, U. H.; Lee, M.; Wang, S.; Liu, W.; Winey, K. I.; Gibson, H. W.; Colby, R. H. *Macromolecules* **2012**.
18. Gwee, L.; Choi, J.-H.; Winey, K. I.; Elabd, Y. A. *Polymer* **2010,** 51, (23), 5516-5524.
19. Imaizumi, S.; Kokubo, H.; Watanabe, M. *Macromolecules* **2011,** 45, (1), 401-409.
20. Lai, J. T.; Filla, D.; Shea, R. *Macromolecules* **2002,** 35, (18), 6754-6756.
21. *Polymer Handbook*, *Fourth Edition*. John Wiley & Sons, Inc.: 1999.
22. Liu, S.; Montazami, R.; Liu, Y.; Jain, V.; Lin, M.; Heflin, J. R.; Zhang, Q. M. *Appl. Phys. Lett.* **2009,** 95, (2), 023505/1-023505/3.
23. Liu, S.; Montazami, R.; Liu, Y.; Jain, V.; Lin, M.; Zhou, X.; Heflin, J. R.; Zhang, Q. M. *Sens. Actuators, A* **2010,** A157, (2), 267-275.
24. Decher, G.; Hong, J. D. *Makromol. Chem., Macromol. Symp.* **1991,** 46, (Eur. Conf. Organ. Org. Thin Films, 3rd, 1990), 321-7.
25. Hawker, C. J.; Bosman, A. W.; Harth, E. *Chemical Reviews* **2001,** 101, (12), 3661-3688.
26. Mather, B. D.; Baker, M. B.; Beyer, F. L.; Berg, M. A. G.; Green, M. D.; Long, T. E. *Macromolecules* **2007,** 40, (19), 6834-6845.
27. Matyjaszewski, K.; Xia, J. *Chemical Reviews* **2001,** 101, (9), 2921-2990.
28. Chiefari, J.; Chong, Y. K.; Ercole, F.; Krstina, J.; Jeffery, J.; Le, T. P. T.; Mayadunne, R. T. A.; Meijs, G. F.; Moad, C. L.; Moad, G.; Rizzardo, E.; Thang, S. H. *Macromolecules* **1998,** 31, (16), 5559-5562.
29. Ran, R.; Yu, Y.; Wan, T. *Journal of Applied Polymer Science* **2007,** 105, (2), 398-404.
30. Truong, N. P.; Jia, Z.; Burges, M.; McMillan, N. A. J.; Monteiro, M. J. *Biomacromolecules* **2011,** 12, (5), 1876-1882.
31. Tigelaar, D. A.; Waldecker, J. R.; Peplowski, K. M.; Kinder, J. D. *Polymer* **2006,** 47, (12), 4269-4275.
32. Bonhôte, P.; Dias, A.-P.; Papageorgiou, N.; Kalyanasundaram, K.; Grätzel, M. *Inorganic Chemistry* **1996,** 35, (5), 1168-1178.
33. Vila, J.; Franjo, C.; Pico, J. M.; Varela, L. M.; Cabeza, O. *Port. Electrochim. Acta* **2007,** 25, (1), 163-172.
34. Koberle, P.; Laschewsky, A. *Macromolecules* **1994,** 27, (8), 2165-2173.
35. Wu, T.; Beyer, F. L.; Brown, R. H.; Moore, R. B.; Long, T. E. *Macromolecules* **2011,** 44, (20), 8056-8063.
36. Gierke, T. D.; Munn, G. E.; Wilson, F. C. *ACS Symposium Series* **1982,** 180, (Perfluorinated Ionomer Membr.), 195-216.
37. Bennett, M. D.; Leo, D. J.; Wilkes, G. L.; Beyer, F. L.; Pechar, T. W. *Polymer* **2006,** 47, (19), 6782-6796.
38. Liu, Y.; Liu, S.; Lin, J.; Wang, D.; Jain, V.; Montazami, R.; Heflin, J. R.; Li, J.; Madsen, L.; Zhang, Q. M. *Appl. Phys. Lett.* **2010,** 96, (22), 223503/1-223503/3.
39. Thomas, D. B.; Convertine, A. J.; Myrick, L. J.; Scales, C. W.; Smith, A. E.; Lowe, A. B.; Vasilieva, Y. A.; Ayres, N.; McCormick, C. L. *Macromolecules* **2004,** 37, (24), 8941-8950.

40. Odian, G., *Principles of Polymerization, Fourth Edition*. John Wiley & Sons, Inc.: 2004.
41. Ledwith, A. *Accounts Chem. Res.* **1972,** 5, (4), 133-9.
42. Ledwith, A.; Purbrick, M. D. *Polymer* **1973,** 14, (10), 521-522.
43. Wilkes, J. S.; Zaworotko, M. J. *J. Chem. Soc., Chem. Commun.* **1992**, (13), 965-7.
44. Gale, R. J.; Gilbert, B.; Osteryoung, R. A. *Inorg. Chem.* **1978,** 17, (10), 2728-9.

5.8 Supporting Information

5.8.1 RAFT synthesis of polystyrene with S,S'-bis(α,α'-dimethyl-α"-acetic acid)-trithiocarbonate (TTC).

The reaction kinetics for the TTC-mediated homopolymerization of styrene are shown in **Figure 5.11**, and the reaction exhibited pseudo-first order kinetics to 50 h and 25% monomer conversion, which suggested that the reaction proceeded in a controlled fashion. Thomas et al. observed similar deviations from the pseudo-first order reaction kinetics at higher monomer conversions for the RAFT polymerization of acrylamide, and they attributed such a change to a reduction in radical concentration in the main RAFT equilibrium and/or a change in the propagation rate constant.[39]

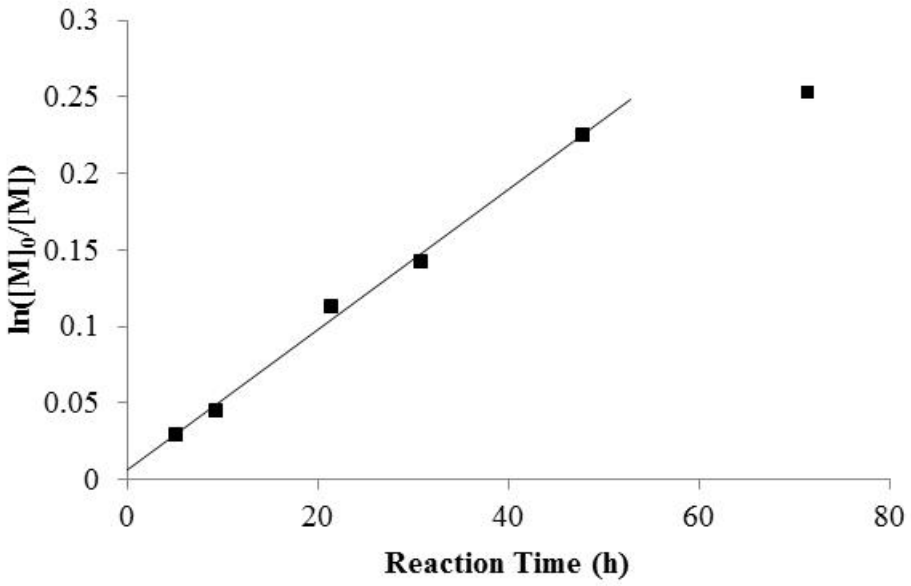

Figure 5.11 Kinetic plot of TTC-mediated homopolymerization of styrene

Figure 5.12 illustrates the molecular weights and PDIs of the poly(Sty) products as a function of the monomer conversion. The absolute weight-average molecular weights of the poly(Sty) samples agreed well with the theoretical prediction, while the PDIs of the samples decreased as the reaction progressed. As expected, both observations confirmed that TTC-mediated homopolymerization of styrene was well-controlled.

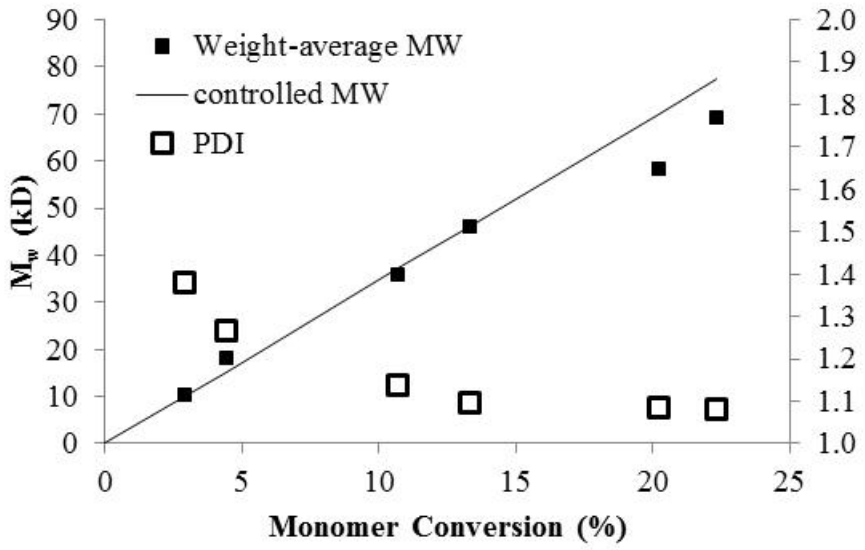

Figure 5.12. Weight-average molecular weight and PDI *vs.* conversion for TTC-mediated homopolymerization of styrene

5.8.2 Synthesis of poly(*n*BA) in the presence of TEA.

Scheme 5.3 illustrates the conventional free radical polymerization of *n*BA in the presence of TEA in benzene. Varying molar ratios of TEA to *n*BA (e.g. 25/100, 50/100, 60/100, 100/100) were charged to the reaction mixtures, while the initiator to monomer concentration was maintained at 0.5 wt%. In a typical polymerization reaction, *n*BA (0.25 g, 2.0 mmol), TEA (0.10 g, 1.0 mmol), and AIBN benzene solution (0.25 g, 0.50 wt%) were charged to a 10-mL, round-bottomed flask. The reaction mixture was sparged with ultrahigh purity nitrogen for 5 min and then placed into an oil bath at 65 °C for 12 h. The reaction products were isolated via vacuum removal of the reaction solvent and subsequently subjected to molecular weight characterizations using size exclusion chromatography in THF.

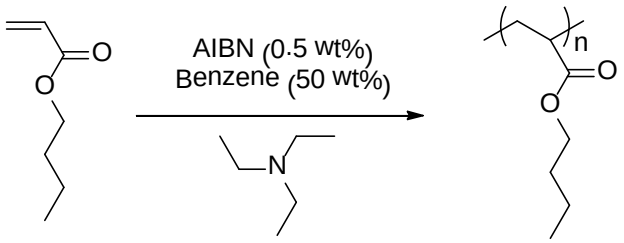

Scheme 5.3 Conventional free radical polymerization of *n*BA in the presence of TEA in benzene

The absolute molecular weights for poly(*n*BA) were determined using the light scattering detector with a dn/dc value of 0.07 m L/g. The degrees of polymerization, X_n, for poly(*n*BA) were calculated using the following equation:

$$\overline{X_n} = \frac{M_w}{128}$$

Figure 5.13 plots the reciprocal of X_n for poly(*n*BA) as a function of the molar concentration ratio of TEA to *n*BA in the feed. The molecular weights of poly(*n*BA) decreased as the molar ratios of TEA increased in the feed, and we attributed that to the chain transfer from the acrylic radicals to TEA during the polymerization reactions. The chain transfer constant C_s was calculated using the following equation[40]:

$$\frac{1}{\overline{X_n}} = \frac{R_i}{2R_p} + C_s\frac{[TEA]}{[nBA]}$$

The calculated C_s value of 0.0240 is significant and is on the same order as that for chain transfer from methyl acrylate radicals to triethylamine (Cs ~ 0.0400).[21] Since the successes of controlled radical polymerization techniques rely on minimizing the propensity of propagating free radical chain ends to undergo undesirable chain transfer or termination, the tendency of acrylic radicals to chain transfer to tertiary amines presents challenges toward incorporating DMAEA into block copolymers.

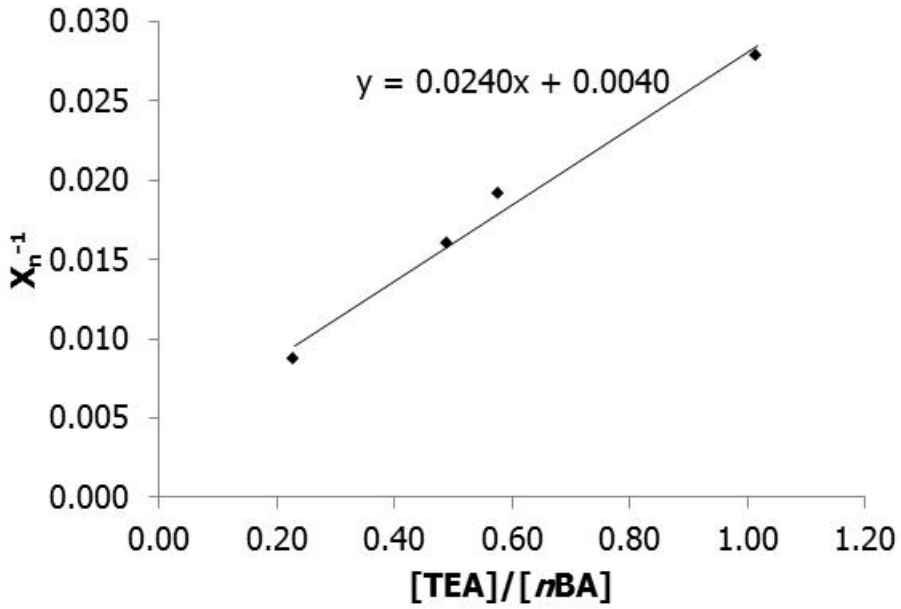

Figure 5.13 Reciprocal of X_n for poly(*n*BA) *vs.* the molar concentration ratios of TEA to *n*BA in the feed

5.8.3 Photo-oxidation of amines

Molecules that contain atoms with lone pairs of electrons such as O, N, or S are prone to losing an electron to form cation radicals. Ledwith studied the synthesis of tris(*p*-bromophenyl)aminium ion and reported that *N*-vinylcarbazole (NVC) dimerized upon reaction with the tris(*p*-bromophenyl)aminium ion in CH_2Cl_2-CH_3OH solvent system (as shown in **Figure 5.14**).[41] Such dimerization reaction is a special example of aromatic carbonyl compounds and dye molecules oxidizing amines. Ledwith and Purbrick further investigated the initiation of free radical polymerization using photo-excited aromatic carbonyl compunds.[42] They reported that the effect of varying initiator concentration on rate of polymerization of methyl methacrylate was rather complex.

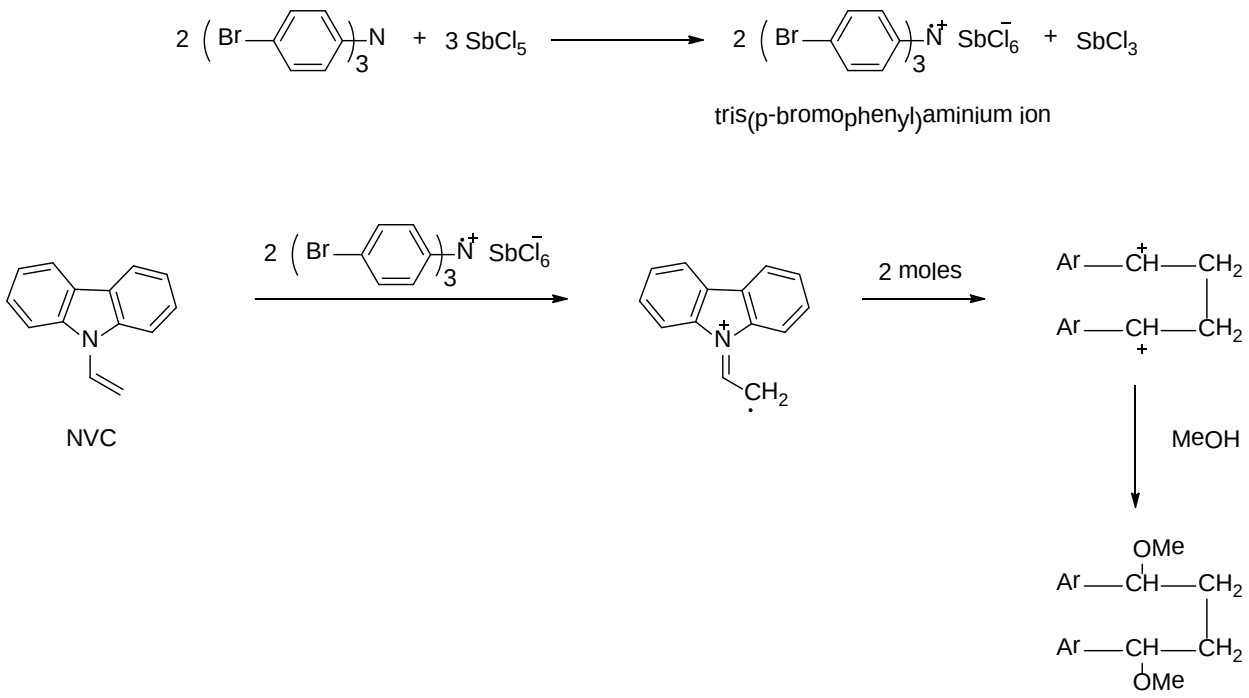

Figure 5.14 Synthesis of tris(p-bromophenyl)aminium ion and its reaction with NVC

5.8.4 Determining the molarity of DMAEA units in the DMAEA triblock copolymer.

Figure 5.15 shows the chemical structure and the ^{1}H NMR spectrum of poly[Sty-*b*-(*n*BA-*co*-DMAEA)-*b*-Sty]. The integration of the resonances at "a", "b" and "c" was used to calculate the mol% of Sty, *n*BA and DMAEA units in the triblock copolymers as follows:

$$mol\%_{sty} = \frac{100c}{c+b}\%$$

$$mol\%_{nBA} = \frac{100(b-a)}{c+b}\%$$

$$mol\%_{DMAEA} = \frac{100a}{c+b}\%$$

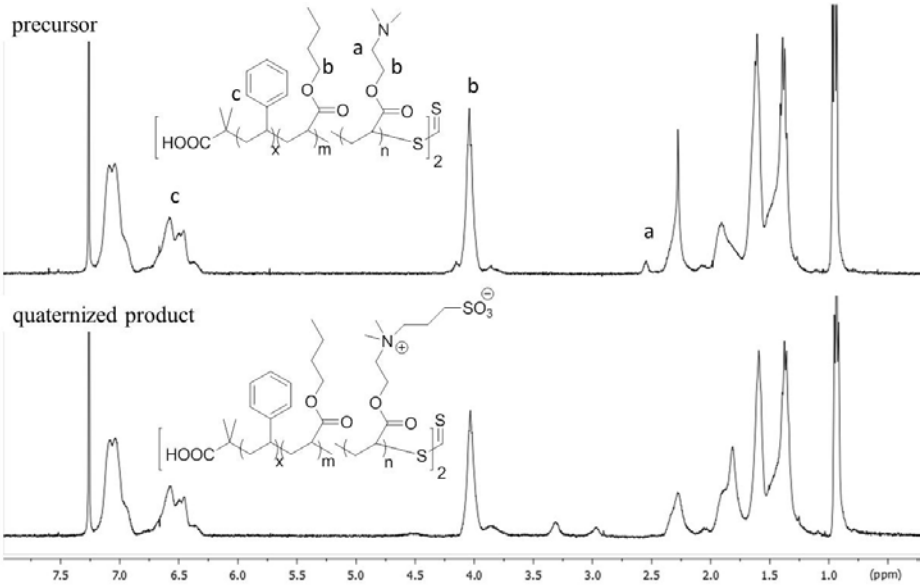

Figure 5.15. Chemical structures and ^{1}H NMR spectra of DMAEA- and SB-DMAEA-containing triblock copolymers. The acrylate central block contained both *n*BA and DMAEA derivatives.

It is known that Sty, *n*BA and DMAEA monomers have molecular weights of 104 g/mol, 128 g/mol and 143 g/mol, respectively. Hence, the molarity of DMAEA in 1 g of DMAEA triblock copolymer is calculated as follows:

$$molarity\ of\ DMAEA = \frac{mol\%_{DMAEA}}{\left(104 \times mol\%_{sty} + 128 \times mol\%_{nBA} + 143 \times mol\%_{DMAEA}\right)} mol$$

5.8.5 Functionalization of DMAEA triblock copolymers for sulfobetaine-containing derivatives.

Figure 5.15 also shows representative ^{1}H NMR spectrum for the SB-DMAEA triblock copolymer. The resonance at “a” in the neutral precursor is assigned to the protons on the methylene unit next to the tertiary amine functionality in DMAEA. Its

complete shift in the zwitterionic product confirmed that the quaternization reaction was quantitative.

5.8.6 Impact of ionic liquids on the glass transition temperatures of poly(Sty-*b*-acrylate-*b*-Sty) membranes.

Figure 5.16 compares the second heat DSC traces for EMIm TfO and DMAEA triblock copolymer with and without the ionic liquid.

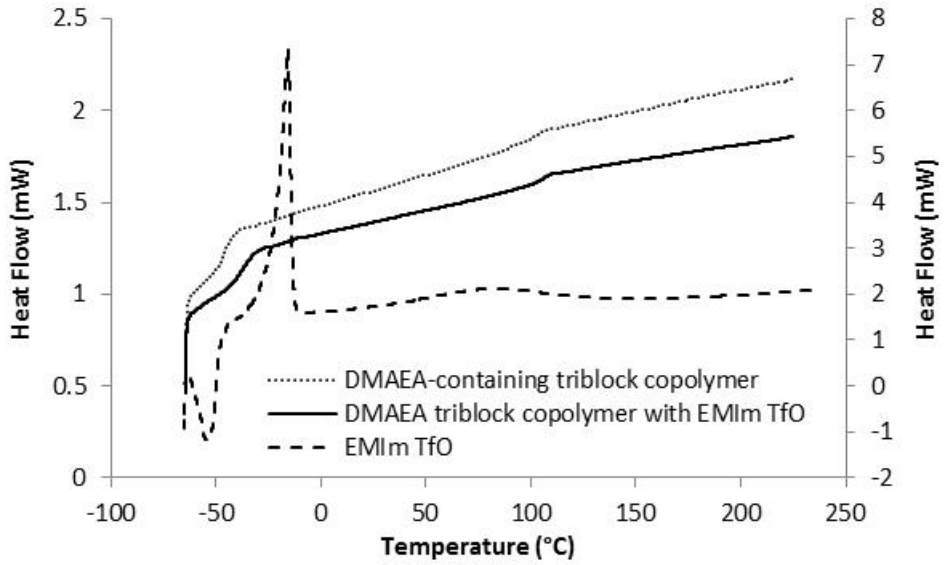

Figure 5.16. DSC traces for EMIm TfO and DMAEA-containing triblock copolymers with and without the ionic liquid.

Figure 5.17 compares the second heat DSC traces for EMIm TfO and SB-DMAEA triblock copolymer with and without the ionic liquid.

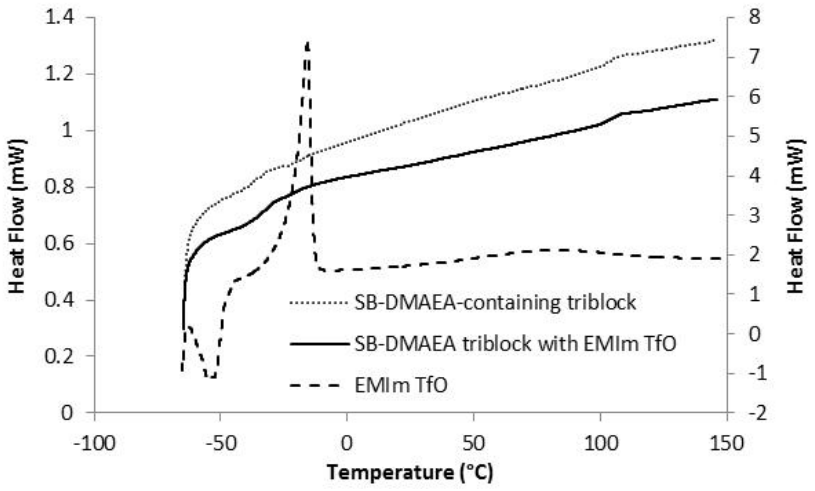

Figure 5.17. DSC traces for EMIm TfO and SB-DMAEA-containing triblock copolymers with and without the ionic liquid.

5.8.7 Electrochemical Stability of Ionic Liquids.

Osteryoung group published the first paper on 1-butylpyridinium chloride-aluminium chloride mixtures (BPC-$AlCl_3$).[43] In basic compositions, where $AlCl_3$ mole fraction is less than 0.5, the butylpyridinium cation is easily reduced. Wilkes and Hussey et al. screened various cations, as shown in **Figure 5.18**, for improved electrochemical stability. They found that the dialkylimidazolium cations stood out with a 0.9 V more negative reduction potential than that of BPC-$AlCl_3$. The 1-ethyl-3-methylimidazolium cation based chloroaluminate ionic liquids exhibit electrochemical window of > 3.0 V, and they are of great interest from an electrochemical perspective.[44]

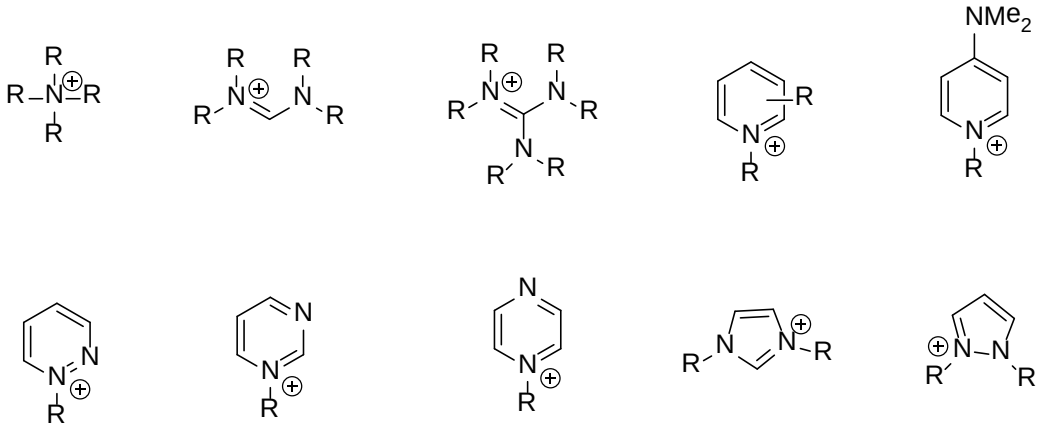

Figure 5.18 Choice of cations in ionic liquids

Galinski et al. summarized the electrochemical stability of various ionic liquids at different electrode materials from the literature.[41] The electrode materials include Pt, W, glassy carbon (GC), and graphite (G). **Table 5.2** lists the electrochemical stability windows for representative imidazolium cation-containing ionic liquids. The authors noted that halide anions undergo anodic oxidation at relatively low potentials, while amide anions are oxidized at relatively high anodic potentials. They also reported that tetraalkylammonium-based ionic liquids exhibited better stability than their imidazolium counterparts due to their lower cathodic reduction potentials.

Table 5.2. Electrochemical stability of imidazolium ionic liquids

Imidazolium Ionic Liquids	Cathodic Limit (V)	Anodic Limit (V)	Electro-Chemical Window	Working Electrode	Reference Electrode
$[EtMeIm]^+[F]^-$	0.7	2.4	3.1	Pt	Pt
$[EtMeIm]^+[BF_4]^-$	-1.6	1	2.6	Pt	Ag|Ag+
	-2.1	2.2	4.3	Pt	Ag|AgCl
	1.0	5.0	4.0	GC	$Li|Li^+$
$[EtMeIm]^+[CF_3SO_3]^-$	-1.8	2.3	4.1	Pt	$I^-|I_3^-$
$[EtMeIm]^+[N(CF_3SO_2)_2]^-$	-1.8	2.5	4.3	Pt	$I^-|I_3^-$
	-2.0	2.1	4.1	Pt	Ag wire
	-2.0	2.5	4.5	Pt	$Ag|Ag^+$
$[EtMeIm]^+[N(C_2F_5SO_2)_2]^-$	-2.0	2.1	4.1	GC	Ag wire
$[EtMeIm]^+[(CN)_2N]^-$	-1.6	1.4	3.0	Pt	Ag wire
$[BuMeIm]^+[Br]^-$	-2.0	0.2	2.2	Pt	$Ag|Ag^+$
$[BuMeIm]^+[BF_4]^-$	1.2	5.0	4.2	GC	$Li|Li^+$
	-1.6	4.5	6.1	W	Pt
	-1.6	3.0	4.6	Pt	Pt
	-1.8	2.4	4.2	Pt	$Ag|Ag^+$
$[BuMeIm]^+[PF_6]^-$	-1.1	2.1	3.2	Pt	Ag wire
	-2.3	3.4	5.7	Pt	Pt
	-1.9	2.5	4.4	Pt	$Ag|Ag^+$
$[BuMeIm]^+[N(CF_3SO_2)_2]^-$	-2.0	2.6	4.6	Pt	$Ag|Ag^+$
$[EtMeMeIm]^+[N(CF_3SO_2)_2]^-$	-2.0	2.4	4.4	Pt	$I^-|I_3^-$
$[PrMeIm]^+[N(CF_3SO_2)_2]^-$	1.0	5.3	4.3	GC	$Li|Li^+$

The molecular weights listed in **Table 5.3** and **Table 5.4** are relative to polystyrene standards. The AIBN to CTA ratio refers to the molar ratio of AIBN to TTC in the feed.

Table 5.3 Molecular weights of samples shown in **Figure 5.1**

Sample	AIBN : CTA	M_n (kg/mol)	M_w (kg/mol)	PDI
PS	1 : 10	69.0	82.3	1.19
Triblock-100	1 : 20	71.8	100	1.39
Triblock-116		80.7	116	1.44
Triblock-128		89.6	128	1.43

Table 5.4 Molecular weights of samples shown in **Figure 5.3** and **Figure 5.4**

Sample		AIBN : CTA	M_n (kg/mol)	M_w (kg/mol)	PDI
	PS precursor	1 : 8.5	63.8	75.2	1.18
	Tertiary amine-containing triblock	1 : 14	72.9	109	1.50
	Zwitterionic triblock	derived from sample above			
	PS precursor	1 : 11	41.0	52.3	1/28
	Poly(Sty-*b*-*n*BA-*b*-Sty)	1 : 7.0	74.0	89.0	1.20

Chapter 6 Impact of Electrostatic Interactions in the Low T_g Center Blocks on the Thermomechanical Properties and the Morphological Development of ABA Triblock Copolymers

(*Tianyu Wu, Mingqiang Zhang, Robert B. Moore, and Timothy E. Long**)

Department of Chemistry, Macromolecules and Interfaces Institute, Virginia Tech, Blacksburg, Virginia 24061-0212

6.1 Abstract

RAFT synthesized poly(sty-*b*-*n*BA-*b*-sty) triblock copolymer phase separates into long-range ordered morphologies in the solid state due to the incompatibility between the poly(*n*BA) phases and the poly(sty) phases. In this study, we introduced DMAEA into the center blocks of a poly(sty-*b*-*n*BA-*b*-sty), which consisted of ~ 50 v% poly(*n*BA). Subsequent quaternization of the tertiary amines into sulfobetaine functionalities incorporated electrostatic interactions into the low T_g center blocks of the triblock copolymers. Both differential scanning calorimetry (DSC) and dynamic mechanical analysis (DMA) results suggested that the electrostatic interactions enhanced block copolymer phase separation. SAXS results indicated that the presence of the sulfobetaine functionalities in acrylate phases increased electron density differences between the phases, and led to better defined scattering profiles. TEM results confirmed that the block copolymers of designed molecular weights exhibited lamellar morphologies, and the lamellar spacing increased with the amount of electrostatic interactions for the zwitterionic triblock copolymers.

Key Words: Block Copolymer, Zwitterion, Morphology, SAXS, TEM

6.2 Introduction

Block copolymers are macromolecules composed of sequences, or blocks, of chemically distinctive repeat units.[1] They have exhibited a range of segregated phases from lamellar to hexagonally packed cylinders to spheres in the bulk state. Comprehensive theoretical treatments of AB diblock, or ABA triblock, copolymers revealed that three experimentally controllable factors determined the phase behaviors of the block copolymers: 1) the overall degree of polymerization N, 2) the volume fractions f of the components, and 3) the Flory-Huggins interaction parameter χ for the chosen block pairs.[2, 3] The first two parameters were tunable through polymerization stoichiometry, while the third was intrinsic to the choice of the block pairs. The product χN dictates the block copolymer phase state. Earlier experimental efforts in understanding the microphase separation of block copolymers focused on styrene, isoprene and butadiene-containing polymers due to their compatibility with the "living" anionic polymerization technique.[4, 5]

Over the past fifteen years, the development of controlled radical polymerization techniques, such as NMP,[6, 7] ATRP[8] and RAFT, [9] have expanded the library of block copolymers that are suitable for morphological studies. Ruzette et al. reported molecular disorder and mesoscopic order in polydisperse acrylic block copolymers synthesized using nitroxide-mediated polymerization.[10] Jullian et al. correlated morphological structures and rheological behaviors of di- and triblock copolymers of poly(sty) and poly(*n*-butyl acrylate), and explored their potential in pressure sensitive adhesive applications.[11] Porto et al. synthesized a zwitterion-containing diblock copolymer using

ATRP in aqueous media, and demonstrated that it self-assembled into well-defined nanostructures.[12]

Meanwhile, Weiss and coworkers were among the first to investigate the influence of electrostatic interaction on the morphological development of lightly sulfonated poly[styrene-*b*-(ethylene-*co*-butylene)-*b*-styrene], where the charged functionalities resided in the outer blocks. They reported that both the sulfonation level and the counter-cation choice impacted the extent of block copolymer microphase separation.[13-15] Gao et al. studied chain dynamics in coronas of poly(styrene-*b*-sodium acrylate) ionomer aggregates, and found that the mobility of the poly(sty) segments depended on their distance from the ionic cores and the size of the cores.[16] More recently, Goswami et al. elucidated the influence of sulfonation on a poly(styrene-*b*-isoprene) diblock copolymer with Monte Carlo and Molecular Dynamics simulation.[17] Weber et al. synthesized a styrenic diblock copolymer, in which one of the blocks contained imidazole functionalities. [18] They found that, upon alkylating the imidazole rings, both the compositions and the morphology of the diblock copolymers impacted their ionic conductivities.

In the present work, we employed the RAFT polymerization technique, and synthesized two series of poly(sty-*b*-acrylate-*b*-sty) triblock copolymers, where the center acrylate block contained moderate amounts of tertiary amine functionalities. In each series, the outer blocks were of identical molecular weights, while the center blocks were either of controlled molecular weights or controlled chemical compositions. Subsequent quaternization of the amines resulted in triblock copolymers that contained lightly charged center blocks. Through a correlation of thermal, thermomechanical and

morphological characterizations, we aimed to elucidate the impact of elecrostractic interactions in the low T_g center blocks on the morphological development, as well as the thermomechanical performance, of ABA triblock copolymers.

6.3 Experimental

Materials. S,S'-bis(α,α'-dimethyl-α''-acetic acid)-trithiocarbonate (TTC), the RAFT agent, was synthesized according to a literature procedure.[19] 1,3-Propanesultone (Aldrich, 99+%), methanol (Fischer Scientific, HPLC grade), chloroform (Fischer Scientific, Optima®), Ruthenium Tetroxide (EMS, 0.5% stabilized aqueous solution), and EpoFix™ cold-setting embedding resin (EMS) were used as received. Styrene (sty, Aldrich, ReagentPlus®, ≥99%), *n*-butyl acrylate (*n*BA, Alfa Aesar, 98+%) and 2-(dimethylamino)ethyl acrylate (DMAEA, Aldrich, 98%) were deinhibited using neutral alumina columns, and further distilled under reduced pressure from calcium hydride. Azobisisobutyronitrile (AIBN, Aldrich, 98%) was recrystallized from methanol.

RAFT synthesis of poly(sty-*b*-acrylate-*b*-sty). Poly(sty) precursors (52 kD, PDI: 1.28 and 82kD, PDI: 1.19) were synthesized with TTC and AIBN according to a reported procedure. For controlled center block lengths, the acrylic block insertion reactions were monitored using in situ FTIR spectroscopy at 814 cm^{-1}. In a typical reaction, poly(sty) precursor (2.0 g, 52 kD, 38 μmol), *n*BA monomer (20.0 g, 156 mmol) and AIBN (0.7 mg, 4.3 μmol) were charged to a 50 mL, round-bottomed flask equipped with a magnetic stir bar. Depending on the targeted center block compositions, the acrylic monomers contained 0, 1, 3, 5 or 10 mol% DMAEA. The reaction mixture was subjected to three freeze-pump-thaw cycles to remove oxygen impurities and cannulated into a sealed reaction flask equipped with a FTIR insertion probe and a magnetic stir bar under ultra-

high purity nitrogen atmosphere. A preheated 65 °C oil bath was then raised to the reaction vessel to initiate the polymerization. Upon reaching the targeted monomer conversion, the reaction product was precipitated into methanol, and dried in a vacuum oven at 65 °C overnight. Triblock copolymers of fixed center block compositions were synthesized using a master batch, and sampled over time.

Quaternization of DMAEA triblock copolymers. The calculation for the stoichiometry of the quaternization reaction was also detailed in the previous report. Specifically, upon full dissolution of the neutral triblock copolymer in chloroform, 10 equivalence of 1,3-propanesultone was charged to the chloroform solution of the triblock copolymer. The exhaustive functionalization reaction was refluxed for 20 h. The quaternized product was precipitated into methanol and vacuum dried.

Instrumentation. ^{1}H NMR spectra were obtained on a Varian Unity 400 MHz spectrometer in $CDCl_3$. Size exclusion chromatography (SEC) determined the molecular weights of the polymers at 35 °C in THF at 1 mL·min^{-1} flow rate. The THF SEC system was equipped with a Waters 717plus autosampler, a Waters 515 HPLC pump, three Polymer Laboratories PLGel 5μm Mixed-C columns, and a Waters 2414 differential refractive index detector. Relative molecular weights to polystyrene standards for all the samples were reported using the Empower Pro software package. Differential scanning calorimetry (DSC) measurements were performed on a TA Q2000 instrument at a heating rate of 10 °C/min from -65 °C. The first heat scans concluded at 150 °C, and traces of the second heats were reported. Dynamic mechanical analysis (DMA) was performed on a TA Q800 analyzer in tension mode, at 1 Hz frequency, 15 μm amplitude, and 3 °C/min heating rate from -90 °C. Triblock copolymer membranes were first cast from 0.1 g·mL^{-1}

chloroform solutions into a PTFE mold to achieve film thicknesses of approximately 0.30 mm. The cast films were dried at room temperature overnight, and annealed at 120 °C for 8 h under vacuum.

Small angle X-ray scattering (SAXS) data were collected using a Rigaku S-Max 3000 SAXS system, equipped with 3 pinholes and a copper rotating anode emitting X-ray with a wavelength of 0.154 nm (Cu Kα). Two-dimensional SAXS patterns were obtained using a fully integrated 2D multiwire, proportional counting, gas-filled detector, with an exposure time of 1 hour. Raw data were corrected for absorption and background noise, and then azimuthally averaged. All SAXS data were analyzed using the SAXSGUI software package to obtain radially integrated SAXS intensity *vs.* scattering vector q plots. For all SAXS experiments, the sample-to-detector distance was 1603 mm, and the q range was calibrated using a silver behenate standard.

TEM specimen approximately 70 nm thick were cryo-sectioned using a RMC Product's PowerTome PC-CRX Ultramicrotome at -60 °C. The solvent-cast and annealed films were embedded in a cured epoxy matrix prior to cryo-microtoming. The formulation of the epoxy matrix consisted of 5 g of epoxy resin and 0.8 g of hardener. The microtomed sections were collected from a 60/40 DMSO/H_2O mixture, stained with a 0.5% RuO_4 aqueous solution in the vapor phase and stored in a desiccator at room temperature prior to imaging. TEM experiments were performed using a Carl Zeiss EM10CA transmission electron microscope operated at 100 kV. Images were collected with a charge-coupled device (CCD) camera, and analyzed using ImageJ.

6.4 Results and Discussions

6.4.1 Synthesis of poly(sty-*b*-acrylate-*b*-sty)

Figure 6.1 illustrated the TTC-mediated RAFT polymerization of DMAEA triblock copolymers and subsequent quaternization with 1,3-propanesultone. The center blocks consisted of random copolymers of *n*BA and DMAEA, where the targeted DMAEA concentrations were 0, 1, 3, 5 and 10 mol%. The resulting triblock copolymers are referred to as poly(sty-*b*-*n*BA-*b*-sty), DMAEA (1 mol%), DMAEA (3 mol%), DMAEA (5 mol%) and DMAEA (10 mol%), respectively. In our previous report, we confirmed that the synthesis of DMAEA (10 mol%) triblock copolymer proceeded in a controlled fashion.

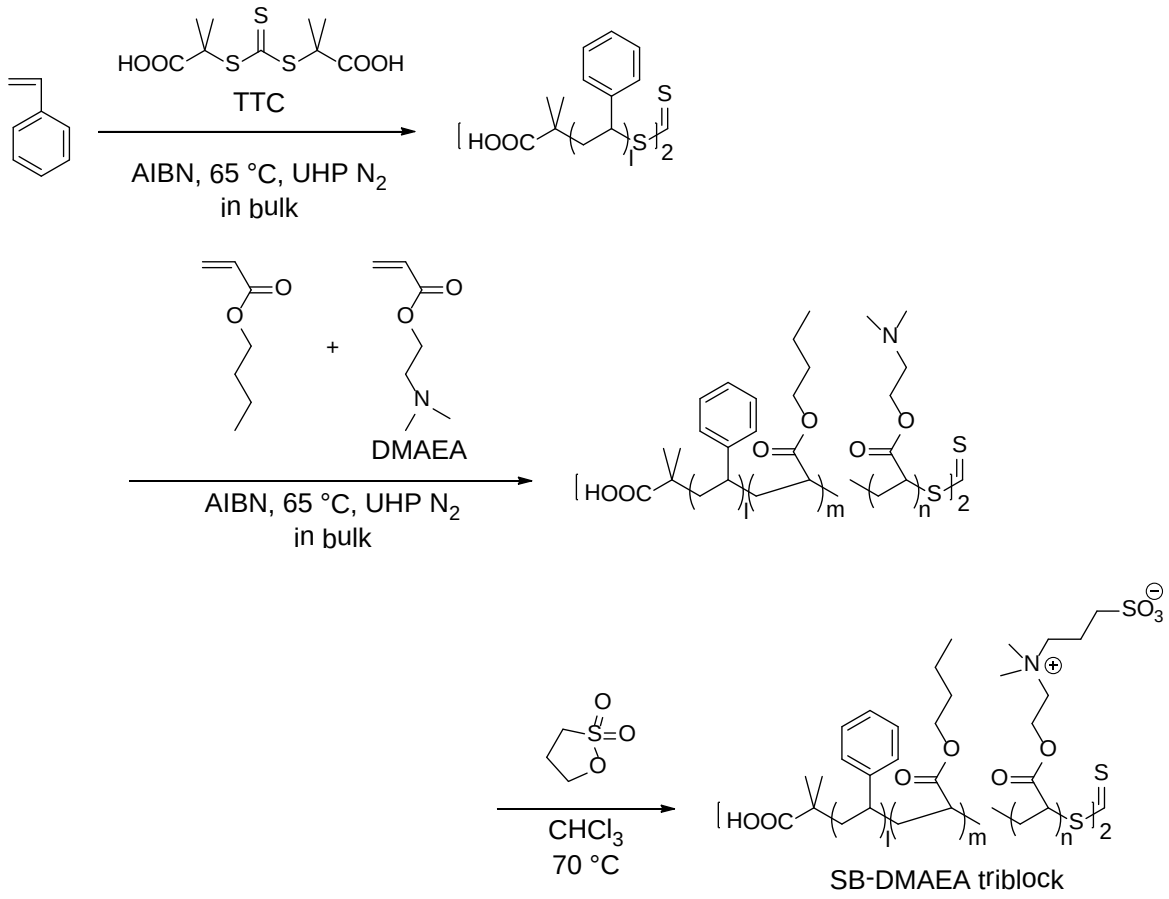

Figure 6.1 Synthesis of poly(sty-*b*-acrylate-*b*-sty) triblock copolymers and subsequent quaternization with 1,3-propanesultone

Figure 6.2 showed the size exclusion chromatograms for the poly(sty) precursor and the DMAEA triblock copolymers that contained 0, 1, 3 and 5 mol% DMAEA in the center blocks. The SEC traces for the triblock copolymers shifted nicely from the poly(sty) precursor, and fell into a relatively narrow molecular weight window.

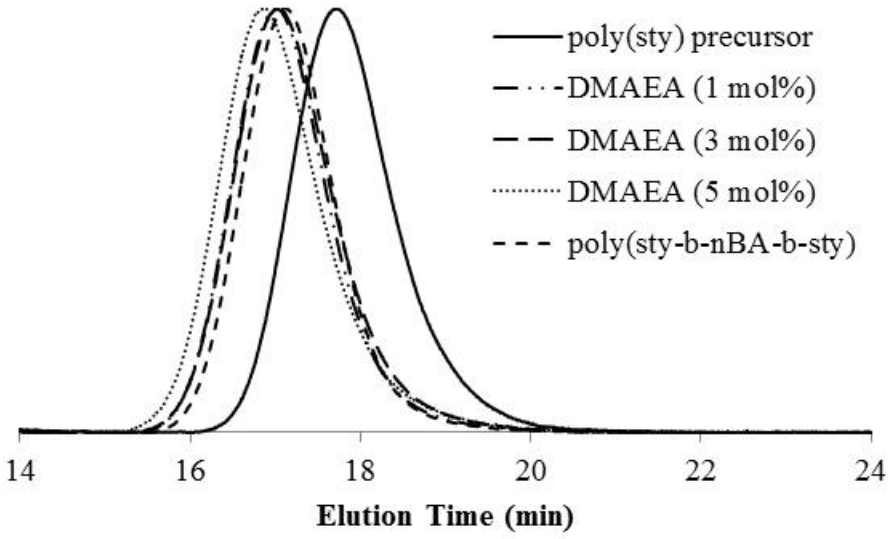

Figure 6.2. Size exclusion chromatography traces for a poly(sty) precursor and the corresponding DMAEA triblock copolymers of controlled center block lengths, but varying DMAEA compositions

Table 6.1 listed the molecular weights, as well as the PDIs, of the four triblock copolymers that contained less than 10 mol% DMAEA in the center blocks. The SEC results suggested that the triblock copolymers were of comparable center block lengths. Coincidentally, the molecular weights of the triblock copolymers increased slightly with the amount of DMAEA in the center acrylic blocks. The volume fractions of the poly(sty) phases in the triblock copolymers were estimated from their ^{1}H NMR spectra and the density of poly(sty) and poly(*n*BA). Details of the calculations are provided in the supporting information.

Table 6.1 Molecular weights of poly(sty-*b*-acrylate-*b*-sty). The DMAEA triblock copolymers contained 1 ~ 5 mol% DMAEA in the acrylic center blocks.

Sample	M_n (kD)	M_w (kD)	PDI	φ_{sty}
Poly(sty) precursor	41.0	52.3	1.28	1.00
Poly(sty-*b*-*n*BA-*b*-sty)	74.0	89.0	1.20	0.57
DMAEA (1 mol%) triblock	72.1	92.5	1.28	0.54
DMAEA (3 mol%) triblock	69.7	89.2	1.28	0.52
DMAEA (5 mol%) triblock	74.0	98.8	1.33	0.45

6.4.2 Glass transition temperatures of poly(sty-*b*-acrylate-*b*-sty)

The DSC traces for the triblock copolymers are included in the supporting information. The results revealed that both neutral and zwitterionic triblock copolymers had two glass transition temperatures, in agreement with our previous report. The lower $T_{g,1}$ at ~ -40 °C corresponded to the poly(acrylate) phase, while the higher $T_{g,2}$ at ~ 100 °C corresponded to the poly(sty) phases. **Figure 6.3** plotted both glass transition temperatures of the triblock copolymers *vs.* the functional acrylate concentration in the center blocks. The lower $T_{g,1}$s for the neutral triblock copolymers decreased slightly as the amount of DMAEA in the center blocks increased, while the higher $T_{g,2}$s remained unchanged at ~ 85 °C. Krause and coworkers studied the dependence of block copolymer glass transition temperatures on their molecular weights with styrene-dimethysiloxane (S-DMS) diblock copolymers, styrene-butadiene (S-B) diblock copolymers and styrene-butadiene-styrene (S-B-S) triblock copolymers.[20, 21] They reported that the S-DMS diblock copolymers had a much lower threshold poly(sty) molecular weight, above which the T_gs of the poly(sty) phases were independent of the low T_g compositions. They attributed such observation to more phase-mixing between the PS and the PB than between the PS and the PDMS phases. Here, we speculate that the molecular weights of both poly(sty) and poly(acrylate) blocks in the triblock copolymers were below their

respective threshold molecular weights, and the two phases were somewhat mixed. As a result, the lower $T_{g,1}$ of the neutral triblock copolymers decreased with increasing DMAEA in the center blocks, which coincided with slight increases in acrylic center block lengths, while the higher $T_{g,2}$ of ~ 85 °C persisted with fixed poly(sty) block lengths.

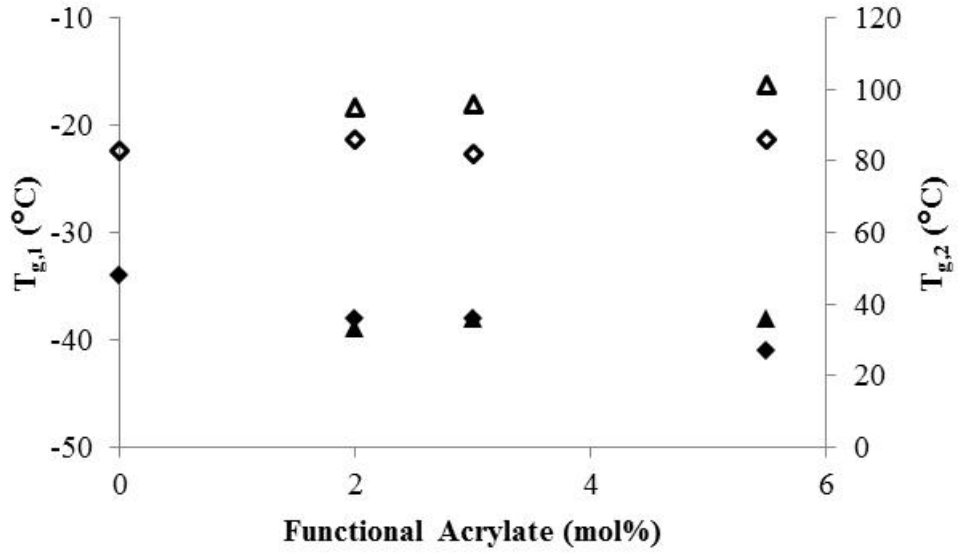

Figure 6.3. Glass transition temperatures of DMAEA triblocks (diamonds) and SB-DMAEA triblocks (triangles) with varying amounts of functional acrylate in the center blocks. Filled data points are for $T_{g,1}$, while open data points are for $T_{g,2}$.

Quaternization of the DMAEA functionalities in the acrylic center blocks increased the higher T_gs for the triblock copolymers to ~100 °C, typical for poly(sty) above its M_e, and slightly decreased $T_{g,1}$ for the acrylic phases of SBDMAEA (1 mol%) and SBDMAEA (3 mol%). These trends suggested that the incorporation of electrostatic interactions into the low T_g center blocks enhanced block copolymer phase separation. However, as the amount of the zwitterionic functionalities in the acrylic center block increased to 5 mol%, the effect of the electrostatic interaction-induced physical

crosslinking became more dominant. As a result, the $T_{g,1}$ for the SBDMAEA (5 mol%) increased upon quaternization.

6.4.3 Thermomechanical properties of poly(sty-*b*-acrylate-*b*-sty)

Figure 6.4 plotted DMA results for both DMAEA (3 mol%) triblock and SB-DMAEA (3 mol%) triblock copolymers. The "storage moduli *vs.* temperature" and the "tan δ *vs.* temperature" traces for the "3 mol%" triblock copolymers were representative of those for the "1 mol%" and the "5 mol%" triblock copolymers. The DMA results for the other two data sets are provided in the supporting information. All samples investigated here exhibited rubbery plateaus with plateau moduli of ~ 100 MPa. The thermomechanical transition at ~ 35 °C corresponded to the glass transition temperature of the poly(acrylate) phase, while the onset of the rubbery flow corresponded to the T_g of the poly(sty) phase. The DMA results agreed well with the DSC results that the quaternization of DMAEA in the center blocks enhanced block copolymer phase separation, and extended the rubbery plateaus for the quaternized triblock copolymers to ~ 100 °C.

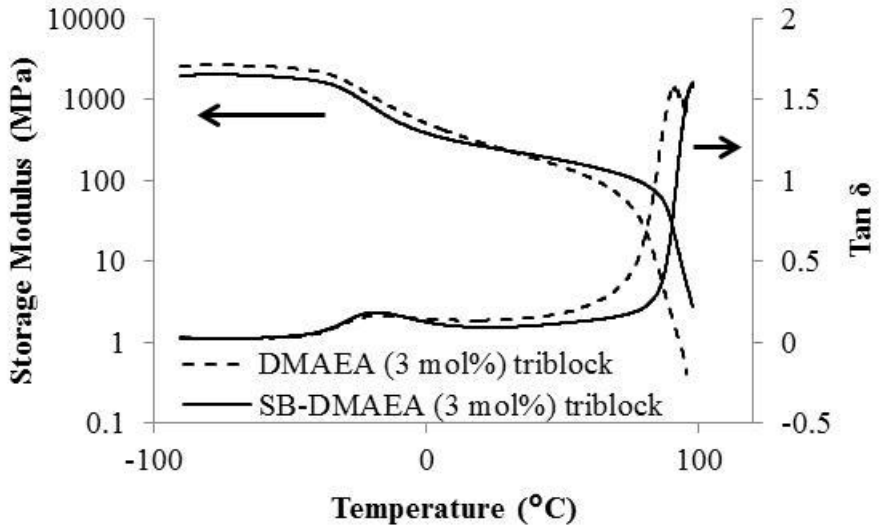

Figure 6.4. DMA traces for a DMAEA triblock copolymer that contained 3 mol% DMAEA in the center block and its SB-DMAEA counterpart

6.4.4 Morphologies of poly(sty-*b*-acrylate-*b*-sty)

Figure 6.5 plotted the small-angle X-ray scattering intensities for poly(sty-*b*-*n*BA-*b*-sty) membranes as a function of q, the scattering vector. The "not stained" sample was cast from a 0.1 g/mL chloroform solution, and characterized without further treatment. The "stained" sample was cut from the "as cast" membrane, and stained with a 0.5 wt% RuO_4 aqueous solution in the vapor phase for 4 hours. For the "not stained" sample, a scattering peak at ~0.34 nm^{-1} was observed, while another scattering feature at ~0.17 nm^{-1} was noticeable. The scattering peak at ~0.34 nm^{-1} corresponded to a characteristic dimension of ~ 18 nm. Yamamoto et al. reported similar SAXS results for a 30k poly(sty-*b*-*n*BA) diblock copolymer around room temperature.[22] They noted that the shape of SAXS traces for the diblock copolymers were temperature dependent. Specifically, the primary scattering feature at ~ 0.17 nm^{-1} appeared as a peak only at temperatures below 20 °C or above 60 °C. Since the electron densities of poly(sty) and

poly(*n*BA) were 340 e·nm^{-3} and 356 e·nm^{-3}, respectively, the authors speculated that the temperature-dependent SAXS profiles for the diblock copolymer resulted from volume changes in the two phases.

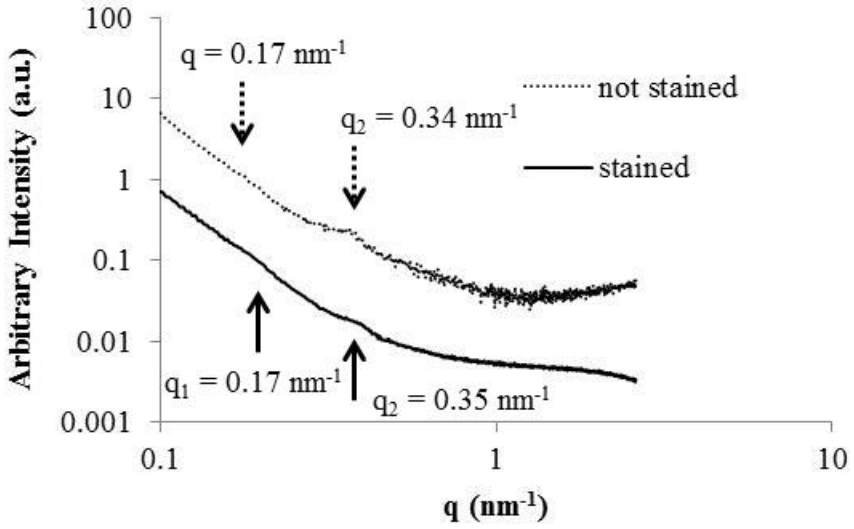

Figure 6.5. SAXS traces for poly(sty-*b*-*n*BA-*b*-sty) with and without RuO_4 staining

Trent et al. studied the use of RuO_4 in the selective staining of polymer samples to improve their electron density contrast for TEM characterization.[23] They reported that RuO_4 selectively stained aromatic structures, but not poly(methyl methacrylate). Here, we employed RuO_4 to selective stain the poly(sty) phases in poly(sty-*b*-*n*BA-*b*-sty) to improve the electron density contrast between the two phases for both SAXS and TEM characterizations. For the SAXS experiment, the "as cast" membrane was stained in the vapor phase for 4 h, while the cryo-microtomed TEM specimen were stained in the vapor phase for 40 ~ 90 min. The SAXS trace for the "stained" sample, as shown in **Figure 6.5**, suggested that the staining of the "as cast" membrane further decreased electron density contrast between the two phases. Since the poly(sty) phases initially had lower electron

density than the poly(*n*BA) phases, we attributed the observed phenomenon to the inefficient staining of the "as cast" membrane in bulk.

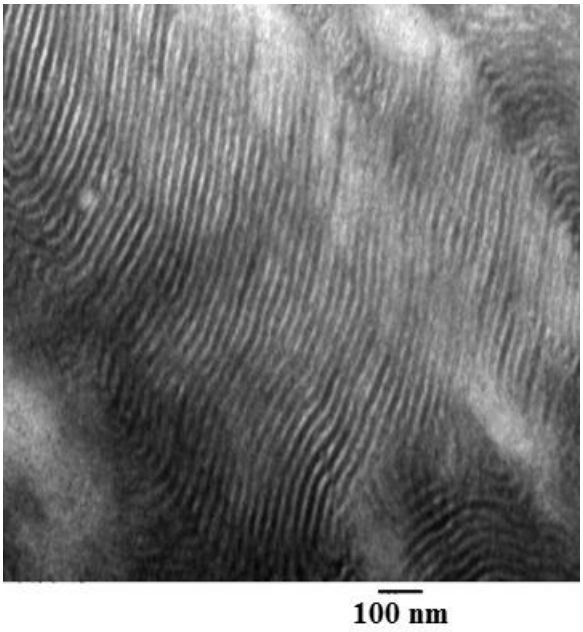

Figure 6.6. TEM image of RuO_4-stained poly(sty-*b*-*n*BA-*b*-sty)

Figure 6.6 showed a TEM image of a RuO_4 stained poly(sty-*b*-*n*BA-*b*-sty) triblock copolymer sample. The dark phases corresponded to the poly(sty) phases, while the bright phases corresponded to the poly(*n*BA) phases. The TEM result confirmed that RuO_4 selectively stained the poly(sty) phases. However, the lamellar spacing of ~ 35 nm observed in TEM was twice as large as the characteristic dimension calculated from q_2 in **Figure 6.5** for the "unstained sample" using SAXS. The SAXS and the TEM results for poly(sty-*b*-*n*BA-*b*-sty) agreed well if the primary scattering peak in SAXS indeed existed.

SAXS traces for all six triblock copolymers are provided in the supporting information. **Figure 6.7** overlaid SAXS traces for the DMAEA (3 mol%) triblock copolymer and its zwitterionic counterpart. Similar to that for poly(sty-*b*-*n*BA-*b*-sty), the neutral triblock copolymer exhibited only one scattering peak at ~ 0.39 nm^{-1}. In

comparison, the SB-DMAEA triblock copolymers exhibited three distinctive scattering features. The broad scattering peaks at q of ~1.5 nm^{-1} were characteristic of the ionomer peaks in charge-containing polymers,[24] and their intensity increased as the amount of the electrostatic interaction increased in the center blocks. The other two scattering peaks appeared at q of ~0.21 nm^{-1} and ~0.41 nm^{-1}, respectively. The ratio of 1:2 for the two scattering vectors suggested that the quaternized triblock copolymers hosted lamellar morphologies.

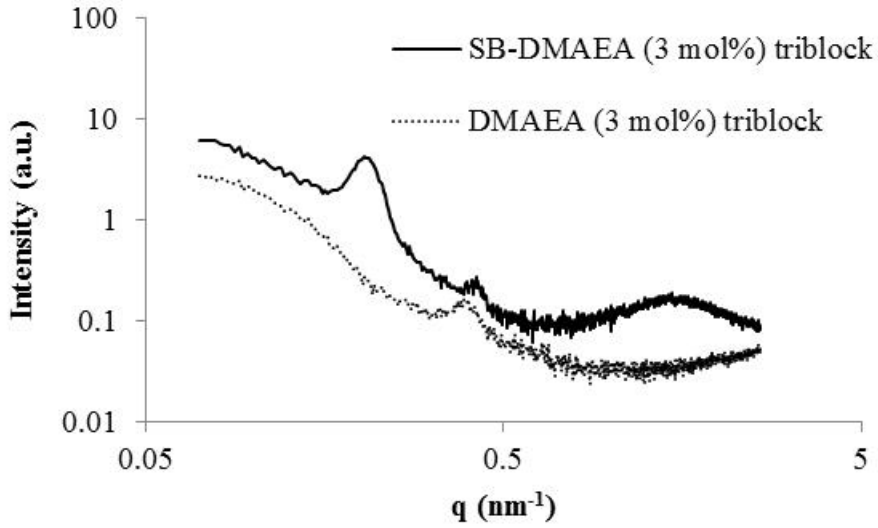

Figure 6.7. SAXS traces for DMAEA (3 mol%) triblock copolymer and its SB-DMAEA counterpart. The traces were shifted along the "Intensity"-axis.

Weiss and coworkers varied the degree of sulfonation in the outer blocks of poly[styrene-*b*-(ethylene-*co*-butylene)-*b*-styrene], and observed two distinct microphase separated morphologies.[14, 15] They reported that the sizes of both the ionic domains and the block domains were independent of the sulfonation levels, while the extent of microphase separation decreased with increasing sulfonation level and with increasing strength of the ionic interactions, i.e. $Na^+ > Zn^{2+} > H^+$. Floudas and coworkers studied the

influence of zwitterion placement on the morphology and the viscoelastic behaviors of poly(styrene-*b*-isoprene) diblock and poly(styrene-*b*-isoprene-*b*-styrene) triblock copolymers.[25-27] They observed ionic aggregates in the poly(isoprene) phases at low temperature when the zwitterion was linked to the poly(isoprene) chain end, but reported similar ion association in the poly(sty) phases only at high temperatures when the zwitterion was attached to the high T_g end. Here, the characteristic dimensions of the scattering features for DMAEA and SBDMAEA triblock copolymers are summarized in **Table 6.2**. We assumed that the only scattering peak observed for the DMAEA triblock copolymers corresponded to their secondary scattering peaks.

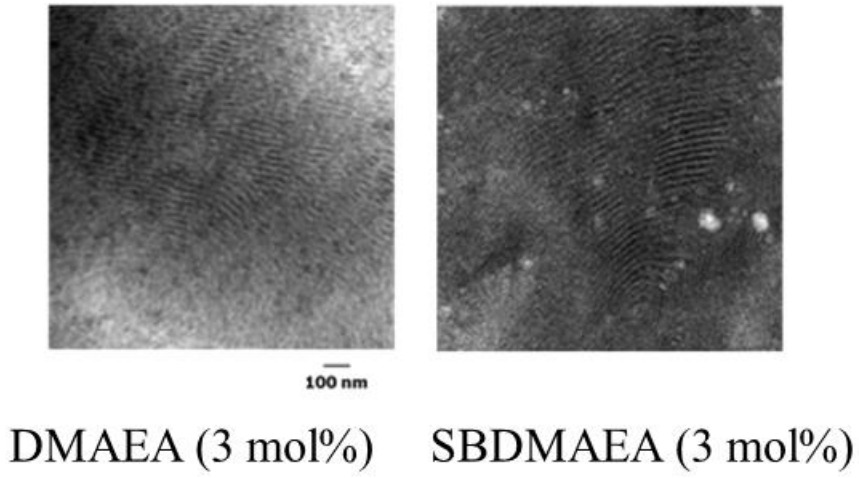

Figure 6.8. Representative TEM images of DMAEA triblock and SB-DMAEA triblock copolymers

Figure 6.8 showed TEM images of DMAEA (3 mol%) triblock and SB-DMAEA (3 mol%) triblock copolymers. The TEM images were representative of the other triblock copolymers, and both exhibited lamellar morphologies. Such long-range ordered morphologies for the quaternized triblock copolymers agreed with their SAXS profiles. The TEM images of the DMAEA triblock copolymers confirmed that the observed

scattering features in their SAXS traces corresponded to the secondary scattering peak. The measured characteristic dimensions of the lamellae, as shown in **Table 6.2**, indicated that, upon the introduction of the electrostatic interactions, the domain sizes contracted slightly. The appearance of the ionomer peak agreed well with previous reports.

Table 6.2. Summary of the characteristic dimensions for both DMAEA triblock and SB-DMAEA triblock copolymers determined using both SAXS and TEM

Functional Acrylate	mol% of functional acrylate in the center blocks	Characteristic Dimensions (nm)				
		SAXS			TEM	
		d_1	d_2	d_i	$d_{lamellae}$	d_i
DMAEA	1.8	ND	16.0	ND	36.7 ± 2.4	ND
	3.1		16.2		29.4 ± 2.2	
	4.6		16.9		30.5 ± 4.0	
SB-DMAEA	1.8	29.9	14.9	4.3	28.4 ± 2.2	ND
	3.1	30.7	15.0		29.2 ± 3.8	
	4.6	34.6	17.3	3.9	31.5 ± 3.6	

6.5 Conclusions

Size exclusion chromatography and ^{1}H NMR results confirmed that the in-situ FT-IR technique facilitated the synthesis of poly(sty-*b*-acrylate-*b*-sty) triblock copolymers of comparable molecular weights, but varying DMAEA compositions in the center blocks. Thermal and thermomechanical characterization results of the triblock copolymers indicated that the incorporation of electrostatic interactions into the low T_g center blocks of the ABA triblock copolymers enhanced their microphase separation and increased their higher T_gs, which corresponded to the poly(sty) phases. As a result, the SBDMAEA triblock copolymers exhibited extended rubbery plateaus compared with their neutral analogs. TEM results indicated that all triblock copolymers had lamellar

morphologies. However, only the zwitterionic triblock copolymers showed SAXS profiles that were characteristic of the lamellar morphology.

6.6 Acknowledgements

This material is based upon work supported by the U.S. Army Research Laboratory and the U.S. Army Research Office under grant number W911NF-07-1-0339 and grant number W911NF-07-1-0452 Ionic Liquids in Electro-Active Devices (ILEAD) MURI. Parts of this work were carried out using instruments in the Nanoscale Characterization and Fabrication Laboratory, a Virginia Tech facility operated by the Institute for Critical Technology and Applied Science. Parts of the TEM images were acquired with the assistance from Kathy Lowe at Virginia-Maryland Regional College of Veterinary Medicine.

6.7 References

1. Bates, F. S.; Fredrickson, G. H. *Annual Review of Physical Chemistry* 1990, 41, (1), 525-557.
2. Leibler, L. *Macromolecules* 1980, 13, (6), 1602-1617.
3. Bates, F. S. *Science* 1991, 251, (4996), 898-905.
4. Hashimoto, T.; Nagatoshi, K.; Todo, A.; Hasegawa, H.; Kawai, H. *Macromolecules* 1974, 7, (3), 364-73.
5. Bates, F. S.; Berney, C. V.; Cohen, R. E. *Macromolecules* 1983, 16, (7), 1101-8.
6. Hawker, C. J.; Bosman, A. W.; Harth, E. *Chemical Reviews* 2001, 101, (12), 3661-3688.
7. Mather, B. D.; Baker, M. B.; Beyer, F. L.; Berg, M. A. G.; Green, M. D.; Long, T. E. *Macromolecules* 2007, 40, (19), 6834-6845.
8. Matyjaszewski, K.; Xia, J. *Chemical Reviews* 2001, 101, (9), 2921-2990.
9. Chiefari, J.; Chong, Y. K.; Ercole, F.; Krstina, J.; Jeffery, J.; Le, T. P. T.; Mayadunne, R. T. A.; Meijs, G. F.; Moad, C. L.; Moad, G.; Rizzardo, E.; Thang, S. H. *Macromolecules* 1998, 31, (16), 5559-5562.
10. Ruzette, A. V.; Tence-Girault, S.; Leibler, L.; Chauvin, F.; Bertin, D.; Guerret, O.; Gerard, P. *Macromolecules* 2006, 39, (17), 5804-5814.
11. Jullian, N.; Rubatat, L.; Gerard, P.; Peyrelasse, J.; Derail, C. *Journal of Rheology* 2011, 55, (2), 379-400.

12. Porto, L. C.; Aissou, K.; Giacomelli, C.; Baron, T.; Rochas, C.; Pignot-Paintrand, I.; Armes, S. P.; Lewis, A. L.; Soldi, V.; Borsali, R. *Macromolecules* 2011, 44, (7), 2240-2244.
13. Lu, X.; Steckle, W. P., Jr.; Hsiao, B.; Weiss, R. A. *Macromolecules* 1995, 28, (8), 2831-9.
14. Lu, X.; Steckle, W. P., Jr.; Weiss, R. A. *Macromolecules* 1993, 26, (24), 6525-30.
15. Lu, X.; Steckle, W. P.; Weiss, R. A. *Macromolecules* 1993, 26, (22), 5876-84.
16. Gao, Z.; Zhong, X. F.; Eisenberg, A. *Macromolecules* 1994, 27, (3), 794-802.
17. Goswami, M.; Sumpter, B. G.; Huang, T.; Messman, J. M.; Gido, S. P.; Isaacs-Sodeye, A. I.; Mays, J. W. *Soft Matter* 2010, 6, (24), 6146-6154.
18. Weber, R. L.; Ye, Y.; Schmitt, A. L.; Banik, S. M.; Elabd, Y. A.; Mahanthappa, M. K. *Macromolecules* 2011, 44, (14), 5727-5735.
19. Lai, J. T.; Filla, D.; Shea, R. *Macromolecules* 2002, 35, (18), 6754-6756.
20. Krause, S.; Iskandar, M.; Iqbal, M. *Macromolecules* 1982, 15, (1), 105-111.
21. Krause, S.; Lu, Z.; Iskandar, M. *Macromolecules* 1982, 15, (4), 1076-1082.
22. Yamamoto, K.; Matsuzaki, T.; Sakurai, S. *Photon Factory Activit Report* 2007, (24).
23. Trent, J. S.; Scheinbeim, J. I.; Couchman, P. R. *Macromolecules* 1983, 16, (4), 589-598.
24. Eisenberg, A.; Hird, B.; Moore, R. B. *Macromolecules* 1990, 23, (18), 4098-4107.
25. Floudas, G.; Fytas, G.; Pispas, S.; Hadjichristidis, N.; Pakula, T.; Khokhlov, A. R. *Macromolecules* 1995, 28, (14), 5109-5118.
26. Floudas, G.; Pispas, S.; Hadjichristidis, N.; Pakula, T. *Macromolecular Chemistry and Physics* 2001, 202, (9), 1488-1496.
27. Pispas, S.; Floudas, G.; Hadjichristidis, N. *Macromolecules* 1999, 32, (26), 9074-9077.

6.8 Supporting Information

Figure 6.9 and **Figure 6.10** overlaid SAXS traces for neutral and quaternized triblock copolymers of comparable molecular weights, respectively.

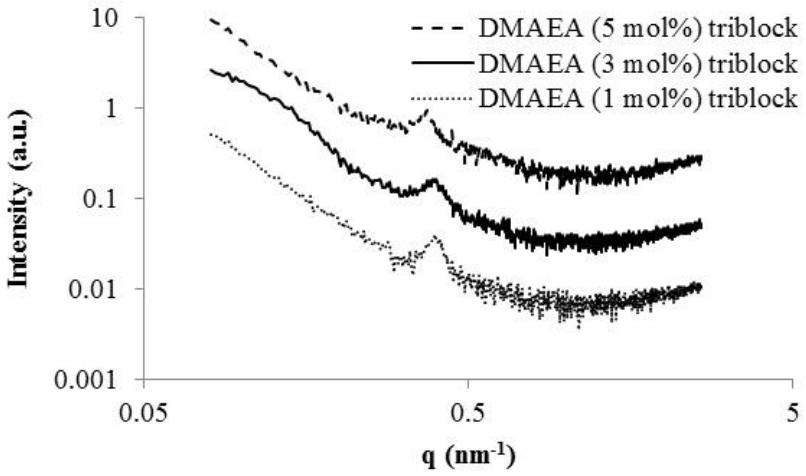

Figure 6.9 SAXS traces for DMAEA triblock copolymers containing varying amounts of DMAEA in the center blocks. The traces were shifted along the "Intensity"-axis.

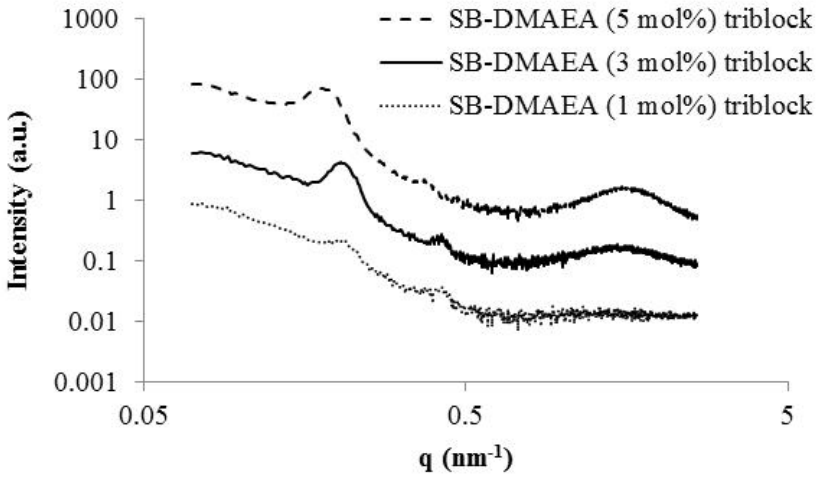

Figure 6.10. SAXS traces for SB-DMAEA triblock copolymers containing varying amounts of SB-DMAEA in the center blocks. The traces were shifted along the "Intensity"-axis.

The amount of SBDMAEA in the zwitterionic triblock copolymers impacted the scattering intensity corresponding to the zwitterionic aggregates. In addition, the incorporation of electrostatic interactions enabled the appearance of the primary

scattering peak, which were missing the SAXS profiles for the DMAEA triblock copolymers, for the triblock copolymers.

Figure 6.11 plotted the half width of the tanδ peaks in DMA for the triblock copolyemers as a function of their DMAEA compositions. The results suggested that the glass transition of the poly(acrylate) phases sharpened upon the introduction of the electrostatic interactions.

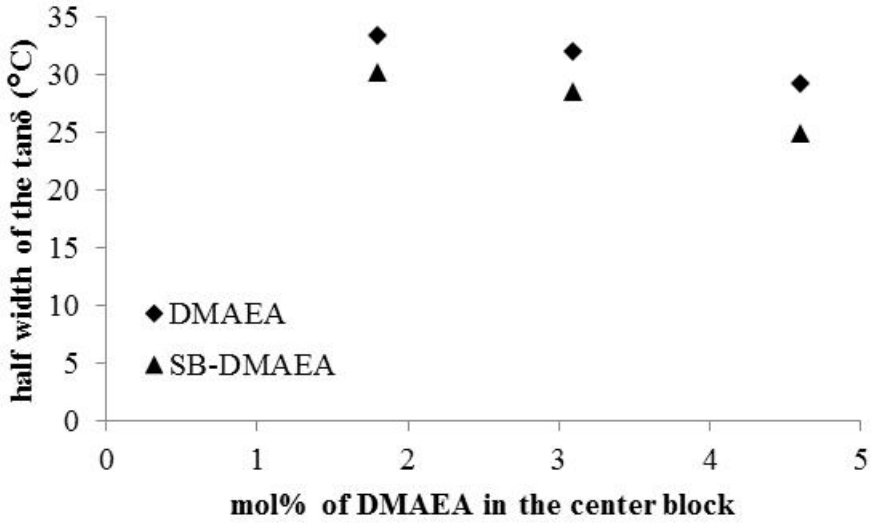

Figure 6.11. Half width of the tanδ peak in DMA for DMAEA triblock and SBDMAEA triblock

Figure 6.12 showed TEM images of the triblock copolymers of comparable molecular weights. All samples exhibited features characteristic of the lamellar morphology. However, as the amount of SBDMAEA increased in the center blocks, light areas of irregular shape appeared in the TEM images. We speculate that the "wet technique" used for TEM specimen collection might have contributed to the observed features.

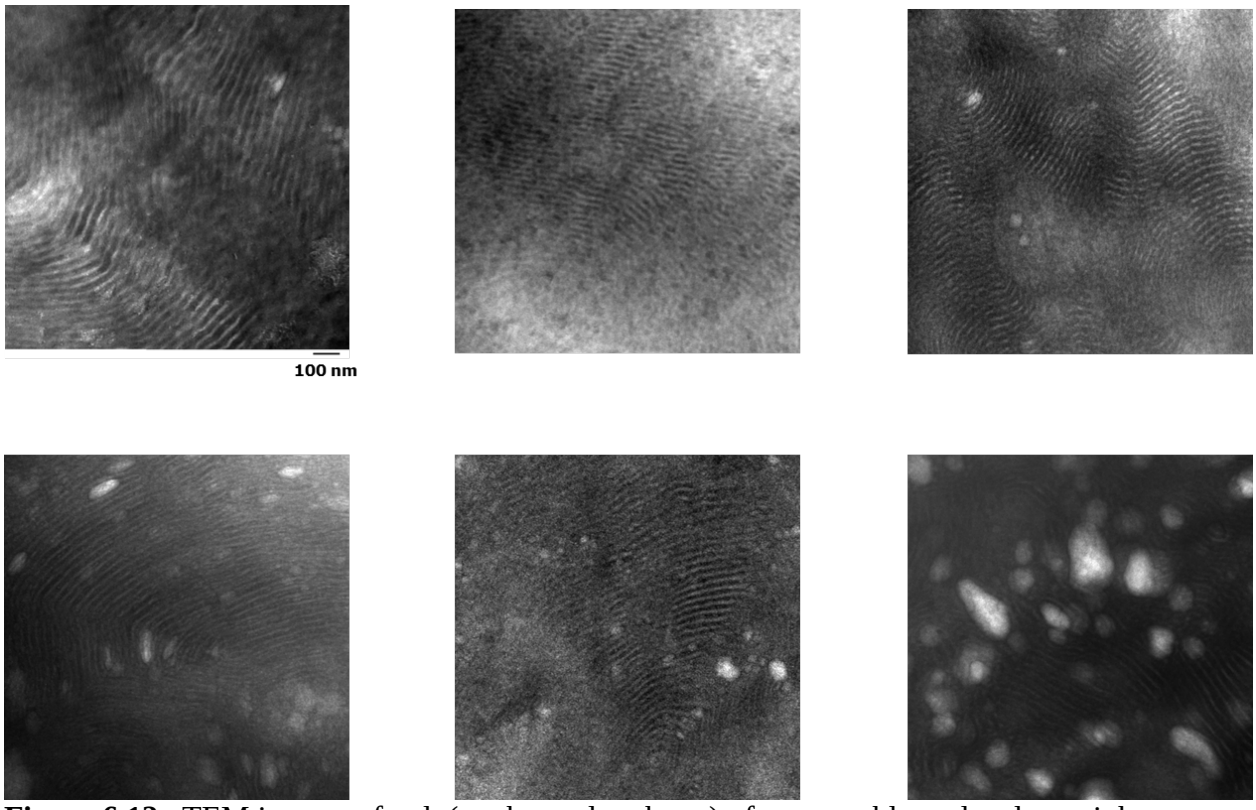

Figure 6.12. TEM images of poly(sty-b-acrylate-b-sty) of comparable molecular weights

Table 6.3 summarized the molecular weights of DMAEA triblock copolymers of the same center block compositions, but varying center block lengths. The triblock copolymers were derived from the sample poly(sty) precursor, and contained ~ 10 mol% DMAEA in the center blocks.

Table 6.3. Molecular weights of poly[sty-*b*-(*n*BA_{92}-*co*-$DMAEA_8$)-*b*-sty] of varying center block lengths.

Sample	M_n (kD)	M_w (kD)	PDI	φ_{sty}
Poly(sty) precursor-82	69.0	82.3	1.19	1.00
DMAEA triblock-100	71.8	100	1.39	
DMAEA triblock-116	80.7	116	1.44	0.45
DMAEA triblock-128	89.6	128	1.43	0.41

Figure 6.13 and **Figure 6.14** plotted the SAXS profiles for the DMAEA and SBDMAEA triblock copolymers on the same plot. The scattering profiles for the neutral triblock copolymers were quite noisy, while those for the zwitterionic triblock copolymers exhibited multiple scattering features that corresponded to both the block copolymer domains and the ionomer domains. The SAXS results for the zwitterionic triblock copolymers indicated that the sizes of the block copolymer domains for the SBDMAEA triblock copolymers increased as the center block molecular weight increased. Meanwhile, the scattering feature for the zwitterionic aggregates remained unchanged.

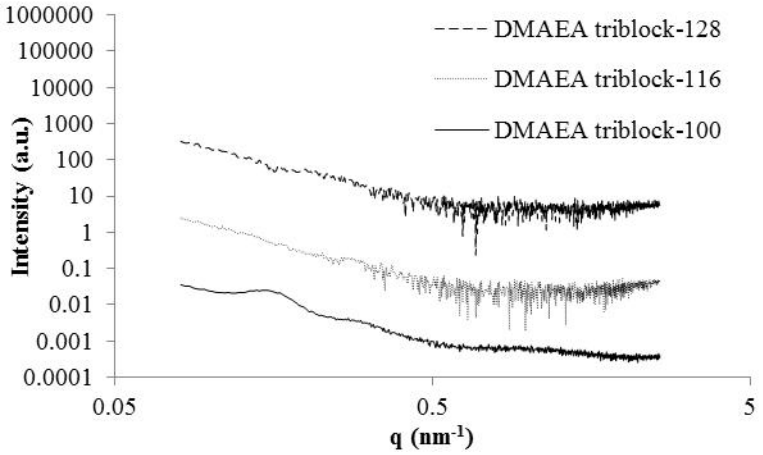

Figure 6.13. SAXS traces for poly[sty-*b*-(*n*BA$_{92}$-*co*-DMAEA$_{8}$)-*b*-sty] of varying center block lengths. The abbreviations indicate the weight-average molecular weights of the samples (in KD). The traces were shifted along the "Intensity"-axis.

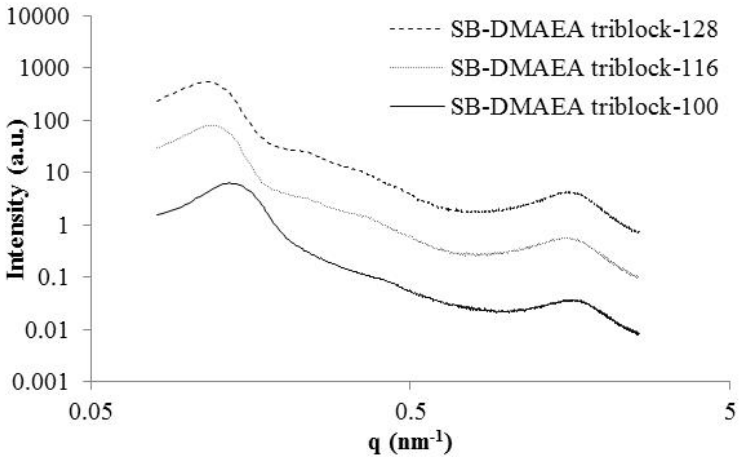

Figure 6.14. SAXS traces for poly[sty-*b*-(*n*BA$_{92}$-*co*-SB-DMAEA$_8$)-*b*-sty] of varying center block lengths. The traces were shifted along the "Intensity"-axis.

Figure 6.15 and Figure 6.16 showed the DMA traces for the neutral and the zwitterionic triblock copolymers. The thermomechanical transitions that led to rubbery flow for all triblock copolymers persisted around ~ 100 °C. For the neutral triblock copolymers, the plateau moduli decreased as the center block molecular weights increased.

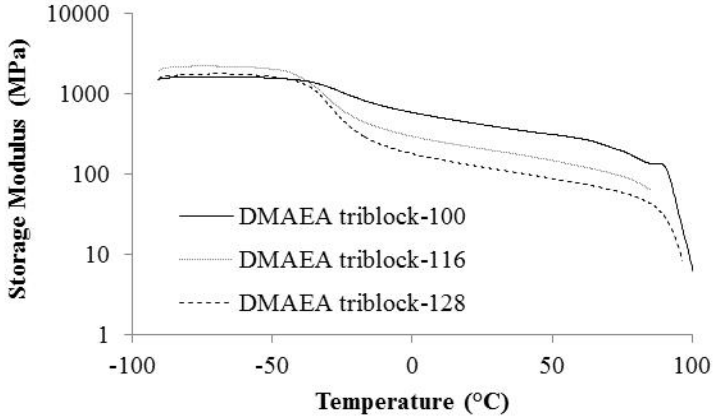

Figure 6.15. DMA traces for poly[sty-*b*-(*n*BA$_{92}$-*co*-DMAEA$_8$)-*b*-sty] of varying center block lengths.

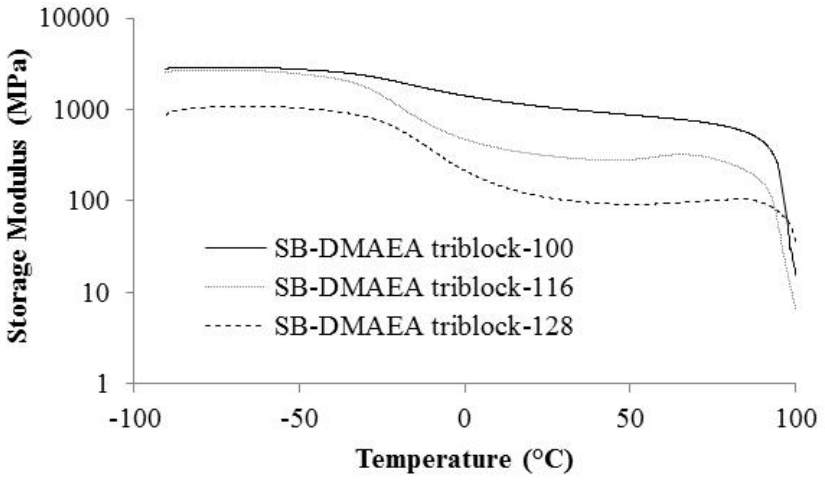

Figure 6.16 DMA traces for poly[sty-*b*-(*n*BA$_{92}$-*co*-SB-DMAEA$_{8}$)-*b*-sty] of varying center block lengths.

Chapter 7 Controlled Radical Polymerization of Tertiary Amine- and Imidazole-Containing Acrylates

(*Tianyu Wu, Shijing Cheng and Timothy E. Long**)

Department of Chemistry, Macromolecules and Interfaces Institute, Virginia 24061

*To whom correspondence should be addressed: Email telong@vt.edu

7.1 Abstract

Conventional free radical polymerization of styrene, methyl methacrylate and *n*-butyl acrylate revealed that the acrylate radicals were much more susceptible to chain transfer to polymers than the styrenic and the methacrylic radicals. As a result, CFRP synthesized poly(acrylate)s are branched. Controlled radical polymerization processes (e.g. RAFT, ATRP and NMP) mediate the reactivity of the acrylic radical and enable the synthesis of well-defined linear poly(alkyl acrylate)s. However, functional groups such as tertiary amine and imidazole on acrylic monomers interfere with the controlled radical polymerization of functional acrylates. In this work, we studied RAFT polymerization of acrylates with both *n*BA and a novel imidazole-containing acrylate. Model CFR and RAFT polymerization of *n*BA in the presence of triethyl amine and *N*-methyl imidazole revealed the interference of the functional group on the polymerization of acrylate. Various RAFT agents, RAFT agent to initiator ratios, degree of polymerization and monomer feed concentrations were screened with an imidazole-containing acrylate for optimized RAFT polymerization conditions. The results suggest that the controlled radical polymerization of functional acrylates, such as 2-(dimethylamino)ethyl acrylate

and 4-((3-(1H-imidazole-1-yl)propanoyl)oxy)-butyl acrylate (ImPBA), remained challenging.

Key Words: functional acrylate, RAFT

7.2 Introduction

Acrylic polymers are an important class of macromolecules that include both poly(acrylate)s and poly(α-substituted acrylate)s such as poly(methacrylate)s and poly(cyanoacrylate)s. They have found a wide range of applications in adhesives, coatings,[1, 2] textiles,[3] bone cements,[4] smart biocompatible materials,[5, 6] and liquid-crystalline thermosets.[7, 8] The presence of the α-substituents impacts both the reactivity of the vinyl bonds and the glass transition temperatures of the corresponding polymers. Acrylates have exhibited facile reactivity most suitable for photolithography, while poly(acrylate)s have lower glass transition temperatures than their α-substituted counterparts.

Jansen et al. studied the effect of molecular structure on the maximum rate of photoinitiated polymerizations with 56 acrylate monomers.[9, 10] They revealed a direct correlation between the calculated Bolzmann-averaged dipole moments of the acrylic monomers and their measured maximum rate of polymerization. They also noted that the hydrogen bonding within the monomers impacted both the tacticity of the resulting polymers and the rate of polymerization. Decker and Moussa investigated the reactivity of acrylate monomers that contained cyclic carbonate structures under UV irradiation.[11] They reported that these new monomers offered high reactivity and extensive cure to yield hard but still flexible polymer material after short UV exposure. Guymon and Bowman probed the polymerization and segregation behavior of *n*-decyl acrylate in a smectic liquid crystal.[12] They found that the polymerization rate increased dramatically as the temperature decreased and the order of the liquid crystalline media increased. They

also developed a kinetic model that described molecular interactions within similar monomer/smectic liquid crystal systems.

Mahdavi et al. employed photo-lithography to cure poly(glycerol-*co*-sebacate acrylate) into a dense array of fibrils that mimic gecko's feet.[13] They modified the surface of those fibrils with oxidized dextran to optimize the adhesives properties of the array for medical applications and demonstrated that the polyester based polymer network was biodegradable and biocompatible. Chan et al. also mimicked gecko feet with a cross-linked poly(*n*-butyl acrylate) elastomer for adhesive properties and presented a design strategy that uses surface wrinkles as patterns to control the adhesion.[14] Hern and Hubbell incorporated Arg-Gly-Asp (RGD) peptide sequence onto acrylate monomers and photopolymerized them into hydrogels.[15] They found that the RGD functionalized hydrogels promoted the spreading of human foreskin fibroblasts, while unfunctionalized hydrogel exhibited poor adhesion.

Meanwhile, due to the facile reactivity of the acrylic radicals, the controlled radical polymerization of functional acrylates such as 2-dimethylaminoethyl acrylate (DMAEA) remained challenging. Yamago et al. reported the synthesis of a 12 k PDMAEA with a PDI of ~ 1.2 using organotellurium-mediated living radical polymerization (TERP).[16] Monteiro and coworkers explored the controlled polymerization of DMAEA with methyl 2-(butylthiocarbonothioylthio)propanoate in dioxane.[17, 18] The resulting polymer had molecular weight of ~ 11 k and PDI of 1.26. Rowe et al. RAFT synthesized PDMAEA with *S*-1-dodecyl S'-(α,α-dimethylacetic acid) trithiocarbonate and screened its suitability as the surface modification agent for gadolinium metal-organic frame works.[19] The homopolymer had molecular weights of ~

20k (PDI ~ 1.25). In a parallel effort, Boyer et al. synthesized a 10 k poly(DMAEA) (PDI ~ 1.15) with 3-(benzylsulfanylthiocarbonylsulfanyl)-propionic acid to control the surface charges on gold nanoparticles and the colloidal stability of iron oxide nanoparticles.[20, 21]

More recently, Feng et al. grafted PDMAEA side chains onto a poly(*N*-isopropylacrylamide)-*b*-poly(2-hydroxyethyl acrylate) (PNIPAM-*b*-PHEA) backbone using CuCl/tris(2-(dimethylamino)ethyl)amine-mediated ATRP.[22] They reported that the final graft copolymers had molecular weights of ~ 35k and PDIs of ~ 1.25 and studied the suitability of such graft copolymers in stabilizing colloidal gold nanoparticles. Suchao-in et al. reported the RAFT synthesis of poly(*N*-isopropylacrylamide)-*b*-poly(DMAEA) with 2-(((butylsulfanyl)-carbonothioyl)sulfanyl) propanoic acid and demonstrated its micellization into vesicles under various experimental conditions.[23] The PNIPAAM precursor and the diblock copolymer had low PDIs and molecular weights of 13 k and 28 k respectively. Liu et al. synthesized of a miktoarm star block terpolymer μ-(PS)(PEO)(PDMAEA) (μ-SODA) using a combination of living anionic polymerization and RAFT polymerization.[24] The RAFT polymerization of the PDMAEA block was mediated with a 2-(((dodecylsulfanyl)carbonothioyl)sulfanyl)-2-methylpropanoic acid derivative. The authors reported narrow PDI of 1.10 for a 38 k μ-SODA, which contained 60 wt% of PDMAEA.

In this work, we report the synthesis of a novel imidazole-containing acrylate through Michael-addition reaction between 1,4-butanediol diacrylate and imidazole and efforts in controlling its radical polymerization using the RAFT strategy. Poly(imidazole acrylate)s and their quaternized derivatives exhibit low glass transition temperatures suitable for applications as polymerized ionic liquids.

7.3 Experimental

7.3.1 Materials

Imidazole (Aldrich, ≥99%), magnesium sulfate (Aldrich, ≥97%), 3,5-di-*tert*-4-butylhydroxytoluene (BHT, Aldrich, ≥99%), bromoethane (Aldrich, ≥99%), cyanomethyl dodecyl trithiocarbonate (C-12CM, Aldrich, 98%), 2-(dodecylthiocarbonothioylthio)-2-methylpropionic acid (C-12MP, Aldrich, 98%), 4-cyano-4-[(dodecylsulfanylthiocarbony)-sulfanyl]pentanoic acid (C-12CP, Aldrich, 97%), 1,4-butanediol diacrylate (Alfa Aeser, 99+%), potassium carbonate (Alfa Aeser, anhydrous, 99%), lithium bis(trifluoromethanesulfonimide (LiTFSI, Acros, 99%), tert-butyl methyl ether (Aldrich), acetone (Fisher Scientific, HPLC grade), methylene chloride (Fisher Scientific, HPLC grade), and *N*,*N*-dimethylformamide (Fisher Scientific) were used as received. Azobisisobutyronitrile (AIBN, Aldrich, 98%) and azobis(4-cyanovaleric acid) (V501, Aldrich, ≥98%) were recrystallized from methanol.

7.3.2 Synthesis of 4-((3-(1H-imidazole-1-yl)propanoyl)oxy)-butyl acrylate (ImPBA)

ImPBA was synthesized following a modified literature procedure.[25] Imidazole (23 g, 338 mmol) was first dissolved in *N*,*N*-dimethylformamide (500 mL), and the solution was then charged with 1,4-butanediol diacrylate (100 g, 505 mmol), potassium carbonate (1.27 g, 9.19 mmol), and BHT (1.90 g) to a 1000-mL, round-bottomed flask equipped with a magnetic stir bar. The reaction was allowed to proceed at 25 °C for 90 h. The mixture was then concentrated to 250 mL via rotatory evaporation and diluted with 150 mL deionized water. The aqueous mixture was washed with hexanes (150 mL × 4), and the product was subsequently extracted from the aqueous layer with chloroform (100 mL × 4). The combined extracts were concentrated in a vacuum evaporator to remove all

solvents, and the crude product was finally purified using flash column chromatography on silica gel with tert-butyl methyl ether and acetone in sequence.

7.3.3 Controlled radical polymerization of poly(*n*BA) and poly(ImPBA)

The controlled radical polymerization of *n*BA and ImPBA were performed employing the RAFT strategy. *n*BA was polymerized in the presence of equimolar triethyl amine and *N*-methyl imidazole to mimick the chemical environment of 2-(dimethylamino)ethyl acrylate and ImPBA, respectively, while various RAFT agent/initiator pairs, molar ratios of RAFT agents to initiators, initial monomer concentrations, and targeted degrees of polymerization at full conversion were screened for optimized RAFT polymerization of ImPBA in DMF. In a typical RAFT polymerization of ImPBA, C-12CP (15.2 mg, 0.038 mmol) and V-501 (10.4 mg, 0.037 mmol) were first dissolved in DMF (15 mL) to make a stock initiator solution. ImPBA (0.45 g, 0.0017 mmol) and the stock solution (2.0 mL) were then charged to a 10-mL round-bottomed flask equipped with a magnetic stir bar. The reaction solution was freeze-pump-thawed three times to remove oxygen and then placed into an oil bath at 65 °C for 12 h. For reaction kinetics studies, aliquots were sampled out at predetermined time intervals under ultrahigh purity nitrogen.

7.3.4 Synthesis of poly(ImPBA) and post-polymerization functionalization to poly(EImPBA TFSI)

In a typical polymerization reaction, ImBA (1.0 g, 3.8 mmol), AIBN (5 mg, 30 μmol) and *N*,*N*-dimethylformamide (5mL) were charged to a 50-mL, round-bottomed flask equipped with a magnetic stir bar. The reaction mixture was sparged with ultrahigh purity nitrogen for 10 min and then placed into an oil bath at 65 °C for 20 h. The reaction

product was isolated via vacuum removal of the solvent, dissolved in methanol and finally dialyzed against methanol for 24 h (Spectrum).

Poly(ImPBA) was subsequently quaternized with bromoethane. In a typical quaternization reaction, poly(ImPBA) (0.46 g), bromoethane (1.2 g, 11 mmol) and chloroform (4.5 mL) were charged to a 50-mL, round-bottomed flask equipped with a magnetic stir bar. The reaction was refluxed for 40 h. After rotary evaporation of the solvent, poly(EImPBA Br) was precipitated into diethyl ether from a methanol/water (2/1 v/v) mixture and dried in a vacuum oven at 65 °C. To obtain poly(EImPBA TFSI), poly(EImPBA Br) (0.36 g) and LiTFSI (0.65 g, 2.3 mmol) were separately dissolved in methanol at 10 wt% concentrations. Upon mixing the two solutions at 25 °C, poly(EImPBA TFSI) precipitates appeared. The precipitates were washed with pure methanol for three times and then dried in vacuum oven at 65 °C.

7.3.5 Instrumentation

^{1}H, ^{13}C and ^{19}F NMR spectra were obtained on a JOEL 500 MHz spectrometer in $CDCl_3$, CD_3OD or DMSO-d_6. Aqueous size exclusion chromatography (SEC) determined the molecular weights of poly(ImBA) at 35 °C and 0.8 $mL \cdot min^{-1}$ flow rate (solvent: 54/23/23 H_2O/methanol/acetic acid (v/v/v%), 0.1 M sodium acetate). The Aqueous SEC system was equipped with a Waters 717plus autosampler, a Waters 1515 HPLC pump, two Waters Ultrahydrogel Linear and one Waters Ultrahydrogel 250 columns, a Waters 2414 differential refractive index detector, and a Wyatt miniDAWN multiangle laser light scattering (MALLS) detector operating at a wavelength of 690 nm. The specific refractive index increment value (dn/dc) for poly(ImBA) in the aqueous eluent was determined offline using a Wyatt Optilab T-rEX refractive index detector at 660 nm and

35 °C. Absolute molecular weights for poly(ImPBA) were calculated using the Wyatt ASTRA V software package with a dn/dc of 0.16 $mL \cdot g^{-1}$. Thermogravimetric analysis (TGA) of the samples employed a TA Q500 from 25 °C to 700 °C at a heating rate of 10 $°C \cdot min^{-1}$ under N2 atmosphere. Differential scanning calorimetry (DSC) measurements were performed on a TA Q2000 instrument at a heating rate of 10 °C/min from -65 °C. The first heat scans were concluded at 120 °C, and traces of the second heats are reported.

7.4 Results and Discussions

7.4.1 Conventional free radical polymerization of styrene, methyl methacrylate and *n*-butyl acrylate.

Scheme 7.1 illustrates the conventional free radical polymerization of styrene (Sty), methyl methacrylate (MMA) and *n*-butyl acrylate (*n*BA) under identical reaction conditions. ^{1}H NMR determined monomer conversions after 9 h, and size exclusion chromatography determined the molecular weights of the polymer products in THF. The results are tabulated in **Table7.1**, and the molecular weights are relative to poly(styrene) standards.

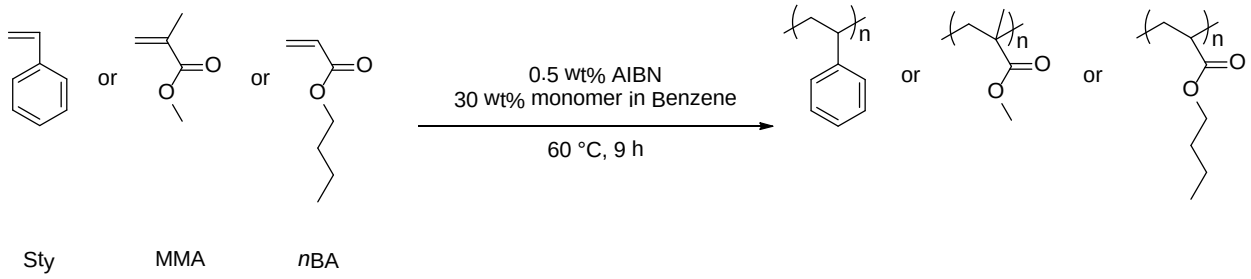

Scheme 7.1 Conventional free radical polymerization of Sty, MMA and *n*BA

Styrene had the lowest monomer conversion among the three monomers at 16% after 9 h, followed by MMA at 46%. *n*BA exhibited the highest monomer conversion of 94% within the same reaction time. The lower PDI of 1.60 for poly(sty) confirmed that the styrenic radicals terminated predominately through radical coupling, while a PDI of 1.89 indicated that the methacrylic radicals terminated mainly through the disproportionation mechanism.[26] In comparison, the molecular weight for the poly(*n*BA) sample was much higher than those for either poly(sty) or poly(MMA). Its higher PDI of 2.46 indicated that the polymer was branched.

Table 7.1 Summary of the conventional free radical polymerization of Sty, MMA and *n*BA

Monomer	Conversion (%)	M_n (kD)	M_w (kD)	PDI
Sty	16	27.6	44.2	1.60
MMA	46	46.9	88.8	1.89
*n*BA	94	222	545	2.46

A number of publications discussed chain transfer reactions involving *n*BA radicals over the past decade.[27-29] **Scheme 7.2** illustrates the mechanism of inter- and intra-molecular chain transfer to polymer in the free radical polymerization of *n*BA. Nikitin and Buback et al. extracted the free radical polymerization rate coefficient for *n*BA intra-molecular chain transfer (backbiting, k_{bb}) and for monomer addition to the resulting mid-chain radical (k_p^t) using pulsed laser polymerization (PLP) size exclusion chromatography (SEC) technique.[30] Hlalele and Klumperman employed in situ NMR to study the radical polymerization of *n*-butyl acrylate.[31-33] They confirmed the coexistence

of both secondary propagating radicals and tertiary mid-chain radicals in the polymerization processes and studied the influence of nitroxide addition on *n*BA polymerization rate. They found that, when free $[DEPN]_0$ was no more than 1 % of initiator [MAMA-DEPN], the polymerization of *n*BA was thermally auto-initiated and the rate of polymerization was independent of $[DEPN]_0$. Ahmad et al. studied chain transfer from *n*-butyl acrylate radicals to poly(*n*BA) in conventional free-radical polymerizations and controlled radical polymerizations (i.e. ATRP, RAFT and NMP) using ^{13}C NMR measurements.[34] The authors concluded that controlled radical polymerization strategies significantly reduced the mol% branches in the resulting polymers. They attributed such observation to the lower concentration of highly reactive short-chain radicals, which were expected to undergo chain transfer to polymers at higher rates, under controlled radical polymerization conditions.

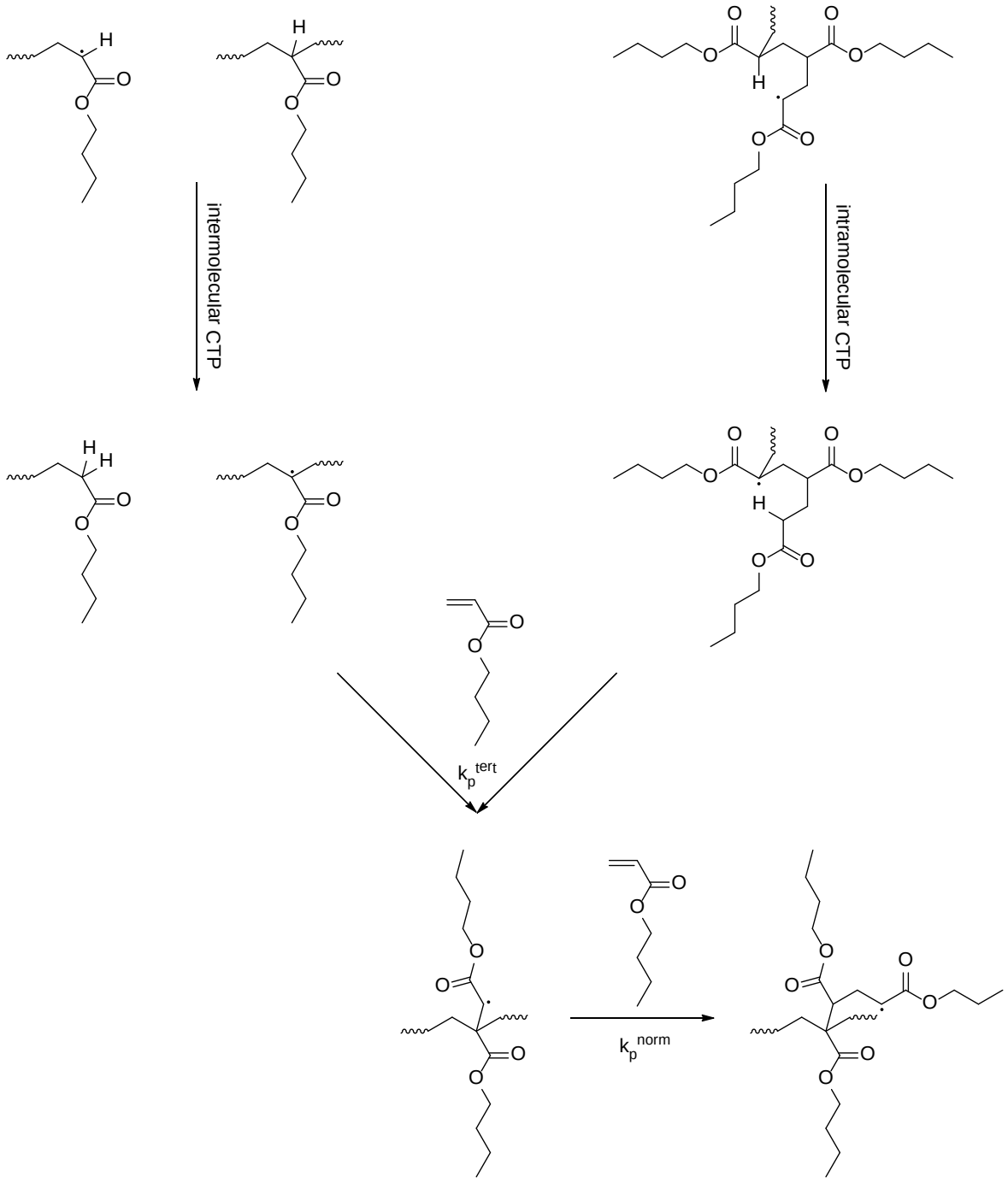

Scheme 7.2 The mechanism of inter- and intra-molecular chain transfer to polymer in the free radical polymerization of *n*-butyl acrylate.

7.4.2 RAFT polymerization of *n*BA with varying CTA and CTA:Ini ratios.

A wide variety of thiocarbonylthio RAFT agents, which include dithioesters, trithiocarbonates, xanthates and dithiocarbamates, have demonstrated their suitability as mediating agents in controlled radical polymerizations. **Figure 7.1** illustrates the structural features of a thiocarbonylthio RAFT agent. The "Z" group modifies addition and fragmentation rates, while the "R" group is the free radical leaving group, which reinitiates polymerization.

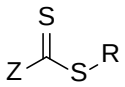

Figure 7.1 Structural features of thiocarbonylthio RAFT agents

We examined the suitability of three commercially available RAFT agents, i.e. C-12MP, C-12CM and C-12CP, in mediating the homopolymerization of *n*BA. The three RAFT agents have the same "Z" group, but different "R" groups, and their chemical structures are shown in **Scheme 7.3**. Both C-12MP and C-12CM were paired with AIBN, while C-12CP was paired with V-501. In all case, *n*BA concentrations were maintained at ~ 1.7 M, and the targeted DPs at full monomer conversion were ~ 570.

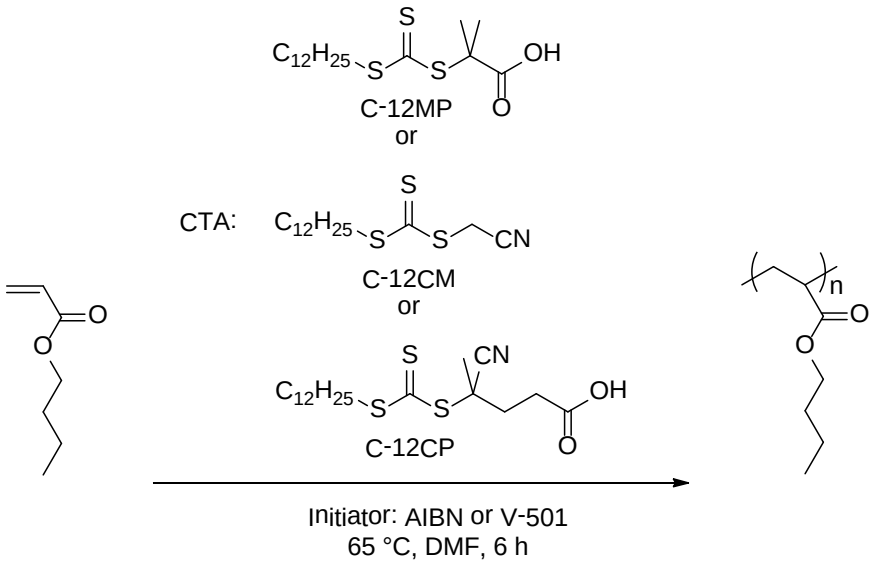

Scheme 7.3 RAFT polymerization of *n*BA with varying RAFT agent/initiator pairs

Table 7.2 compares *n*BA conversions after 6 h for varying CTA choices and at a CTA:Ini ratio of 10:1. Both C-12MP and C-12CP mediated homopolymerization of *n*BA reached ~ 50% conversion. The molecular weights of all three products were of narrow PDIs, suggesting that the impact of acrylic radical transfer to polymer was significantly reduced under RAFT polymerization conditions.

Table 7.2 *n*BA conversion after 6 h with varying CTAs and the molecular weights of the resulting poly(*n*BA)

RAFT Agent	Conversion (%)	Mw (kD)	PDI
C-12MP	46	32.6	1.11
C-12CM	23	18.0	1.10
C-12CP	48	22.1	1.14

Figure 7.2 compares the size exclusion chromatograms of poly(*n*BA) synthesized in the presence of C-12CP at varying CTA to initiator ratios from 10:1 to 1:2. The polymerizations were performed at 2.0 M *n*BA concentrations and with targeted DPs of ~ 650 at full conversions. The reactions were allowed to proceed at 65°C for 75 min, and they reached between 25% and 65% monomer conversions. The results suggested that an increase in initiator concentration led to higher rates of monomer consumption. However, the PDIs broadened as the CTA:Ini ratios decreased. Therefore, careful selection of the CTA:Ini ratio is paramount for efficient polymerization and optimized molecular weight control.

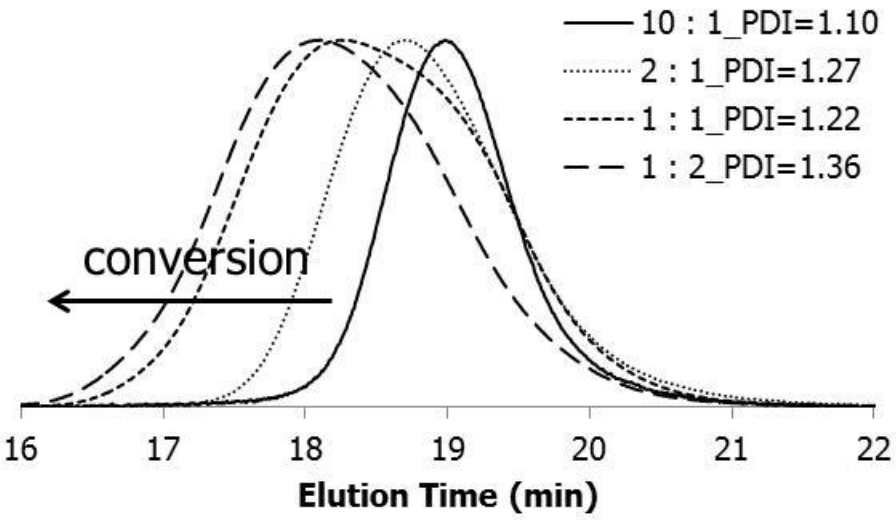

Figure 7.2 Size exclusion chromatogram for C-12CP mediated RAFT polymerization of *n*BA at varying CTA : Ini ratios (10:1 to 1:2)

7.4.3 CFR and RAFT polymerization of *n*BA in the presence of triethylamine (TEA) and 1-methylimidazole (*N*-MIm).

Scheme 7.4 illustrates the conventional free radical polymerization (CFRP) of *n*BA in the presence of triethylamine and C-12CP mediated RAFT polymerization of *n*BA in the presence of *N*-methylimidazole.

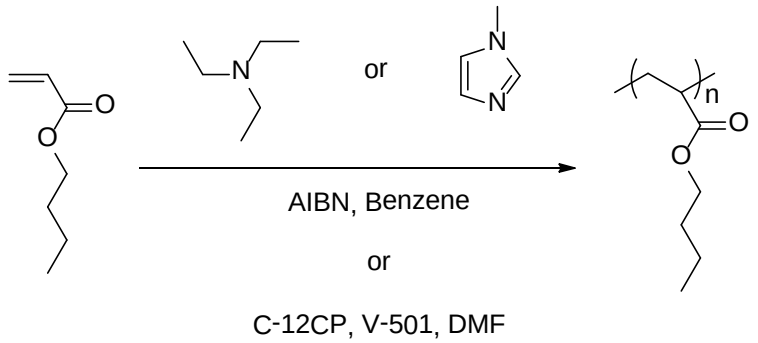

Scheme 7.4. CFR and C-12CP-mediated RAFT polymerization of *n*BA in the presence of triethylamine and 1-methyl imidazole

The CFRP was performed in benzene, while the RAFT polymerization was conducted in DMF. **Figure 7.3** plots the reciprocal of DP for poly(*n*BA) as a function of TEA to *n*BA molar ratios in the feed. All polymerizations were performed with 50 wt% of *n*BA in benzene and 0.5 wt% of AIBN to *n*BA in the feed. All reactions reached ~ 50% monomer conversion in 75 min, and the molecular weights of poly(*n*BA) were reported from the light scattering detector of the SEC with an dn/dc value of 0.07 mL/g. The molecular weights of poly(*n*BA) decreased as the molar ratio of [TEA] in the feed increased. The Mayo equation described the radical chain transfer to the monomer, the solvent and the initiator as follows:

$$\frac{1}{\overline{X_n}} = \frac{R_i}{2R_p} + C_M + C_s\frac{[S]}{[M]} + C_I\frac{[I]}{[M]}$$

The linear plot indicated that the acrylic radicals chain transferred to TEA with a C_s value of 0.024, in agreement with earlier literature reports,[35] and it is significantly high in a radical polymerization process.

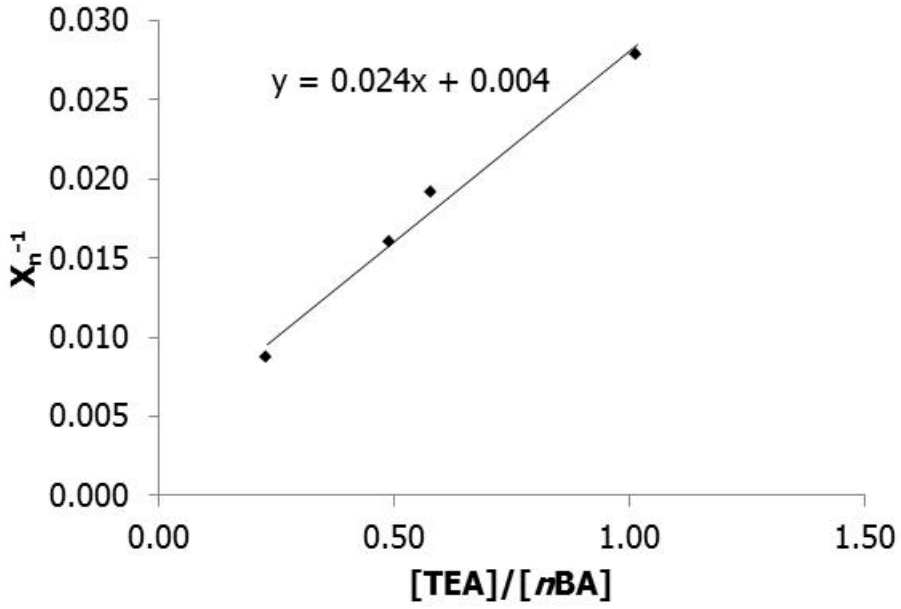

Figure 7.3 X_n^{-1} *vs.* [TEA]/[*n*BA] plot for the homopolymerization of *n*BA in benzene

In comparison, the molecular weights of poly(*n*BA) synthesized using CFRP in the presence of *N*-MIm was independent of [*N*-MIm]/[*n*BA] feed ratio. However, *n*BA did not polymerize at CTA:Ini ratio of 2:1 or higher when equimolar *N*-MIm was presence. **Figure 7.4** plots the reaction kinetics for C-12CP mediated homopolymerization of *n*BA in the presence of equimolar *N*-MIm and at CTA:Ini ratio of 1:1. Despite an inhibition period of ~ 30 min, the polymerization followed pseudo-first order reaction kinetics, which is characteristic of controlled radical polymerization. Coote attributed the initial rate retardation to the slow fragmentation of the polymeric RAFT-adduct radical through ab inito calculations.[36]

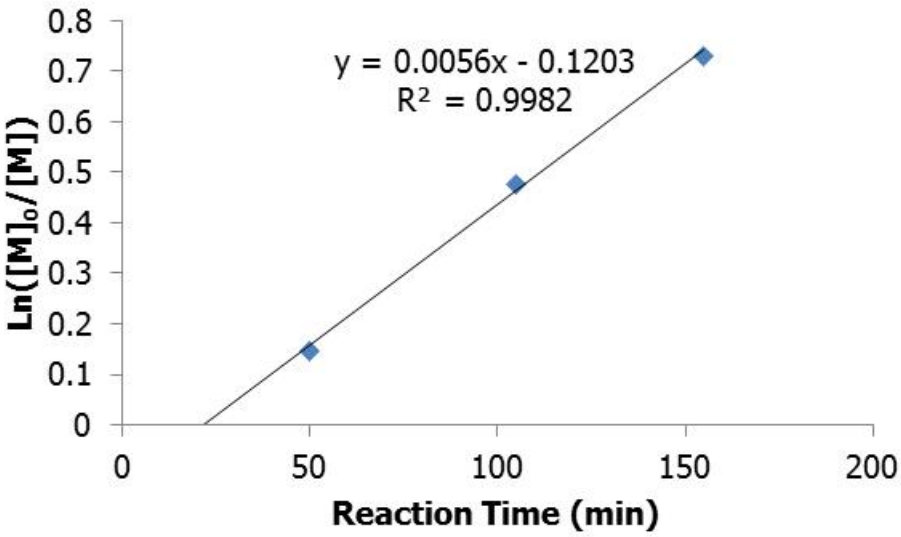

Figure 7.4 Reaction kinetics for C-12CP mediated polymerization of *n*BA in the presence of equal molar 1-MIm and at CTA:Ini ratio of 1:1

Figure 7.5 plots both the weight-average molecular weights of poly(*n*BA) and their PDIs as a function of monomer conversions for C-12CP mediated RAFT polymerization of *n*BA in the presence of *N*-MIm. While the actual molecular weights of poly(*n*BA) were within the vicinity of the theoretical prediction, their linear trend crossed the theoretical molecular weight prediction at ~ 40% conversion with a smaller slop. In addition, the PDIs of the samples increased from 1.14 at 14% conversion to 1.33 at 52% conversion. Here, we demonstrated the controlled radical polymerization of *n*BA in the presence of *N*-MIm using RAFT with C-12CP at CTA:Ini ratio of 1:1. However, it was more challenging than in the absence of *N*-MIm.

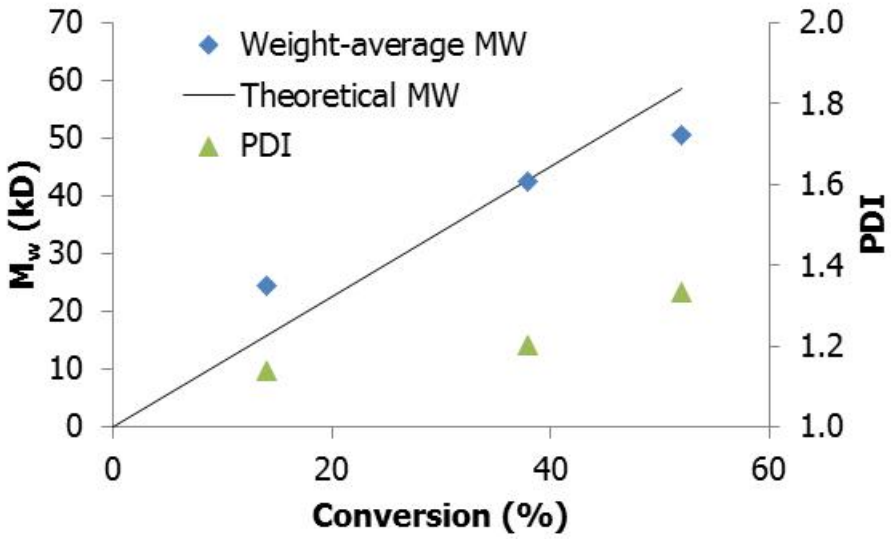

Figure 7.5 Weight-average molecular weight and PDI *vs.* conversion plot for C-12CP-mediated RAFT polymerization of *n*BA in the presence of *N*-MIm at CTA:Ini ratio of 1:1

7.4.4 Synthesis of 4-((3-(1H-imidazole-1-yl)propanoyl)oxy)-butyl acrylate (ImPBA).

The synthesis of ImPBA followed a modified literature procedure,[25] in which excess of 1,4-butanediol diacrylate was used to minimize difunctional Michael adduct (**Scheme 7.5**). Unreacted 1,4-butanediol diacrylate and BHT impurity were removed during the hexane washes, while K_2CO_3 remained in the aqueous phase during the chloroform extractions. ImPBA was then isolated from the crude using flash column chromatography. TLC results showed that ImPBA had a R_f of ~ 0 in tert-butyl methyl ether and a R_f of ~ 0.4 in acetone, while trace residue of 1,4-butanediol diacrylate had a R_f of ~ 0.8 in tert-butyl methyl ether. Therefore, tert-butyl methyl ether was first used as the eluent to remove 1,4-butanediol diacrylate impurity, and acetone was then chosen to collecte ImPBA. The final product had a yield of 40%. **Figure 7.6** shows the 1H NMR spectrum of ImPBA obtained in $CDCl_3$.

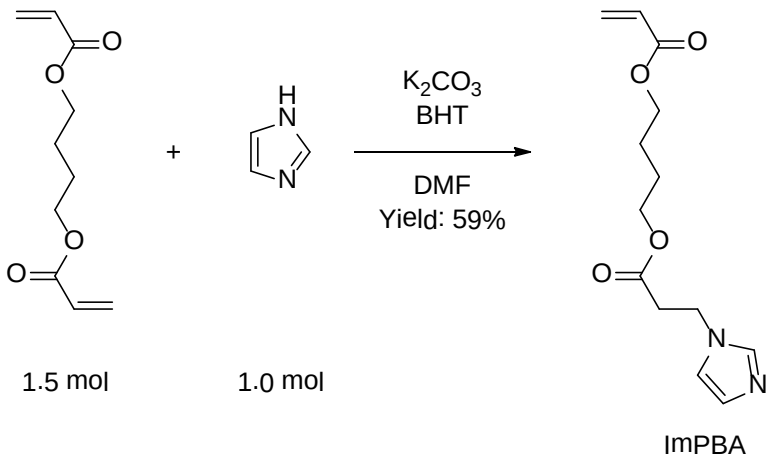

Scheme 7.5. Synthesis of 4-((3-(1*H*-imidazol-1-yl)propanoyl)oxy)butyl acrylate (ImPBA)

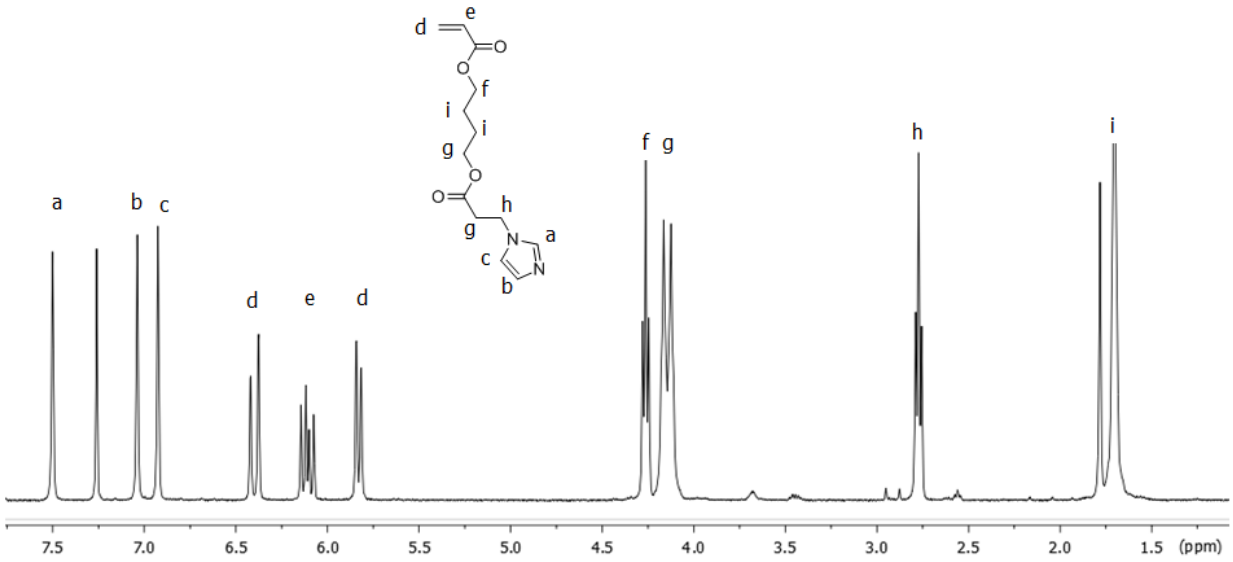

Figure 7.6 ^{1}H NMR of ImPBA in $CDCl_3$

7.4.5 Polymerization of ImPBA, subsequent quaternization with bromoethane and anion exchange to poly(EImPBA TFSI).

Scheme 7.6 illustrates the conventional free radical polymerization of poly(ImPBA) and subsequent post-polymerization modifications that yielded

poly(EImPBA TFSI). **Figure 7.7** compares the ^{1}H NMR of the poly(ImPBA) precursor and the poly(EImPBA TFSI) product.

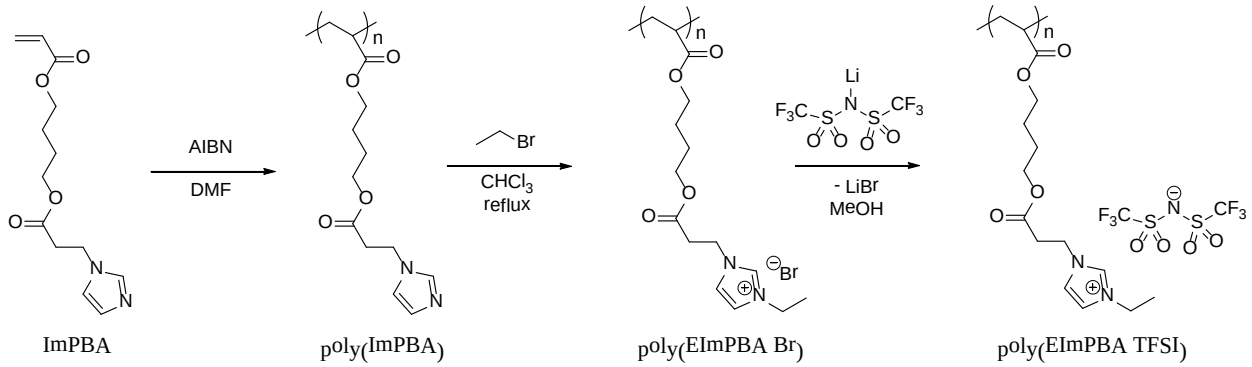

Scheme 7.6. Conventional free radical polymerization of ImPBA, quaternization of poly(ImPBA) with bromoethane and subsequent anion exchange with LiTFSI

Poly(ImPBA) precipitated out of chloroform upon quaternization with bromoethane. The ^{1}H resonances at “a”, “b” and “c” corresponded to the three protons on the imidazole ring in poly(ImPBA), while those at “a’”, “b’” and “c’” corresponded to the three protons on the imidazolium ring in poly(EImPBA TFSI). The complete shift of imidazole resonances to the imidazolium resonances confirmed that the quaternization reaction proceeded to 100% conversion. Since poly(EImPBA Br), LiTFSI and LiBr are all soluble in methanol, reprecipitation of poly(EImPBA TFSI) into methanol was sufficient to remove all impurities.

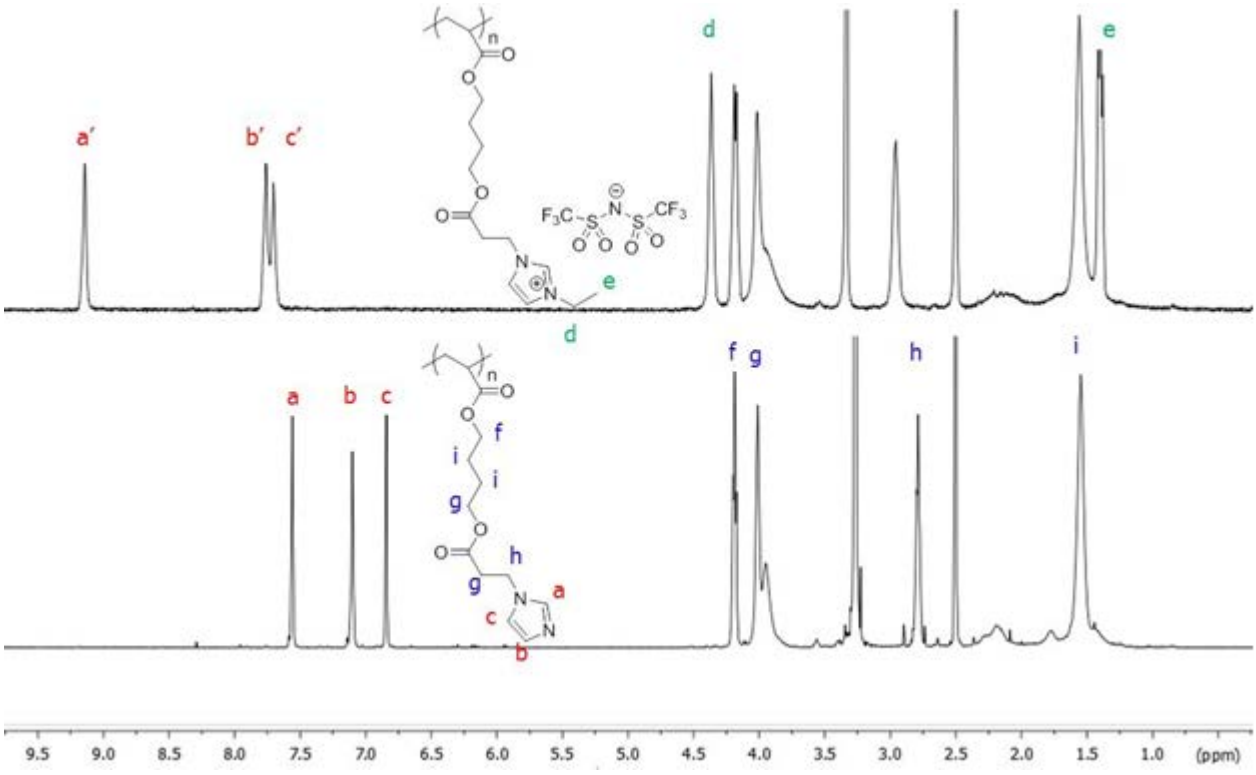

Figure 7.7 ^{1}H NMR of poly(ImPBA) and poly(EImPBA TFSI) obtained in DMSO-d_6

7.4.6 Thermal properties of poly(ImPBA) and its quaternized derivatives.

Table 7.3 lists the glass transition temperatures and the 5% weight loss temperatures of poly(ImPBA), poly(EImPBA Br) and poly(EImPBA TFSI). All three polymers exhibited sub-zero glass transition temperatures. Quaternization of poly(ImPBA) with bromoethane increased its T_g from -26 °C to -12 °C. Subsequent anion exchange of the Br anion to bulkier TFSI anion resulted in lower T_g of -28 °C, in agreement with earlier literature reports. In addition, the choice of the counter-anion also impacted the thermal stability of the quaternized poly(ImPBA). While poly(ImPBA) and poly(EImPBA Br) exhibited similar $T_{d,5\%}$ temperatures of ~ 220 °C, anion exchange of Br to TFSI improved the Td,5% of poly(EImPBA TFSI) to 324 °C. These results

suggested that anion exchange of quaternized poly(ImPBA) allowed great tunability toward their thermal properties.

Table 7.3 Thermal properties of poly(ImPBA) and its quaternized derivatives

Sample	T_g (°C)	$T_{d,5\%}$ (°C)
Poly(ImPBA)	-26	225
Poly(EImPBA Br)	-12	221
Poly(EImPBA TFSI)	-28	324

7.4.7 Reaction condition screening for optimized RAFT polymerization of ImPBA.

Scheme 7.7 illustrates the RAFT polymerization of ImPBA. All three RAFT agents (i.e. C-12MP, C-12CM and C-12CP) and varying molar ratios of chain transfer agents (CTA) to initiators (Ini) (i.e. 10:1, 2:1, 1:1, and 1:2) were screened for optimized controlled radical polymerization of ImPBA. In all reactions, ImPBA concentrations were maintained at ~ 0.75 M, and the targeted DPs at full monomer conversion were ~ 300.

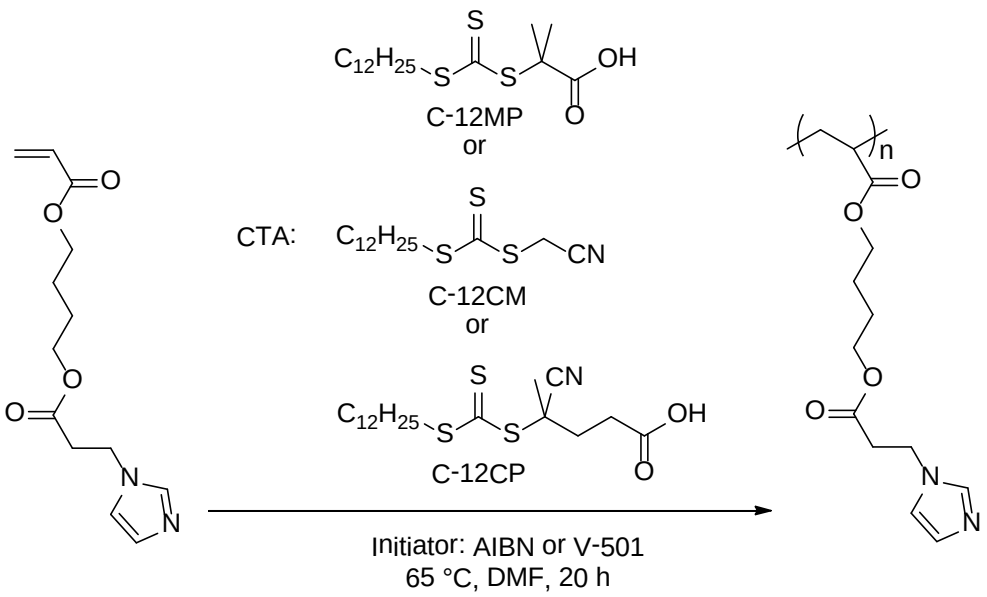

Scheme 7.7 Synthesis of poly(ImPBA) in the presence of RAFT agents with varying "R" groups

Table 7.4 compares ImPBA conversion after 20 h for varying CTA choices and CTA:Ini ratios. As expected, little monomer conversion was observed at CTA:Ini ratio of 10:1 for any of the selected CTAs. Increasing the initiator concentrations led to higher monomer conversions over the same reaction time. In addition, C-12CP was much more efficient at mediating the homopolymerization of ImPBA at CTA:Ini ratios of 2:1 than either C-12MP or C-12CM. Size exclusion chromatography results determined that ImPBA polymerized with C-12CP at CTA:Ini ratio of 1:1had PDI of 1.24.

Table 7.4. ImPBA conversion after 20 h with varying CTAs and CTA:Ini ratios

	Monomer Conversion (%)		
CTA : Ini	C-12MP	C-12CM	C-12CP
10 : 1		0	5
2 : 1	0	0	50
1 : 1	0	94	92
1 : 2	98	90	94

Figure 7.8 plots the reaction kinetics for C-12CP-mediated RAFT polymerization of ImPBA at C-12CP:V-501 feed ratio of 1:1, [ImPBA] of 0.75 M and $DP_{100\%}$ of 300. The results indicated that the reaction followed pseudo-first order reaction kinetics, which was characteristic of controlled radial polymerization reactions, after a 150 min inhibition period. The inhibition period was longer than that observed for the RAFT polymerization of *n*BA in the presence of equimolar *N*-MIm under the same reaction conditions. The k_{app} of 4.3×10^{-5} s^{-1} was half of the k_{app} for the RAFT polymerization of *n*BA in the presence of *N*-MIm.

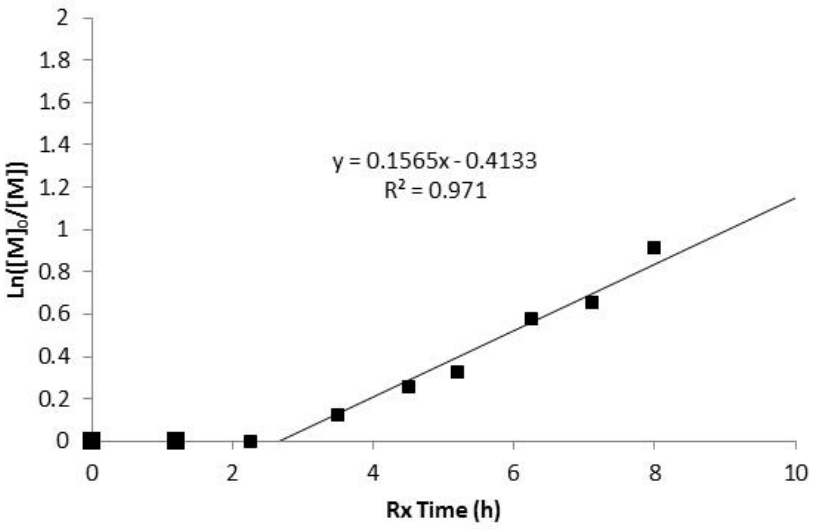

Figure 7.8 Reaction kinetics for C-12CP-mediated RAFT polymerization of ImPBA at 65 °C, C-12CP:V-501 feed ratio of 1:1, [ImPBA] of 0.75 M and $DP_{100\%}$ of 300.

Figure 7.9 plots the size exclusion chromatograms for poly(ImPBA) sampled out over time. As the reaction proceeded, the SEC chromatograms shifted toward shorter elution time, which corresponded to higher molecular weights.

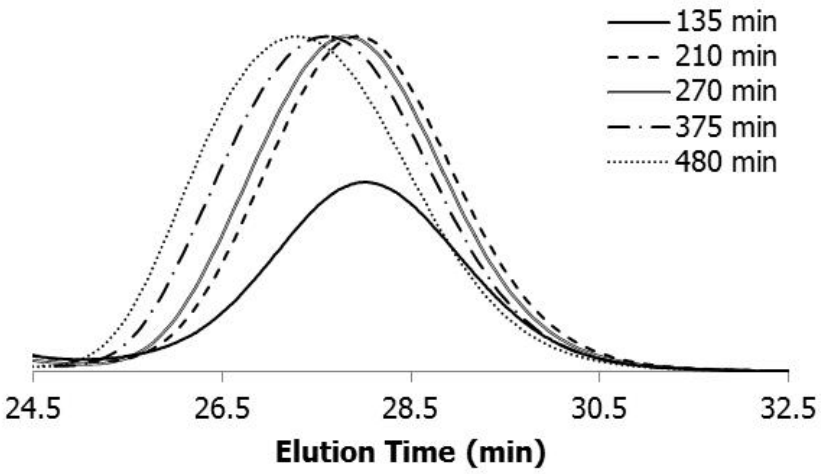

Figure 7.9 Aqueous size exclusion chromatogram for poly(ImPBA) sampled out over time

Figure 7.10 plots the molecular weights and PDIs of RAFT synthesized poly(ImPBA) as a function of the reaction conversion. While the PDIs of all samples remained < 1.2, The molecular weight plot indicated that the radical process was not well-controlled.

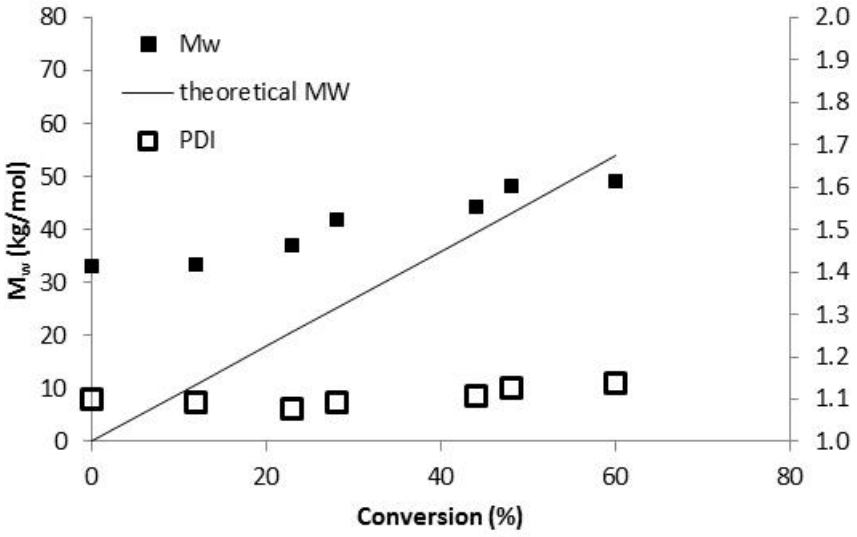

Figure 7.10 Weight-average molecular weight and PDI *vs.* conversion plot for C-12CP-mediated RAFT polymerization of ImPBA at CTA:Ini ratio of 1:1

7.5 Conclusions

Conventional free radical polymerization of Sty, MMA and *n*BA revealed that the acrylate radicals were much more susceptible to chain transfer to the polymer than methacrylic and styrenic radicals. As a result, CFRP synthesized poly(acrylate)s are often branched. Controlled radical polymerization process (e.g. RAFT, ATRP and NMP) significantly minimized the impact of acrylic radical transfer. However, controlled radical polymerization of functional acrylates, such as DMAEA and ImPBA, remained challenging.

7.6 Acknowledgements

This material is based upon work supported by the U.S. Army Research Office under grant number W911NF-07-1-0452 Ionic Liquids in Electro-Active Devices (ILEAD) MURI.

7.7 References

1. Gorelov, Y. P.; Mekalina, I. V.; Trigub, T. S.; Shalaginova, I. A.; Sentyurin, E. G.; Bogatov, V. A.; Aizatulina, M. K. *Russian Journal of General Chemistry* 2011, 81, (5), 1036-1041.
2. Francis, L. F.; Grunlan, J. C.; Sun, J.; Gerberich, W. W. *Colloids and Surfaces A: Physicochemical and Engineering Aspects* 2007, 311, (1–3), 48-54.
3. Ye, H.; Li, Z.; Chen, G.; Zhou, S.; Cai, J. *Adv. Mater. Res. (Durnten-Zurich, Switz.)* 2011, 331, (Advances in Textile Engineering), 229-236.
4. Boesel, L. F.; Reis, R. L. *Progress in Polymer Science* 2008, 33, (2), 180-190.
5. Lutz, J.-F. *Journal of Polymer Science Part A: Polymer Chemistry* 2008, 46, (11), 3459-3470.
6. Vauthier, C.; Dubernet, C.; Fattal, E.; Pinto-Alphandary, H.; Couvreur, P. *Advanced Drug Delivery Reviews* 2003, 55, (4), 519-548.
7. Barclay, G. G.; Ober, C. K. *Progress in Polymer Science* 1993, 18, (5), 899-945.
8. Lub, J.; Broer, D. J.; Wegh, R. T.; Peeters, E.; I van der Zande, B. M. *Molecular Crystals & Liquid Crystals* 2005, 429, (1), 77-99.
9. Jansen, J. F. G. A.; Dias, A. A.; Dorschu, M.; Coussens, B. *Macromolecules* 2002, 35, (20), 7529-7531.
10. Jansen, J. F. G. A.; Dias, A. A.; Dorschu, M.; Coussens, B. *Macromolecules* 2003, 36, (11), 3861-3873.
11. Decker, C.; Moussa, K. *Die Makromolekulare Chemie, Rapid Communications* 1990, 11, (4), 159-167.
12. Guymon, C. A.; Bowman, C. N. *Macromolecules* 1997, 30, (18), 5271-5278.
13. Mahdavi, A.; Ferreira, L.; Sundback, C.; Nichol, J. W.; Chan, E. P.; Carter, D. J. D.; Bettinger, C. J.; Patanavanich, S.; Chignozha, L.; Ben-Joseph, E.; Galakatos, A.; Pryor, H.; Pomerantseva, I.; Masiakos, P. T.; Faquin, W.; Zumbuehl, A.; Hong, S.; Borenstein, J.; Vacanti, J.; Langer, R.; Karp, J. M. *Proceedings of the National Academy of Sciences* 2008, 105, (7), 2307-2312.
14. Chan, E. P.; Smith, E. J.; Hayward, R. C.; Crosby, A. J. *Advanced Materials* 2008, 20, (4), 711-716.
15. Hern, D. L.; Hubbell, J. A. *Journal of Biomedical Materials Research* 1998, 39, (2), 266-276.
16. Yamago, S.; Iida, K.; Yoshida, J.-i. *Journal of the American Chemical Society* 2002, 124, (46), 13666-13667.
17. Truong, N. P.; Jia, Z.; Burges, M.; McMillan, N. A. J.; Monteiro, M. J. *Biomacromolecules* 2011, 12, (5), 1876-1882.

18. Truong, N. P.; Jia, Z.; Burgess, M.; Payne, L.; McMillan, N. A. J.; Monteiro, M. J. *Biomacromolecules* 2011, 12, (10), 3540-3548.
19. Rowe, M. D.; Chang, C.-C.; Thamm, D. H.; Kraft, S. L.; Harmon, J. F.; Vogt, A. P.; Sumerlin, B. S.; Boyes, S. G. *Langmuir* 2009, 25, (16), 9487-9499.
20. Boyer, C.; Whittaker, M. R.; Chuah, K.; Liu, J.; Davis, T. P. *Langmuir* 2009, 26, (4), 2721-2730.
21. Boyer, C.; Priyanto, P.; Davis, T. P.; Pissuwan, D.; Bulmus, V.; Kavallaris, M.; Teoh, W. Y.; Amal, R.; Carroll, M.; Woodward, R.; St Pierre, T. *Journal of Materials Chemistry* 2010, 20, (2), 255-265.
22. Feng, C.; Shen, Z.; Li, Y.; Gu, L.; Zhang, Y.; Lu, G.; Huang, X. *Journal of Polymer Science Part A: Polymer Chemistry* 2009, 47, (7), 1811-1824.
23. Suchao-In, N.; De Bruyn, H.; Perrier, S.; Chirachanchai, S. *Journal of Polymer Science Part A: Polymer Chemistry* 2009, 47, (24), 6783-6788.
24. Liu, C.; Hillmyer, M. A.; Lodge, T. P. *Langmuir* 2009, 25, (24), 13718-13725.
25. Cheng, S.; Zhang, M.; Dixit, N.; Moore, R. B.; Long, T. E. *Macromolecules* 2012, 45, (2), 805-812.
26. Odian, G., *Principles of Polymerization*. Fourth Edition ed.; John Wiley & Sons, Inc.: Hoboken, New Jersey, 2004.
27. Barner-Kowollik, C. *Macromol. Rapid Commun.* 2009, 30, (23), 1961-1963.
28. Maeder, S.; Gilbert, R. G. *Macromolecules* 1998, 31, (14), 4410-4418.
29. Plessis, C.; Arzamendi, G.; Leiza, J. R.; Schoonbrood, H. A. S.; Charmot, D.; Asua, J. M. *Macromolecules* 1999, 33, (1), 4-7.
30. Nikitin, A. N.; Hutchinson, R. A.; Buback, M.; Hesse, P. *Macromolecules* 2007, 40, (24), 8631-8641.
31. Hlalele, L.; Klumperman, B. *Macromolecules* 2011, 44, (14), 5554-5557.
32. Hlalele, L.; Klumperman, B. *Macromolecules* 2011, 44, (17), 6683-6690.
33. Hlalele, L.; Klumperman, B. *Macromolecules* 2011, 44, (18), 7100-7108.
34. Ahmad, N. M.; Charleux, B.; Farcet, C.; Ferguson, C. J.; Gaynor, S. G.; Hawkett, B. S.; Heatley, F.; Klumperman, B.; Konkolewicz, D.; Lovell, P. A.; Matyjaszewski, K.; Venkatesh, R. *Macromol. Rapid Commun.* 2009, 30, (23), 2002-2021.
35. *Polymer Handbook, Fourth Edition*. John Wiley & Sons, Inc.: 1999.
36. Coote, M. L. *Macromolecules* 2004, 37, (13), 5023-5031.

Chapter 8 Overall Conclusions

Zwitterions are unique functionalities that exhibit strong inter- and intra-molecular electrostatic interactions. Earlier literature focused on their potential in thermoplastic elastomers, while recent research efforts aimed at harnessing their structural similarities to phospholipids that exhibit anti-fouling characteristics. In this dissertation, we successfully designed and synthesized 2-[butyl(dimethyl)amino]ethyl methacrylate methanesulfonate (BDMAEMA MS) as the cationic analog to 3-[[2-(methacryloyl-oxy)ethyl](dimethyl)ammonio]-1-propanesulfonate (SBMA). *n*-butyl acrylate (*n*BA) based acrylic copolymers containing SBMA and BDMAEMA MS of varying charge compositions were polymerized. ^{1}H NMR results confirmed good agreement between the monomer feed and copolymer compositions. Small- angle X-ray scattering traces from both zwitterionomers and cationic analogs were fit very well, using a hard sphere model combined with a structure factor incorporating liquid-like interparticle interference. The modeling results revealed that the zwitterionomers contained fewer, but larger, ionic aggregates than the cationic analogs in a given sample volume. The superior elastomeric performances observed for the zwitterionomers compared to their cationic analogs coincided with their more well-defined microphase-separated morphologies. The stronger ion-ion interactions in the zwitterionomers were thus postulated to produce rubbery plateaus in DMA and better mechanical performance. The stronger zwitterionic interaction offers the potential to uptake conductive diluents, such as ionic liquids, while maintaining their mechanical strength for advanced electro-mechanical applications.

Zwitterionomer / ionic liquid binary compositions prepared using the "swelling" and the "cast with" processing methods exhibited very different thermomechanical performance, morphologies and ionic conductivity. Dynamic mechanical analysis showed that the "swollen" membranes maintained their thermomechanical performance with up to 18 wt% EMIm ES, while that of the "cast with" membranes decreased gradually as the ionic liquid contents in the composite membranes increased. Quantitative analysis of the SAXS data revealed that the sample processing methods impacted the distribution of ionic liquid inside the composite membranes. Specifically, for the "swollen" membranes, the zwitterionic aggregates existed prior to the introduction of ionic liquid into the membranes, and they resisted the intercalation of ionic liquid during the swelling process. Conversely, for the "cast with" membranes, the presence of the polar guest molecules during the membrane casting process hindered the formation of the zwitterionic aggregates, which functioned as the physical crosslinks in the "swollen" membranes. Impedance spectroscopy results showed that the ionic conductivity for the "swollen" membranes plateaued at ionic liquid concentrations higher than 12 wt%. This deviation from the exponential increase in ionic conductivity was likely the result of the persistence of the zwitterionic aggregates in the "swollen" membranes as well. In summary, the zwitterionic aggregates in poly(*n*BA-*co*-SBMA) served as both the physical crosslinks and the host sites for ionic conductive guest molecules. In order to optimize both thermomechanical performance and ionic conductivity of the polymer / ionic liquid binary compositions, it is desirable to have reinforcing mechanism, such as crystallinity or hydrophobic interactions, which are insensitive to the polar guest molecules.

We explored the synthesis of high molecular weight poly[sty-*b*-(*n*BA-*co*-DMAEA)-*b*-sty] using reversible addition-fragmentation chain transfer (RAFT) polymerization. The tertiary amine functionality in DMAEA would afford the triblock copolymers tunable polarity toward polar guest molecules, such as ionic liquids, upon quaternization. However, model study on 2-(dimethylamino)ethyl acrylate (DMAEA) revealed that acrylic radicals had high chain transfer tendencies toward the tertiary amine-containing monomer, which is undesirable in controlled radical polymerization processes. The measured chain transfer constant, C_s, of 0.0634 is close to that reported for the chain transfer between methyl acrylate radicals and triethylamine. Despite the inherent high C_s for DMAEA, we obtained poly[sty-*b*-(*n*BA-*co*-DMAEA)-*b*-sty] with relatively narrow PDIs through lowering the radical concentration, as well as that of DMAEA, in the RAFT polymerization procedure.

Both triblock copolymers that contained ~ 10 mol% neutral, or quaternizied, DMAEA showed much improved affinity toward EMIm TfO, an ionic liquid, while their *n*BA-containing counterpart was incompatible with the ionic liquid. Thermal and thermomechanical analyses of the block copolymer and their composite membranes revealed that they all had two distinctive glass transition temperatures at ~ -40 °C and ~ 100 °C. The lower T_g corresponded to the acrylate phases, where the ionic liquid resided, while the higher T_g corresponded to the IL-free poly(sty) phases, which served as the physical crosslinks in the membranes. The triblock copolymer / EMIm TfO binary compositions exhibited rubbery plateaus between -20 °C and 100 °C and plateau moduli of ~ 100 MPa, both of which are desirable for applications in electromechanical transducers. Actuator fabricated from poly[sty-*b*-(*n*BA-*co*-DMAEA)-*b*-sty] indeed

showed electro-responsiveness. The synthesis of poly[sty-*b*-(*n*BA-*co*-DMAEA)-*b*-sty] demonstrated here provided tunability for further understanding the structure-morphology-performance relationship of polymer-based electromechanical transducers.

In-situ FT-IR technique facilitated the synthesis of poly(sty-*b*-acrylate-*b*-sty) triblock copolymers of comparable molecular weights, but varying DMAEA compositions in the central blocks. Thermal and thermomechanical characterization of the resulting triblock copolymers indicated that the incorporation of electrostatic interactions into the low T_g central blocks of the ABA triblock copolymers enhanced their microphase separation and increased their higher T_gs, which corresponded to the poly(sty) phases. As a result, the SBDMAEA triblock copolymers exhibited extended rubbery plateaus compared with their neutral analogs. TEM results indicated that all triblock copolymers had lamellar morphologies. However, only the zwitterionic triblock copolymers showed SAXS profiles that were characteristic of the lamellar morphology.

Novel imidazole-containing acrylates were synthesized employing Michael-addition reactions. The monomers varied in the spacers between the acrylate and the imidazole functionalities. Conventional free radical polymerization of Sty, MMA and *n*BA revealed that the acrylate radicals were much more susceptible to chain transfer to the polymer than methacrylic and styrenic radicals. As a result, CFRP synthesized poly(acrylate)s are often branched. Controlled radical polymerization process (e.g. RAFT, ATRP and NMP) significantly minimized the impact of acrylic radical transfer. However, controlled radical polymerization of functional acrylates, such as DMAEA and ImPBA, remained challenging. The homopolymers of these novel imidazole-containing

acrylates and their quaternized derivatives exhibited potential as nucleic acid delivery agents.

Chapter 9 Suggested Future Work

9.1 Explore the applicability of solution rheology in elucidating the semi-dilute solution morphologies of strongly associated polymers

Chapter 4 of this dissertation reported the impact of processing methods (e.g. "swelling" *vs.* "cast with") on the morphology and the property of zwitterionomer / ionic liquid binary compositions. We focused on the solid state properties of the composite membranes and attributed the decreasing thermomechanical performance with increasing ionic liquid contents for the "cast with" membranes to more homogeneous distribution of ionic liquids in the zwitterionomer membranes. **Figure 9.1** compares the steady shear viscosities of the 10 wt% zwitterionomer in chloroform at 15 °C. The wt% of EMIm ES, the ionic liquid, is relative to the dry mass of the zwitterionomer in the solutions. The results showed drastically lower steady shear viscosities for ternary solutions that contained higher EMIm ES contents, in agreement with our hypothesis. Cheng and Long et al. employed dynamic mechanical analysis to evaluate the influence of electrostatic interactions on flow activation energies of phosphonium-containing triblock copolymers.[1] However, the application of solution rheology in the morphological characterization of semi-dilute polymer solutions is not well-documented in the literature. Our preliminary results indicated that solution rheology provided us with a sensitive tool to explore the impact of guest molecule on the molecular interactions between strongly associating polymers in solution.

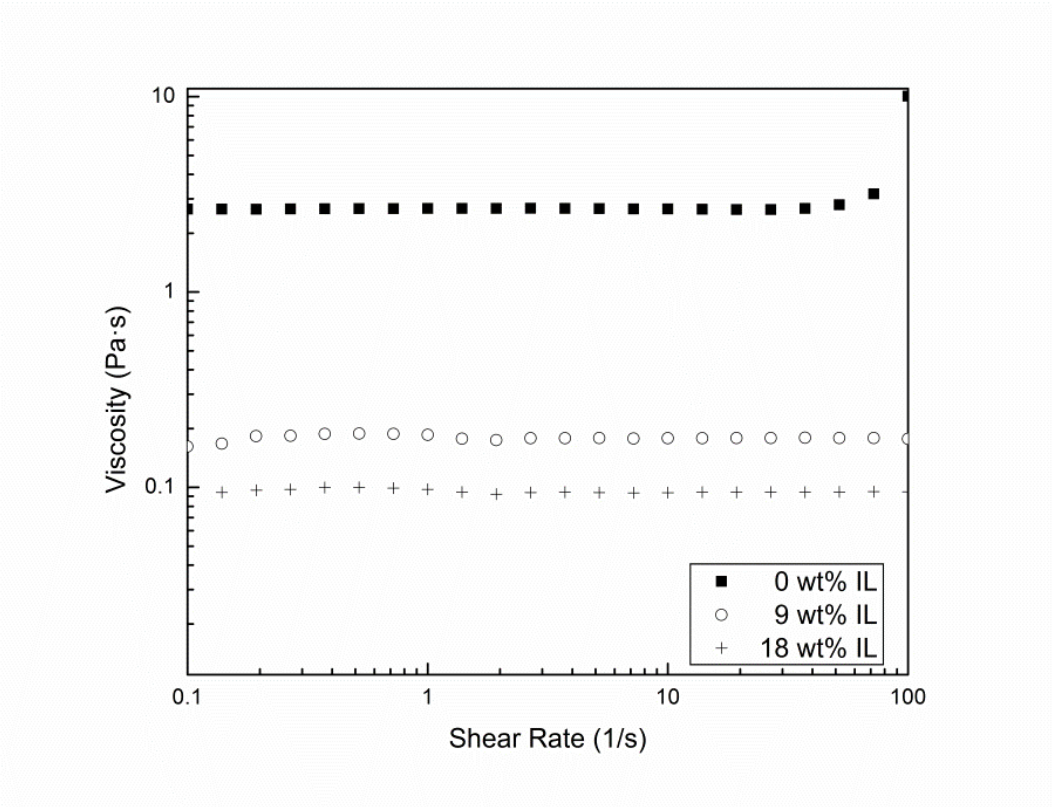

Figure 9.1 Steady shear viscosities of 10 wt% poly(*n*BA$_{90}$-*co*-SBMA$_{10}$) chloroform solutions at 15 °C. The ternary solutions contained 0, 9 and 18 wt% 1-ethyl-3-methylimidazolium ethanesulfate to the polymer.

9.2 Fine tune the affinity of poly(sty-*b*-acrylate-*b*-sty) toward polar guest molecules

In Chapter 5, we reported the impact of moderate amounts of 2-dimethylaminoethyl acrylate (DMAEA) incorporation into poly(sty-*b*-acrylate-*b*-sty) on its affinity toward ionic liquids. **Figure 9.2** showed representative swelling profiles for the DMAEA-triblock, the zwitterionic SB-DMAEA triblock and the poly(sty-*b*-*n*BA-*b*-sty) control toward 1-ethyl-3-methylimidazolium triflate (EMIm TfO). All triblock copolymers had comparable molecular weights, and the functional triblock copolymers contained 10 mol% DMAEA derivatives in the central blocks.

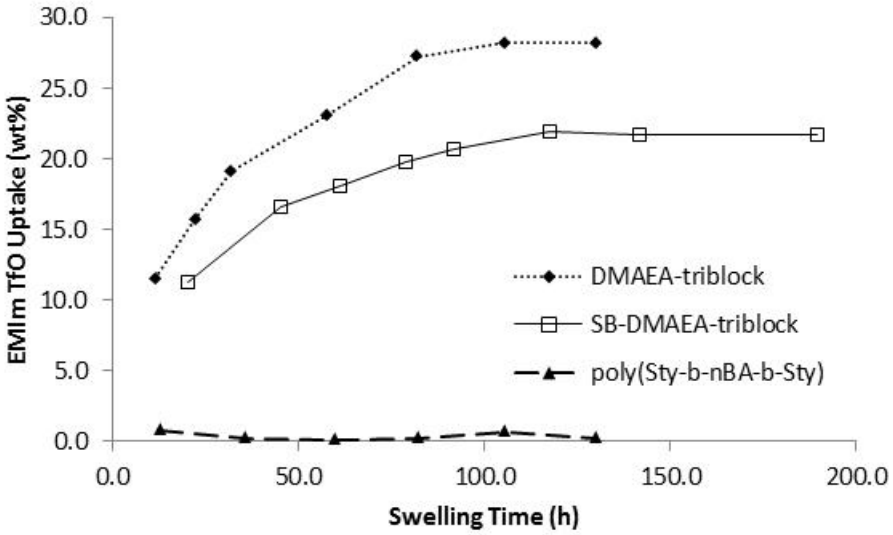

Figure 9.2 Swelling profiles for the ABA triblock copolymers with EMIm TfO

Figure9.3 showed the still images of the electro-mechanical actuators fabricated from both DMAEA-derived triblock copolymers under a 4 V applied potential. A follow-up study should vary the amounts of functional acrylates in the central blocks and evaluate its impact of the swelling capacity, as well as the actuation performance, of the triblock copolymers.

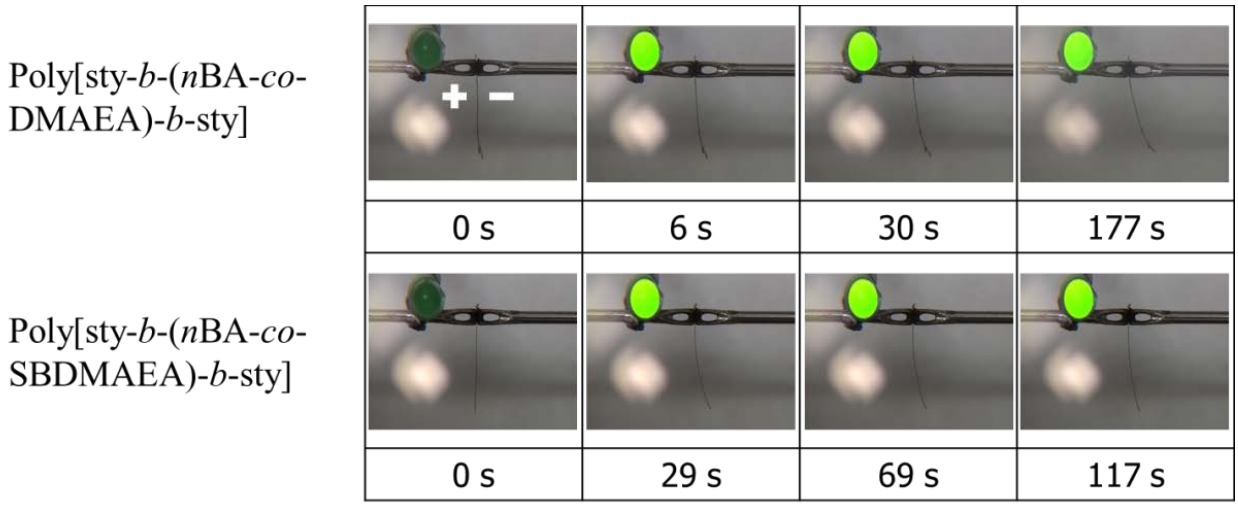

Figure 9.3 Still images of electromechanical transducers fabricated from EMIm TfO swollen poly(sty-*b*-acrylate-*b*-sty), a poly(allylamine hydrochloride) / anionic gold nanoparticle conductive nanocomposite, and gold electrodes under an applied potential of 4 V.

In addition, contact angle measurements with various ionic liquids on different triblock copolymer substrates might elucidate the molecular origin for the varying capacity of the triblock copolymers toward different ionic liquids.

9.3 Controlled radical polymerization of functional acrylates

Chapter 7 of this dissertation discussed the chain transfer issues that existed in the conventional free radical polymerization of acrylates. Recent developments in controlled radical polymerization techniques have enabled the synthesis of poly(acrylate)s with narrow PDIs.[2] However, controlled radical polymerization of functional acrylates remained challenging. Monteiro and coworkers explored RAFT polymerization of 2-dimethylaminoethyl acrylate (DMAEA) for applications as nucleic acid delivery agents.[3, 4] Gu and Lodge synthesized an ABA triblock copolymer that contained 2-bromoethylacrylate (BrEA) in the central block for gas separation performances.[5] Both

DMAEA and BrEA enable facile quaternization of the precursor polymers for polymerized ionic liquids. The novel imidazole-containing acrylates that we reported in this dissertation are similar functional acrylates. **Figure 9.4** illustrated the CRP of ImBA with various RAFT agents. Preliminary results indicated that the RAFT polymerized poly(ImBA) had relatively narrow PDIs. It is promising to control the radical polymerization of such imidazole-containing acrylates under appropriate conditions.

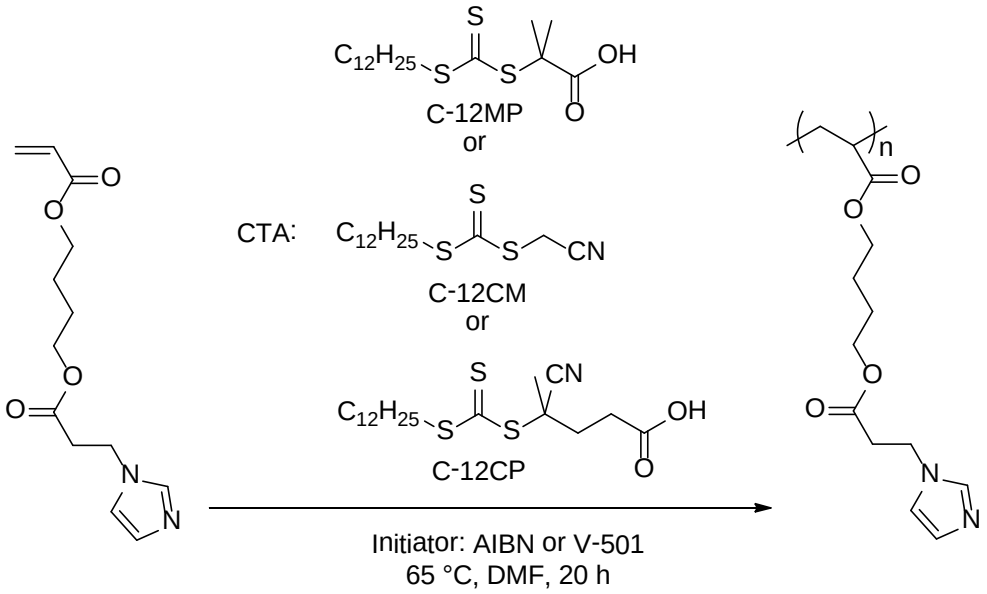

Figure 9.4 RAFT polymerization of ImBA with different CTAs

9.4 Novel zwitterionic poly(acrylate)s for pressure sensitive adhesives

Acrylic (co)polymers are one of few polymers that exhibit tack without functional additives. They are unique candidates for applications in pressure sensitive adhesive. Meanwhile, Nielson and coworkers explored zwitterionic compounds as tackifiers or plasticiers in adhesive formulations and provided adhesive compositions comprising zwitterionic copolymers.[6, 7] In this dissertation, we reported the syntheses of a series of novel imidazole-containing acrylates using Michael-addition reactions. The chemical structures of the novel acrylates are shown in **Figure 9.5**, and they vary in the chemical

structures of the spacers. It would be interesting to explore the pressure sensitive adhesive properties of compositions that contain theses functional acrylates.

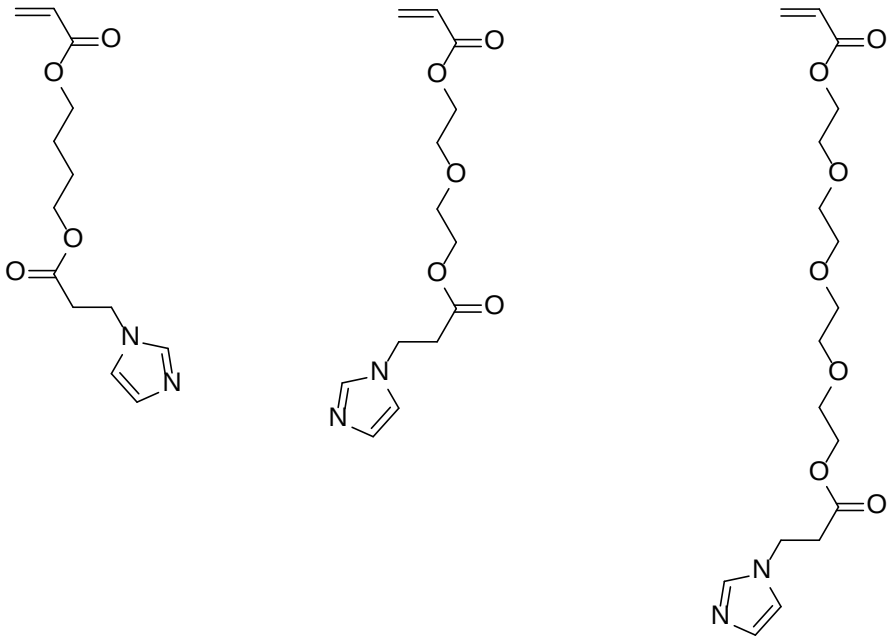

Figure 9.5 Chemical structures of the novel imidazole-containing acrylates

9.5 Influence of oligo(ethylene oxide) placement on the colloidal stability of imidazolium polycation / DNA polyplexes.

Kwoh et al. conjugated PEG to poly-L-lysine to sterically stabilize the resulting polyplexes at neutral charge ratios by shielding the surfaces.[8] Hemp and Long et al. synthesized similar AB diblock copolymers for nonviral gene delivery.[9] A stabilizing block of either oligo(ethylene glycol$_9$) methyl ether methacrylate or 2-(methacryloxy)ethyl phosphorylcholine provided colloidal stability, and the phosphonium-containing cationic block induced electrostatic nucleic acid complexation. While the block copolymer strategy exhibited great potential in stabilizing polyplexes, the synthesis of the block copolymers remained challenging. **Figure 9.6** illustrates the

chemical structures of three imidazolium polycations. Poly(EVIm Br) is not OEGylated, while poly(EImDEGA Br) is internally OEGylated and poly[M(EO)2Vim Br] is externally OEGylated. The syntheses of the three imidazolium polycations was either described in Chapter 7 of this dissertation or adopted from literature procedures.[10]

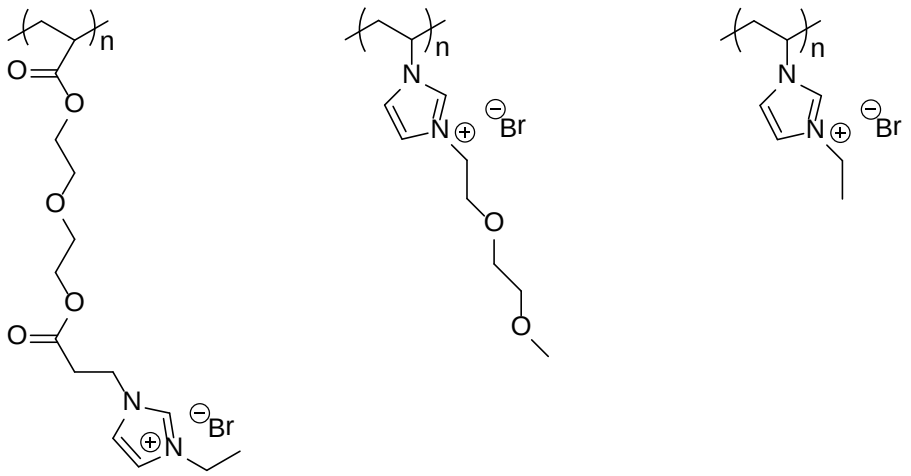

Figure 9.6 Chemical structures of imidazolium polycations with and without OEGylation

Figure 9.7 shows the colloidal stability of the imidazolium polycation / DNA polyplexes in Dulbecco's modified Eagle's media (DMEM) at N/P ratios of 2. The experimental conditions were adopted from a literature procedure.[9] All polyplexes maintained hydrodynamic diameters of ~ 100 nm in RNAse-free water over 24 h. In comparison, the hydrodynamic radii of the same polyplexes doubled or tripled upon dispersing into DMEM. More importantly, only those derived from poly[$M(OE)_2$VIm Br], which contained external OEGylation, exhibited colloidal stability in DMEM over 24 h. These results indicated that the placement of oligo(ethylene oxide) on imidazolium polycations had a profound impact on the colloidal stability of their complexes with DNA. External OEGylation of quaternizable polyamines and polyimidazoles may

provide simpler alternatives to block copolymers that exhibit both nucleic acid delivery capability and colloidal stability under physiological conditions.

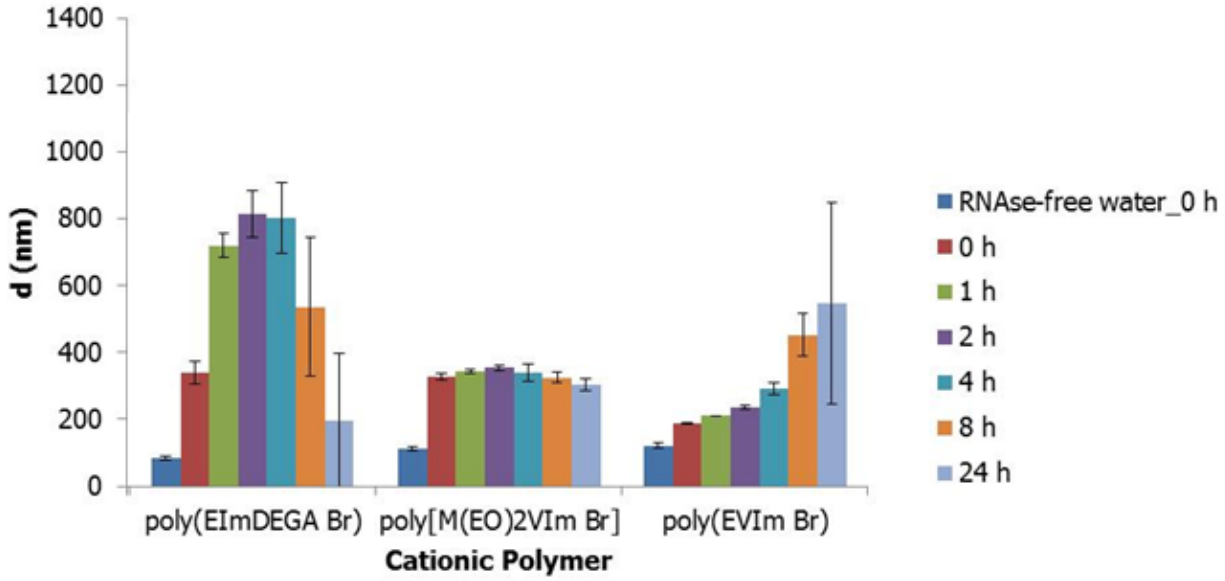

Figure 9.7 Hydrodynamic radii of the polyplexes in RNAse-free water or DMEM over time

Figure 9.8 illustrates imidazolium polycations that bear external oligo(ethylene oxide) units, and they are suitable candidates for future screening of nucleic acid delivery agents with colloidal stability under physiological conditions.

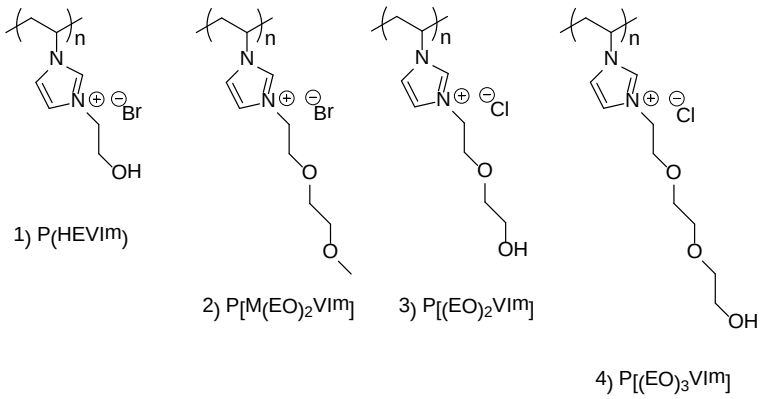

Figure 9.8 Imidaozlium polycations that bear externally oligo(ethylene oxide) unites

9.6 References

1. Cheng, S.; Beyer, F. L.; Mather, B. D.; Moore, R. B.; Long, T. E. *Macromolecules* **2011,** 44, (16), 6509-6517.
2. Ahmad, N. M.; Charleux, B.; Farcet, C.; Ferguson, C. J.; Gaynor, S. G.; Hawkett, B. S.; Heatley, F.; Klumperman, B.; Konkolewicz, D.; Lovell, P. A.; Matyjaszewski, K.; Venkatesh, R. *Macromol. Rapid Commun.* **2009,** 30, (23), 2002-2021.
3. Truong, N. P.; Jia, Z.; Burges, M.; McMillan, N. A. J.; Monteiro, M. J. *Biomacromolecules* **2011,** 12, (5), 1876-1882.
4. Truong, N. P.; Jia, Z.; Burgess, M.; Payne, L.; McMillan, N. A. J.; Monteiro, M. J. *Biomacromolecules* **2011,** 12, (10), 3540-3548.
5. Gu, Y.; Lodge, T. P. *Macromolecules* **2011,** 44, (7), 1732-1736.
6. Nielson, K. E.; Li, K.; Rayner, T. J. Adhesive compositions and adhesive tapes comprising novel zwitterionic copolymers. 1998-42980 6133391, 19980317., 2000.
7. Nielson, K. E.; Li, K.; Rayner, T. J. Adhesive compositions with zwitterionic tackifiers and plasticizers for adhesive tape. 1998-40024 6106940, 19980317., 2000.
8. Kwoh, D. Y.; Coffin, C. C.; Lollo, C. P.; Jovenal, J.; Banaszczyk, M. G.; Mullen, P.; Phillips, A.; Amini, A.; Fabrycki, J.; Bartholomew, R. M.; Brostoff, S. W.; Carlo, D. J. *Biochimica et Biophysica Acta (BBA) - Gene Structure and Expression* **1999,** 1444, (2), 171-190.
9. Hemp, S. T.; Smith, A. E.; Bryson, J. M.; Allen, M. H.; Long, T. E. *Biomacromolecules* **2012**.
10. Green, M. D.; Salas-de la Cruz, D.; Ye, Y.; Layman, J. M.; Elabd, Y. A.; Winey, K. I.; Long, T. E. *Macromolecular Chemistry and Physics* **2011,** 212, (23), 2522-2528.